UNIVERSITÀ DEGLI STUDI DI PADOVA

UNIVERSITÀ DEGLI STUDI DI PADOVA

DIPARTIMENTO DI FISICA E ASTRONOMIA "GALILEO GALILEI"

SCUOLA DI DOTTORATO DI RICERCA IN ASTRONOMIA
XXIX CICLO

GALAXIES ON THE ROAD TO QUENCHING

Direttore della scuola di dottorato: Prof. Giampaolo Piotto
Supervisore: Dott. Bianca Maria Poggianti
Correlatore: Dott. Benedetta Vulcani, Dott. Alessia Moretti
Controrelatori: Prof. Simona Mei, Dott. Alessandro Boselli

Dottoranda: Angela Paccagnella

Alla mia famiglia

"Equipped with his five senses,
man explores the universe around him
and calls the adventure Science."
Edwin Powell Hubble

Ringraziamenti

Con questi ringraziamenti si chiude un percorso straordinario. Non avrei potuto chiedere di più, come ricercatrice e come persona, a questi tre anni di dottorato.

Un ringraziamento speciale va alla mia relatrice, Dr.ssa Bianca Poggianti, non solo per l'immenso contributo teorico e metodologico offertomi e la sua dedizione a seguirmi nella mia ricerca ma anche per l'esempio che è stata per me di intelligenza, correttezza, amore per la ricerca e professionalità che costituirà sempre per me un modello da perseguire nella vita e nel lavoro.

Ho avuto inoltre la fortuna di collaborare con la Dott.ssa Benedetta Vulcani e la Dott.ssa Alessia Moretti a cui dedico un secondo grande grazie. Il loro contributo, dalle chiacchierate davanti ad un caffè, alle piccole correzzioni di ortografia fino alla discussione dei risultati, è sempre stato essenziale.

Nessuno dei molteplici passi che mi hanno portato a completare questo percorso sarebbe inoltre stato possibile senza la guida di un gruppo strepitoso, sotto ogni punto di vista. Per questo ringrazio Marco, Giovanni Fasano, Jacopo, Jara, Daniela e l'intero WINGS team.

Un sentito ringraziamento al Dott. Alessandro Boselli e alla Prof. Simona Mei, per aver letto con pazienza ed attenzione questo lavoro ed avermi aiutato a renderlo migliore.

Voglio, inoltre, ringraziare tutti i colleghi con cui ho condiviso lezioni, impegni, preoccupazioni e frustrazioni, oltre a idee e soddisfazioni. Sono stati per me più veri amici che semplici compagni. In particolare Alessandra, Andrea, Pietro, Giacomo ed Elena, compagni di avventure dentro e fuori dal Dipartimento.

Non avrei mai potuto concludere questo lavoro se non avessi avuto il sostegno della mia famiglia che mi ha seguita con affetto e pazienza, incentivandomi anche nei momenti più duri.

Un ultimo ringraziamento a Francesco. Il suo amore, la sua pazienza e la sua comprensione mi hanno letteralmente permesso di vedere il mondo. Che regalo stupendo.

Abstract

This thesis explores the properties of galaxies that reside in high density regions in the local Universe. The driving motivation is to shed light on how galaxies stop forming stars and the role played by the environment in this process. A wide variety of environmentally-related quenching mechanisms have been proposed and the smoking gun proving that these are actually transforming galaxies from being star forming to passive is the existence of a population of galaxies in transition with intermediate features. In this Thesis I will mainly focus on the properties of two population of galaxies: those that are forming stars at a reduced level compared to other galaxies at similar mass, and those that have recently and abruptly interrupted their star formation.

The data exploited in this Thesis come from surveys which focus on different environments in the local Universe: the WIde-field Nearby Galaxy-cluster Survey (WINGS, Fasano et al. 2006) with its recent extension OmegaWINGS (Gullieuszik et al., 2015a, Moretti et al. submitted) and the Padova Millennium Galaxy and Group catalogue (PM2GC, Calvi et al. 2011).

The Thesis starts with a characterization of the WINGS survey and then focuses on the new OmegaWINGS data, illustrating the most important aspects of the photometric and spectroscopic observations. I will describe in detail my personal contribution to the survey, from the data analysis to the redshift and velocity dispersion measurements, to the membership assignments. I will also present the complete galaxy catalog built from the combination of the two cluster surveys considered.

While halo mass estimates are quite easily obtained for clusters, at the group regime it is less straightforward to derive robust measurements. I will then present a procedure I developed to compute halo masses from observable quantities for the PM2GC. My approach exploits mock galaxy catalogs extracted from the De Lucia & Blaizot (2007) semi-analytic model, run on the Millennium Simulation (Springel et al. 2005).

Subsequently, I will discuss the methods adopted to compute the galaxy stellar properties, exploiting both spectroscopic and photometric information.

Using the data from the WINGS+OmegaWINGS surveys, I will present an analysis of the ongoing Star Formation Rate (SFR) and the Specific Star Formation Rate (SSFR) - stellar mass (M_*) relations in field and cluster mass limited samples. I contrast trends in the different environments and, in clusters, at different clustercentric distances. The main result is that in clusters a population of galaxies with a reduced SFR is detected, named transition galaxies, which is much rarer in the field. The spatial location of these galaxies, together with the analysis of the star formation histories, colors and average ages, suggest that transition galaxies have had a reduced SFR for the past 2-5 Gyr. This is compatible with a strangulation scenario, even if other processes like ram pressure stripping can not be excluded.

I characterize the properties of post starburst (PSB) galaxies, which are galaxies that abruptly interrupted their star formation sometimes during the past < 1.5 Gyr and present recognizable features in their spectra (no emission and Hδ in absorption). Exploiting an observed magnitude limited sample drawn from WINGS+OmegaWINGS, I will present the first complete characterization of PSBs in clusters and contrast their properties to those of passive (PAS) and emission line (EML) galaxies. The main finding is that the incidence of PSBs increases from the outskirts toward the cluster centers and, more gently, from the least toward the most luminous and massive clusters. PSBs have stellar masses, magnitudes, colors and morphologies intermediate between PAS and EML galaxies, typical of a population that has recently become passive. The phase-space analysis and the velocity dispersion profiles also suggest that PSBs represent a combination of galaxies with different accretion histories. In particular, PSBs with the strongest Hδ are consistent with being recently accreted. This analysis suggests that as a galaxy is accreted onto a cluster and approaches the cluster virialized region, ram pressure stripping (or other interactions) induces either a burst of the star formation with a subsequent fast quenching, or simply a fast quenching and this is more efficient in more massive clusters.

I then characterize the PSB population also in smaller systems. Combining the WINGS+OmegaWINGS and PM2GC data, I will show how the fraction of PSB galaxies and the quenching efficiency depend on the halo mass, and increase from single galaxies, to binaries, groups and clusters. In the different environments, different physical mechanisms are probably responsible for the production of PSB galaxies, but all of them produce a truncation of star formation on short time-scales. If ram pressure stripping is the most likely candidate in clusters, gravitational interaction between galaxies could be

more efficient in lower density regions.

To conclude, the role of environment is undisputed in driving the galaxy evolution. In this Thesis I identified two possible evolutionary pathways related to the end of star formation in clusters: one requires a gradual reduction of star formation (long time-scale quenching t>2Gyr), the other a rapid truncation of the star formation activity (t∼0.1Gyr). Comparing the fraction of PSBs to the fraction of galaxies in transition, it appears that the short timescale star-formation quenching channel contributes two times more than the long timescale one to the growth of the passive population in clusters. The emerging picture is that ram pressure stripping is probably the most successful process affecting star formation in clusters, followed by strangulation. Other mechanisms might play a role, even though they most likely take place in lower density environments.

Riassunto

L'obiettivo del lavoro presentato in questa tesi è la caratterizzazione osservativa delle proprietà delle galassie, per vincolarne gli scenari di formazione ed evoluzione. In particolare, mi sono concentrata nel determinare come l'ambiente in cui evolvono le galassie influisca sul processo di formazione stellare nelle regioni ad alta densità nell'Universo locale.

Tra i diversi meccanismi proposti come responsabili del quenching, ovvero la tendenza delle galassie a smettere di produrre stelle, quelli relativi all'ambiente sembrano svolgere un ruolo cruciale. La prova che confermerebbe l'azione primaria di questi meccanisimi dovrebbe essere l'esistenza, in ammassi e gruppi di galassie, di una popolazione di galassie in transizione con caratteristiche intermedie.

Con lo scopo dunque di identificare questa nuova popolazione, mi concentrerò sullo studio delle proprietà di due particolari classi di galassie: quelle che stanno formando stelle ad un livello ridotto rispetto ad altre galassie di massa simile, e quelle che hanno recentemente, e molto probabilmente bruscamente, interrotto la loro formazione stellare.

Utilizzerò i dati provenienti da diverse campagne osservative: la WIde-field Nearby Galaxy-cluster Survey (WINGS, Fasano et al. 2006) con la sua recente estensione OmegaWINGS (Gullieuszik et al., 2015a; Moretti et al., 2017), e il Padova Millennium Galaxy and Group catalogue (PM2GC, Calvi et al. 2011).

La prima parte della tesi è riservata alla descrizione delle survey WINGS e OmegaWINGS. Particolare attenzione sarà dedicata alla presentazione degli aspetti più importanti delle osservazioni fotometriche e spettroscopiche di OmegaWINGS, in cui sono stata personalmente coinvolta. Descriverò in dettaglio il mio contributo alla survey, che va dall'analisi dei dati alle misurazioni di redshift e dispersione di velocità, all'individuazione delle galassie appartenenti agli ammassi. Presenterò dunque il catalogo completo costruito dalla combinazione delle due survey considerate.

Mentre è relativamente facile ricavare una stima della massa di alone per gli ammassi,

è più complicato ottenere misurazioni affidabili per i gruppi. Ho quindi sviluppato una procedura per derivare le masse di alone per i dati PM2GC da quantità osservabili, che descriverò in dettaglio. Tale procedura utilizza cataloghi di galassie estratti dai modelli semi analitici di De Lucia & Blaizot (2007), applicati alla Millennium Simulation (Springel et al. 2005).

Successivamente, descriverò i metodi adottati per il calcolo delle proprietà delle galassie, sfruttando le informazioni provenienti da osservazioni spettroscopiche e fotometriche.

Utilizzando i dati WINGS+OmegaWINGS, discuterò l'analisi delle relazioni tra il tasso di formazione stellare (SFR), il tasso specifico di formazione stellare (SSFR) e la massa stellare di una galassia (M_*), nel campo e negli ammassi, in campioni limitati in massa. Confronterò gli andamenti nei diversi ambienti e, negli ammassi, a diverse distanze dal centro. Il risultato principale è l'individuazione di una popolazione di galassie in ammasso con SFR ridotta, denominate galassie in transizione, che è molto più rara nel campo. La distribuzione spaziale di queste galassie, insieme all'analisi della storia di formazione stellare, dei colori ed età medie, suggeriscono che le galassie in transizione abbiano avuto un SFR ridotta per circa 2-5 Gyr. Questo è compatibile con uno scenario di "strangulation", anche se altri processi come la ram pressure stripping non possono essere esclusi.

Successivamente caratterizzerò le proprietà delle galassie cosiddette post starburst (PSB), cioè galassie che hanno bruscamente interrotto la loro formazione stellare all'incirca 1 miliardo di anni fa e che presentano caratteristiche ben riconoscibili nei loro spettri (nessuna emissione e Hδ in assorbimento). Sfruttando un campione limitato in magnitudine apparente estratto dai dati WINGS + OmegaWINGS, presenterò la prima caratterizzazione completa di galassie PSB in ammasso e confronterò le loro proprietà con quelle di galassie passive (PAS) e con righe di emissione (EML). Il principale risultato riguarda il numero relativo di galassie PSB, che aumenta leggermente dalla periferia verso il centro degli ammassi e dall'ammasso meno luminoso/massiccio a quello più luminoso/massiccio.

Le galassie PSB hanno proprietà, quali masse stellari, magnitudini, colori e morfologie, intermedie tra le PAS e EML, tipiche di una popolazione che è recentemente diventata passiva. L'analisi dello spazio delle fasi e dei profili di dispersione di velocità indicano anche che le PSB rappresentano una combinazione di galassie con diverse storie di accrescimento. In particolare, PSB con forte Hδ sono consistenti con l'essere state recentemente accresciute.

Questa analisi suggerisce che, nel processo di accrescimento di una galassia su un ammasso, all'avvicinarsi alla regione virializzata, per effetto della ram pressure stripping (o di altre interazioni) viene indotto un rapido quenching, preceduto o meno da un forte

episodio di formazione stellare; inoltre quest'effetto è più forte in ammassi più massicci.

Descriverò successivamente la popolazione di PSB in sistemi più piccoli. Combinando i dati WINGS+OmegaWINGS ai dati PM2GC, mostrerò come la frazione di galassie PSB e l'efficienza del quenching dipendano dalla massa dell'alone e aumentino andando da galassie singole, a sistemi binari, gruppi e ammassi. Nei diversi ambienti, diversi meccanismi fisici sono probabilmente responsabili per la produzione di galassie PSB, ma tutti producono un troncamento della formazione stellare su brevi scale temporali. Mentre negli ammassi la ram presssure stripping sembra essere il candidato più probabile, l'interazione gravitazionale tra galassie potrebbe essere più efficiente nelle regioni a bassa densità.

Dal confronto tra la frazione di PSB e di galassie in transizione, si può dedurre che il canale di quenching più rapido constribuisce circa due volte di più alla crescita della popolazione di galassie passive rispetto al canale di quenching più lento. Il quadro che emerge è che la ram pressure stripping è probabilmente il processo che maggiormente incide sul quenching della formazione stellare negli ammasi, seguito dalla strangulation. Altri meccanismi potrebbero influire, anche se probabilmente con effetto maggiore in ambienti a minore densità.

Contents

Publications

Thesis publications

Paccagnella, A., Vulcani, B., Poggianti, B. M., Moretti, A., Fritz, J., Gullieuszik, M., Couch, W., Bettoni, D., Cava, A., D'Onofrio, M., and Fasano, G. (2016). *Slow Quenching of Star Formation in OMEGAWINGS Clusters: Galaxies in Transition in the Local Universe*, ApJ, 816:L25.

Paccagnella A. Vulcani, B., Poggianti B. M., Fritz, J., Fasano, G., Moretti, A., Jaffe' Y. L., Biviano A., Gullieuszik, M., Bettoni, D., Cava, A., Couch, W, and D'Onofrio, M. (2016). *OmegaWINGS: The first complete census of post starburst galaxies in clusters in the local universe*, ApJ Submitted.

Paccagnella, A., Vulcani, B., Poggianti, B. M., Fritz, J., Fasano, G., Moretti, A., Calvi R. (2016). *The incidence of post starburst galaxies in the different environments in the local universe*, ApJ to be submitted.

Gullieuszik, M., Poggianti, B. M., Fasano, G., Zaggia, S., **Paccagnella, A.**, Moretti, A., Bettoni, D., D'Onofrio, M., Couch, W. J., Vulcani, B., Fritz, J., Omizzolo, A., Baruffolo, A., Schipani, P., Capaccioli, M., and Varela, J. (2015). *OmegaWINGS: OmegaCAM-VST observations of WINGS galaxy clusters*, A&A, 581:A41.

Gullieuszik, M., Poggianti, B. M., Fasano, G., Zaggia, S., **Paccagnella, A.**, Moretti,

A., Bettoni, D., D'Onofrio, M., Couch, W. J., Vulcani, B., Fritz, J., Omizzolo, A., Baruffolo, A., Schipani, P., Capaccioli, M., and Varela, J. (2015). *OmegaWINGS: A VST Survey of Nearby Galaxy Clusters*, The Messenger, 160, 13-17.

Moretti M., Gullieuszik M., Poggianti B. M., **Paccagnella A.**, Couch, W. J., Vulcani, B., Bettoni, D., Fritz, J., Cava, A., Fasano, G., and D'Onofrio, M. (2016). *OmegaWINGS spectroscopy of local clusters of galaxies over 1 square degree*, ArXiv e-prints.

Other publications

Poggianti, B. M., Fasano, G., Omizzolo, A., Gullieuszik, M., Bettoni, D., Moretti, A., **Paccagnella, A.**, Jaffe', Y. L., Vulcani, B., Fritz, J., Couch, W., and D'Onofrio, M. (2016). *Jellyfish Galaxy Candidates at Low Redshift*, AJ, 151:78.

Vulcani, B., Poggianti, B. M., Fritz, J., Fasano, G., Moretti, A., Calvi, R., and **Paccagnella, A.** (2015). *From Blue Star-forming to Red Passive: Galaxies in Transition in Different Environments*, ApJ, 798:52.

Guglielmo, V., Poggianti, B. M., Moretti, A., Fritz, J., Calvi, R., Vulcani, B., Fasano, G., and **Paccagnella, A.** (2015). *The star formation history of galaxies: the role of galaxy mass, morphology and environment*, MNRAS, 450:2749–2763.

1 Introduction

1.1 Galaxy formation

Understanding the evolution of the Universe, and how matter evolved from a relatively homogeneous primordial gas after the Big Bang into the diversity of galaxies and cosmic structures seen today, remains a major goal of modern astronomy.

Over the past decades, constraints on the properties of galaxies over cosmic time have remarkably improved, as our understanding of the processes that shape galaxies. Despite this, several new questions remain to be answered: How do galaxies build up their stellar mass by forming stars? What physical processes drive the star-formation in galaxies and how does the star formation rate change over cosmic time, galaxy properties, and the type of environment a galaxy inhabits? How are galaxies affected by these physical processes?

In the local Universe, where galaxies represent the end-products of all cosmic processes, galaxies exhibit a staggering diversity of properties. These diverse properties are exemplified in the Hubble Sequence classification scheme (Hubble, 1926), which illustrates the various morphologies of galaxies according to a *tuning fork* diagram (see figure 1.1). Even today galaxies can be grouped into four broad classes:

- Elliptical galaxies are spheroidal systems dominated by old stellar populations, lack significant ongoing star formation, and are generally massive and red.
- Lenticulars or S0s have a smooth light distribution, show a disk/lens and a predominant spheroidal component and may have structural bars.
- Spiral galaxies have disks, are bluer due to young stellar populations from ongoing star formation, and are divided into barred and normal spirals, depending on whether

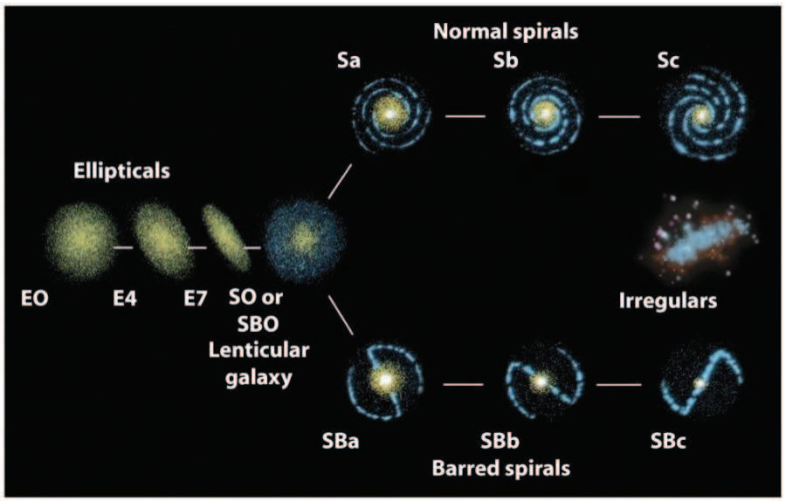

Figure 1.1: Schematic representation of the Hubble tuning fork for galaxy classification (from cyberneticinc.com). Galaxies are grouped as ellipticals (E), lenticulars (S0s), spirals (S and Sb if a bar present) and irregulars.

or not a bar is detected. They are usually ordered according to the bulge to disk brightness ratio.

- Irregular galaxies are characterized by an irregular shape, sometimes with evidence of gravitational disruption in the form of tidal tails.

The assembly of the Hubble Sequence is one of the most widely studied phenomena, as extensively discussed for example in the review of Sandage (2005) and van den Bergh (1998), and yet it has not been fully understood. Many properties of the galaxy population change along the sequence, indicating that it actually reflects a sequence in physical properties of galaxies whose variation has to be linked to different channels of formation and evolution.

In an attempt to address this issue, statistical studies of galaxy populations in the local Universe have revealed correlations between galaxy properties and provided constraints on their evolution. These studies have found that red elliptical "early-type" galaxies are the oldest and most massive galaxies, and preferentially inhabit dense regions of the Universe such as galaxy clusters, while blue star-forming "late-type" galaxies are less massive and more frequent in emptier regions of space (see section 1.2 and Dressler, 1980). Early interpretation of these differences resulted in a simple model in which elliptical galaxies formed early in the Universe's history and rapidly evolved, until their star formation

ended. However, the reason for this early and rapid evolution is not obvious. This simple "monolithic collapse" model places the formation of galaxies at high-redshift from a rapid burst of star formation when massive gas clouds collapse (Eggen et al., 1962; Larson, 1974, 1975), and then requires a passive evolution to the present day with little to no additional star formation or morphological changes.

More recent advances based on observations and cosmological simulations of a cold dark matter (CDM) dominated Universe point to the paradigm of hierarchical structure formation, where galaxies form, owing to the cooling of hot gas, within dark matter halos that form from the gravitational collapse around peaks in the initial density field (Mo and Fukugita, 1996; Sheth and Tormen, 2002). Despite the several evidences supporting this "bottom-up" model, with smaller structures forming first and later merging into larger systems, there are still some unresolved problems. Indeed, it has long been known that galaxies do not share this trend, at least in their star formation history. Massive galaxies are dominated by old stellar populations, in contrast to spiral galaxies, that appear to have actively formed stars over the last billion years, and are dominated by young stellar populations. Moreover, the average mass of star forming galaxies declines with decreasing redshift. This trend, named "downsizing" by Cowie et al. (1996), is not necessarily in contrast with the hierarchical clustering of dark matter halos. It has been suggested that internal feedback mechanisms could reconcile this anti-hierarchical behavior of galaxies with the standard dark matter bottom up model (Bower et al., 2006; Croton et al., 2006): the suppression of late gas condensation in massive halos due to the AGN activity gives rise to shorter formation time-scales for more massive galaxies (De Lucia et al., 2006), while supernovae could efficiently delay the star formation in low mass systems, in qualitative agreement with the observed trends.

After the assembly, halos and galaxies evolve simultaneously and the evolution of a galaxy is driven by the evolution of its host halo. If the halo is accreted by a larger one, the galaxy will be affected as well, experiencing, for example, the stripping of the hot gas reservoir that served as fuel for the star formation. More generally, the various properties of galaxies are strictly related to the environment in which they are evolving. In the next sections I will give an overview of the main observational evidences of the environmental effects and of the physical processes that are involved, driven by the motivation that a fraction of galaxies will be processed at some point through dense environments.

1.2 Observational evidence for environmental effect

Much of the early thinking about the effect a galaxy's environment has on its properties was driven by a few key observations. I review these early results and some of the most recent correlations.

The morphology-density relation

In his pioneering work based on photographic plates of 55 rich galaxy clusters, obtained using the Las Campanas 2.5-m and the Kitt Peak 4-m telescopes, Dressler (1980) found that in clusters the fraction of early type galaxies increases with the galaxy density and/or clustercentric radius (Whitmore et al., 1993) (see Fig.1.2). This correlation between galaxy morphology and its environment, called the *morphology-density* relation, appeared universal, as it holds in both structurally regular (dynamically 'relaxed') and irregular (clumpy, 'non-relaxed') nearby clusters and also in groups and in the field environment (Bhavsar, 1981; de Souza et al., 1982; Postman and Geller, 1984). Whitmore and Gilmore (1991), re-examining the 55 clusters studied by Dressler, argued that the morphology-radius relation -the correlation between morphology and clustercentric distance- is tighter than the morphology-density relation thus being more fundamental (see also the recent results of Fasano et al., 2015). Moreover, when the morphology-density relation was proved to hold also for clusters at intermediate redshifts ($z \sim 0.3 - 0.5$) (Dressler et al., 1997; Fasano et al., 2000), the viewpoint of Whitmore and collaborators was almost bailed out. In this redshift range, however, the relation was found very weak or even absent for irregular clusters.

In the subsequent decade, several authors studied the morphology-density relation in different ranges of redshift and stellar masses. Most of them agreed that this relation is already in place at $z \sim 0.5$, also in groups, and out to $z \sim 1$ in clusters (Treu et al., 2003; Postman et al., 2005; Desai et al., 2007; Wilman et al., 2009) and that the evolution of the morphological fractions strongly depends on galaxy mass (Nuijten et al., 2005; Oesch et al., 2010; Vulcani et al., 2011).

Besides the dependence on redshift, some authors have also analyzed the morphological fractions as a function of the global cluster properties. In particular, Desai et al. (2007) found a mild dependence of the morphological fractions on the cluster velocity dispersion, while the growth of the spiral/S0 fraction with redshift was found by Poggianti et al. (2009) to be stronger for low-mass than for high-mass clusters. Fasano et al. (2015), studying the nearby cluster population, found that the link between morphology and local

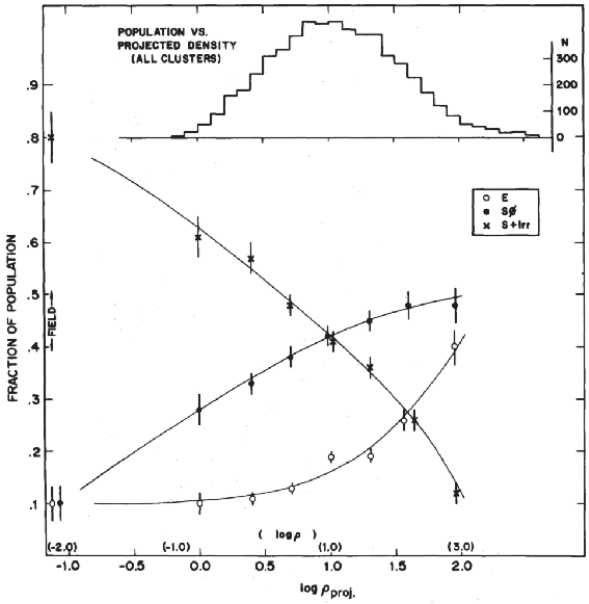

Figure 1.2: The morphology-density relation reproduced from Dressler (1980). The fractions of E, S0, and spiral plus irregular galaxies are shown as functions of the projected local density (in galaxies per square megaparsec). The upper histogram shows the number distribution of galaxies found in these environments, for a sample of over 6000 galaxies in 55 rich clusters. The fraction of spiral galaxies falls steadily for increasing local density, compensated by a corresponding rise in the fraction of elliptical and S0 galaxies. Identical trends have been found to hold for galaxies in poorer groups, but the dependence weakens or disappears in groups where the crossing time is comparable to the age of the universe.

density is preserved just in dynamically evolved regions. A specific effect of the cluster environment on the spiral/S0 fraction is claimed by Calvi et al. (2012), based on the sharp enhancement/dearth of S0s/late types found in clusters at low redshift, compared to other environments (single galaxies, binary systems, poor/rich groups). The SDSS and 2dF surveys made it possible to extend the study to low density regions, confirming the increase of the fraction of red, bulge dominated galaxies with galaxy-density (Goto et al., 2003; Hogg et al., 2003; Balogh et al., 2004a).

Color-Magnitude relation

Galaxy clusters have proven to be very useful laboratories for the study of galaxy formation and evolution. Indeed, it is well established that many galaxy properties in the nearby Universe correlate strongly with their environment. Beside the morphology-density relation described in the previous section, at low redshift a clear bimodality in the colors

of cluster galaxies, strictly linked to the morphological type, emerged (see for example the works of Conselice 2006; Wang et al. 2007). The "blue cloud" is dominated by spirals and irregular galaxies, and the prominent ridge of red galaxies (the so-called "red sequence") is mainly populated by E/S0 galaxies. This implies that morphology correlates at some level with the stellar population content (and hence color). Early works by Baum (1959); Faber (1973) and Caldwell (1983) established the existence of a red sequence of cluster ellipticals in the local Universe and showed that these galaxies have systematically redder colors with increasing luminosity. Later on, Visvanathan and Sandage (1977) and Sandage and Visvanathan (1978a,b) found that this color-magnitude relation (CMR) is universal. In the past decade, a number of studies have shown that the CMR of elliptical galaxies holds at progressively higher redshifts, at least up to z= 1.4 (e.g. Ellis et al., 1997; Stanford et al., 1998; van Dokkum et al., 2000; van Dokkum and Stanford, 2001; Blakeslee et al., 2003; Mei et al., 2006; Lidman et al., 2008; Mei et al., 2009; Jaffé et al., 2011). As a consequence, the CMR is, arguably, one of the most powerful scaling relations obeyed by the early-type galaxy population at the cores of clusters, encoding important information about their formation history.

Innumerable studies have investigated the origin of this relation, and the reasons why a galaxy either belongs to it, or falls below in the blue cloud. The CMR is usually characterized by a linear relation, defined by a zero point, slope and color scatter. Its slope has traditionally been interpreted as the direct consequence of a mass-metallicity relation (e.g. Faber, 1973; Larson, 1974; Gallazzi et al., 2006). The common underlying idea is that this mass-metallicity sequence originates from the fact that more massive galaxies have deeper potential wells and retain metal enriched stellar ejecta more effectively than less massive ones (Larson, 1974; Dekel and Silk, 1986; Tremonti et al., 2004; De Lucia et al., 2004; Kobayashi et al., 2007; Finlator and Davé, 2008).

An alternative interpretation in which the CMR is predominantly an age sequence would imply that the relation changes significantly with redshift as less massive galaxies approach their formation epochs. This possibility was ruled out by observations of clusters at intermediate redshift that showed that the slope of the CMR evolves little with redshift (Kodama and Arimoto, 1997; Kodama et al., 1998).

Nevertheless, weak age trends along the CMR have been claimed (e.g. Ferreras et al., 1999; Poggianti et al., 2001; Nelan et al., 2005), even though it seems clear that they are not the main physical driver. The small observed scatter can result from a small age difference at given galaxy mass, as suggested by Bower et al. (1992).

The tightness of the relation then implies an early formation epoch (z $>$ 2–3; e.g.

Bower et al., 1992; Mei et al., 2009). and a very synchronized star-formation histories for these galaxies.

This homogeneity of histories of early-type galaxies in clusters needs to be contrasted with a number of other results and considerations. An example is the so-called "progenitor bias". Given that the population of early-type galaxies observed in distant clusters does not necessarily comprises all the early-type galaxies existing at $z = 0$, morphological transformations might occur in clusters (see below) and change later-type star forming galaxies into some of the early-type galaxies present in clusters today. Because of this, in distant clusters only those galaxies that were already assembled as early-type and stopped forming stars at high redshift would be observed.

This, together with other findings, suggest that the color-magnitude sequence of clusters today must be composed of a variegated population of galaxies that had a variety of star formation histories. Though probably the mass-metallicity relation remains the main driver of the CM relation, intricate age and metallicity effects must be at work.

Star formation suppression in cluster galaxies

The first attempt to study the star formation activity in clusters was carried out back in the 80's by Kennicutt and Kent (1983) who showed that Virgo cluster galaxies have, on average, a lower star formation activity, redder colors and lower HI gas content than their field counterpart. Since then, several authors proved that strongly star-forming galaxies are mostly found in low-density environments, while the cores of massive clusters are full of massive, early-type galaxies dominated by old stellar populations both in the local universe (e.g. Baldry et al., 2006; van den Bosch et al., 2008; Gavazzi et al., 2010; Peng et al., 2010; Wetzel et al., 2012; Rasmussen et al., 2012; Haines et al., 2013) and out to z$\sim$ 1 (e.g., Patel et al., 2009; Cooper et al., 2010; Muzzin et al., 2012; Raichoor and Andreon, 2012; Mok et al., 2013; Woo et al., 2013; Nantais et al., 2013; Kovač et al., 2014; Tal et al., 2014). In a hierarchical universe, clusters grow by accreting galaxies from less dense environments. This picture clearly emerges from numerical simulations in the ΛCDM cosmology (e.g. the Millennium simulation, Springel et al. 2005), where satellite galaxies continuously feed regions of higher density (central galaxies, groups, clusters) at the intersection of multiple filaments. Thus, in order to form/maintain this star formation density relation, galaxy properties need to be altered upon infall into a cluster: star formation needs to be suppressed. This is in turn believed to be causally linked to the lack of cold star forming gas (e.g. Haynes and Giovanelli, 1984; Gavazzi et al., 2006; Fabello et al., 2012; Catinella et al., 2013; Hess and Wilcots, 2013; Boselli et al., 2016). The combination of

Hα and HI data has been crucial for understanding the nature of the underlying physics for the quenching of the star-formation activity in cluster galaxies (see e.g. Gavazzi et al., 2013a,b). These works have indeed shown that the quenching of the star formation activity follows the stripping of the atomic gas.

Various physical mechanisms have been proposed over the years to remove (or consume) gas and quench star formation in galaxies within massive clusters, but there is currently no clear consensus on the cause of this gas depletion. More gentle mechanisms, which are more difficult to observe directly, could also lead to the quenching of star formation, as will be discussed in the following section.

It is important to observationally specify the environment where galaxy properties start to change and how much they change. While galaxies within clusters strongly exhibit the above environmental dependencies, such trends can extend to galaxies beyond the virial radius. Important hints on the origin of the observed trends could come also from the study of the periphery of clusters and of groups. Recently, several authors have noted an enhanced quiescent fraction and reduced HI emission in galaxies out to two-four virial radii (Balogh et al., 2000; von der Linden et al., 2010; Wetzel et al., 2012) as well as for dwarf galaxies around lower mass groups.

The luminosity function of galaxies in clusters

For understanding the formation history and evolution of the galaxies in galaxy clusters, the galaxy luminosity function (LF), i.e. the number density of galaxies at a given luminosity, is a powerful tool for describing the fundamental properties of galaxies. In the early studies, a single Schechter function was suggested as an analytic form to describe the "universal" LF of galaxies in clusters (Schechter and Peebles, 1976) and field environment (Madgwick et al., 2002; Blanton et al., 2005).

The study of the LF in clusters has two main purposes: the comparison of the LF shape in clusters and in the field, to obtain information on the influence of environment on the formation and overall statistics of cluster galaxies; and the investigation of differences in the LFs of different clusters, both at similar or different redshifts, as markers of the effect of evolution in the star formation of galaxies.

The effect of evolution on the shape of the LF was investigated already by Dressler (1978a,b,c), who noted that clusters with massive cD galaxies tend to have a steeper bright end of the LF and suggested that galaxy cannibalism in cluster cores could help in shaping the LF. Since then, many studies have been carried out to establish the properties of the LF for field and cluster galaxies, based either on individual clusters or on stacked cluster

samples (see Boselli and Gavazzi 2006 for a comprehensive review). The results of these studies have been discordant. While several investigations have brought a picture of an universal cluster LF (Lugger, 1986; Colless, 1989; Paolillo et al., 2001; Popesso et al., 2005), other studies have highlighted clear differences in the LF of cluster and field -indicating that the faint end slope of the LF is steeper in clusters- or of different clusters (Dressler, 1978c; López-Cruz et al., 1997; Garilli et al., 1999; Goto et al., 2002; De Propris et al., 2003; Hansen et al., 2005; Trentham et al., 2005).
A change in the LF shape with cluster-centric distance was also observed in numerous studies (e.g. Beijersbergen et al., 2002; Goto, 2005) and mainly ascribed to the effect of galaxy harassment on dwarf galaxies (see Moore et al., 1996, and the following section). In particular, these studies found that the LF becomes shallower and dimmer with decreasing cluster-centric distance, which is attributed to the interaction between infalling galaxies and the intracluster medium (ICM) via ram-pressure stripping and tidal disruption in the cluster core.
Recent studies on clusters LFs have therefore been focused on galaxies LFs at fixed distance from the cluster center in terms of R_{200} (Popesso et al., 2006; Moretti et al., 2015), finding somewhat contradictory results. In particular Moretti et al. (2015), studying the WINGS clusters LF out to $0.5 \times R_{200}$ found that the steepening at fainter luminosities is less pronounced than the one found for SDSS clusters. WINGS clusters display a wide variety of LFs shapes, but this does not seem to correlate with cluster properties (traced by the X luminosity and by the clusters velocity dispersions.)

Evolution of cluster galaxies

There have also been direct evidence for cluster galaxy evolution. Galaxy morphology is one of the most fundamental properties of galaxies subject to change with redshift. Dressler et al. (1997) found that the morphology-density relation varies with redshift: in clusters the fraction of elliptical galaxies is as large or larger than in low redshift clusters, but the S0 fraction in 2-3 times smaller, with a proportional increase of the spiral fraction. Fasano et al. (2000) showed that the S0 to elliptical ratio is 5 times larger at z=0 than at z$\sim$0.5, while no further evolution of the S0 fraction in clusters at $z \sim 1$ has been found (Postman et al., 2005; Desai et al., 2007; Wilman et al., 2009). In contrast, the elliptical fraction appears to remain constant (Desai et al., 2007). This have been interpreted as evidence of the transformation of star forming spirals into passive S0s by the effect of the environment. Other galaxy properties also change with time. Butcher and Oemler (1978, 1984) found that fractions of blue galaxies are larger in the past, showing that cluster

galaxies evolve from blue to red (so-called the Butcher-Oemler effect, see also Dressler et al. 1994; Couch et al. 1994, 1998; Poggianti et al. 2006). The Butcher-Oemler effect may not be an exclusively cluster specific effect and cannot be used as an explanation of the different population inhabiting cluster and field environments. Indeed, it has also been shown that in the field the star formation rate increases with z as well (Lilly et al., 1995; Rowan-Robinson et al., 1997; Tresse and Maddox, 1998; Bell et al., 2005); galaxies were producing far more stars at intermediate redshift than they are doing at z=0 independently on environment.

Several other observational evidences of the role of the environment have been studied since the pioneering work of Dressler, concerning both tracers of the stellar component and the gas content. Important clues come for example from the study of the mass function (Baldry et al., 2006; Bamford et al., 2009; Bolzonella et al., 2010; Vulcani et al., 2012; von der Linden et al., 2010; Calvi et al., 2013), of the mass-size relation (Huertas-Company et al., 2013a,b; Weinmann et al., 2009; Poggianti et al., 2013; Cooper et al., 2012; Mei et al., 2012; Raichoor and Andreon, 2012; Delaye et al., 2012) and of the atomic gas content of galaxies (Haynes and Giovanelli, 1984; Giovanelli and Haynes, 1985; Gavazzi, 1989; Boselli, 1994; Solanes et al., 2001; Gavazzi et al., 2005; Chung et al., 2009; Cortese et al., 2011; Serra et al., 2012). .

All these observations prove that galaxies evolve moving from the field to cluster, changing their color from red to blue, and their morphology from late-type to early-type. A complete review of all these correlations is beyond the scope of this introduction, that aimed only at highlighting the importance of the external quenching in shaping the life of a galaxy.

1.3 The physical processes acting in clusters

Theoretical understanding of the possible mechanisms responsible for the observed environmental correlations is critical. While there are many possible explanations, below I describe the most plausible and well developed ideas, as summarized by Boselli and Gavazzi (2006) and De Lucia (2010). Three main classes of processes are considered: (1) interplay between galaxies and intra-cluster medium (2) galaxy-galaxy gravitational interaction. (3) gravitational interaction between a galaxy and the cluster potential.

1.3.1 Interplay between galaxies and intra-cluster medium

- **Ram pressure stripping** Galaxies traveling through a dense (10^{-3}–10^{-4}atoms/cm^3) and hot ($10^7 - 10^8$K) intra-cluster medium (ICM) suffer a strong ram-pressure stripping that sweeps cold gas out of the stellar disc (Gunn and Gott, 1972). Ram-pressure stripping can effectively remove the interstellar medium (ISM) if it overcomes the gravitational pressure anchoring the gas to the disk:

$$\rho_{ICM} V_{gal}^2 \geq 2\pi G \Sigma_{star} \Sigma_{gas} \tag{1.1}$$

  where ρ_{ICM} is the density of the ICM, V_{gal} the galaxy velocity inside the cluster, Σ_{star} is the stellar surface density and Σ_{gas} the gas surface density. The role of ram pressure gas stripping on early and late type galaxies has been extensively modeled by N-body and SPH simulations (e.g. Abadi et al., 1999; Quilis et al., 2000; Vollmer et al., 2001). Despite the intrinsic differences, these models established that ram pressure is sufficient to remove part of the ISM on time scales of the order of the cluster crossing time (a few 10^9 yr), when typical ICM density and cluster velocity dispersion are assumed. The efficiency of this process depends on several factors, such as the inclination of the galaxy disk with respect to trajectory (face-on interaction are more efficient) or the type of orbit, with radial orbits being more efficient due to the higher velocities. Moreover, ram pressure is expected to be more efficient at removing gas from low mass objects than from massive spirals. The interaction between the hot ICM and the cold ISM could also be responsible for an enhanced star formation activity in cluster galaxies, increasing cloud-cloud collision and cloud collapse (Evrard, 1991; Bekki and Couch, 2003).

  The models of Elmegreen and Efremov (1997) show that the star formation activity can increase up to a factor of 2 in high density, rich clusters on time scale of the order of 10^8 yr, while on longer time scales galaxies become quiescent. The old stellar component is unperturbed during ram pressure interaction.

  Extreme examples of gas stripping are the so-called "jellyfish galaxies" (e.g. Fumagalli et al., 2014; Fossati et al., 2016; Ebeling et al., 2014; Poggianti et al., 2016). Before leading to a complete gas ablation, ram pressure produces significant compression ahead of the galaxy and the possible formation of "tentacles" of material behind the main body of the galaxy (see figure 1.3). Jellyfish galaxies have been known in nearby clusters for many years. Usually, only a few galaxies per clus-

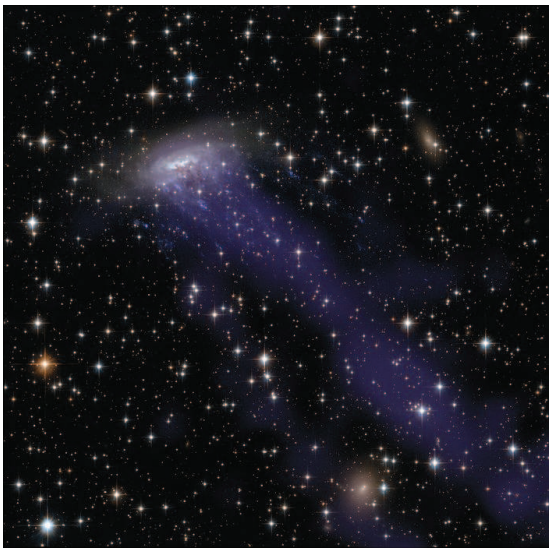

Figure 1.3: This image combines NASA/ESA Hubble Space Telescope observations with data from the Chandra X-ray Observatory. As well as the electric blue ram pressure stripping streaks seen emanating from ESO 137-001, a giant gas stream can be seen extending towards the bottom of the frame, only visible in the X-ray part of the spectrum. Credit: NASA, ESA, CXC.

ter have been studied, in a handful of clusters (e.g. Virgo, Coma, A1367, A3627, Shapley Kenney and Koopmann, 1999; Sun et al., 2006; Yoshida et al., 2008; Yagi et al., 2010; Smith et al., 2010; Hester et al., 2010; Merluzzi et al., 2013; Kenney et al., 2014). A few examples have been identified in clusters at z∼0.2-0.4 (Cortese et al., 2007; Owers et al., 2012; Ebeling et al., 2014; Rawle et al., 2014), and there is accumulating evidence for a correlation between the efficiency of the stripping phenomenon and the presence of shocks and strong gradients in the X-ray ICM (Owers et al., 2012; Vijayaraghavan and Ricker, 2013).

- **Strangulation or starvation** Current theories of galaxy formation suggest that when a galaxy is accreted onto a larger structure, the gas supply can no longer be replenished by cooling that is suppressed by the removal of the hot gas halo associated with the infalling galaxy (Larson et al., 1980; Font et al., 2008; McCarthy et al., 2008). This process, introduced by Larson et al. (1980) to explain the transformation from spirals to S0s, has been given the quite violent name of 'strangulation' (or 'starvation' or 'suffocation') and it represents one important element of semi-analytic models of galaxy formation. On time scales of a few Gyr, the star formation would exhaust the available gas, quenching further star formation activity. If this process

is combined with a relatively efficient supernovae feedback, galaxies that fall into a larger system consume their cold gas very rapidly, moving onto the red-sequence on quite short time-scales.

- **Thermal evaporation** Another mechanism to slow down the star formation rate of galaxies is thermal evaporation of the cold gas in disk galaxies via heat conduction from the surrounding hot ICM (Cowie et al., 2003). If the ICM temperature is high compared to the galaxy velocity dispersion, at the interface between the hot ICM and the cold ISM, the temperature of the ISM rises rapidly and the gas evaporates. The mass loss rate is proportional to the dimension of the galaxy and to the density and temperature of the ICM. A typical galaxy (of radius 15 kpc and $5 \cdot 10^9 M_\odot$ of atomic gas) can be completely stripped on time-scales of the order of some $10^7 - 10^8$ yr.

All of the above mechanisms need relatively high density hot intra-cluster gas, and thus are likely to happen in the central region of clusters. Although several authors indicated that these mechanisms cannot explain the suppression of star formation as far as several Mpc from the center of a cluster (Balogh et al., 1997; Kodama and Smail, 2001; Lewis et al., 2002), Fujita et al. (2003) pointed out that these mechanisms can happen in cluster sub-clump regions (small groups around a cluster). The above mechanisms mainly affect the star formation rate of a galaxy, compared with the following dynamical mechanisms which directly affect the (stellar) morphology of a galaxy.

1.3.2 Galaxy-galaxy gravitational interaction

- **Mergers** Galaxy mergers and more generally strong galaxy-galaxy interactions, act on all the constituents of the galaxy, including gas, stars, dust and dark matter, with an efficiency that depends on the gravitational bounding of the different systems. They are commonly viewed as a rarity in massive clusters: due to the high relative velocities of galaxies in the dense cluster cores, tidal interactions are more frequent but have a shorter duration than in the field (t $\sim 10^8$ yr). Simulations (Byrd et al., 1990) showed that the typical perturbation induced by a single high speed encounter among cluster galaxies is too small to significantly affect the star formation rate. Mergers are certainly more efficient in the infalling group environment and may therefore represent an important 'preprocessing' step in the evolution of cluster galaxies. Mergers drive gas towards the center of galaxies, where it can trigger a

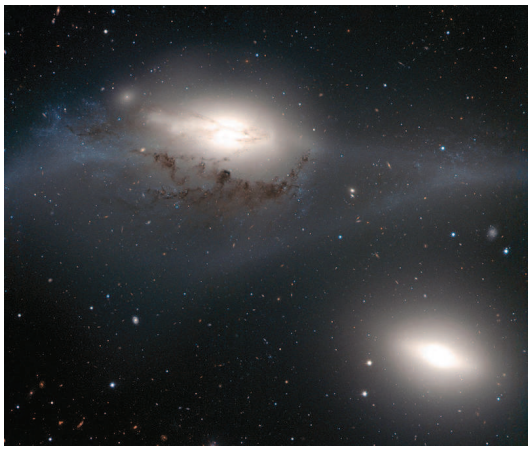

Figure 1.4: This striking image, taken with the FORS2 instrument on the Very Large Telescope, shows a beautiful yet peculiar pair of galaxies, NGC 4438 and NGC 4435, nicknamed The Eyes. The larger of these, at the top of the picture, NGC 4438, is thought to have once been a spiral galaxy that was strongly deformed by collisions in the relatively recent past. The two galaxies belong to the Virgo Cluster and are about 50 million light-years away. This photograph was produced by European Southern Observatory (ESO).

burst of star formation and fuel the central black hole whose feedback can heat the remaining gas and eventually quench star formation. Numerical simulations (see Mihos, 2004) have shown that close interactions can lead to a strong internal dynamical response driving the formation of spiral arms and, in some cases, of strong bar modes. Sufficiently close encounters can completely destroy the disc, leaving a remnant whose properties resemble those of an elliptical galaxy. Hence, late type galaxies can be transformed into early types with a central bulge component (Driver et al., 2006; Drory and Fisher, 2007). Typical examples of cluster galaxies which recently underwent a merging are NCG 4438 and NCG 4435, the eyes galaxies in Virgo (figure 1.4).

- **Harassment** Galaxy harassment (Moore et al., 1996; Boselli and Gavazzi, 2006) is a mechanism that strips a galaxy of part of its mass and drives morphological transformation as a consequence of the combined effect of multiple high-speed galaxy-galaxy close ($\sim$50 kpc) encounters and the interaction with the potential of the cluster as a whole. Harassment has the potential to change any internal property of a galaxy within a cluster, within several crossing times (multiple encounters needed). Anyway, numerical simulations indicate that the efficiency of this process is largely limited to low-luminosity hosts, due to their slowly rising rotation curves and their low-density

cores (Moore et al., 1999). Therefore harassment might have an important role in the formation of dwarf elliptical galaxies and S0s, while it is less able to explain the evolution of bright cluster galaxies.

1.3.3 Gravitational interaction between a galaxy and the cluster potential

Not only tidal interactions between galaxies can induce some relevant perturbation, but also tidal interactions between galaxies and the whole cluster potential, inducing gas inflow, bar formation, nuclear and perhaps disk star formation. Models by Fujita (1998); Valluri (1993) and Henriksen and Byrd (1996) showed that tidal compression of galactic gas via interaction with the cluster potential can accelerate molecular clouds of disk galaxies falling towards the core, increasing the star formation rate. The efficiency of this process naturally depends on the cluster to galaxy mass ratio, the distance of the galaxy from the center and the galaxy radius. The first galaxies to experience this kind of interaction are large galaxies passing within few hundreds of kpc of the cluster center. The net result could be a first increase of the nuclear activity of cluster galaxies and eventually a decrease of the total gas consumed through star formation events, while a complete removal of the gas due directly to the interaction in unlikely.

Obviously, other processes are needed to complete this scenario (e.g. AGN feedback, preprocessing), but the ones listed above are expected to produce the most important changes in the cluster galaxy population.

1.3.4 Comparison between the various processes

The identification of the perturbing mechanism responsible for quenching star formation activity of galaxies in high density regions has become one of the major challenges of modern extragalactic astronomy. Different mechanisms may have different effects and act on different time scales. Following Boselli and Gavazzi (2006); Boselli et al. (2016), I conclude this introduction comparing the various processes and their effect on the galaxy population in clusters, discussing the relative time scales necessary to affect star formation, their probability and efficiency as a function of clustercentric distance.

Indeed, the three classes of processes discussed in the previous sections have significantly different effect on gas and/or stellar component of a galaxy. Gravitational interactions can on one hand be at the origin of the nuclear activity, inducing nuclear gas infall,

but also contribute to heating up stellar disk and increase the bulge to disk ratio. These interactions are thus able to transform spirals into lenticulars even if, as already discussed, given the high velocity dispersion of clusters, the probability of galaxies to be perturbed by such processes is very low. The tidal interactions with the cluster potential are expected to be even less efficient in stripping the gas from the galaxy. On the contrary, interactions with the hot ICM can efficiently remove the outer gas and quench star formation, directly -ram pressure - or via strangulation but can hardly increase the bulge to disk ratio, as requested to explain the morphological segregation.

The time scales necessary to reduce the star formation activity obviously depend on the kind of interaction. Galaxy-galaxy interactions have typically long time scales, some Gyr (the relaxation time of the cluster). Galaxy harassment is more efficient due to the contribution of the potential well of the cluster, but still several 10^9 yr are needed. Time scales for ram pressure stripping instead are shorter, $\sim 10^9$ yr (one crossing time), and are even shorter for gas removal due to thermal evaporation (10^8 yr). Models (Bekki et al., 2002; McGee et al., 2014) indicate that the time scale for galaxy strangulation is of the order of some Gyr.

Note that, in this scenario, these timescales should be considered as lower limits since the star formation activity gradually decreases once the gas is removed, thus extending the time during which a galaxy can form stars.

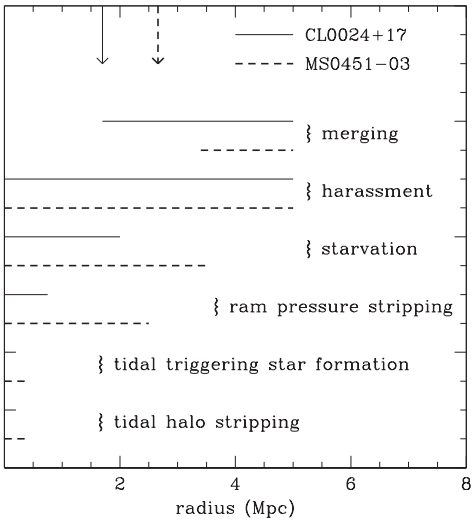

Figure 1.5: Schematic diagram showing the the radial range of action of the different environmental processes than can affect the star formation in galaxies. Solid and dashed lines correspond to the two clusters studied by Moran et al. (2007).

The identification of the clustercentric radius at which the various processes occurs is another critical point in this picture (see figure 1.5 for a schematic representation of the radial range of different processes.) The galaxy-ICM interactions are most efficient close to the cluster center, where the density and the temperature of the ICM, as well as the velocity of galaxies, reach their maxima. In these regions also the perturbation induced by the cluster potential are most efficient. Although the duration of the interactions might be shorter than in the cluster outskirts, the frequency of galaxy-galaxy interactions reaches the maximum in the densest central regions. Because of the combined action of galaxy-galaxy and galaxy-cluster gravitational interactions, galaxy harassment might also be effective at the cluster periphery. For similar reasons, starvation and preprocessing might be effective well outside the cluster core and even outside the virial radius.

1.4 This thesis

As discussed above, the motivation to simultaneously study galaxies and the structures that host them is strong. Observations show overwhelming evidence for a dependence of galaxy properties and evolution on environment. Surveys of the galaxy population in the local universe have found that the distribution of many galaxy properties, including color, morphology and star formation rate (SFR), are bimodal. Galaxy bimodality is likely a consequence of star formation in some galaxies being quenched, shut off. A wide variety of quenching mechanisms have been proposed to match the observed distributions of galaxy properties and among these the ones related to the environment seem to play a crucial role. The smoking gun proving that these are actually transforming galaxies -moving them form the blue cloud to the red sequence- would be the existence of a population of galaxies in transition with intermediate properties. The purpose for the work carried out in this thesis is precisely to investigate the galaxy population in groups and clusters to identify these transitional galaxies. In this framework, trying to understand how, where and when quenching occurs, I present an analysis of both galaxies and their hosting structures, from the most extreme tail of the distribution of halo masses, that is galaxy clusters, to groups and low-mass halos. To do so, I will exploit mainly two different data sets: the **WIde-field Nearby Galaxy-cluster Survey (WINGS)** (Fasano et al., 2006) together with its recent extension **OmegaWINGS** (Gullieuszik et al., 2015a; Moretti et al., 2017) and the **Padova-Millennium Galaxy and Group Catalogue (PM2GC)** (Calvi et al., 2011), which are described in detail in **Chapters 2 and 3**. In those Chapters I will mainly focus on my personal contribution to the projects.

Chapter 4 is dedicated to the presentation of the properties of the galaxy population, derived either from the spectroscopy or the photometry. Galaxy stellar masses, star formation histories and average stellar ages are derived by analyzing their integrated spectra by means of the spectrophotometric code SINOPSIS (Fritz et al. 2007, 2011, 2014). Morphologies are obtained from the MORPHOT tool (Fasano et al. 2012) applied to B and V images.

Chapters 5 and 6 include the main scientific results of my analysis. In Chapter 5 I study how the ongoing star formation rate (SFR) and the specific star formation rate (SSFR) vary with stellar mass and environment within the cluster sample. I present an analysis of the incidence of each population (star forming, passive and galaxies in transition) and a characterization of their star formation histories, colors and average ages. Trends of the different galaxy populations are described as a function of the clustercentric distance and of the cluster properties.

In **Chapter 6** I focus on galaxies that have recently quenched their star formation and investigate the processes that led to this suppression. I investigate the occurrence and properties of post starburst galaxies (PSB) in clusters and compare them to those of passive and star forming galaxies. Trends are investigated as a function of both clustercentric distance and global cluster properties. Including also the PM2GC data sample, I study the dependence of the PSB fraction on the halo mass of the system. At the end of the Chapter, I also compare the population of galaxies in transition to that of PSBs, to characterize the different channel that lead galaxies on the road to quenching.

Finally, the conclusions of this thesis are summarized in **Chapter 7**, where future work prospects are also described.

Throughout this thesis, I assume the Hubble constant $H_0 = 70\,\mathrm{km\,s^{-1}\,Mpc^{-1}}$, the total matter density $\Omega_m = 0.30$, the density of dark energy at the present day $\Omega_\Lambda = 0.70$. All magnitudes used in this thesis are Vega magnitudes, unless otherwise stated.

The work presented in this thesis was carried out in close collaboration with Dr. Bianca Maria Poggianti, my thesis Supervisor. Moreover, part of this thesis reflects the work that I have carried out during my visit to the KAVLI Institute for the Physics and Mathematics of the Universe (JP) in collaboration with Dr. Benedetta Vulcani; and during my visit to the Australian Astronomical Observatory (AUS), in collaboration with Dr. Warrick Couch.

2

The cluster samples

In this chapter I give an overview of the cluster samples I used in my analysis. I present the main characteristic of the WINGS survey and focus on the new OmegaWINGS data, describing the most important aspects of the photometric and spectroscopic observations. I describe the data analysis and redshift measurements that allowed to assign membership and estimate the velocity dispersion. I also derived the spectroscopic completeness corrections as a function of both magnitude and clustercentric distance. Finally, I present the complete galaxy catalog built from the match of the two cluster surveys.

The work I carried out on the OmegaWINGS data has been included in Gullieuszik et al. (2015a); Moretti et al. (2017).

2.1 WINGS

The WIde-field Nearby Galaxy-cluster Survey (WINGS) (Fasano et al., 2006; Moretti et al., 2014) is an all-sky ($|b| > 20°$) multi-wavelength survey of clusters of galaxies with $0.04 < z < 0.07$, X-ray selected from ROSAT All Sky Survey data (Ebeling et al., 1996, 1998, 2000). The goal of the project is the systematic study of the local cosmic variance of the cluster population and of the properties of cluster galaxies as a function of cluster properties and local environment. The cluster sample includes 77 clusters (41 in the Southern Hemisphere and 36 in the Northern Hemisphere), covering a wide range of velocity dispersion (σ_{cl} ∼500-1300 km/s) and X-ray luminosity ($L_X \sim 0.2 - 5 \times 10^{44}$ erg/s).

The core of the WINGS project is the optical (B, V) imaging survey (Varela et al., 2009). It provides photometric data for a huge sample of galaxies (∼550,000) covering a $34' \times 34'$ field of view, corresponding to at least about a clustercentric distance of $0.6R_{200}$, as well as structural and morphological information for a sub-sample (∼50,000) of relatively bright galaxies.

R_{200} is defined to be the radius delimiting a sphere with interior mean density 200 times the critical density and is used as an approximation for the cluster virial radius. The R_{200} values for the WINGS clusters are computed from the velocity dispersion using the formula from Poggianti et al. (2006):

$$R_{200} = 1.73 \left(\frac{\sigma_{cl}}{1000(km/s)} \right) \frac{1}{\sqrt{(\Omega_\Lambda + \Omega_M (1+z_{cl})^3)}} h^{-1} \qquad (Mpc) \qquad (2.1)$$

where σ and z are the cluster's velocity dispersion and median redshift, respectively.WINGS observations were taken with the Wide Field Camera mounted at the prime focus of the INT-2.5m telescope in La Palma (Canary Island, Spain) and with the Wide Field Imager mounted at the Cassegrain focus of the MPG/ESO 2.2 m telescope in La Silla (Chile) for the northern and southern clusters, respectively. The optical imaging has been complemented by a spectroscopic survey for a subsample of 48 clusters, obtained with the spectrographs WYFFOS@WHT and 2dF@AAT (Cava et al., 2009), by a near-infrared (J, K) survey for a subsample of 28 clusters obtained with WFCAM@UKIRT (Valentinuzzi et al., 2009), and by U broad-band (Omizzolo et al., 2014) and Hα narrow-band imaging for a subsample of 17 clusters, obtained with wide-field cameras at different telescopes (INT, LBT, Bok).

The spectroscopic selection was based on the (B, V) WINGS photometry. The aim of the target selection strategy was to maximize the chances of observing galaxies at the cluster redshift without biasing the cluster sample. Galaxies with total magnitude V≤20, a fiber aperture V≤ 21.5 and with a color within a 5 kpc aperture of $(B-V) \leq 1.4$ were selected. These selection limits were applied so as to reject background galaxies, much redder than the cluster red sequence and to avoid any bias in the colors of the selected galaxies. The exact cut in color was varied slightly from cluster to cluster in order to account for the redshift variation and to optimize the observational setup.

A spectroscopic completeness correction for each cluster was determined as the ratio of the number of spectra yielding a redshift to the total number of galaxies in the photometric catalog, as a function of both V-band magnitude and clustercentric distance.

These observations have yielded redshifts for 6137 galaxies, which have been used to

Cluster	z	N_z	σ_W kms^{-1}	$log(L_X)$ $10^{44}ergs^{-1}$	R_{200} Mpc
A0119	0.0444	158	866 ±55	44.51	2.10
A0151	0.0532	92	762 ±57	44.00	1.84
A0160	0.0438	40	784 ±111	43.58	1.90
A0193	0.0485	40	761 ±86	44.19	1.84
A0376	0.0476	66	949 ±90	44.14	2.29
A0500	0.0678	89	729 ±55	44.15	1.75
A0671	0.0507	20	956 ±130	43.95	2.31
A0754	0.0547	132	961 ±57	44.90	2.32
A0957x	0.0451	65	704 ±52	43.89	1.70
A0970	0.0591	117	771 ±42	44.18	1.85
A1069	0.0653	40	690 ±68	43.98	1.65
A1291	0.0509	27	413 ±65	43.64	1.0
A1631a	0.0461	126	717 ±38	43.86	1.73
A1644	0.0467	176	1051 ±58	44.55	2.54
A1795	0.0633	53	658 ±81	45.05	1.58
A1831	0.0634	17	444 ±68	44.28	1.07
A1983	0.0447	45	522 ±36	43.67	1.26
A1991	0.0584	35	625 ±73	44.13	1.50
A2107	0.0410	36	626 ±83	44.04	1.52
A2124	0.0666	30	596 ±58	44.13	1.43
A2169	0.0578	37	524 ±60	43.65	1.26
A2382	0.0641	152	835 ±58	43.96	2.00
A2399	0.0578	125	716 ±46	44.00	1.72
A2415	0.0575	98	698 ±52	44.23	1.68
A2457	0.0584	56	648 ±51	44.16	1.56
A2572a	0.0390	21	546 ±103	44.01	1.33
A2589	0.0419	35	830 ±98	44.27	2.01
A2593	0.0417	53	627 ±67	44.06	1.52
A2622	0.0610	38	732 ±68	44.03	1.76
A2626	0.0548	36	679 ±60	44.29	1.64
A3128	0.0600	207	900 ±38	44.33	2.16
A3158	0.0593	177	1090 ±53	44.73	2.62
A3266	0.0593	225	1389 ±66	44.79	3.34
A3376	0.0461	92	814 ±56	44.39	1.97
A3395	0.0500	125	755 ±49	44.45	1.82
A3490	0.0688	83	660 ±47	44.24	1.58
A3497	0.0680	82	724 ±48	44.16	1.73
A3556	0.0479	114	584 ±45	43.97	1.41
A3560	0.0489	118	717 ±43	44.12	1.73
A3809	0.0627	104	561 ±40	44.35	1.35
IIZW108	0.0483	27	549 ±42	44.34	1.33
MKW3s	0.0444	32	539 ±37	44.43	1.31
RX0058	0.0484	22	696 ±119	43.64	1.68
RX1022	0.0548	25	582 ±91	43.54	1.40
RX1740	0.0441	20	540 ±66	43.70	1.31
Z2844	0.0503	33	529 ±84	43.76	1.28
Z8338	0.0494	53	686 ±71	43.90	1.66
Z8852	0.0408	53	696 ±67	43.97	1.69

Table 2.1: WINGS-List of the 48 clusters in the spectroscopic sample, their mean redshift, number of member galaxies, velocity dispersion, X-ray luminosity and R_{200}.

derive cluster velocity dispersions and membership for the cluster galaxies. Table 2.1 lists the 48 WINGS clusters and the main properties derived from the available spectroscopy.

To maximize the scientific outcome of the data, the whole WINGS dataset and products have become publicly available using the Virtual Observatory tool (Moretti et al., 2014).

2.2 OmegaWINGS

The WINGS sample is unique, as none of the low-z surveys investigate a large sample of clusters and cluster galaxies in such detail. Its greatest limitation is that it covers only the cluster cores, missing the more external regions. Crucially, what is missing is coverage out to at least the virial radius and into the outer regions, to link clusters with the surrounding population and the field.

To go beyond this limitation, a new observational program has been performed, following the previous work, but with a field of view four times larger (1 deg^2)than that of WINGS: OmegaWINGS. The great asset of OmegaWINGS is not just to quadruple the WINGS area, but to cover the virial region and extend to the infall region out to $2.5R_{200}$. This allows to investigate the transition environment between the cluster cores, with their dense and hot intracluster medium, and the filaments and groups feeding the cluster.

The survey includes a photometric campaign for 48 clusters that were randomly selected from the WINGS targets observable from Paranal and a spectroscopic follow-up for a subsample of 33 clusters. The position of the target clusters observed by the OmegaWINGS survey are shown in Fig. 2.1.

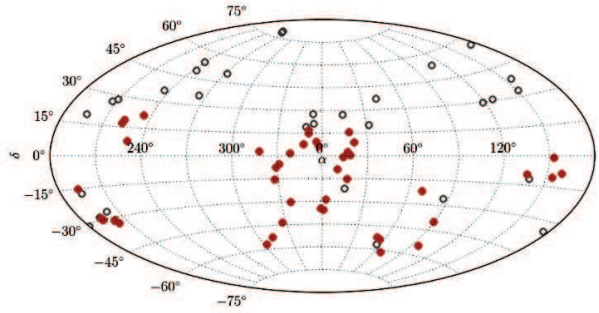

Figure 2.1: OmegaWINGS target clusters are shown as filled circles, all WINGS clusters are shown as open circles.

2.2.1 Photometric observations

The cluster sample has been imaged in the optical Johnson filters (B,V) with OmegaCam, the wide-field imager for the Cassegrain focus of the VLT Survey Telescope (VST). The VLT is a 2.6m wide field optical telescope equipped with OmegaCAM (Kuijken, 2011), a camera that samples the $\sim$1 deg^2 VST field of view with a mosaic of 32 4k$\times$2k CCDs. OmegaWINGS target clusters were randomly selected from the 57 WINGS clusters that can be observed from VST ($\delta < 20\,\mathrm{deg}$). Observations started in October 2011 and were concluded in September 2013.

All clusters were observed for 25 minutes in each band, with a median seeing of $1''$ in B and V band, and $1.3''$ and $1.2''$ in 80% of the B- and V-band images, respectively. The observations, data reduction and photometric catalogs are described in Gullieuszik et al. (2015). The data were reduced with a modified version of the ESO-MVM ALAMBIC reduction package (see Vandame 2004, Bouy et al., 2015), developing ad hoc cross-talk and gain harmonisation and CCD control procedures. Special care was taken for illumination correction, using OmegaCAM observations of standard stellar fields. The source extraction and measure of photometric and structural parameters was performed using SEXTRACTOR (Bertin and Arnouts, 1996).

Photometric calibration was made using WINGS stars as local standards fitting the difference between calibrated WINGS photometry (B_{STD}, V_{STD}) and instrumental OmegaCAM magnitudes (b, v) as a function of the $(\mathrm{B\text{-}V})_{STD}$ color through equations:

$$B_{STD} - b = a_B(B-V)_{STD} + b_B$$
$$V_{STD} - v = a_V(B-V)_{STD} + b_V$$

The results for all OmegaWINGS clusters are listed in Table A.1 of Gullieuszik et al. (2015a). The star-galaxy classification was done following the criteria used for the original WINGS survey, as described in Varela et al. (2009). Some of the faintest objects, with properties between those of stars and galaxies, have been classified as unknowns. The quality of the source classification mostly depends on the seeing conditions during the B- and V-band observations and decreases at increasing magnitudes: at a magnitude $V \sim 22.0$ mag the 50% of the sources in each cluster has been classified.

In order to perform a consistency check of both the photometric calibration and the star/galaxy classification, I compared OmegaCAM data with those provided by the WINGS photometric survey matching the two catalogs with a tolerance of $1.5''$. I determined the photometric differences $(V - V_{WINGS})$ and $(B - B_{WINGS})$ for the objects that

are classified as galaxies in both catalogs, and found that they do not depend on either magnitude or color with a 3-σ clipped standard deviation smaller than 0.1 mag. I also checked if there is a dependence of these differences on the position on the mosaic, finding no significant offset. An external check to test the relative accuracy of OmegaWINGS photometry across the OmegaCAM FoV and the spatial stability was also performed by comparing OmegaWINGS photometry with that of SDSS. In the V band the relative photometric accuracy is $\leq\sim$ 0.03 mag for all clusters. The dispersions of ΔB are 0.04-0.06 mags. The photometric zero-point in all calibrated catalogs has been found to also be constant across the whole mosaic and no residual systematic effects were detected.

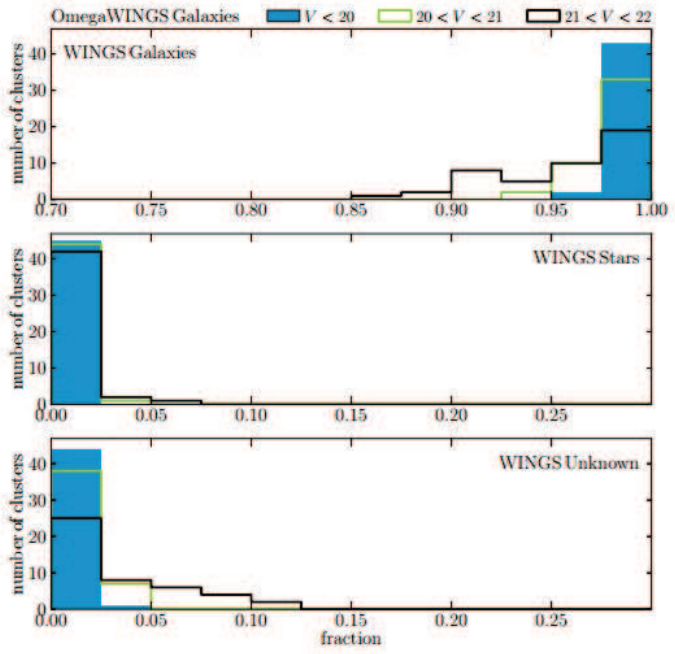

Figure 2.2: Fraction of objects classified as galaxies in OmegaWINGS that have been classified as galaxies (upper panel), stars (central panel), or with unknown classification (lower panel) in WINGS. In each panel, the solid blue, green, and black histograms show objects in three different magnitude bins, as indicated in the legend. Figure from Gullieuszik et al. (2015a).

I also compared the OmegaWINGS source classification to that of WINGS, in order to check its reliability. Figure 2.2 illustrates the results. For each cluster I divided the sources classified as galaxies in OmegaWINGS into three magnitude bins: $V < 20$ mag, $20 < V < 21$ mag, and $21 < V < 22$ mag and calculated how many OmegaWINGS

galaxies were classified as galaxy, star, and unknown in WINGS. In all but two clusters, the fraction of bright ($V < 20$ mag) OmegaWINGS galaxies classified as galaxies in WINGS is >97.5%. In more than 50% of the clusters the number of faint OmegaWINGS galaxies with unknown classification in WINGS is negligible; in all other clusters, this fraction is still lower than 10%. There are no OmegaWINGS galaxies with $V < 20$ mag classified as stars in WINGS in any cluster. The fraction of galaxies misclassified as stars in WINGS is also negligible (<5%) for fainter galaxies ($20 < V < 22$ mag). This analysis proves that the OmegaWINGS galaxy classification is highly reliable for objects with $V < 20$ mag. This is the magnitude range used to select the targets for the spectroscopic follow-up survey (see section 2.2.2).

The astrometric accuracy of the catalogs was tested against the 2MASS and SDSS DR8 (when available) stellar catalogs. The distributions of the differences in α and δ coordinates have always negligible mean values and typical dispersions of $0.2''$ (2MASS) and $0.07''$ (SDSS).

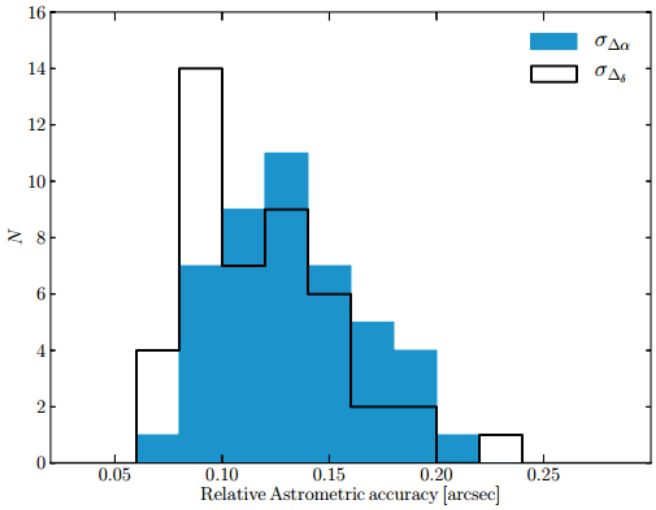

Figure 2.3: Dispersion of the distributions of sky-coordinate differences between OmegaWINGS and WINGS positions of all stars in each 46 OmegaWINGS fields. Only stars brighter than $V = 20$were used. Figure from Gullieuszik et al. (2015a).

As an additional test of the astrometric calibration accuracy, I compared the sky-coordinates of all stars in OmegaWINGS and WINGS catalogs. The dispersion of the $\Delta\alpha$ and $\Delta\delta$ distributions is a robust indicator of the accuracy of the astrometric calibration,

as WINGS was calibrated independently. The results are presented in fig. 2.3 and confirm that the internal astrometry calibration is accurate at a level always better than 0.2″. The mean values of the distributions are 0.1″ for both right ascension and declination.

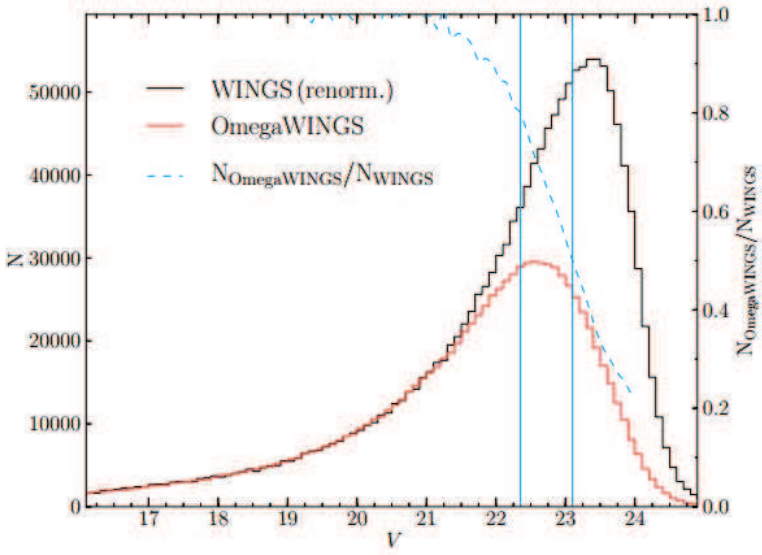

Figure 2.4: V-band magnitude distribution of all objects in the OmegaWINGS and WINGS database. WINGS magnitude distribution was re-normalised to match the total number of sources with $16 < V < 21$ *mag. The ratio of OmegaWINGS to WINGS magnitude distributions is shown as a dotted line; the corresponding scale is shown on the right-hand axis. The vertical lines are traced at the magnitude corresponding to a ratio of 0.5 and 0.8 (50% and 80% completeness level). Figure from Gullieuszik et al. (2015a).*

The OmegaWINGS photometric completeness was estimated as the ratio of OmegaWINGS to WINGS magnitude distributions (see Fig. 2.4): the 50% completeness level is reached at V = 23.1 mag, the 80% level at V = 22.4 mag. This result is based on the assumption that WINGS photometry is complete at least up to V $\sim$ 23 mag. I therefore performed an additional test by fitting an exponential relation to the bright tail of the OmegaWINGS histogram in Fig. 2.4. The completeness factor was obtained as the ratio of the observed magnitude distribution to the best-fit exponential model. Following this approach, 50% and 80% completeness are found at V = 23.3 and 22.7 mag, respectively, confirming the previous results within reasonable uncertainties.

Sextractor photometric catalogs were produced and are released by Gullieuszik et al. (2015a) at CDS (Gullieuszik et al., 2015b). Catalogs and reduced images will also be part of the next release version of the WINGS database. The B- and V-band OmegaCAM

images have provided the targets for the following spectroscopic follow-up.

2.2.2 Spectroscopic data: observations and data reduction

A spectroscopic follow-up for a subsample of 33 clusters imaged by OmegaCAM has been carried out at the 3.9m Anglo Australian Telescope (AAT) using the AAOmega spectrograph (Smith et al.2004; Sharp et al. 2006). The main strategy for selecting spectroscopic targets was similar to the one applied to the WINGS survey and has been made on the basis of magnitude and color. First of all, objects classified as galaxies and with a total magnitude brighter than V=20 mag were selected; the sources were subsequently divided into bright and faint according to their V aperture magnitude inside the fiber diameter ($2.16''$). Bright sources have $V_{fib} \leq 20.5$ mag, faint sources have $20.5 \leq V_{fib} \leq 21.5$. For (almost) each cluster there are two configurations, hereafter bright and faint, with integration times of 1 and 2 hours respectively. Some observations have been carried out under non optimal weather conditions and the total exposure time was increased to reach a sufficient signal-to-noise ratio for all targets. A color cut approximately at $(B-V) = 1.20$ mag was also considered to minimize the contamination from background galaxies and exclude extremely red sources. The exact cut in color was varied slightly from cluster to cluster in order to account for the redshift variation and to optimize the observational setup. The further selection was random, with the only priority assigned according to the location of the targets with respect to the original WINGS regions: the targets located outside the original WINGS analyzed regions had the highest priority, followed by the targets located inside the WINGS images but without a spectrum (intermediate priority), and by the targets located inside the WINGS region and with a previously determined redshift (lowest priority).

The spectroscopic observations were obtained over the course of 5 different runs, started in August 2013 and completed in September 2015, using the AAOmega dual-beam spectrograph at AAT. This instrument is designed to allow the acquisition of up to 392 simultaneous spectra of objects anywhere within a two degree field on the sky. It consists of a wide-field corrector, an atmospheric dispersion compensator and a robot gantry which positions optical fibers on the sky. Science fibers are arranged into a pseudo-slit which feeds into a single collimator and then separates into the blue and red arms of the system via a dichroic beam splitter.

AAOmega can be configured, using different grisms, to observe the entire optical spectrum over the wavelength range 3800-9000 Å, with a small overlap between the red and

blue arms. In particular the 580V and the 385R grisms were used, which have a resolution of 1300 (FWHM=3.5-6 Å).

For all configurations, 25 sky fibers were allocated, and 6 for the guide stars, adding $\sim$ 360 possible science fibers per observing configuration. The position of the sky fibers were defined by visually inspecting OmegaWINGS images and looking for 25 regions with no sources uniformly distributed over the entire field of view. Science targets have then been positioned on the field by using the configuration software, which takes into account the priorities described in the previous section using a Simulated Annealing (SA) algorithm. A tumbling mechanism with two field plates allows the next field to be configured while the current field is being observed.

Table 2.2 contains the median seeing of each run, along with the number of nights, the number of observed targets and the total success rate (i.e. the rate of successful redshift measurements over the total of assigned fibers in the run). For the detailed observing log of each configuration refer to Moretti et al. (2017) where the seeing and the percentage of observed galaxies with reliable redshift measurements are also listed.

Science exposures lasted 20 min, so the one hour exposure for the bright configurations consisted of 3×20 minutes single ones, and the faint configurations were observed for 6×20 minutes. Prior to each sequence, an arc frame and a fiber flat were taken. The arc frame is used to calibrate the wavelength scale of the spectra and the fiber flats are used to determine the locations of the spectra on the CCD. Bias frames and dark frames were taken daily. The data reduction was performed using the dedicated pipeline 2dfdr, which properly handles science and calibration (flat–field and arc) exposures, producing wavelength calibrated spectra for each arm. After having produced the single blue and red arm corrected spectra, the procedure spliced them together in order to get a single spectrum covering the entire observed spectral range. The sky subtraction was performed using the dedicated algorithm by Sharp and Parkinson (2010), that implements the Principal Component Analysis to derive an optimal sky estimate starting from dedicated sky exposures.

The signal to noise of AAOmega spectra averaged over the entire spectrum goes from $\approx$ 11-22 (median and mean, respectively) for the bright configurations and $\approx$ 6-6 for the faint configurations. Fig. 2.5 shows the distributions of the median signal to noise (top panel), and the 68% confidence limit for the observed configurations (lower panel). Left plot refers to the bright configurations, right plot to the faint configurations. The total number of observed spectra is 18995.

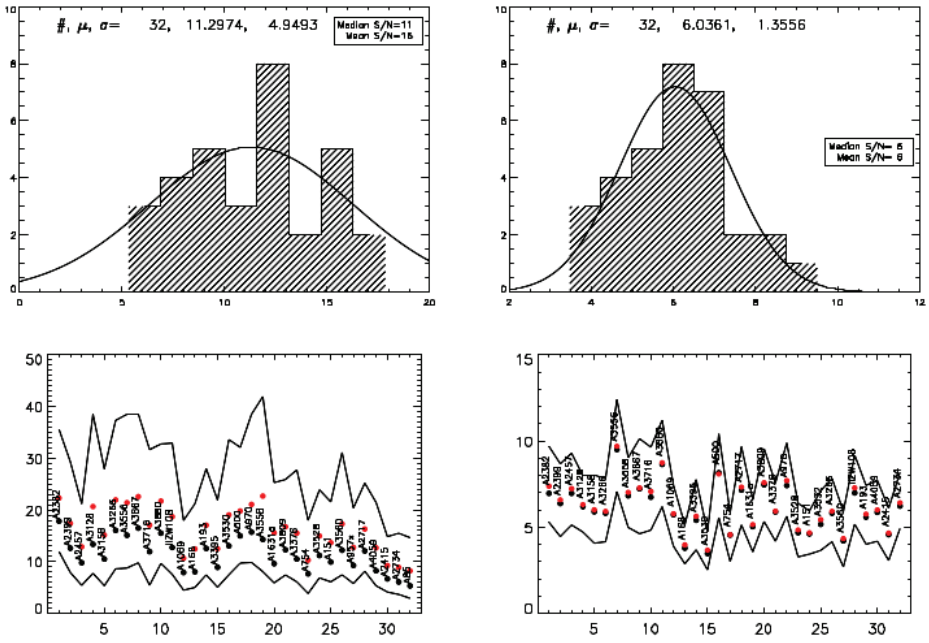

Figure 2.5: Overall signal to noise distributions for the bright (left) and faint (right) configurations. Top panels show the distributions of the measured signal–to–noise in the observed configurations (32 are bright and 32 are faint with superimposed the gaussian fit to the distributions. The numbers in the inset indicate the mean and median signal to noise. The lower panels show for each configuration the mean (red) and median (black) signal–to-noise together with the 68% confidence limits. Figure from Moretti et al. (2017)

Run	nights	targets	success rate
August 2013	6	10+2	97.2
December 2013	3	5+3	89.0
July 2014	2	2+2	97.4
January 2015	5	4+4	92.8
September 2015	2	3+5	95.6

Table 2.2: Number of observing nights, number of observed targets with both faint and bright configurations plus the number of configurations not completed, and average success rate of redshifts measurements for each observational run.

2.2.3 Redshifts

Galaxy redshifts were measured on the spliced spectra, i.e. those extending over the entire wavelength range, in order to have information both from the blue part of the spectra, where most optical absorption lines are present at the sample redshifts, and from the

red part of the spectra, where the Hα+NII region is located. The night sky residuals, present in specific regions of the spectra, have been replaced by interpolated values before measuring the redshifts.

A semi-automatic procedure based on the IRAF's Radial Velocity Package RVSAO (Kurtz and Mink, 1998) has been applied to these cleaned spectra. Two independent redshift estimates were obtained from the two main tasks in the package: XCSAO and EMSAO. XCSAO, using mainly absorption lines, cross-correlates the Fourier transform of an object's spectrum against the transforms of a set of template spectra with known spectral shifts to obtain a velocity and error. EMSAO finds emission lines in a spectrum and computes the observed centers, getting individual shifts and errors for each line as well as a single velocity combining all of the lines. The redshifts are measured as radial velocities in units of cz and are subsequently converted to heliocentric values. I, along with other 4 people, inspected a subset of the spectra by eye to verify the redshift measurements and to ensure that the best matching template was chosen. The results were averaged if the two values from the two packages were compatible, while emission line redshifts were preferred in case of different determinations or if the absorption line redshift could not be measured. Spectra without emission lines were assigned a redshift on the basis of the cross-correlation technique only. Errors on the redshifts (see Kurtz and Mink, 1998) are the errors of the combined measurements of both absorption and emission features if the two have been averaged together to get the redshift, and are single errors on the measurements that do not have emission lines, or where the absorption line cross-correlation is uncertain. This procedure allowed to assign a redshift determination to 17985 of the 18995 AAOmega observed spectra in 33 clusters, with an average success rate of $\sim 95\%$.

With these observations the number of WINGS clusters with spectroscopic follow-up was greatly enlarged, adding the clusters A85, A168, A2717, A2734, A3530, A3532, A3528, A3558, A3667, A3716, A3880 and A4059 and new redshifts to 21 clusters within the old WINGS spectroscopic survey. To build the final catalogs and assign memberships, I matched the fields covered by both the WINGS and the OmegaWINGS observations and identified common objects based on a positional match within 3.6 arcsec (I checked that this distance value allowed to recover common objects -those with the lower priorities, see section 2.2.2- without including close-by galaxies). Given the selection criteria and the priorities described before, common objects account only for approximately the 10% of the galaxies in each field. When the difference between the two redshift measures was greater than the given tolerance of 0.002, the OmegaWINGS value was chosen as the final redshift.

To further complete the redshift sample, I searched for objects in different literature catalogs (SDSS, NED, SIMBAD, NOAO and DR7) that are present in the parent photometric catalog used to select the spectroscopic targets and added them to the final catalog.

Figures 2.6 summarize the results of this process for the 33 OmegaWINGS clusters: RA DEC position of the spectroscopic targets in WINGS (blue crosses), OmegaWINGS (green squares), common objects (red triangles) and literature targets (black stars) are shown.

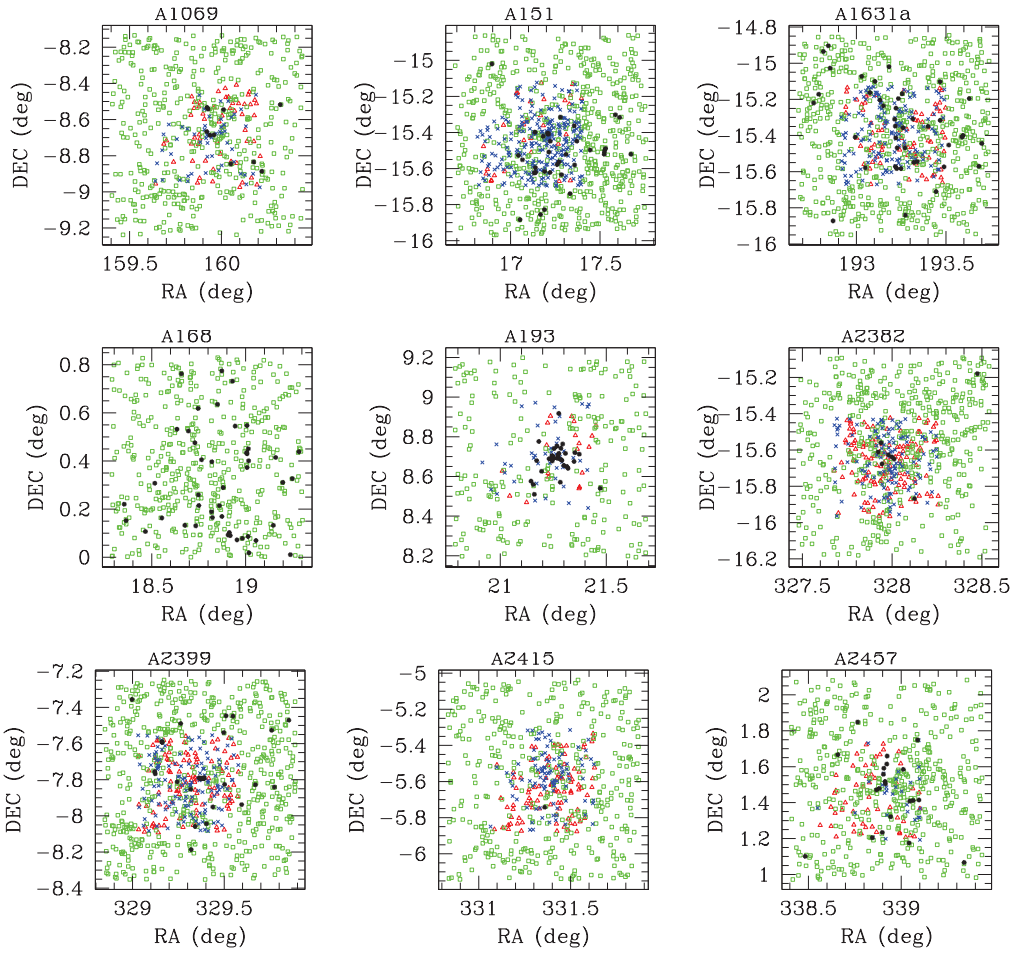

Figure 2.6: RA DEC position of spectroscopic targets in WINGS only (blue crosses) and AAOmega only (green squares). Red triangles mark the common objects while black stars are the targets from the literature.

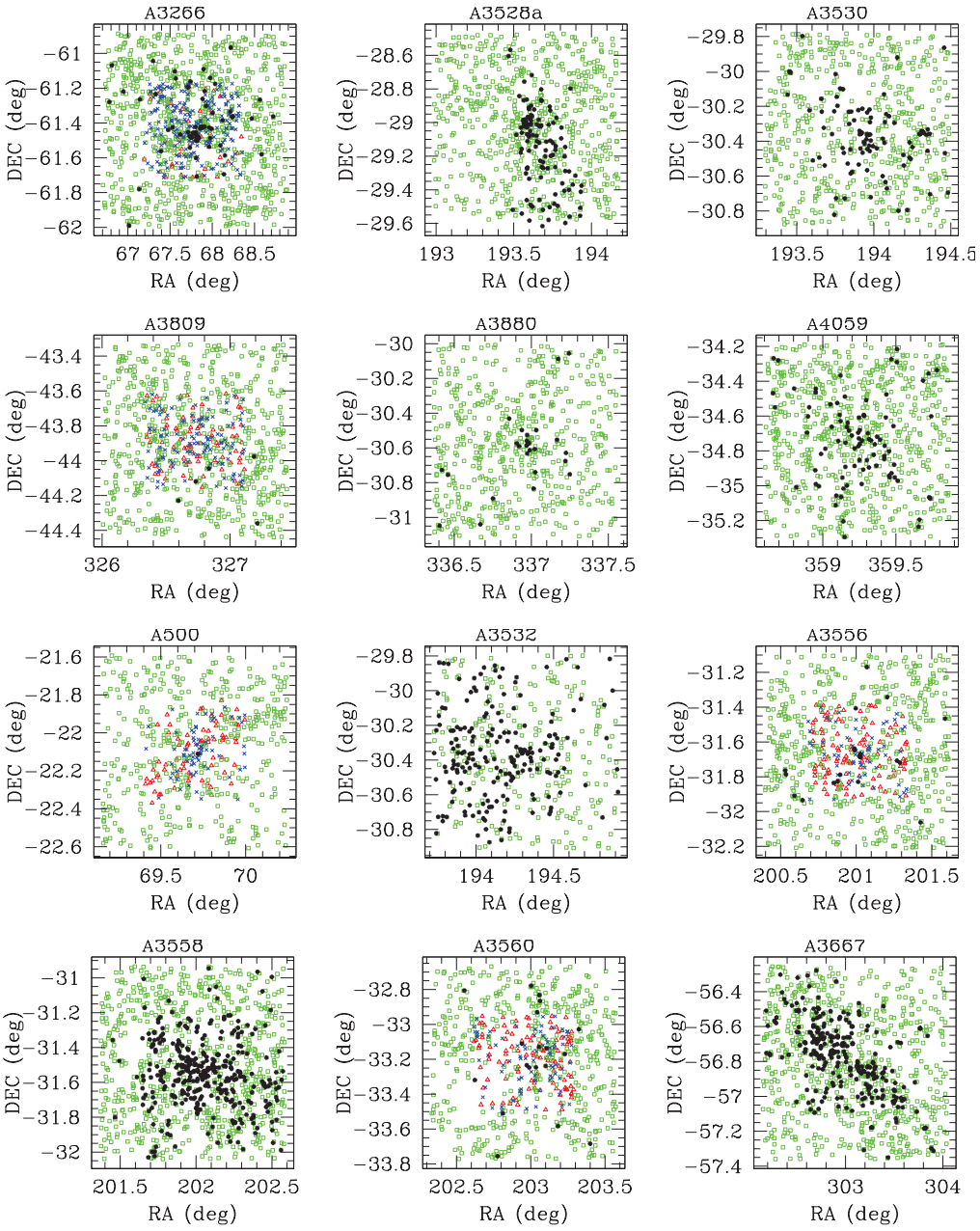

Fig.2.6 continued.

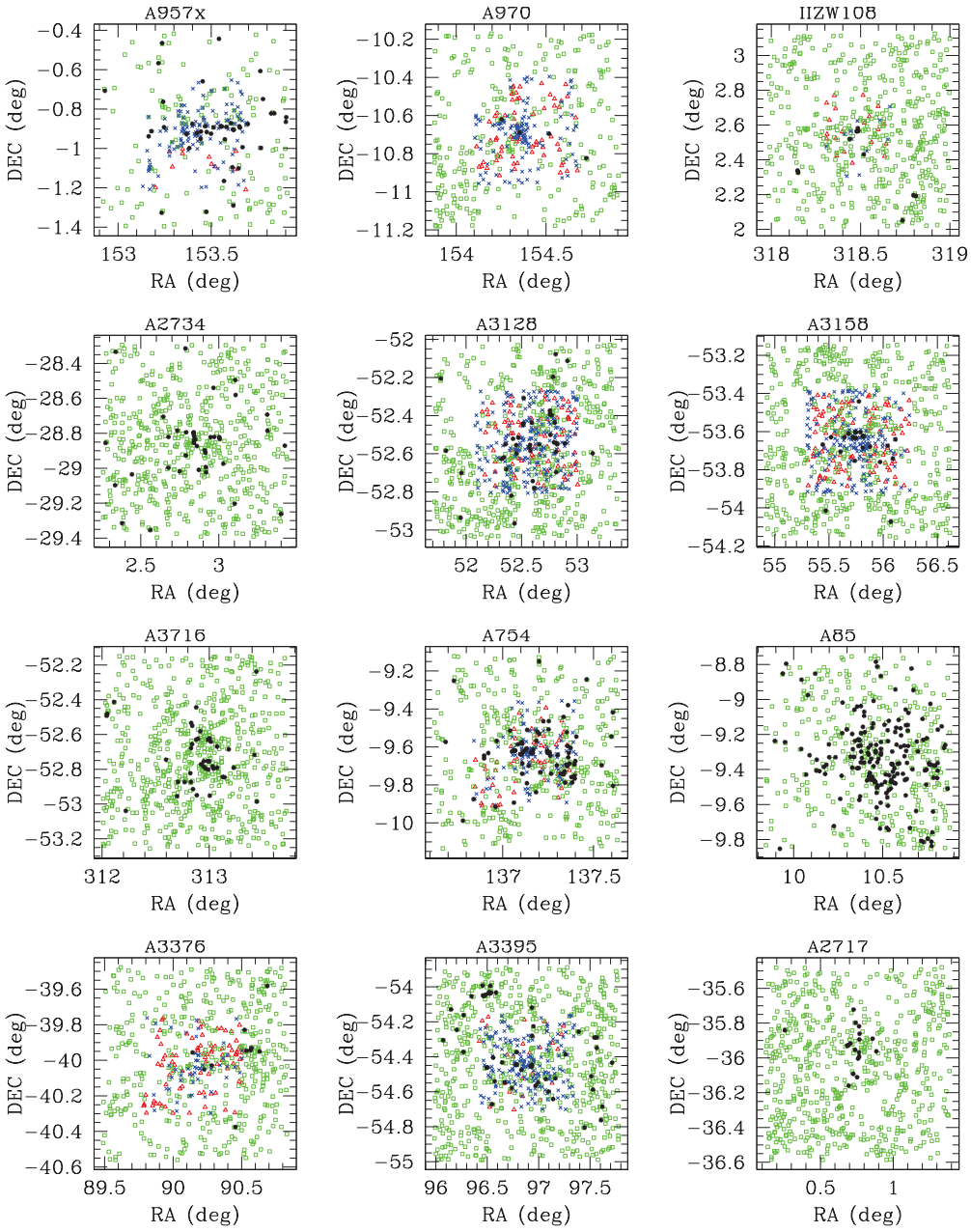

Fig.2.6 continued.

2.2.4 Velocity dispersion and membership

Due to projection effects, any cluster kinematic data sample inevitably contains galaxies that are not bound to the cluster and therefore are not good tracers of its gravitational potential. This issue is even more problematic for the OmegaWINGS observations, given the very large field of view of the observations, that may be heavily contaminated by objects in the external regions. It is very important to determine as accurately as possible which galaxies belong to the clusters and which ones have to be considered as non members.

In order to give a reliable estimate of these parameters, I therefore adopted an iterative procedure, as in Cava et al. (2009), following an improved $\pm 3\sigma$ clipping algorithm (Yahil and Vidal, 1977), which includes the weighted gap method (e.g. Girardi et al., 1993) and interactively removes galaxies outside R_{200}. The procedure starts by eliminating candidates whose velocities, given by $v = cz$, are outside a given fixed range (in our case those with $|v - v_{cl}| > 0.015$, corresponding to ~ 4000 km/s), where a first estimate of v_{cl} is obtained looking at the mean cluster redshifts in the WINGS catalog. I proceeded as follows. Starting from the galaxies in this redshift range and in the whole field of view, I applied the weighted gap method. Gaps are defined as $g_i = v_i + 1 - v_i$ for the sorted velocities and weights as $w_i = i(N-i)$ for $i = 1, .., N-1$ for N galaxies. The weighted gap is defined as $\frac{\sqrt{g \cdot w}}{MM(\sqrt{g \cdot w})}$ where MM is defined to be the mean of the central 50% of the data set. The presence of gaps greater than 3 suggests the possibility of substructures that can alter the velocity dispersion determination. I visually inspected the velocity histograms to decide whether or not the gap found highlights the presence of a substructure and, if this is the case, galaxies to one side of the weighted gap were removed.

After the redefinition of the main structures, I computed the mean redshift z_{cl} and the rest frame velocity dispersion σ_{cl} for each cluster using the biweight robust location and scale estimators (based on the ROSTAT routine, Beers et al., 1990) and an iterative 3σ clipping until convergence in σ is reached. I used the projected spatial distribution to define a further radius-dependent cut, meaning that at each iteration I determined R_{200} and considered only galaxies within this radius to compute the velocity dispersion.

The final values (listed in table 2.3) are then used to select member galaxies as those having $|z_i - z_{cl}| < 3\sigma_{cl}$. No selection has been applied on the distance of member galaxies from the cluster center, here defined as the brightest cluster galaxy (BCG).

Our estimates of cluster redshifts and velocity dispersions are in good agreement with those given by Cava et al. (2009), except for A3395, where I measured a much larger velocity dispersion (1206 km/s instead of 755 km/s). This could be due to the larger extent

of the OmegaWINGS fields, that reach in this case R_{200}, while the WINGS spectroscopic survey just reached $\sim 0.5R_{200}$.

The redshifts and velocity dispersions that are given in Tab.2.3 were derived by using only redshifts from the OmegaWINGS and WINGS surveys, therefore excluding additional redshifts present in the literature. The errors quoted were obtained using the classical jackknife technique (Efron, 1982). In four of our clusters the procedure suggests the

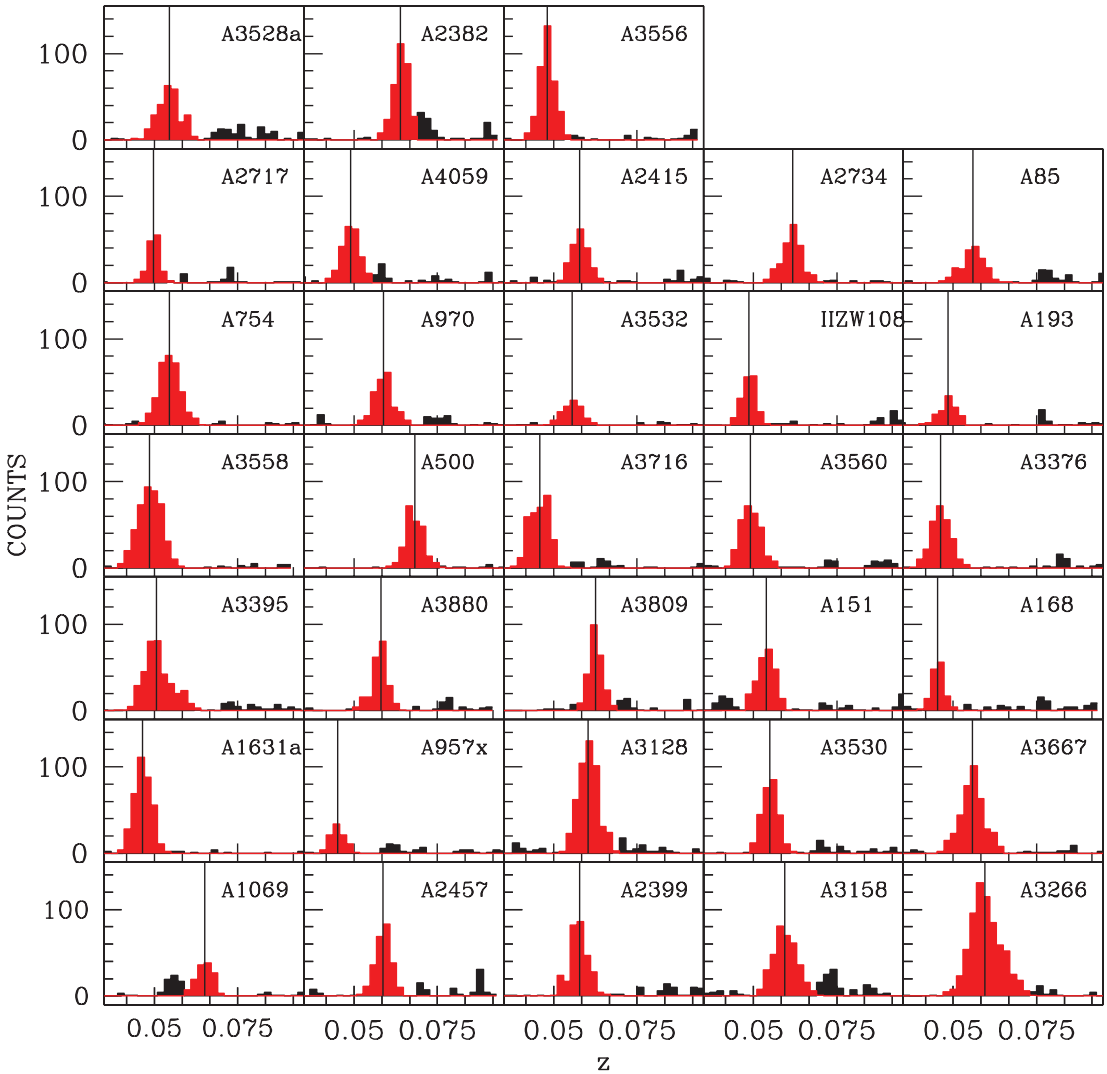

Figure 2.7: Histograms of the data sample in the redshift range $0.03 \leq z \leq 0.09$ *where fore/background objects are visible (black histograms). In red are histograms for cluster members defined using a* 3σ *cut.*

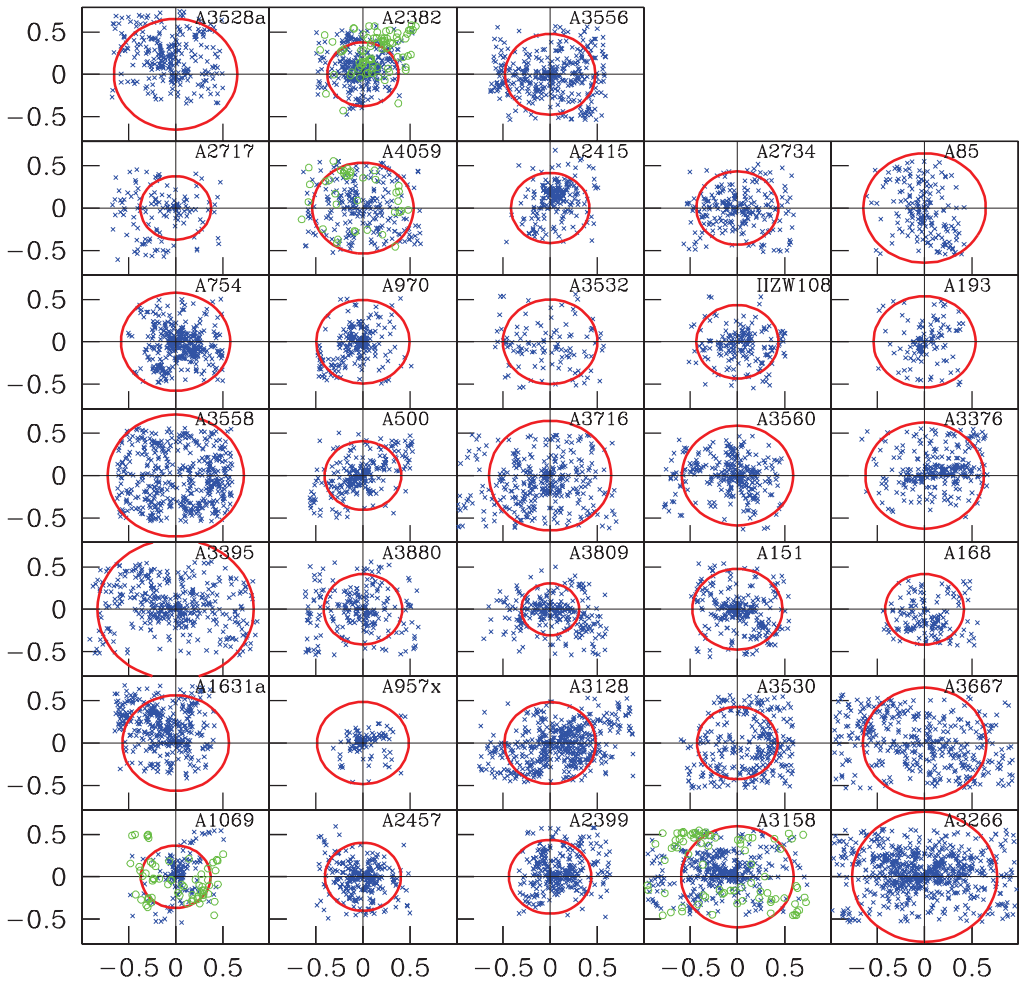

Figure 2.8: RA DEC position of member galaxies. The circle of radius R_{200} is plotted in red, centered on the old WINGS center coordinates. In green RA DEC position of galaxies in the substructure, when detected.

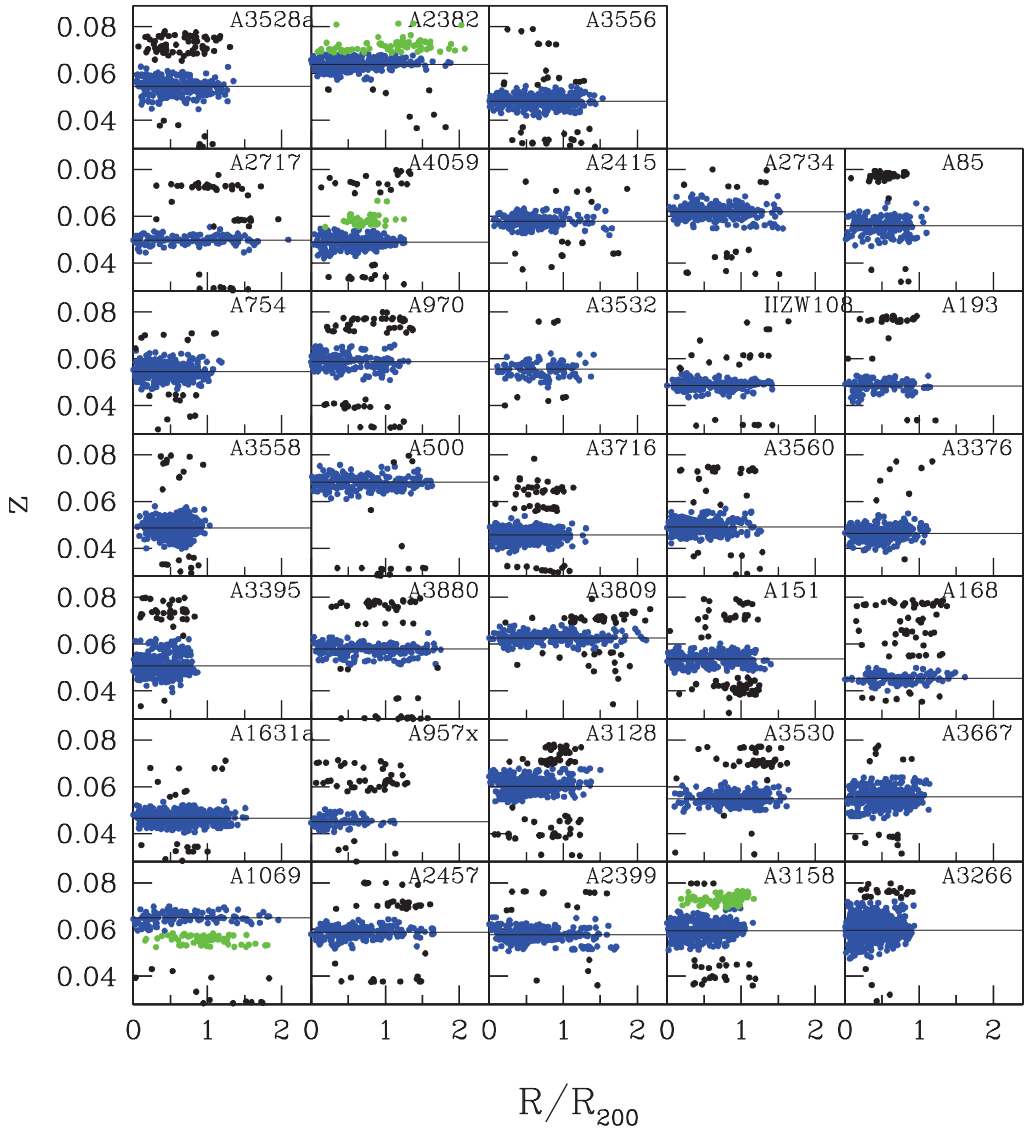

Figure 2.9: Redshift diagrams of the data sample in the range $0.03 \leq z \leq 0.09$ *as a function of the normalized radius* (R/R_{200}). *Blue points indicate cluster members, green points possible substructures, the horizontal line is the mean cluster redshift. Black points are back/foreground galaxies.*

presence of a secondary structure, with a slightly different velocity (shown in Tab.2.3, last column). More details will be given in Biviano et al. (in preparation) where the presence of substructures will be analyzed with a dedicated algorithm. Table 2.3 lists the number of targets observed with AAOmega with a reliable redshift determination (col. 2), the number of new cluster members (col. 3), the total number of members (including the ones present only in the WINGS spectroscopic catalog) that contributed to the velocity dispersion determination (col. 4), the velocity dispersion and its error in col. 5. The R_{200} (in Mpc, col. 6) and M_{200} (10^{13} $M_\odot$, col. 7) were derived following Poggianti et al. (2006) using equation 2.1 and

$$M_{200} = 1.2 \cdot 10^5 \left(\frac{\sigma_{cl}}{1000(kms^{-1})} \right)^3 \frac{1}{\sqrt{(\Omega_\Lambda + \Omega_M (1+z_{cl})^3)}} h^{-1} \qquad (10^{10} M_\odot) \qquad (2.2)$$

using the cluster velocity dispersion σ_{cl} and the cluster redshift z_{cl}.

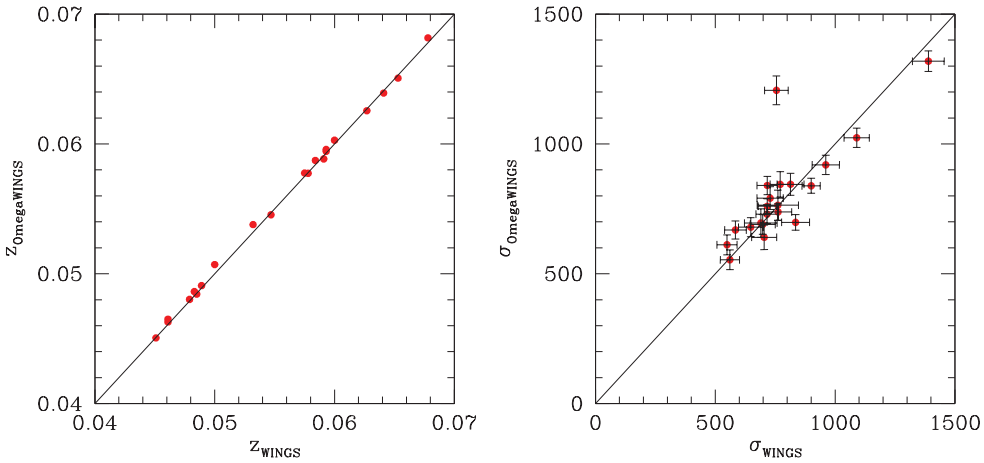

Figure 2.10: Comparison between WINGS and OmegaWINGS cluster redshifts (left panel) and velocity dispersions (right panel).

2.2.5 Completeness

It is very important to know the completeness level of the spectroscopic observations as this is a factor that must be accounted for anytime one wants to use the spectroscopic sample to study magnitude-dependent properties. I calculated the spectroscopic completeness as a function of both magnitude and radial distance (to account for the crowding of the fibers spectroscope near the clusters center) based on the selection made from the available

Cluster	N_z	$N_{memb,OW}$	$N_{memb,tot}$	z_{cl}	$\sigma \pm \sigma_{err}$	R_{200}	M_{200}	z_{gap}
A1069	496	107	130	0.0651	695±54	1.7	55.9	0.058
A151	623	165	248	0.0538	738±32	1.8	52.4	0.0
A1631a	673	288	369	0.0465	760±28	1.8	64.8	0.0
A168	459	141	141	0.0453	546±38	1.3	178.9	0.0
A193	239	72	101	0.0484	764±57	1.8	382.4	0.0
A2382	594	271	322	0.0639	698±30	1.7	73.7	0.069
A2399	678	234	291	0.0577	729±35	1.7	44.1	0.0
A2415	482	144	194	0.0578	690±37	1.7	98.4	0.0
A2457	535	232	249	0.0587	679±36	1.6	51.3	0.0
A2717	610	135	135	0.0498	544±46	1.3	172.4	0.0
A2734	556	220	220	0.0618	780±48	1.9	294.0	0.0
A3128	584	333	480	0.0603	838±28	2.0	54.4	0.0
A3158	621	243	357	0.0594	102±37	2.5	28.3	0.069
A3266	877	479	678	0.0596	131±39	3.2	67.2	0.0
A3376	519	229	263	0.0463	844±42	2.0	27.4	0.0
A3395	652	244	369	0.0507	120±55	2.9	169.3	0.0
A3528a	627	262	262	0.0545	101±46	2.4	82.3	0.0
A3530	530	275	275	0.0548	674±38	1.6	102.6	0.0
A3532	250	107	107	0.0555	805±61	1.9	99.4	0.0
A3556	625	328	359	0.048	668±34	1.6	101.1	0.0
A3558	706	442	442	0.0486	100±33	2.4	129.9	0.0
A3560	580	244	283	0.0491	840±35	2.0	100.4	0.0
A3667	687	386	386	0.0558	101±42	2.4	87.2	0.0
A3716	609	327	327	0.0457	848±26	2.0	38.3	0.0
A3809	695	189	244	0.0626	553±38	1.3	74.8	0.0
A3880	543	216	216	0.058	688±56	1.7	27.0	0.0
A4059	686	229	229	0.049	752±38	1.8	71.4	0.055
A500	478	187	227	0.0682	791±43	1.9	54.9	0.0
A754	423	250	338	0.0545	919±36	2.2	79.2	0.0
A85	359	172	172	0.0559	982±55	2.4	158.4	0.0
A957x	154	48	92	0.0451	640±47	1.5	175.6	0.0
A970	331	136	214	0.0588	844±49	2.0	56.6	0.0
IIZW108	504	162	171	0.0486	611±38	1.5	50.1	0.0

Table 2.3: OmegaWINGS main results: column (2), (3) and (4) give the number of redshifts derived from OmegaWINGS spectroscopy, the number of OmegaWINGS members and the total number of members (including WINGS results), respectively. Column (5) gives the estimated mean cluster redshift, while column (6) gives the velocity dispersion and its error, as derived from the number of members listed in column (4). Columns (8) and (9) are the R_{200} (in Mpc) and M_{200} (in units of $10^{13} M_{\odot}$) derived from eq. 2.1 and 2.2 respectively. The last column lists the secondary redshift.

optical B and V photometry. Following the selection criteria described above, the exact cut in the color-magnitude diagram varied slightly from cluster to cluster. Moreover, given that the spectroscopic catalogs of 21 out of the 33 clusters include the WINGS redshift measurements, I had to join the WINGS and OmegaWINGS photometric catalogs used to select the spectroscopic targets. To be consistent, I considered for the whole cluster sample the complete photometric catalog.

The magnitude completeness is defined as:

$$C(m) = \frac{N_z}{N_{ph}}(m) \tag{2.3}$$

where N_z is the number of galaxies with measured redshifts and N_{ph} is the number of galaxies in the parent photometric catalog, taking into account the cuts in color and magnitude, for each given magnitude bin of width 0.5 mag.

Recall that the candidates have to obey to the following conditions:
1. $V_{tot} \leq 20$
2. $20.5 \leq V_{fib} < 21.5$ for the faint configuration or $V_{fib} < 20.5$ for the bright configuration
3. $(B\text{-}V)_{tot}$ bluer than the one defined by the cluster red sequence

where V_{fib} is the V-band magnitude inside the $2.''16$ aperture, V_{tot} is the total V magnitude and $(B\text{-}V)_{tot}$ is the color computed from the total B and V magnitudes. The radial completeness function is defined, analogously as the ratio between the number of targets with redshift with respect to the number of candidates in the parent photometric catalog in the same radial bin:

$$C(r) = \frac{N_z}{N_{ph}}(r) \tag{2.4}$$

where radial bins have been chosen to have the same area. Radial bins have been defined in terms of R/R_{200}, and the subtended area is $\pi/4$. For the most spatially extended observations/lowest R_{200} clusters we were able to define up to 13 bins. Fig.2.12 shows the single clusters radial completeness, where the external bins with lower statistics (less than 20 members) have been outlined with larger dots. The total weight for each galaxy in the catalog is defined as:

$$W(m,r)_i = \frac{1}{C(m)_i \cdot C(r)_i} \tag{2.5}$$

In the clusters having also the WINGS redshift measurements, the net result is a pretty flat behavior of both the magnitude and radial completeness functions. For the remaining sample the central area is not properly covered by the data and the radial completeness

function decreases.

Finally, I computed the two completeness functions merging the catalog with the literature redshifts.

Figures 2.11 and 2.12 show for each OmegaWINGS field the magnitude and radial completeness computed without (blue circles) and with (red squares) literature. Big symbols indicate bins with low statistics (fewer than 20 points). Dashed lines (blue and red) indicate the total completeness for the two samples.

2.3 Summary

In this Chapter I have described in detail the cluster sample I will use in this thesis. I have briefly presented the WINGS survey, whose data served as the starting point for the new survey OmegaWINGS that extends the previous project. The OmegaWINGS photometric and spectroscopic observations have been described, with particular focus on my contribution to the different steps of the data reduction and analysis. Combining these data with those already available in the WINGS database, I compiled the complete cluster catalog. A summary of the important quantities can be found in table 2.4.

Using an iterative 3σ clipping scheme, I derived rest frame velocity dispersions for the 33 OmegaWINGS clusters and assigned membership. A total of 8891 galaxies turn out to be members of the OmegaWINGS cluster sample, thereby almost two and a half times the number of known members in the WINGS survey.
I will discuss the properties of the galaxy population in Chapter 4.

Starting from to these data, together with the general field sample that will be presented in Chapter 3, I will carry out a systematic study of all the main galaxy properties in relation to their environment.

Name	$N_{cluster,phot}$	$N_{cluster,spec}$	$N_{galaxies,z}$	$N_{members}$
WINGS	77	48	6137	3647
OmegaWINGS	48	33(21)	17985	8891(1394)

Table 2.4: The numbers of clusters and galaxies in the WINGS and OmegaWINGS surveys. The number of clusters in the photometric (col. 1) and spectroscopic (col. 2) campaigns are given.Col.3 list the number of galaxies with successful redshift determination and col. 4 the number of member galaxies. For OmegaWINGS, the quantities within brackets indicate common objects with WINGS .

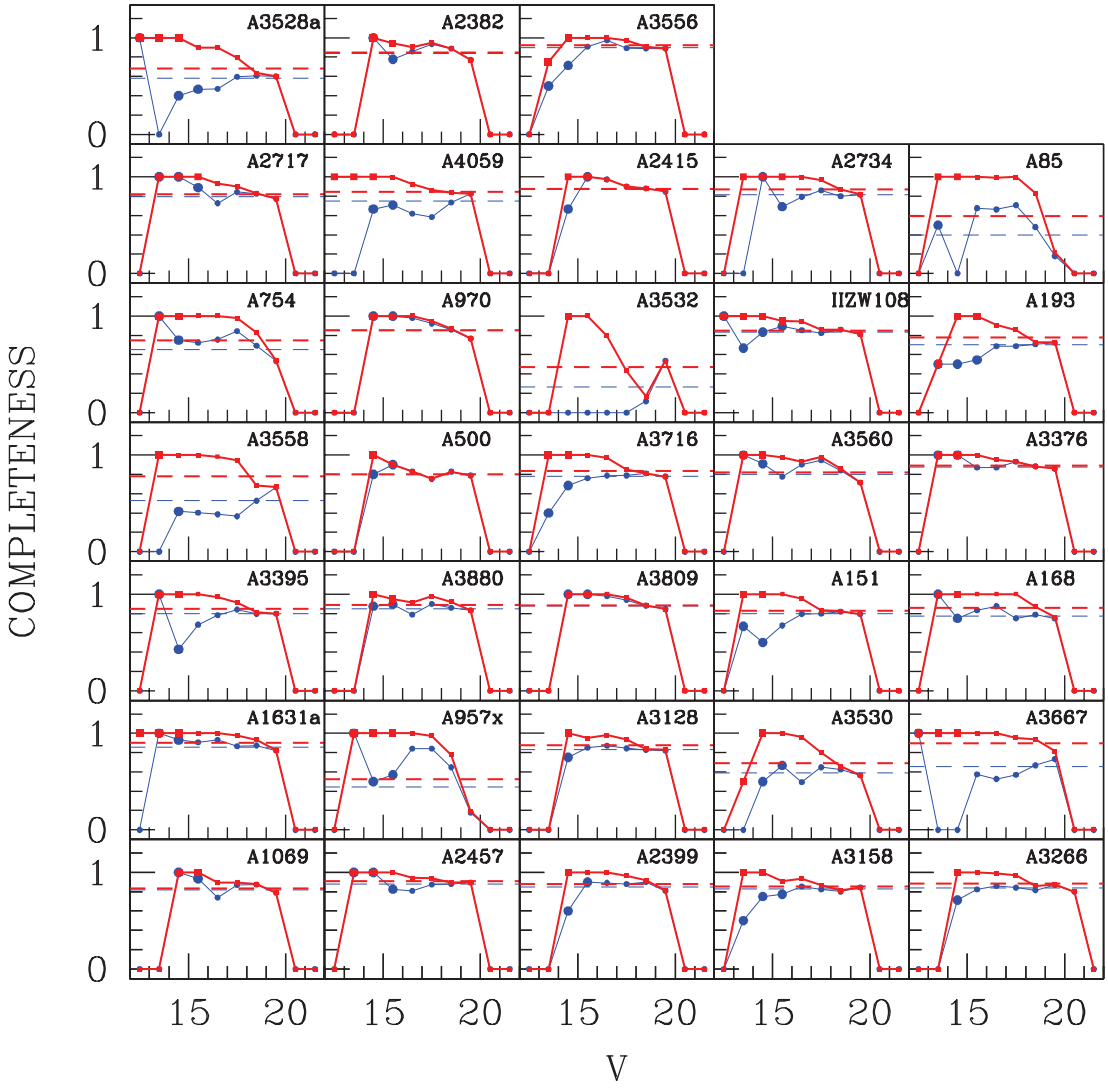

Figure 2.11: Completeness as a function of the V magnitude for the 33 OmegaWINGS clusters. Blue dots represent the OmegaWINGS+WINGS catalog, red squares the full catalog that includes the literature. Large dots represent bins with low statistic (fewer than 20 points). Dashed lines indicate the total completeness for the two samples

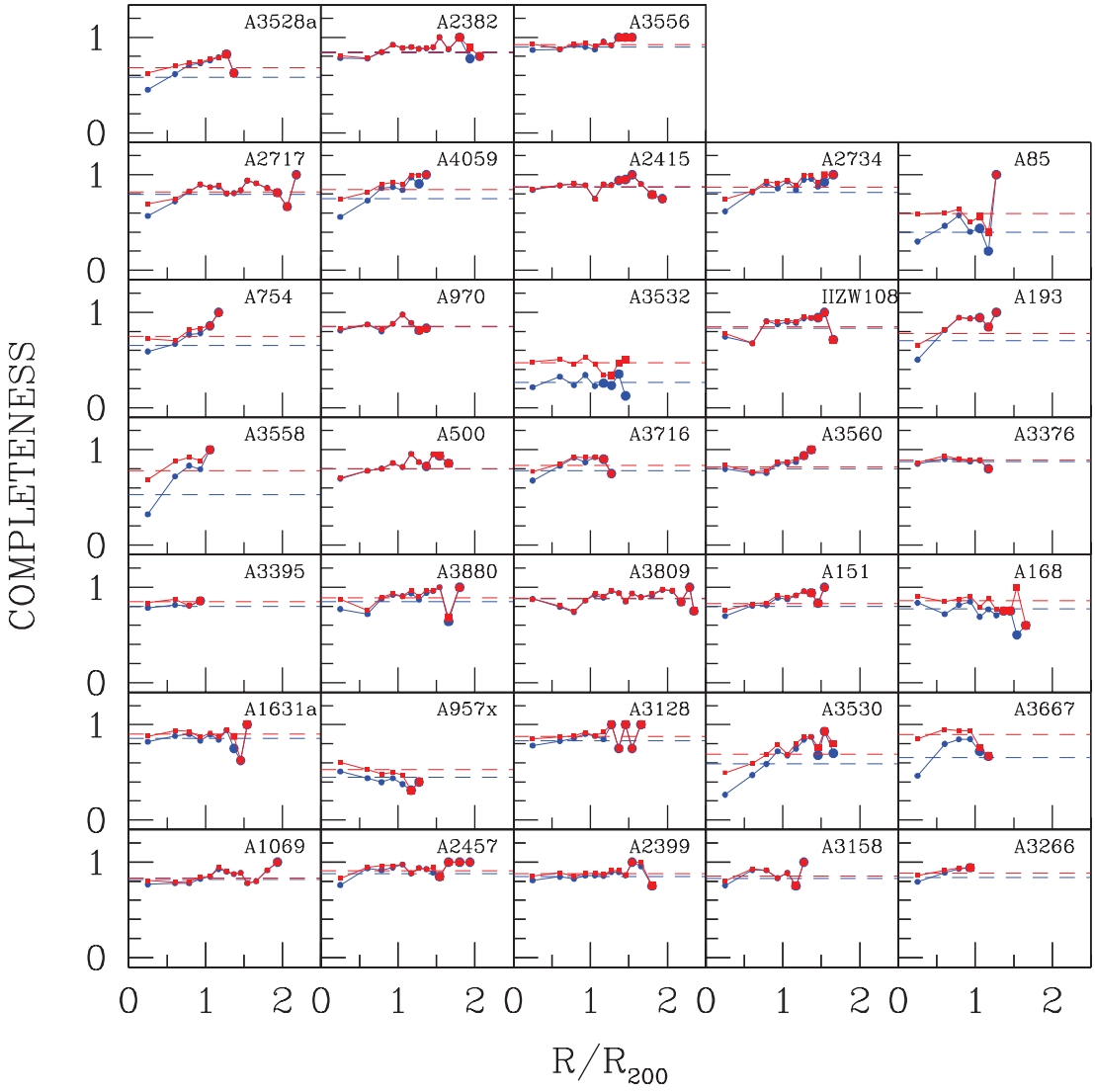

Figure 2.12: Completeness as a function of the distance from the cluster center (BCG) for the 33 OmegaWINGS clusters. Blue dots represent the OmegaWINGS+WINGS catalog, red squares the full catalog that includes the literature. Large dots represent bins with low statistic (fewer than 20 points). Dashed lines indicate the total completeness for the two samples.

3

The general field sample: PM2GC

In this Chapter I present the general field sample extracted from the PM2GC database: galaxies are selected according to their B rest frame magnitude and assigned to groups, binary or single systems thanks to a Friend of Friend algorithm. Exploiting a mock galaxy catalog built from semi-analytic models run on the Millennium Simulation I derived a simple method to broadly distinguish high and low contaminated groups and obtained a functional formulation to compute halo masses from observables quantities.

The results of the analysis presented in this Chapter have been used by Guglielmo et al. (2015), Vulcani et al. (2015), Poggianti et al. (2016) and Calvi et al. (2016, in prep.) and will be presented in Paccagnella et al. (2017, in prep.).

3.1 Introduction

One of the challenges of this work is that of building a continuous distribution of halo masses going from isolated galaxies to pairs, groups and clusters to link the properties of galaxies to those of their halo. As already discussed in Chapter 1, while the effects induced by the environment on the properties of the galaxy population have been widely studied in massive clusters, where they are strongest, they have been found to persist at least down to virial masses of $\sim 10^{12} M_{\odot}$ (e.g. Weinmann et al., 2006; Wetzel et al., 2012). A few studies in the past have investigated the correlation between galaxy properties and halo mass using group catalogs (e.g. Martínez et al., 2002; Yang et al., 2005; Balogh et al., 2004b) but a detailed analysis spanning the entire halo mass range in an homogeneous

sample is still missing.

Indeed, while halo masses are easy to estimate for massive systems, such as clusters or very rich groups, based on the velocity dispersion of their member galaxies, this method is not very reliable for small groups with only a few members or for even smaller systems such as binaries and single galaxies. A different approach to estimate halo masses needs to be considered. I have developed a technique that exploits mock galaxy catalog from semi analytic models to link the distribution of galaxies to that of dark matter halos. As demonstrated in Yang et al. (2003, 2007, 2008), the mass of a dark matter halo associated with a group is tightly correlated with both the total stellar mass of member galaxies and to the mass of the most massive galaxy in the system. Based on this idea, I derived two different estimates of the halo mass. This method has the advantage that is equally applicable to groups spanning the entire range in richness, including single galaxies and binaries.

3.2 The PM2GC catalog

The Padova Millennium Galaxy and Group Catalogue (PM2GC) (Calvi et al., 2011) is a database representative of the general field population in the Local Universe that was created to satisfy the requirements of high quality imaging and spectroscopic completeness. The galaxy sample was built on the basis of the Millennium Galaxy Catalogue (MGC) (Liske et al., 2003; Cross et al., 2004; Driver et al., 2005), a deep and wide B-imaging survey along an equatorial strip of $0.6deg \times 73deg$ covering an area of $\sim 38deg^2$ obtained with the Isaac Newton Telescope (INT) and consists of 144 overlapping fields. The catalog contains about one million of objects, spanning the magnitude range $16 \leq B_{MGC} \leq 24$, reduced by the Cambridge Astronomy Survey Unit (CASU) (Irwin and Lewis, 2001) and classified using SEXTRACTOR. A sample of galaxies was selected from the MGCz catalog, the spectroscopic extension of the MGC. It was built on the Two-Degree Field Galaxy Redshift Survey (2dFGRS, Colless et al., 2001) and the Sloan Digital Sky Service-EDR (SDSS-EDR/DR1 York et al., 2000), in which the MGC survey region is fully contained, and complemented with redshifts taken at the AAT using the 2dF facility (Driver et al., 2005), as well as redshifts from the NASA Extragalactic Database (NED), the 2dF QSO Redshif Survey (2QZ), the Paul Francis' Quasar Survey and some low surface brightness galaxies. The total spectroscopic completeness is greater than 96% for $B_{MCG} < 20$, therefore a statistical completeness correction to the sample is not needed.

The description of the selection and the properties of galaxy groups, as well as a

detailed characterization of the different environments constructed by means of a Friends-of-Friends (FoF) algorithm is fully described in Calvi et al. (2011). Here I summarize the key steps made to build the catalog. A restricted sample of galaxies brighter than $M_B = -18.7$ and with a spectroscopic redshift in the range $0.03 \leq z \leq 0.11$ (3210 galaxies) was selected. Absolute magnitudes were obtained K-correcting the observed SEXTRACTOR magnitudes, with K-corrections taken from Poggianti and Barbaro (1997).

The approach used to identify galaxy groups is based on a plain FoF algorithm according to which two galaxies are physically related and join the same group if their distances in the projected direction and in the line of sight are less than some fixed thresholds, called 'linking lengths', that connect together all galaxies within a particular linking volume, chosen to be a cylinder. Starting from a trial group found by the described algorithm for galaxies brighter than $M_B = -18.7$, with defined median geometric center, redshift and velocity dispersion, an iterative procedure was performed that assign memberships based on a 3σ clipping routine and a distance dependent cut. This process was repeated until convergence. Only those galaxies that are within $1.5R_{200}$ from the group center and 3σ from the group redshift were considered as members of the final groups. The result is a catalog of 176 groups of galaxies with at least three members, in the redshift range $0.04 \leq z \leq 0.1$, containing in total 1057 galaxies and representing 43% of the total general field population at that redshift.

In general, most of the groups contain fewer than 10 members, 63% have less than 5 members and 43% have only three members. The median redshift and velocity dispersion of the sample are $z = 0.0823$ and $\sigma = 191.8$ km/s respectively. The range of velocity dispersion is between 100 km/s and 800 km/s.
Galaxies that do not satisfy the group membership criteria at $0.03 \leq z \leq 0.11$ and with no friends (1141) were classified as field-single, those with only one friend within 1500 km/s and 0.5 $h^{-1}Mpc$ (490) were called field-binary. All galaxies in the environments described above are collected in the "general field" sample.

I will discuss the properties of the galaxy population in Chapter 4. Here I anticipate that stellar masses have been computed following the Bell and de Jong (2001) formulation (see 4.2.2). The methods and the presentation of the catalogs are described in Calvi et al. (2011), and the samples are available on-line on the web page of the MNRAS paper and of the MGC.

3.3 Estimates of the halo masses from simulations

Here I describe how I exploited mock catalogs to test the performance of the FoF algorithm and to assign halo masses to the systems in the PM2GC.

3.3.1 The Millennium Galaxy Run

I took advantage of publicly available galaxy catalogs from semi-analytic models run on the Millennium Simulation (Springel et al., 2005). The Millennium simulation is based on a cold dark matter (ΛCDM) cosmological model of structure formation, with a dark energy field. The basic assumptions are those of an inflationary universe, dominated by dark matter particles, leading to a bottom–up hierarchy of structure formation, via collapsing and merging of small dense halos at high redshifts, into the large virialized systems such as groups and clusters that contain the galaxies that we observe today. The simulation was carried out using a modified version of the publicly available code GADGET2 (Springel et al., 2001), evolving 10^{10} particles of an individual mass $8.6 \times 10^8 h^{-1} M_\odot$, in a cubic region of the Universe of side $500 h^{-1} Mpc$, from redshift $z = 127$ to the present day and with a spatial resolution of $5 h^{-1} kpc$.

The cosmological parameters assumed are $\Omega_m = \Omega_{dm} + \Omega_b = 0.25$, $\Omega_b = 0.045$, $\Omega_\Lambda = 0.75$, $h = 0.73$, $n = 1$, and $\sigma_8 = 0.9$. The Hubble constant is characterized as $100\ h\ kms^{-1}\ Mpc^{-1}$, while σ_8 is root mean square linear mass fluctuation within a sphere of radius $8 h^{-1} Mpc$ extrapolated to $z = 0$, n is the spectral index of the primordial power spectrum. These cosmological parameters are consistent with a recent combined analysis from first year WMAP data (Sánchez et al., 2006) and the 2dF Galaxy Redshift Survey.

The derived dark matter halo catalogs include halos down to a resolution limit of 20 particles, which yields a minimum halo mass of $1.72 \times 10^{10} h^{-1} M_\odot$. Halos in the simulation are found using a FoF group finder, tuned to extract halos with overdensities of at least 200 relative to the critical density. Within a FoF halo, substructures are identified using the SUBFIND algorithm (Springel et al., 2001) as locally overdense regions in the density field of the background halo. In the Millennium simulation, 64 time-slices of the locations and velocities of all the particles were stored, spread approximately logarithmically in time between $z = 127$ and 0. From these timeslices, merger trees are built by combining the tables of all halos found at any given output time, a process which enables to trace the growth of halos and their subhalos through time within the simulation. More detailed descriptions of the simulation itself and of the post-processing can be found in Springel et al. (2005).

3.3.2 The semi-analytic model

The Millennium Simulation has had enormous success in matching the large-scale structure seen in observational surveys of the Universe, but it does not provide any information on how the "normal matter" behaves within this dark matter framework. The analytic treatment of the baryonic component is quite complex, involving nonlinear physics and several mechanisms such as the cooling of gas onto galaxies, the conversion of gas into stars and the feedback produced by supernovae or Active Galactic Nuclei (AGN). Because of this, in the framework of the cosmological simulations, there are still major difficulties in the modeling of the physics involved in galaxy formation. One successful approach that has been developed to circumvent this problem is the so-called "semi-analytic modeling". This technique attempts to construct a coherent set of analytic approximations which describe the nonlinear equations governing the physical processes inherent to galaxy formation. The aim is to predict the properties of galaxies and how they evolve with cosmic time, starting from dark matter Monte Carlo merger trees.

Some of the earliest attempts to construct a self-consistent semi-analytic model of galaxy formation began with White and Frenk (1991); Cole (1991) and Lacey and Silk (1991). Since then, numerous studies (Baugh et al., 1999, 1998; Somerville and Primack, 1999; Cole et al., 2000; Hatton et al., 2003; Monaco et al., 2007) have extended and improved this original framework.

Semi analytic models rely on simplified assumptions and require the treatment of the various processes only through parametric forms and the introduction of free parameters that have to be set through the comparison with observational data. This formulation in general takes the form of differential equations for the time evolution of the galaxies that describe, with the mentioned level of approximation, radiative cooling of gas, star formation, AGN feedback and the effects due to the re-ionization due to the UV background. The morphological transformation and the process of metal enrichment are modeled as well. Moreover, to be consistent with observations, population synthesis models are applied to predict spectra and magnitudes for the stellar light emitted by the galaxies, including simplified models for the dust attenuation.

In this work the semi-analytic model of De Lucia and Blaizot (2007) has been chosen. This model is applied onto the halo merger trees constructed using the halo catalogs of the Millennium Simulation introduced earlier following the method described by Springel et al. (2005) and Croton et al. (2006) and has been the first variant of the "Munich" models family that has been made publicly available. It includes prescriptions for supernova-driven

winds, follow the growth of supermassive black holes, and include a phenomenological description of AGN feedback. The model is calibrated to reproduce the $z = 0$ luminosity function in the K- and J -bands. It also provides stellar masses and rest-frame Vega magnitudes, which include the effect of the dust in the Buser (1978) system, calculated using the models of Bruzual and Charlot (2003).

The extractions presented in Vulcani et al. (2014) were used to reproduce the observed field selecting portions of "simulated sky" corresponding to square boxes of $\sim 38 deg^2$ (30×30Mpc) at z=0.06. To match the observed field sample, the boxes extracted are 323 physical Mpc deep. To account for cosmic variance, 10 simulated field samples were selected and will be used separately. No pre-selection on halo mass was applied to these boxes. At the resolution of the Millennium Simulation, halos with $M_{200} \sim 10^{13} M_{\odot}$ contain on average about 15 galaxies within the virial radius, with stellar masses larger than $M_* \sim 10^9 M_{\odot}$. For each halo or sample of galaxies, information on the halo mass, the virial radius, the xyz coordinates in the box and the velocity dispersions are available. Velocity dispersions have been computed using all galaxies within R_{200} and more massive than $M_* \sim 5 \times 10^8 M_{\odot}$, that is the resolution limit of the simulation. Each galaxy is characterized by a unique ID, the type (central,satellite or orphan) , the position in the box, the stellar mass and rest-frame Vega magnitudes. The observed-frame Sloan *ugriz* were also extracted. Instead of using the stellar masses provided by the models, following Vulcani et al. (2014), I used the stellar masses estimated using the Bell & de Jong formulation.[1] As a consistency test, Vulcani et al. (2014) performed a comparison between these stellar masses and the ones provided by the De Lucia and Blaizot (2007) catalog, based on the Bruzual and Charlot (2003) model. They found a good agreement, with an absolute median difference of 0.08.

Since the main aim of this analysis is to exploit the information obtained from the simulation to predict the halo mass of the systems in the PM2GC, a "sim-projected" sample was also extracted: all quantities were computed from the 10 simulated fields with the same methods that have been applied on the PM2GC data. Simulated galaxies were projected on the xy plane and those with absolute magnitude above the PM2GC limit (M_B=-18.7) were selected. The same FoF algorithm used to define the systems in the PM2GC sample was also applied to this "sim-projected" galaxy sample in order to identify groups, binary systems and single galaxies.

This sample will be compared to the 10 "simulated" fields that includes the 3D estimates provided by the simulation. The number of systems in the two different samples,

[1] Details on the procedure are given in section 4.2.2

Catalog	Groups	Binaries	Singles
simulated	851	1345	18923
sim-projected	1647	2115	9682

Table 3.1: Number of groups, binary systems and single galaxies in the simulated and sim-projected samples.

summed over the 10 fields, are given in Tab. 3.1.

This analysis also allows to check the performance of the FoF algorithm, estimating its incompleteness and contamination.

3.3.3 The contamination of the sim-projected groups

Any selection of group members will have some fraction of false positives, i.e. interlopers selected as members that do not belong to a group, and false negatives, i.e. true member galaxies missed by the selection.

The comparison between the sim-projected groups identified by the PM2GC FoF algorithm and the simulated groups whose properties (e.g. member galaxies, velocity dispersion etc.) are provided by the simulation, allowed to estimate the contamination of the PM2GC group catalog.

The contamination is defined as the fraction of interlopers. Formally, it corresponds to $f_i = N_i/N$, where N is the number of selected members and N_i is the number of interlopers $N_i = N - N_{true}$. For the sim-projected sample I found that more than 50% of the groups have a contamination higher than 50%.

To properly account for this contaminated population, I looked for a relation that links observable quantities and distinguish between "real" groups and "fake" ones. I found that the velocity dispersion of sim-projected groups σ, that is an output of the FoF algorithm, and the total stellar mass of member galaxies $logM^{MS}_{*,tot}$, correlate well for groups with $f_i < 0.3$ that arrange themselves in a well-defined region in the $\sigma - logM^{MS}_{*,tot}$ plane (Fig. 3.1). To distinguish these groups, I divided the $\sigma - logM^{MS}_{*,tot}$ plane in two regions with a line whose equation is meant to maximize the fraction- bigger than 85%- of real groups on one side (left):

$$LogM_* = 0.003 \cdot \sigma + 10.40 \tag{3.1}$$

In Figure 3.2 the distributions of the fraction of interlopers for the two classes of groups are shown: the majority of groups lying on the left side of eq. 3.1 ($> 60\%$) have a low fraction of interlopers, while almost all ($\sim$80%) groups on the right side are highly contaminated. Given that highly contaminated groups would naturally induce a huge

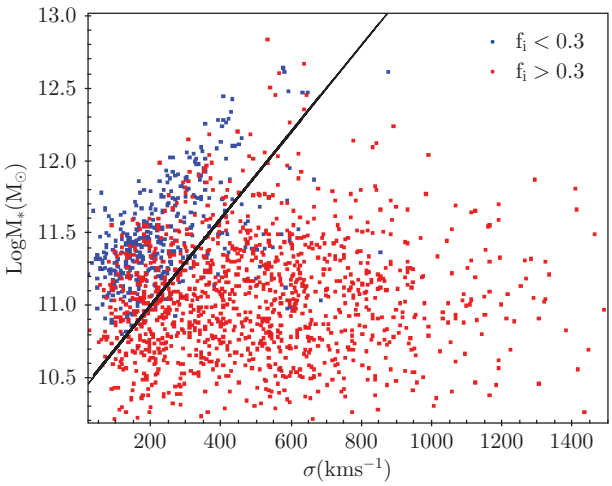

Figure 3.1: LogM$_*$(total stellar mass)-σ for the FoF simulated groups. Blue and red dots indicate respectively group with a fraction of interlopers smaller and bigger than 30%. The black line dividing the plane in two is the one defined by equation 3.1.

scatter in the determination of the halo mass, in the following analysis I will consider only those groups having $logM^{MS}_{*,tot} > 0.003 \cdot \sigma + 10.40$.

3.3.4 Halo mass of the sim-projected sample

The starting point is to assign halo masses to the groups in the sim-projected catalog. Even if in principle the mass of the halo in which each simulated galaxy is embedded is known, linking FoF groups to one halo mass is not straightforward. In the simulated sample one can take advantage of all the information coming from the Millennium Simulation thus having a unique correspondence between galaxies and the dark matter halo of the system to which they belong. On the contrary, in the sim-projected catalog, because of projection effects, galaxies located in different simulated halos seem to belong to the same sim-projected group. Thus, some fraction of the group members are not true members but are central galaxies that exist within a smaller simulated halos.
To get the most reliable halo mass for groups with more than 3 galaxies, I first chose the mass corresponding to the simulated halo to which the majority of the sim-projected group galaxies belongs. Then, I calculated the number of lost members N$_{lost}$: if N is the total number of galaxies in the simulated halo, N$_{true}$ is the number of true members that are selected as members of the sim-projected group, $N_{lost} = N - N_{true}$. If the number of galaxies in the sim-projected group is N_{tot} and $N_{lost} > N_{tot}$, I chose the next halo in

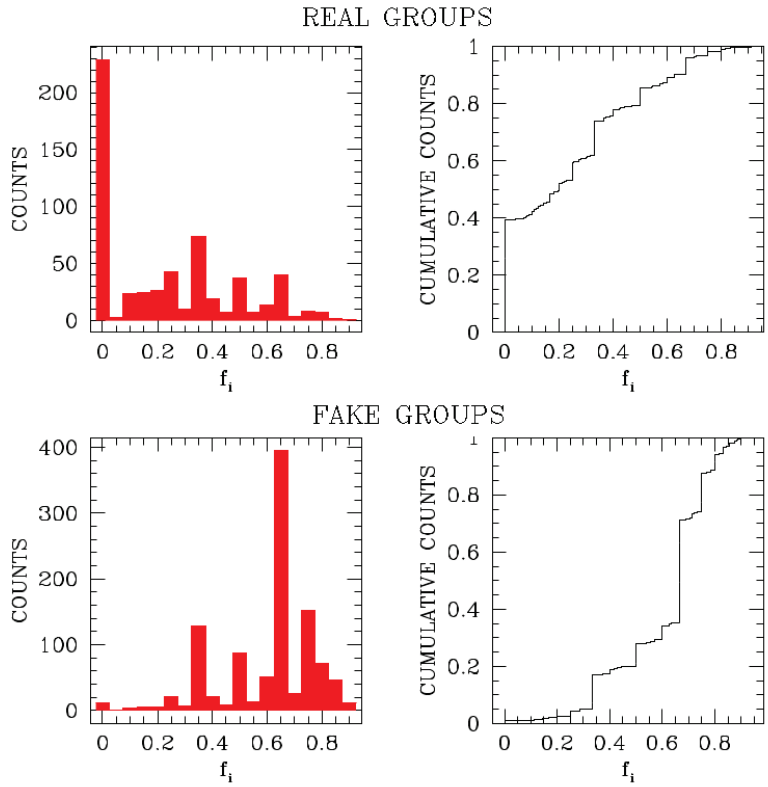

Figure 3.2: Counts and cumulative distribution of the contamination f_i in "real groups" (upper panel) and "fake" groups (lower panel). f_i is defined as the fraction of interlopers in the sim-projected groups.

frequency and recalculated the different quantities. If the number of galaxies in this new simulated halo N' is closer to N_{tot}, I rejected the first halo and considered the second one as the one corresponding to the sim-projected group and iterated the process, otherwise I kept the first one (see figure 3.3 for a schematic representation of these quantities). In the case that all galaxies in the group belong to different simulated halos, (38% of the groups) I assigned to the sim-projected group the mass of the halo corresponding to the most massive galaxy (hereafter MMG) and flagged the group (see below for further discussion).

Regarding galaxies in binary systems, if the two members did not belong to the same simulated halo, I assigned to the sim-projected binary the mass of the halo of the MMG. For single galaxies the associated halo mass is the one of the simulated halo that contains the galaxy. For the sake of clarity, in the following I will refer to this estimate of the halo mass as M_{halo}^{MS}. For each sim-projected system three main quantities are now available:

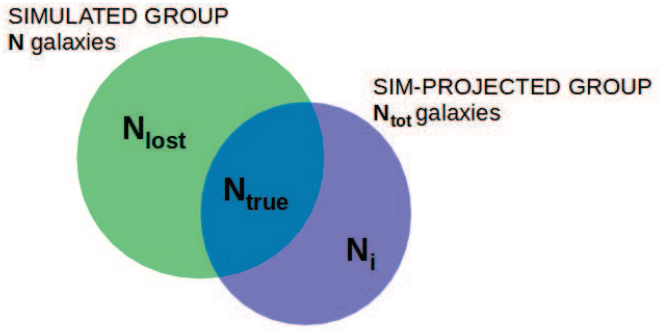

Figure 3.3: Schematic representation of the simulated and sim-projected groups with the relative quantities: N is the number of galaxies in the simulated halo, N_{tot} is the number of galaxies in the sim-projected group selected by the FoF algorithm, N_{lost} and N_{true} are respectively the number of galaxies of missed and successfully identified by the FoF algorithm and N_i is the number of interlopers.

halo mass M^{MS}_{halo}, the stellar mass of the MMG $M^{MS}_{*,MMG}$ and the total stellar mass $M^{MS}_{*,tot}$, defined as the sum of the stellar masses of the galaxies in the FoF system selected above the PM2GC magnitude limit ($M_B = -18.7$).

The Stellar-to-halo Mass Relation

The dark halo mass can be connected to the stellar mass of the MMG of a system by assuming a one-to-one and monotonic relationship between the two. Figure 3.4 illustrates, for the 10 sim-projected samples, that indeed a strong correlation between these two variables exists. Despite the fact that the scatter of $\mathrm{M}^{MS}_{*,MMG}$ at a fixed halo mass is significant, there is an overall trend for the MMG stellar mass to increase with total the halo mass M^{MS}_{halo}. If we adopt the functional form suggested by Yang et al. (2003) and Moster et al. (2010), this relation can be approximated to high accuracy by:

$$\frac{M^{MS}_{*,MMG}}{M_{halo}} = \left(\frac{M}{M_0}\right)_0 \left[\left(\frac{M_{halo}}{M_1}\right)^{-\beta} + \left(\frac{M_{halo}}{M_1}\right)^{\gamma}\right]^{-1} \tag{3.2}$$

This relation has four free parameters: the normalization of the stellar-to-halo mass (SHM) ratio $(m/M)_0$, a characteristic mass M_1, where the SHM ratio is equal to $(M/M)_0$, and two slopes β and γ which indicate the behavior of $M^{MS}_{*,MMG}/M^{MS}_{halo}$ at the low and high mass ends, respectively. The values of these parameters are strongly related to the stellar

mass function. Varying M_1, we expect a drastic change in the shape of the relation, with higher/lower values corresponding to many more/less massive galaxies and too few/many low massive galaxies. This is because M_1 is the characteristic mass corresponding to the highest stellar-to-halo mass ratio. Keeping M_1, β, and γ fixed and only varying $(m/M)_0$ corresponds to changing the stellar mass of the galaxy that lives inside each halo by a

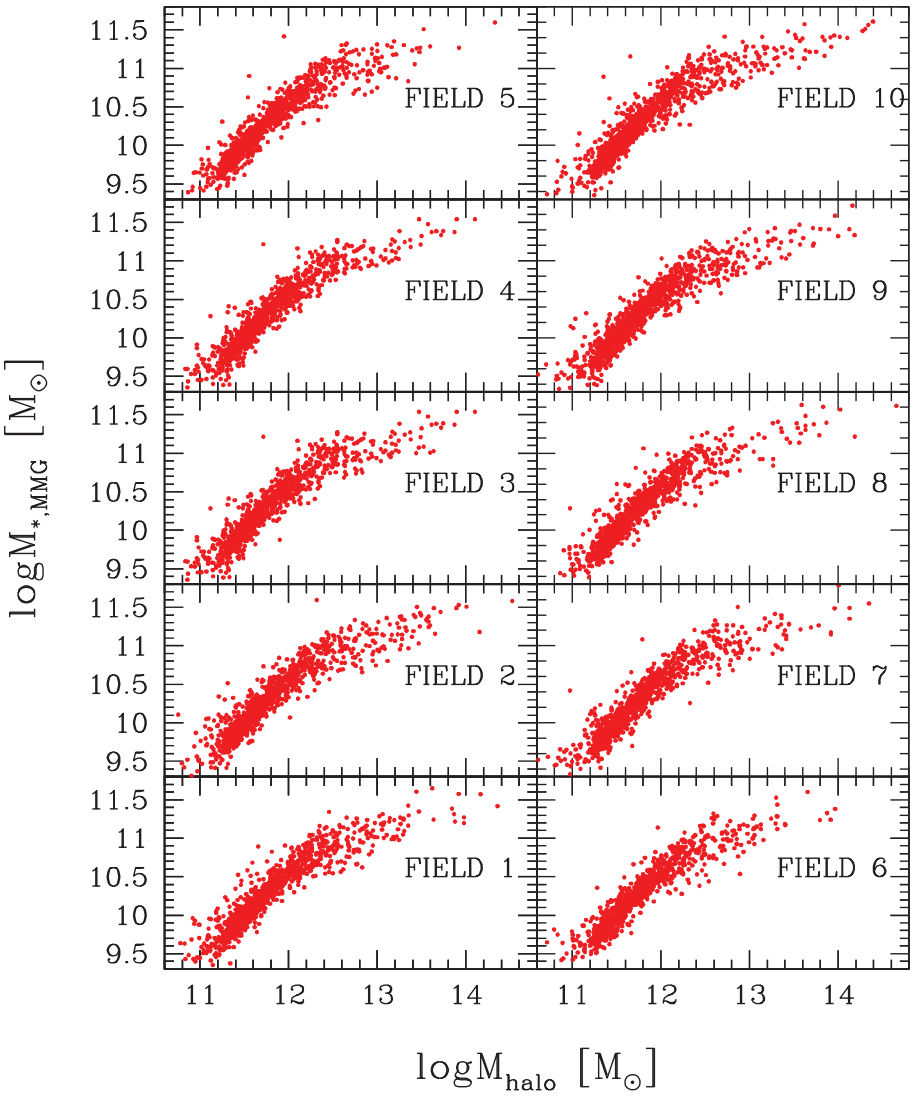

Figure 3.4: Stellar mass of the most massive galaxy as a function of the main halo for groups in the 10 sim-projected fields (red).

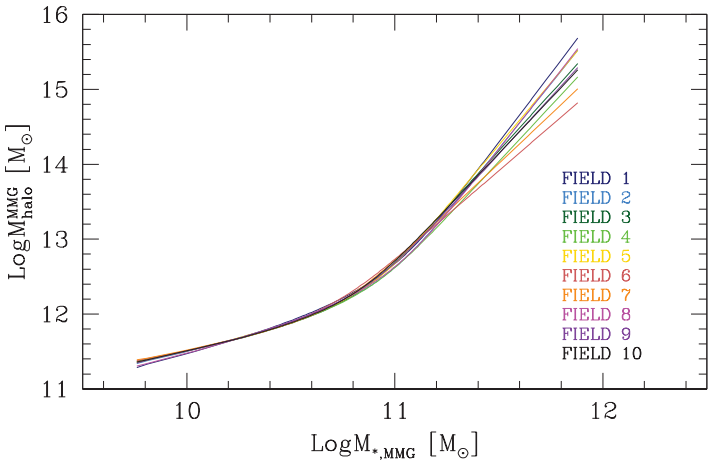

Figure 3.5: Fitted curves for Stellar-to-halo Mass Relationship in the 10 sim-projected samples.

constant factor, being directly linked to the value of the normalization of the stellar mass function. The values of β and γ are given respectively by the low-mass and high-mass slope of the stellar mass function. To constrain these parameters and account for the

MS Field	M/M_0	$\log M_1$	β	γ
1	0.076	11.987	-0.512	0.727
2	0.081	11.933	-0.736	0.711
3	0.082	11.812	-1.023	0.674
4	0.083	11.849	-0.910	0.665
5	0.081	11.874	-0.866	0.699
6	0.076	11.688	-1.251	0.582
7	0.079	11.734	-1.267	0.618
8	0.079	11.971	-0.587	0.717
9	0.080	11.841	-0.859	0.671
10	0.081	11.790	-1.031	0.660

Table 3.2: Fitting results for Stellar-to-halo Mass Relationship in the 10 sim-projected samples.

cosmic variance I fitted the 10 sim-projected samples extracted from the 10 simulated fields implementing a nonlinear least-squares Marquardt-Levenberg algorithm. This gives ten different sets of parameters, listed in table 3.2, yielding the same number of fitted curves, shown in Fig. 3.5.

Equation 3.2 needs to be inverted in order to get the halo mass from the stellar mass of the MMG. I therefore applied the bisection method: I generated an input array of halo

masses that covers, with a high sampling, the whole interval of M_{halo}^{MS} and from equation 3.2 got the array of stellar masses. I searched in this last array for the stellar mass that is closer to our input mass and linked it to the corresponding halo mass. This numerical solution generates errors that are completely negligible with respect to both the precision of the stellar mass estimate (0.2 dex) and the internal scatter of the fit, which is discussed below. Hereafter I refer to halo masses derived through this technique as M_{halo}^{MMG}.

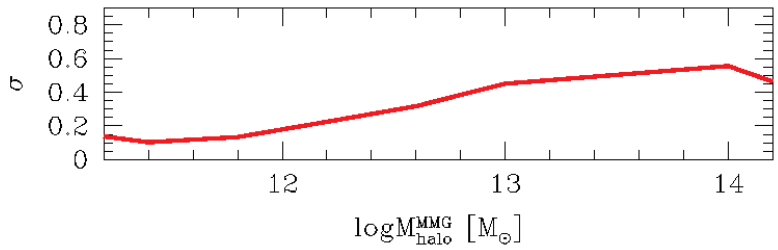

Figure 3.6: Residual standard deviation of the $M_{halo}^{MS} - M_{halo}^{MMG}$ relation plotted as a function of M_{halo}^{MMG}.

Clearly, the assumption of a one-to-one relation between the stellar mass and the halo mass is oversimplified. In reality, due to the several factors (i.e. the intrinsic scatter in the relation between the halo mass and the true most massive galaxy of the system or the incompleteness and contamination introduced by the group finder) this relation contains some scatter, which results in errors in the inferred group masses. Figure 3.6, shows the scatter of the M_{halo}^{MMG}-M_{halo}^{MS} relation obtained as the mean of the ten residual standard deviations calculated in bins of logarithmic fitted halo mass. The results indicate that the scatter increases with the halo mass, as expected given the change in the slope of the SHM relation at the high-halo mass end.

The Total Stellar-to-halo Mass Relation

As demonstrated in Yang et al. (2005), the mass of a dark matter halo associated with a group is tightly correlated with the total stellar mass of all member galaxies down to some luminosity. This is further illustrated in Figure 3.7, where the correlations between the halo mass M_{halo}^{MS} assigned to the mock systems and the total stellar mass for the 10 sim-projected fields are shown. I remind here that galaxies located in groups, binaries and single systems were considered all together (excluding highly contaminated groups, see sect. 3.3.3) and that the total stellar mass has been computed including only galaxies

brighter than the PM2GC magnitude limit of $M_B = -18.7$. Obviously, for single galaxies, the mass of the MMG and the total stellar mass coincide.

To fit the data, I used an analytic equation with four free parameters that reproduces

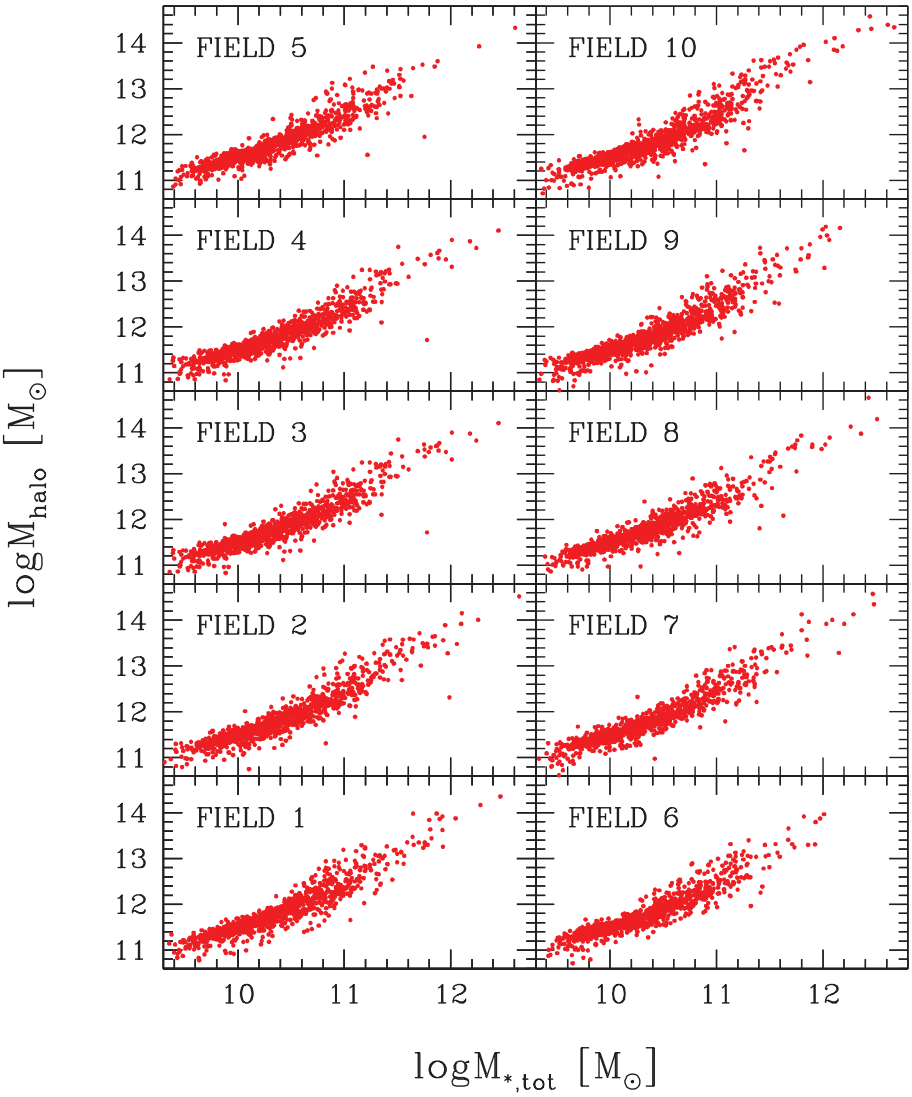

Figure 3.7: Total stellar mass as a function of the main halo for groups in the 10 sim-projected fields (red). The blue lines are the best fit results obtained using equation 3.3.

quite well the relation:

$$logM_{halo} = a + d\left[arctan\left(\frac{M^{MS}_{*,tot} - b}{c}\right)\right] \tag{3.3}$$

The same nonlinear least-squares fitting algorithm described in the previous section has been applied to the sim-projected samples in order to get the ten different sets of parameters (see Fig. 3.7 and table 3.3). To quantify the scatter of this relation, as done before, I compared the assigned halo mass, hereafter M^{tot}_{halo} and the mock halo mass M^{MS}_{halo} and computed the mean standard deviation for the residuals. The results are plotted against the fitted halo mass M^{tot}_{halo} in Fig. 3.9. The scatter increases with halo mass, but is limited to 0.4 dex along the whole mass range.

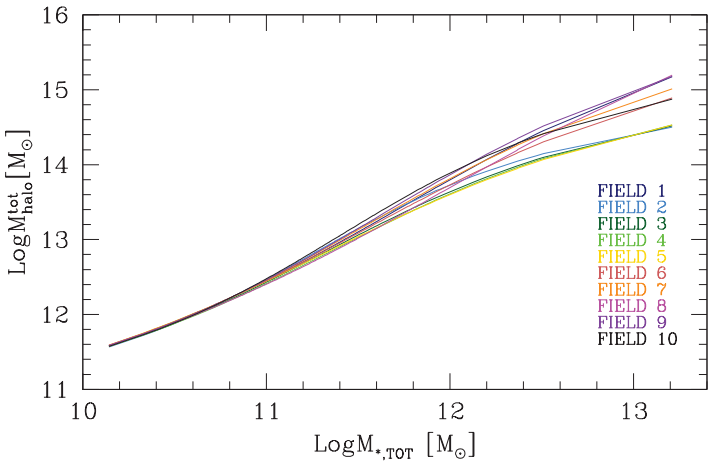

Figure 3.8: Fitted curves for total stellar mass to halo relationship in the 10 sim-projected samples.

Finally, Figure 3.10 compares the distribution of halo masses M^{MS}_{halo} (black) to the values inferred from the MMG stellar mass M^{MMG}_{halo} (red) and from the total stellar mass M^{tot}_{halo} (blue). The median values of the distributions are listed in table 3.4 with the errors. Both relationships provide good estimates of the halo mass, the median values being always compatible within the errors with the estimates derived from the simulation. I recall that the whole fitting procedure has been applied to groups identified by the same group finder algorithm run on the observations, thus already contains the scatter introduced with projection effects and interlopers on the estimation of the final halo mass.

MS Field	a	b	c	d
1	13.429	11.734	1.858	2.6
2	12.796	11.241	1.221	1.678
3	12.832	11.32	1.438	1.83
4	12.859	11.364	1.518	1.893
5	12.831	11.326	1.683	2.02
6	13.139	11.54	1.739	2.289
7	13.206	11.554	1.63	2.278
8	13.652	11.967	2.073	2.859
9	13.352	11.64	1.651	2.403
10	13.056	11.402	1.281	1.905

Table 3.3: Fitting results for Total Stellar-to-halo Mass Relationship in the 10 sim-projected samples.

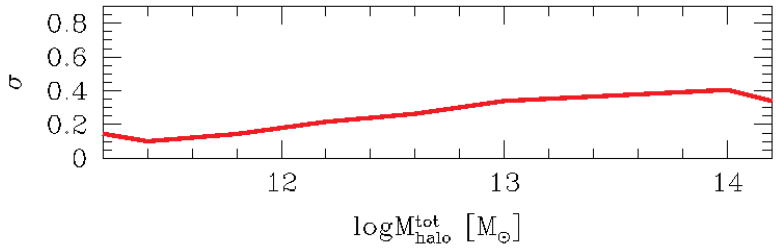

Figure 3.9: Residual standard deviation of the $M^{MS}_{halo} - M^{tot}_{halo}$ relation plotted as a function of M^{tot}_{halo}.

3.4 The PM2GC halo masses

3.4.1 Correcting for the survey edges

An important effect that needs to be accounted for before applying equation 3.3 to the observed sample is due to the survey geometry. A group whose projected area straddles one or more survey edges may have members that fall outside of the survey, thus causing an incompleteness which affects our mass estimate of the group. The geometry I used to quantify this issue is a simplification of the real one that is quite complicated. In particular, I chose to correct for the rectangle that contains the whole field of view and proceed as in Yang et al. (2007). First, I estimated the total stellar mass for each group without taking edge effects into account thereafter, 200 points were randomly distributed within the corresponding halo radius R_{200}. Next I applied the rectangular mask and removed

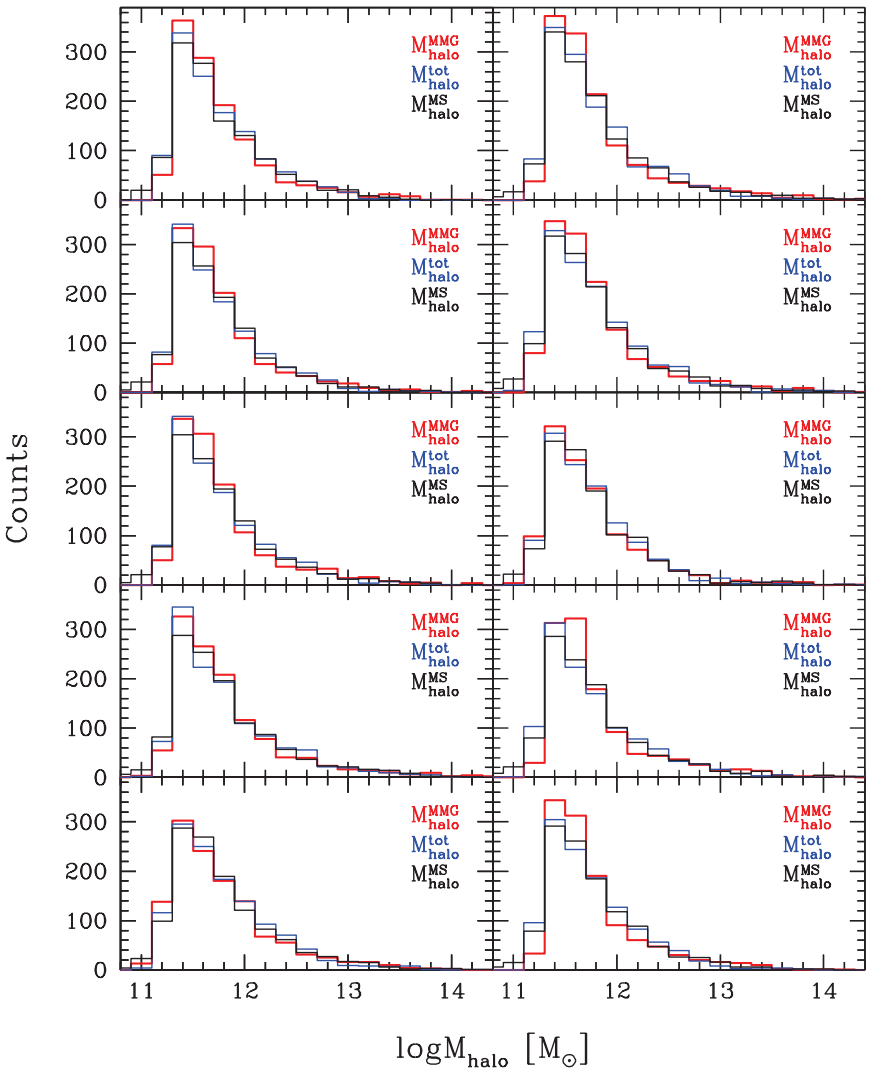

Figure 3.10: Halo mass distributions for the 10 sim-projected samples as derived from the simulation (black), from eq.3.2 (red) and eq.3.3 (blue).

those random points that fall outside of the field region. For each group I computed the number of remaining points, N_r, and define $f_{edge}=N_r/200$ as a measure for the volume of the group that lies within the survey edges. Finally, I multiplied the total stellar mass with $1/f_{edge}$ to correct for the "missing members" outside the edges. This correction, as

$\mathrm{Med}(M_{halo}^{MMG})$	$\mathrm{Med}(M_{halo}^{tot})$	$\mathrm{Med}(M_{halo}^{MS})$
11.63 ± 0.02	11.65 ± 0.02	11.66 ± 0.02
11.66 ± 0.02	11.67 ± 0.02	11.67 ± 0.02
11.64 ± 0.02	11.65 ± 0.02	11.64 ± 0.02
11.63 ± 0.02	11.64 ± 0.02	11.63 ± 0.02
11.62 ± 0.02	11.64 ± 0.02	11.63 ± 0.02
11.63 ± 0.02	11.66 ± 0.02	11.64 ± 0.02
11.63 ± 0.02	11.64 ± 0.02	11.64 ± 0.02
11.63 ± 0.02	11.65 ± 0.02	11.64 ± 0.02
11.63 ± 0.02	11.64 ± 0.02	11.65 ± 0.02
11.64 ± 0.02	11.66 ± 0.02	11.66 ± 0.02

Table 3.4: Median values of the halo mess estimates for the 10 sim-projected samples obtained with eq.3.2 and eq.3.3 and as given by the simulation. The uncertainties on the medians are estimated as $1.253\sigma/\sqrt{N}$.

discussed in Yang et al. (2007) works well for groups with $f_{edge} > 0.6$, that in the PM2GC sample constitute the 96% of the whole sample.

Taking into account the edge correction, I recalculated the stellar mass for each group and flag the ones with $LogM_* > 0.003 \cdot \sigma + 10.4$ that, according to the statistics derived in section 3.3.4, should be the ones with the lower fraction of interlopers.

3.4.2 Halo masses

Finally, I calculated the dark matter halo masses for the whole PM2GC catalog (groups, binaries and single galaxies) exploiting equations 3.2 and 3.3. Due to the different cosmology adopted in the PM2GC and in the Millennium Simulation, I converted the stellar mass estimates of the PM2GC sample by summing a factor of 0.09 to the magnitudes that enter the Bell & DeJong formula, that translates into a factor of ~ 0.032 on the mass.

To take into account the cosmic variance (or, more accurately, sample variance), I computed the final halo mass as the mean of the ten halo masses obtained using the fit parameters listed in tables 3.3 and 3.4 and considered the scatter among them in the errors. The final catalog thus includes the two different halo mass estimates and relative errors. Figure 3.11 shows the results obtained for the group sample: colored crosses represent the values obtained for each set of parameters listed in tables 3.3 and 3.4, while the red dots mark the final mean values.

Figure 3.12 finally shows the distribution of halo masses obtained from eq.3.2 (left) and eq.3.3 (right) for single galaxies (blue), binary systems (red) and groups (green) in

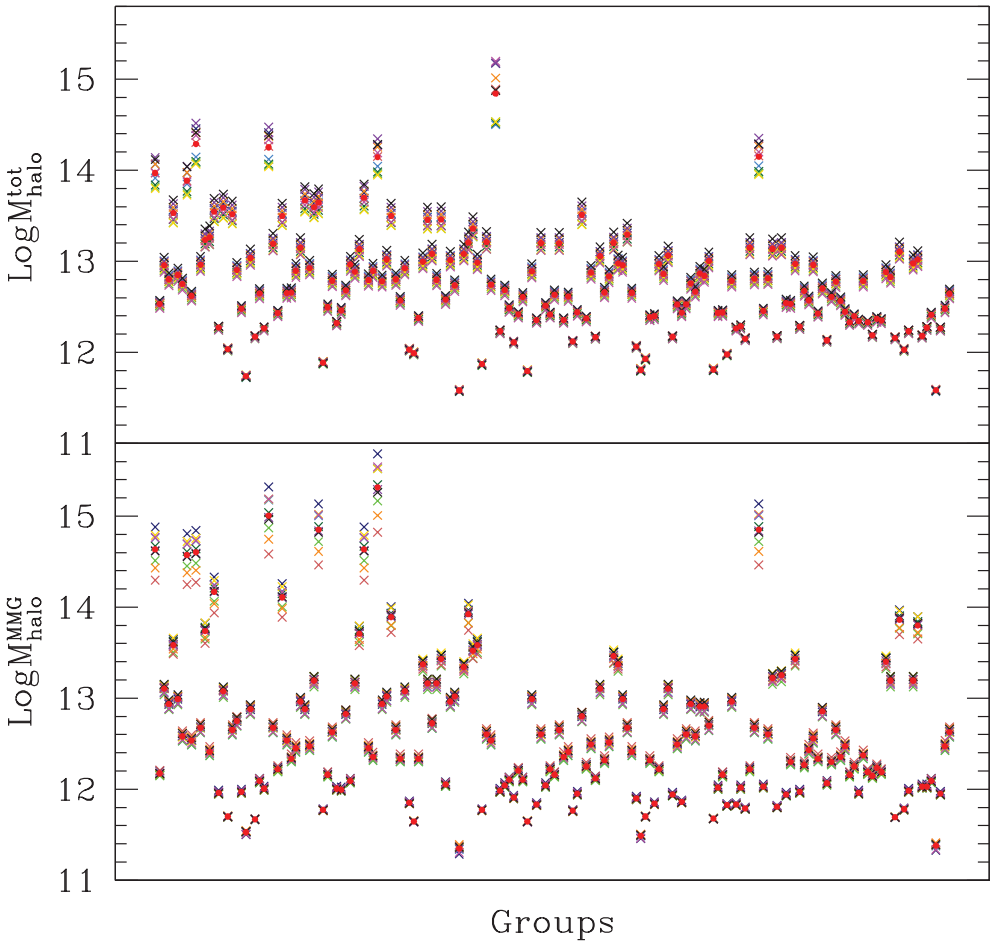

Figure 3.11: Halo masses obtained for the PM2GC group sample exploiting equation 3.2 (lower panel) and 3.3 (upper panel). Colored crosses represent the values obtained for each set of parameters listed in tables 3.3 and 3.4, while the red dots mark the final mean values.

the PM2GC. The median halo masses are marked with arrows and the values are listed in table 3.5.

Given the results of the comparison between the halo masses estimated for the mock catalogs, the relation linking the total stellar mass to the dark matter halo mass seems to produce a better estimate of the true halo mass and thus I consider the mass computed from equation 3.3 for the following applications.

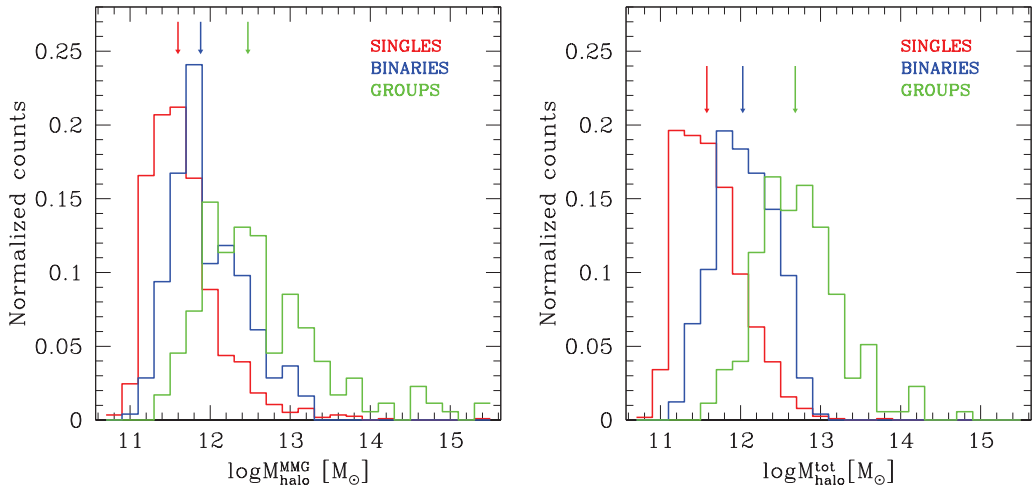

Figure 3.12: Mass distribution of halo masses obtain from eq.3.2 (left) and eq.3.3 (right) for single galaxies (blue), binary systems (red) and groups (green) in the PM2GC.

Sample	$\text{Med}_{sin} \pm \sigma$	$\text{Med}_{bin} \pm \sigma$	$\text{Med}_{gr} \pm \sigma$
logM^{MMG}_{halo}	11.59 ± 0.02	11.88 ± 0.04	12.47 ± 0.08
logM^{tot}_{halo}	11.58 ± 0.02	12.03 ± 0.03	12.68 ± 0.05

Table 3.5: Median values of the halo mess estimates obtained with eq.3.2 and eq.3.3 for single galaxies (col. 2), binary systems (col.3) and groups. The uncertainties on the medians are estimated as $1.253\sigma/\sqrt{N}$.

Below an example of the final catalogs is shown. The complete catalogs will be fully presented in Paccagnella et al. in preparation. The main new properties of a subsample of groups are given in table 3.6. The different columns indicate: (1) PM2GC group serial number; (2) median group redshift; (3) velocity dispersion with its error (km/s); (4) number of member galaxies; (5) R_{200} in Mpc; (6) edge flag; (7) edge correction; (8) Logarithm of the total stellar mass; (9) Logarithm of the stellar mass of the MMG; (10) B-V for the MMG; (11) Logarithm of the halo mass obtained form equation 3.2; (12) Logarithm of the halo mass obtained form equation 3.3; (13 and 14) errors on the halo mass estimates.

In table 3.7 we list the properties of a subsample of binaries. The different columns indicate: (1) PM2GC binary ID; (2) Logarithm of the total stellar mass; (3) Logarithm of the stellar mass of the MMG; (4) B-V for the MMG; (5) Logarithm of the halo mass

obtained form equation 3.2; (6) Logarithm of the halo mass obtained form equation 3.3; (7 and 8) errors on the halo mass estimates.

Table 3.8 gives an example of the catalog for single galaxies. The different columns indicate: (1) MGC ID; (2) redshift; (3 and 4) right ascension and declination at epoch J2000 (5) Logarithm of the stellar mass; (6) Logarithm of the halo mass obtained form equation 3.2; (7) Logarithm of the halo mass obtained form equation 3.3; (8 and 9) errors on the halo mass estimates.

3.5 Summary

In this Chapter I introduced the general field sample extracted from the PM2GC galaxy catalog, a database of groups and galaxies in the local Universe. The sample includes galaxies in the redshift range $0.03 < z < 0.11$ and brighter than $M_B = -18.7$, whose environment (i.e. groups, binaries and single galaxies) was characterized by means of a Friend of Friend (FoF) algorithm.

In order to estimate the halo mass of these systems, I exploited a detailed mock galaxy catalog built from the De Lucia and Blaizot (2007) semi-analytic models run on the Millennium Simulation. To compare simulations to observations, a sample as similar as possible to the observed ones was assembled, selecting portions of "simulated sky" at $z = 0.06$ corresponding to square boxes of $\sim 38 deg^2$. To account for cosmic variance, 10 simulated field samples were selected. A sim-projected catalog was built from these extractions, applying the same FoF algorithm run on the PM2GC sample and all quantities were computed with the same methods that would be used observationally. Halo masses were assigned to these systems exploiting the information given by the simulation. This catalog was used to constrain the parameters of two simple functional forms connecting respectively the mass of the most massive galaxy and the total stellar mass to the dark matter halo mass.

Even if both these relationships are found to produce a good estimate of the true halo mass, the one connecting the the total stellar mass to the halo mass introduces a lower scatter, thus lower errors in the inferred halo masses. I therefore decided to adopt the latter estimate in the following analysis.

From these equation I was able to derive the halo masses of the PM2GC systems, spanning the entire range in richness. In order to assign halo masses to the groups of the PM2GC I first had to correct for edge effect and then recalculate the total stellar mass.

The comparison between the sim-projected and simulated quantities further allowed to

test the performance of the group finder algorithm in terms of contamination by interlopers and distinguish between low and high contaminated groups. I presented the final catalogs for groups, binaries and single galaxies including both values for the halo mass with relative errors.

PM2GC	z	$\sigma \pm \sigma_{err}$	N	R_{200}	edge	f_{edge}	$LogM_*$	$LogM_{MMG}$	$B-V_{MMG}$	$M_{halo,1}$	$M_{halo,2}$	σ_1	σ_2
1000	0.1004	358 ± 46	24	0.844	2	0.87	12.2	11.66	0.938	14.634	13.969	0.18	0.126
1001	0.0813	143 ± 77	5	0.341	1	1.0	11.069	10.74	0.742	12.174	12.532	0.019	0.028
1003	0.0921	43 ± 41	3	0.101	1	1.0	11.278	11.1	0.839	12.936	12.801	0.041	0.043
1004	0.0632	432 ± 58	19	1.037	2	0.98	11.832	11.32	0.899	13.584	13.53	0.06	0.087
1007	0.0944	196 ± 150	6	0.462	1	1.0	11.238	10.96	0.831	12.581	12.749	0.038	0.04
1008	0.0948	423 ± 87	18	0.999	2	0.78	12.127	11.64	0.893	14.572	13.887	0.172	0.117
1009	0.0732	184 ± 176	3	0.438	1	1.0	11.138	10.94	0.938	12.536	12.62	0.036	0.033
1011	0.0912	545 ± 53	56	1.29	2	0.89	12.51	11.65	0.914	14.603	14.289	0.176	0.173
1012	0.0927	171 ± 38	6	0.406	1	1.0	11.4	11.0	1.073	12.675	12.963	0.04	0.053
1013	0.0666	234 ± 57	4	0.56	1	1.0	11.604	11.37	0.812	13.737	13.235	0.074	0.069
1015	0.0977	398 ± 95	20	0.94	1	1.0	11.626	10.88	0.907	12.411	13.264	0.03	0.071
1016	0.0811	233 ± 72	12	0.555	1	1.0	11.843	11.51	0.881	14.17	13.544	0.122	0.088
1021	0.0949	431 ± 66	24	1.018	2	0.915	11.88	11.15	0.764	13.077	13.59	0.04	0.091
1024	0.0597	198 ± 140	5	0.476	1	1.0	11.356	11.03	0.885	12.75	12.904	0.041	0.049
1025	0.05	88 ± 45	5	0.213	1	1.0	11.027	10.58	0.845	11.972	12.48	0.014	0.025
1027	0.0961	153 ± 91	4	0.361	1	1.0	11.455	11.08	0.823	12.881	13.036	0.041	0.057
1031	0.0823	662 ± 81	3	0.146	1	1.0	10.847	10.61	0.544	12.006	12.264	0.014	0.016
1033	0.0952	662 ± 59	61	1.565	2	0.92	12.472	11.78	0.895	15.007	14.252	0.227	0.167
1036	0.0889	266 ± 165	6	0.63	2	0.725	11.805	11.49	0.823	14.108	13.496	0.115	0.085
1037	0.0399	106 ± 99	3	0.258	1	1.0	11.162	10.94	0.896	12.536	12.65	0.036	0.035

Table 3.6: The main new properties of a subsample of groups. The different columns indicate: (1) PM2GC group serial number; (2) median group redshift; (3) velocity dispersion with its error (km/s); (6) number of member galaxies; (5) R_{200} in Mpc; (6) edge flag; (7) edge correction; (8) Logarithm of the total stellar mass; (9) Logarithm of the stellar mass of the MMG; (10) (B-V) for the MMG; (11) Logarithm of the halo mass obtained form equation 3.2; (12) Logarithm of the halo mass obtained form equation 3.3; (13 and 14) errors on the halo mass estimates.

IDbin	LogM$_*$	LogM$_{MMG}$	$B-V_{MMG}$	M$_{halo,1}$	M$_{halo,2}$	σ_1	σ_2
1.0	10.581	10.38	0.819	11.782	11.974	0.007	0.011
2.0	10.193	9.93	0.653	11.457	11.622	0.018	0.009
3.0	10.954	10.91	0.518	12.472	12.39	0.034	0.021
4.0	10.831	10.8	0.81	12.267	12.245	0.023	0.015
5.0	10.241	10.18	0.326	11.626	11.661	0.005	0.009
6.0	10.096	9.99	0.585	11.495	11.546	0.015	0.007
7.0	10.752	10.48	0.845	11.871	12.156	0.011	0.013
8.0	11.271	11.07	0.874	12.854	12.792	0.041	0.043
9.0	9.959	9.86	0.524	11.412	11.446	0.025	0.005
10.0	9.8	9.61	0.262	11.26	11.341	0.043	0.005
11.0	10.552	10.51	0.728	11.9	11.945	0.012	0.011
12.0	10.707	10.68	0.711	12.091	12.107	0.016	0.012
13.0	10.918	10.83	0.832	12.318	12.347	0.026	0.019
14.0	10.931	10.9	0.826	12.451	12.363	0.033	0.02
15.0	10.227	10.11	0.558	11.576	11.649	0.008	0.009

Table 3.7: An example of the catalog for a subsample of binaries. The different columns indicate: (1) PM2GC binary ID; (2) Logarithm of the total stellar mass; (3) Logarithm of the stellar mass of the MMG; (4) B-V for the MMG; (5) Logarithm of the halo mass obtained form equation 3.2; (6) Logarithm of the halo mass obtained form equation 3.3; (7 and 8) errors on the halo mass estimates.

IDMGC	zMGC	RA	DEC	LogM$_*$	M$_{halo,1}$	M$_{halo,2}$	σ_1	σ_2
61514.0	0.084	215.954	-0.248	10.57	11.961	11.963	0.013	0.011
27280.0	0.097	179.891	-0.026	10.2	11.639	11.627	0.004	0.009
11383.0	0.064	161.514	0.147	10.11	11.576	11.557	0.008	0.007
66778.0	0.108	220.11	0.01	9.91	11.443	11.413	0.02	0.004
52268.0	0.108	207.99	-0.188	10.47	11.861	11.865	0.01	0.011
56234.0	0.105	211.446	0.02	10.13	11.589	11.572	0.007	0.008
16076.0	0.081	167.171	0.193	10.56	11.951	11.953	0.013	0.011
13606.0	0.108	164.023	-0.039	9.95	11.469	11.44	0.018	0.005
57725.0	0.08	213.087	-0.158	9.8	11.377	11.341	0.027	0.005
25661.0	0.059	178.081	-0.186	10.21	11.647	11.636	0.004	0.009
60827.0	0.074	215.59	-0.177	9.7	11.314	11.28	0.032	0.008
46480.0	0.098	201.688	-0.17	9.26	11.062	11.051	0.065	0.026
25285.0	0.096	177.455	-0.261	9.6	11.255	11.222	0.04	0.011
60138.0	0.064	214.843	-0.08	9.42	11.15	11.127	0.056	0.019
55832.0	0.047	211.398	0.185	10.76	12.203	12.165	0.02	0.013

Table 3.8: Catalog example for single galaxies. The different columns indicate: (1) MGC ID; (2) redshift; (3 and 4) right ascension and declination at epoch J2000 (5) Logarithm of the stellar mass; (6) Logarithm of the halo mass obtained form equation 3.2; (7) Logarithm of the halo mass obtained form equation 3.3; (8 and 9) errors on the halo mass estimates.

4

The galaxy properties

In this chapter I discuss the method adopted to compute the properties of the galaxy samples studied in the following analysis.
Stellar masses, star formation histories and average stellar ages of galaxies were derived by analyzing their integrated spectra by means of the spectrophotometric code SINOPSIS. The code includes also an automatic routine to measure the equivalent width of the spectral lines. I briefly and schematically recall the main features and parameters of the code.
I also present the MORPHOT tool that have been applied to B and V images in order to get the morphological classification. Photometric information are finally exploited to compute stellar masses through the Bell and de Jong (2001) prescription and define the mass completeness limit of the samples.

4.1 Galaxy properties from spectroscopic information: SINOPSIS

SINOPSIS (**SI**mulati**N**g **OP**tical **S**pectra w**I**th **S**tellar population models) (Fritz et al., 2007, 2011, 2014) is a significantly improved and extended version of the spectrophotometric code developed by Poggianti et al. (2001) to derive the star formation histories of a sample of Luminous Infrared galaxies from their average spectrum. The goal of this model is to reconstruct the star formation history (SFH, hereafter) of galaxies, hence the amount of stars formed at each epoch throughout the galaxy evolutionary history. To this aim, the code measures the mean features of an optical spectrum, namely the average flux in significant portions of continuum–dominated spectral regions, and the equivalent

width (EW) of emission and absorption lines, and tries to find a model that minimizes the differences with these observable features in the data.

This model assumes that an observed spectrum is a combination of simple stellar population spectra, and therefore a galaxy model spectrum is computed by adding the synthetic spectra of Single Stellar Populations (SSPs) of different ages built with a Salpeter (1955) initial mass function (IMF) with stellar masses in the range $0.15 \leq M \leq 120 M_{\odot}$. To compose the final model, each spectrum is first of all multiplied by an appropriate mass value according to the SFH and, before being added, it is extinguished to simulate dust in a uniform screen geometry. The final synthetic spectrum will hence have the form:

$$L_{mod} = \sum_{i=1}^{N_{SSP}} M_i \cdot L_i(\lambda) \cdot 10^{-0.4(A(\lambda) R_V E(B-V)_i)} \tag{4.1}$$

where N_{SSP} is the number of SSPs used, M_i and $L_i(\lambda)$ are the values of stellar mass and luminosity per unit of stellar mass of the i SSP respectively, $A(\lambda)$ represents the extinction law, $E(B\text{-}V)_i$ is the color excess assigned to the i SSP and finally R_V is the ratio of total to selective absorption $A_V/E(B-V)$. Notice that only positive values for extinction are allowed. A significant characteristic of this spectrophotometric model concerns the treatment of dust obscuration. For the sake of generality the Galactic extinction curve ($R_V = 3.1$, Cardelli et al. (1989)) is adopted, but the value of color excess, E(B-V) is left free to vary from one population to another, according to the hypothesis of selective extinction: the youngest stellar populations are expected to be still embedded within the dusty molecular clouds where they formed, thus generally dust extinction will be higher for younger stellar populations (Calzetti et al., 1994; Poggianti and Wu, 2000). This treatment of dust obscuration is not only a more realistic description of the real situation but is also required when one wants to reproduce also the intensity of emission lines, which are the most prominent features of the youngest stars and the most prone to dust extinction.

Concerning metallicities, one of the main hypotheses of the model is that all the stellar populations in a galaxy have a common metallicity value at any age. So a homogeneous value for the metallicity of theoretical spectra is adopted and the model is left free to choose between three different sets of metallicities: sub-solar (Z = 0.004), solar (Z = 0.02) and super-solar (Z = 0.05). Fitting an observed spectrum with a single value of the metallicity is equivalent to assuming that this value belongs to the stellar population that is dominating its light. It is clear that assuming a single value for the SSP's metallicity is a simplifying assumption since, in practice, the stellar populations of a galaxy span

Age interval	[yr]	ΔT [yr]
$(0 \div 2)$	$\times 10^6$	2.0×10^6
$(2 \div 4)$	$\times 10^6$	2.0×10^6
$(4 \div 7)$	$\times 10^6$	3.0×10^6
$(7 \div 20)$	$\times 10^6$	1.3×10^7
$(2 \div 6)$	$\times 10^7$	4.0×10^7
$(6 \div 20)$	$\times 10^7$	1.4×10^8
$(2 \div 6)$	$\times 10^8$	4.0×10^8
$(6 \div 10)$	$\times 10^8$	4.0×10^8
$(1 \div 3.2)$	$\times 10^9$	2.2×10^9
$(3.2 \div 5.6)$	$\times 10^9$	2.4×10^9
$(5.6 \div 10)$	$\times 10^9$	4.4×10^9
$(1 \div 1.41)$	$\times 10^{10}$	4.1×10^9

Table 4.1: The ages and durations (ΔT) of the set of averaged SSP spectra used in SINOPSIS, as it was built according to the criteria explained in the text. Here ΔT is the time interval over which the SFR is assumed to be constant.

a range in metallicity value. A check on the reliability of the mass and star formation histories derived using this method has been performed analyzing synthetic spectra of different SFHs with metallicity that varies as a function of stellar ages, so to simulate the chemical evolution of the galaxy, and it turns out that the way metallicity is treated does not introduce any bias in the recovered stellar mass or SFH (Fritz et al., 2007).

The synthetic spectra for the model were taken from a combination of two different sets that both use Padova evolutionary tracks (Bertelli et al., 1994) and with stellar ages ranging from 10^5 to 20×10^9 years. The first set uses the Jacoby et al. (1984) library of observed stellar spectra in the optical domain for ages younger than 10^9 years and is composed of spectra of 108 different ages, while for older SSPs spectra were taken from the MILES library (Sánchez et al., 2006). Both sets were degraded in spectral resolution, in order to match that of the observed spectra.

The stellar age resolution of this initial set of SSP had to be reduced in order to make it adequate to the capabilities of the spectral analysis. To this aim a new set of stellar population spectra was built, starting from the 108 SSPs, averaging all the SSP spectra with ages within 12 given time intervals. This time intervals were chosen on a physical basis, considering the stellar ages at which the main spectral features change significantly. The chosen age and time intervals are listed in table 4.1. Finally, the emission from ionized gas in the interstellar medium was included by means of the photoionisation code CLOUDY (Ferland, 1996), so that the youngest SSPs display hydrogen and forbidden

emission lines, mainly of oxygen, nitrogen and sulfur. Furthermore, dust emission from circumstellar envelopes of AGB stars has been added as in Bressan et al. (1998).

The code aims to find the combination of 12 mass and extinction values that better fits the observed spectrum. The comparison is done on the flux measured on a certain number of bands in the continuum and on the values of equivalent width of spectral lines both in emission and in absorption. A technique for the automatic measure of the lines EW both in emission and in absorption has hence been developed by Fritz et al. (2007) (see section 4.1.1). The observed errors on the flux are computed by taking into account the local spectral signal-to-noise ratio, while uncertainties on the equivalent widths are derived mainly from the measurements method. Due to the presence of extinction, the search of the combination of parameters that minimizes the differences between the observed and model spectrum is a non-linear problem and it is also under-determined, which means that the number of constraints is lower than the number of parameters. In order to find it, an Adaptive Simulated Annealing algorithm randomly explores the parameters space, searching for the absolute minimum of a standard χ^2 function which is given by:

$$\chi^2 = \sum_{i=1}^{N} \left(\frac{M_i - O_i}{\sigma_i}\right)^2$$

where M_i and O_i denote the quantities measured from the model and observed spectra, respectively, σ_i the observed uncertainties and N the total number of observed constraints.

The solution given with this method is non-unique, due to the limited wavelength range under analysis, together with the age-metallicity degeneracy and the already mentioned non-linearity and underdetermination. To account for this, error-bars are associated to mass, extinction and age values.

4.1.1 Equivalent width computation

When trying to reconstruct the characteristics of the stellar populations in a galaxy, a very important information is carried by the spectral lines. Not only equivalent width values are used as constrains for the model spectrum described in the previous section (note that not all of the line are used as constraints, some are just measured), but are also crucial for the science coming from the analysis of the spectra. For example, the presence and strength of the emission and absorption lines can be used to derive the spectral classification and investigate the frequency of the various spectral types as a function of both the clusters' properties and the galaxies' characteristics (see Chapter 6). Given the

huge number of spectra of the original WINGS sample, Fritz et al. (2007) developed an automatic technique which is capable of measure the EW of lines both in emission and in absorption, being also able to distinguish if the line is absent or if it is dominated by features such as bad sky subtraction or spectral noise. The main issue when computing the EW of a line is an appropriate choice of the continuum level that translates into the correct choice of the value of the full width at zero intensity, $\Delta\lambda$, which is symmetric with respect to the nominal (theoretical) line's center. To find the proper EW value, the algorithm first measures the line over a very short interval $\Delta\lambda$, which under samples the real value; then, various values of the EW are computed as a function of $\Delta\lambda$, which is increased at steps of 1Å, starting from an initial width of 4 to 8 Å, depending on which line is measured, up to ∼80 Å. The correct value of the EW is found, among those measured in this way, by analyzing the EW trend curve. The absolute value of the EW, in general, monotonically increases with $\Delta\lambda$ and the point where the trend curve has its first change in slope is generally where the line should ideally be measured for both emission and absorption lines. An important exception is the case of an absorption + emission profile, which can be easily found in lines such as $H\beta$, or $H\gamma$. In this case, the first change in the slope of the trend curve happens in correspondence to the change from sampling the emission and the absorption profile and is the second change in slope that identifies the correct EW value. The $H\alpha$ line is treated in a different way to consider, when the line is in emission, also the effect of the close two Nitrogen forbidden lines. In this case the trend curve analysis may become too complicated and a fixed $\Delta\lambda \sim 70$ Å is adopted, to safely include both Hα and the Nitrogen lines. The characteristics of the EW trend curve are also used to estimate the error that this method can, at least in principle, introduce to the EW estimate. As already pointed out, the choice of the continuum is critical, given that the EW measurement is quite dependent on its fluctuations, hence, on the local S/N. To account for this an errorbar is defined by taking the semidifference of the EW values measured with a $\Delta\lambda$ of 5 Å smaller and larger, respectively, than the value used for the line measurement. This, together with a factor that depends on the line intensity, is used to compute the error on EW.

4.1.2 The properties of stellar populations

Fitting the main features of an optical spectrum allows to derive the characteristics of the stellar populations whose light we see in the integrated spectrum. Here I briefly describe how the properties of the stellar populations, that will be used for the following analysis,

are derived from the spectrophotometric synthesis. A full description of the measurements and stellar population properties is given in Fritz et al. (2011), together with the validation of the results and the presentation of the complete catalog.

As far as the OmegaWINGS and WINGS spectra are concerned, the galaxy masses and star formation rates have been derived by fitting the fiber spectra and thus suffer from aperture effect: the fiber diameters were 2.16″ (AAT) and 1.6″ (WHT), therefore the spectra cover only the central 1.3 to 2.8 kpc of our galaxies depending on the cluster redshift (see Cava et al. 2009 for details). To recover the galaxy-wide integrated properties, all the derived quantities have been scaled from the fiber to the total magnitude, using the ratio of total to aperture fluxes.

Moreover, due to the configuration of the 2dfdr spectrograph, which is a dual-beam system with two arms overlapping around 5700 Å, for each object observed with this instrument two spectra were obtained, which were spliced into the full final spectrum. Despite the overlap that is quite extended, the region of the spliced spectrum often results quite noisy, due to normalization issues and might significantly alter the SFRs and mass estimates. To avoid this problem, only of the blue part of the continuum, ranging from about 3600 Å to 5700 Å, was fitted. This does not affect the EW measurements used in the following analysis (at our redshifts the interesting lines fall outside the overlapped region) and in this case the spliced spectra were used.

Stellar mass

As already made clear by Longhetti and Saracco (2009) and Renzini (2006), the use of spectral synthesis techniques leads to three different definitions of the stellar mass, namely:

1. the initial mass of the SSP, at age zero; this is nothing but the mass of gas turned into stars;

2. the mass locked into stars, both those which are still in the nuclear-burning phase, and remnants such as white dwarfs, neutron stars and stellar black holes;

3. the mass of stars that are still shining, i.e. in a nuclear burning phase.

It should be noticed that the difference between these three definitions is a function of the stellar age and of the IMF. The code provides masses calculated using all of the aforementioned definitions, but only the masses defined according to definition 2. will be used in the next chapters. Given that the theoretical spectra are given in luminosity per unit of solar mass, to compute the values of stellar mass the model spectrum is converted

to flux by accounting for the luminosity distance factor and the K-correction (which is naturally performed by fitting the spectra at their observed redshifts).

Star formation rate and Star formation history

The search for the best fit-model, as already discussed in section 4.1, is performed using 12 SSPs of different ages, obtained, in turn, by binning a much higher age-resolution stellar age grid. The star formation history is then given as the star formation rate in the 12 bins that is computed by dividing the stellar mass of a given age bin by its duration. Definition 1 of the mass was applied in this calculation. However, there is an intrinsic degeneracy in the typical features of spectra of similar age, hence, an intrinsic limit to the precision of this method in determining the age of the stellar populations that compose a spectrum. This means that we may be not able, in general, to distinguish between patterns of SFH and extinction that differ in the ages of the dominant stellar populations by small amounts, and also that similar spectral features can be obtained with different linear combination of parameters.

I will hence consider as meaningful only the estimates of the SFR in bigger main age bins depending on properties of the stellar populations I aim to describe and I will discuss in the relative sections. Moreover, the current SFR value is taken to be the one referring to the time interval ranging from 0-20My and is calculated by fitting the equivalent width of emission lines, namely Hydrogen (Hα and Hβ) and Oxygen ([OII] at 3727 Å). The lines' luminosity is entirely attributed to star formation processes neglecting other mechanisms that can produce ionizing flux.

The SFRs given as output by SINOPSIS only refer to values normalized to the fiber-aperture magnitude. In order to compute the global value, one should multiply the fiber-SFR by the ratio of total and aperture fluxes.

Starting from the global SFR, I defined as specific star formation rate (SSFR) the SFR per unit of galaxy stellar mass, i.e. $SSFR = SFR/M_*$. By definition, the SSFR dimensionally is the inverse of the timescale of the formation of the entire stellar mass of a galaxy ($[SSFR] = yr^{-1}$). This quantity is an indicator of the contribution of the current star formation process to the stellar mass growth of galaxies. Low SSFRs indicate that the processes of star formation were more active in the past, while high SSFRs mean that a significant fraction of the stellar mass of the galaxy is currently being built.

Average ages

The code provides also an estimate of the average age of a galaxy, weighted on the stellar populations that compose its spectrum. Given that the mass-to-light ratio changes as a function of the age, there are two different definitions that can be given: the mass-weighted and the luminosity-weighted age (see also Fernandes et al., 2003). The latter is directly derived from the spectrum, being weighted in this way towards the age of the stellar populations that dominate the light, while the first definition requires the knowledge of the mass distribution as a function of stellar age, i.e. the SFH. The logarithm of of the luminosity weighted age is given by:

$$\langle \log(T) \rangle_L = \frac{1}{L_{tot}(V)} \times \sum_{i=1}^{N_{SSP}} L_i(V) \times \log(t_i) \tag{4.2}$$

where $L_i(V)$ and $L_{tot}(V)$ are the restframe luminosities of the *i-th* SSP and of the total spectrum, respectively, in the V-band, and t_i the age of the $i-th$ SSP.

$$\langle \log(T) \rangle_M = \frac{1}{M_{tot}} \times \sum_{i=1}^{N_{SSP}} M_i \times \log(t_i) \tag{4.3}$$

and, similarly, M_{tot} and M_i are the total mass and the mass of the *i-th* SSP, respectively. Hence, while the luminosity-weighted age gives an estimate of the age of stars that dominate the optical spectrum, being in this way more sensitive to the presence of young stars, the mass-weighted value is more representative of the actual average age of a galaxy's stellar populations. To compute these values the finest age grid (12 ages) are averaged.

4.2 Galaxies properties from photometric information

4.2.1 Morphologies

For both the WINGS and the PM2GC samples, morphological types were derived from V-band and B-band images respectively using MORPHOT, an automatic tool purposely devised in the framework of the WINGS project (Fasano et al., 2012). MORPHOT was designed with the aim to reproduce as closely as possible visual morphological classifications. It extends the classical Concetration/ Asymmetry/clumpinesS (CAS) classification (Conselice 2003) by using 20 different image-based morphological diagnostics, 14 of them have never been used, while the remaining six (besides the CAS parameters, the Sersic

index, the Gini and M20 coefficients (Lotz et al., 2004)) are actually already present in the literature, although in slightly different forms. We refer the reader to Fasano et al. (2010) and Fasano et al. (2012) for an outlining of the logical sequence and the basic procedures of MORPHOT and an exhaustive description of the tool.

MORPHOT assigns a morphological type (T_M) to each galaxy from -6 (cD) to 11 (irregulars).

The morphological classification of the OmegaWINGS sample is currently underway (Fasano et al. in preparation). For the purposes of this thesis, G.Fasano visually classified the morphologies of the post starburst galaxies in our sample (see Chapter 6) which are not in the original WINGS sample, by inspecting the V-band images.

In the following, I will consider three main morphological classes: ellipticals (MORPHOT type $-5 \leq T_M < -4.25$), S0s ($-4.25 \leq T_M \leq 0$) and late-types ($T_M > 0$).

4.2.2 Galaxy stellar masses

For the WINGS and the PM2GC samples, stellar masses were estimated also following the method proposed by Bell and de Jong (2001). The authors, using spectrophotometric model in conjunction with simplified spiral galaxy evolution models, found a strong correlation between stellar M/L ratio and optical colors of the integrated stellar populations for a wide range of star formation histories. They found that, under the assumption of a universal IMF, relative trends in model stellar M/L with color are robust to uncertainties in stellar population and galaxy evolution modeling, including the effect of modest bursts of star formation. In addition, errors in the dust-reddening estimates do not significantly affect the final derived stellar masses.

Stellar masses were computed by Calvi et al. (2011) and Vulcani et al. (2011) for the PM2GC and WINGS catalogs respectively, using the relation between M/L_B and rest-frame (B-V) color and the equation given by Bell and de Jong (2001):

$$log_{10}(M/L_B) = a_B + b_B(B-V). \tag{4.4}$$

For the Bruzual & Charlot model with a Salpeter (1955) IMF (0.1-125 $M_\odot$) and solar metallicity, $a_B = -0.51$ and $b_B = 1.45$.

For the WINGS sample the total luminosity L_B was derived from the total (SEXTRACTOR AUTO) observed B magnitude (Varela et al., 2009), corrected for distance modulus and Galactic extinction, with k-correction given by Poggianti and Barbaro (1997). The rest frame $(B-V)$ color is the observed color derived from magnitudes measured within

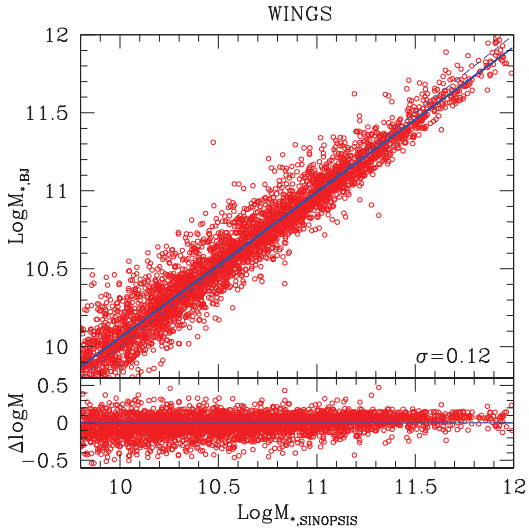

Figure 4.1: Comparison between the masses estimated following the spectrophotometric code SINOPSIS (Fritz et al., 2007, 2011) and those derived from the Bell and de Jong (2001) formulation for the WINGS sample. The blue dashed line is the 1:1 relation, the solid line represents the least square fit for galaxies above the mass completeness limit. The bottom panel shows the difference between the two mass estimates.

a diameter of 10 kpc, corrected for Galactic extinction and k-corrected as the total magnitude.

For PM2GC galaxies, B-band photometry from the MGCz was taken. Rest frame $(B-V)$ color has been computed from the Sloan $g-r$ extinction corrected color. A typical error of $\sim$0.2-0.3 dex was estimated performing a comparison with masses estimated through other methods. In the following, for consistency with the literature, I will use for the PM2GC sample stellar masses estimated following this technique, while I will take advantage of the estimates given by SINOPSIS for the OmegaWINGS+WINGS sample.

Figure 4.1 shows the comparison of the Bell and de Jong (2001) masses and the SINOPSIS stellar masses (computed according to definition n.2, see section 4.1 and converted to the appropriate IMF) for the WINGS sample. Discrepancies are $\sim$0.2 dex, which corresponds to the typical error on the mass estimates. The same test has been performed on the PM2GC stellar masses in Calvi et al. (2011) who found a similar dispersion.

Mass completeness limit

Equation 4.4 has been used also to derive the mass completeness limit of both the OmegaWINGS and PM2GC catalogs (see Vulcani et al., 2011; Calvi et al., 2012). The mass-limited samples ensure completeness, that is, include all galaxies more massive than the limit, regardless of their morphologies and colors. This is the best choice to properly characterize galaxy masses and related properties. The galaxy stellar mass limit was computed as the mass of an object whose observed magnitude is equal to the faint magnitude limit of the survey, and whose color is the reddest color of a galaxy at the higher redshift considered.

For the WINGS and OmegaWINGS sample the magnitude limit is $V = 20$. Considering the distance module of ~ 37.5 of the most distant cluster and the reddest rest-frame color the magnitude limit corresponds to a mass limit of $M_* = 10^{9.8} M_\odot$ in a Salpeter (0.15-120) IMF, above which the sample is unbiased.

As for the PM2GC, the spectroscopic magnitude limit is $M_B = -18.7$. Considering the reddest rest-frame color $(B - V) = 0.9$, the mass limit is $M_* = 10^{10.38} M_\odot$ for a Salpeter IMF.

5

Galaxies in transition in different environments

In this chapter I present a study of the ongoing star formation rate as a function of stellar mass in different environments. I compare the SFR-M_* relation of star forming galaxies in clusters and in the field and look at variations as a function of the clustercentric distance and of the cluster properties. I also investigate the properties of the different galaxy populations and their star formation histories. This allows to put constraints on both the range of local environments where star formation is quenched and the average timescale over which it happens.

The analysis that follows has been published in Paccagnella et al. (2016) and a second paper is in preparation (Calvi et al. in preparation.)

5.1 Introduction

The distribution of many galaxy properties, including color, morphology and star formation rate (SFR), is bimodal, reflecting the existence of two broad types of galaxies: red, old, quiescent early-type galaxies and dust-reddened or blue, late-type disk galaxies with ongoing star formation. This bimodality is related to the variations in the cold gas content, which lead to different levels of star formation and eventually to quenching. Whether the reasons for galaxies getting quenched are internal or external is of critical importance.

The correlation found between SFR and the total M_* (main sequence, MS, Brinchmann

et al., 2004; Noeske et al., 2007; Elbaz et al., 2007; Daddi et al., 2007) has been interpreted as the result of the balancing of inflows of cosmological gas and outflows due to the feedback (Bouché et al., 2010; Lilly et al., 2013), thus being sensitive to any physical mechanism affecting the amount of gas available for star formation. The star formation quenching seems to be stronger in clusters, which have a higher fraction of early-types and a lower fraction of late-type galaxies than the field (e.g., Dressler, 1980; Poggianti et al., 1999; Bai et al., 2009), suggesting that they are extremely effective in cutting off the galaxy's ability to form stars.

Examples of external processes acting in high-density regions, extensively described in Chapter 1, include ram-pressure stripping (Gunn and Gott, 1972), high speed galaxy encounters (galaxy harassment; Moore et al., 1996), galaxy-galaxy mergers (Mihos and Hernquist, 1994), and removal of the warm and hot halo gas (strangulation; Larson et al., 1980; Balogh et al., 2000).

The most direct way to isolate the effects of the environment is to study the trends in the galaxy population mix in clusters, where most of the aforementioned processes are strongly active, and compare them with the field. Furthermore, it is useful to analyze the radial distribution of member galaxies and how their properties change within the clusters, since the cluster-centric distance traces the cluster density profile and is an approximate time-scale for the star formation quenching (Gao et al., 2004).

While so far the SFR-M_* relation has been largely investigated in the field, only few studies focused on clusters. Using local galaxy field samples, Peng et al. (2010) and Wijesinghe et al. (2012) showed that the local density mostly changes the fraction of passive galaxies but has little effect on the SFR-M_* relation. Focusing on one cluster at the time, also Tyler et al. (2013) and Tyler et al. (2014) failed to identify any difference in the SFR distribution of cluster and field galaxies and did not detect any population of galaxies departing from the MS. This implies that the quenching of star formation is a relatively fast transition. On the other hand, von der Linden et al. (2010) ($z < 0.1$) and Haines et al. (2013) ($0.15 < z < 0.3$) found evidence that galaxies in clusters have lower SFRs than galaxies of similar mass in the field. A population of galaxies with reduced SFR at given mass was discovered in clusters by Patel et al. (2009) at $z \sim 0.8$ and Vulcani et al. (2010) at $0.4 < z < 0.8$.

What is still missing is a detailed study of the local cluster population in a statistically meaningful sample.

Moreover, a complete picture can be depicted comparing the galaxy population in local clusters to that of groups, binary systems and single galaxies. This analysis allows

the study of the properties and the evolution of galaxies in the widest possible range of environments in the local Universe.

I adopt a Salpeter (1955) initial mass function in the mass range 0.15-120 $M_\odot$. The cosmological constants assumed are $\Omega_m = 0.3$, $\Omega_\Lambda = 0.7$ and $H_0 = 70$ km s^{-1} Mpc^{-1}.

5.2 Galaxy sample

To characterize the population mix of galaxies in different local and global environments, I take advantage of two data sets, one drawn from the OmegaWINGS survey and the other from the PM2GC catalog.

Given the different mass completeness limit of the two surveys, when the two samples are used together I considered only galaxies with stellar masses above the PM2GC mass limit.

The SFRs, star formation histories (SFHs), M_*, luminosity- and mass-weighted ages (LWA and MWA, respectively) were derived for both data sets by fitting the spectra with the spectrophotometric model described in section 4.1. As already discussed in 4.1.1, emission lines can be measured down to a limit of 2 Å, while any emission measurement below this threshold is considered unreliable. This sets a lower detection limit that translates into a specific star formation rate limit of $10^{-12.5} yr^{-1}$. To be conservative, I considered as star forming only galaxies with $sSFR > 10^{-12} yr^{-1}$, and I have verified that moving the threshold does not severely affect our results.

5.2.1 The cluster sample

For the OmegaWINGS sample, I selected member galaxies belonging to a subsample of 31 clusters (see sec.2.2) with spectroscopic completeness higher than 50% (including OmegaWINGS clusters observed until January 2015 and the WINGS clusters above the requested completeness). I adopted a mass-limited sample considering only galaxies with masses above the limit defined in sec 4.2.2 of $10^{9.8} M_\odot$. This choice ensure completeness, that is, include all galaxies more massive than the limit, with no bias on color or morphological type. Hence, this is the best way to properly characterize galaxy masses and related properties. A field control sample is extracted from the non-member galaxies in the redshift range $0.02 < z < 0.09$. In clusters, I excluded the BCGs and considered all galaxies within $2R_{200}$. According to the analysis of Guglielmo et al. (2015) and Marziani et al. (2016) the AGN contribution can be neglected. I combined the data from all the

clusters together, to have better statistics and characterize average properties.

The final sample consists of 5065 cluster galaxies and 743 field galaxies (respectively 9242 and 1347 galaxies, once weighted for incompleteness).

5.3 Results

5.3.1 The SFR-M_* relation in clusters and field

The main panel of Figure 5.1 shows the SFR-M_* relation for all SF galaxies in the different environments; the right and top panels show the SFR and M_* distributions, above the mass completeness limit, weighted for incompleteness and normalized to the total.

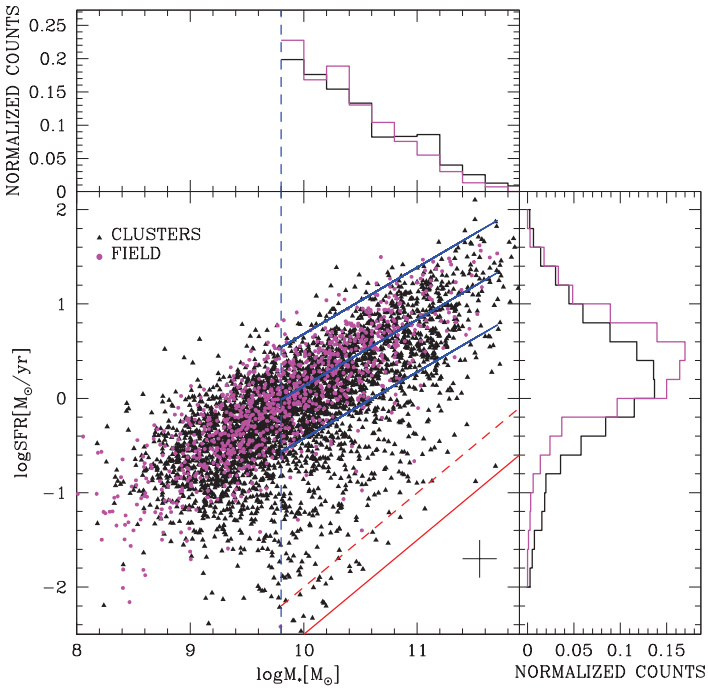

Figure 5.1: Main panel: SFR-M_* relation for cluster (black triangles) and field (magenta circles) galaxies. The blue solid lines indicate the best fit of the field with 1.5σ error, the red solid (dashed) line the $\log sSFR = -12.5(-12)$ *limit. The blue vertical dashed line indicates the mass completeness limit. Typical error-bars on SFR and M_* are indicated in the bottom-right corner. Upper panel: cluster (black) and field (magenta) mass distributions. Right panel: cluster and field SFR distributions above the mass completeness limit. Histograms are normalized to total and weighted for incompleteness.*

Above $M_* > 10^{9.8}$ $M_\odot$, the relation for the field can be fitted, accounting for incompleteness, by the equation

$$\log(SFR) = 0.70 \times \log(M_*/M_\odot) - 6.93 \tag{5.1}$$

with a scatter $\sigma \sim 0.35$ dex. This relation agrees with other MSs at similar redshifts (e.g. Salim et al., 2007; Elbaz et al., 2007) confirming the reliability of our field.

A change of the SFR-M_* relation with the environment is well visible. Even though galaxies in clusters can be as actively star-forming as galaxies in the field, a population with reduced SFRs is evident in the former, while it is much less noticeable in the latter.

To quantify the difference between the different SFR distributions, I performed a Kolmogorov-Smirnov (KS) test that tells whether I can disprove the null hypothesis that two data sets are drawn from the same parent distribution. The test rejects the null hypothesis with a probability $P_{KS} > 99.9\%$ for the SFR weighted distributions and, at a lower level, also for the two weighted mass distributions. To exclude that the differences in the SFR distributions are driven by different mass distributions, we performed 100 Monte Carlo simulations extracting randomly a subsample of SF galaxies with the same mass distribution of the field from the cluster sample. The KS test disproves at a significant level the null hypothesis in 100% of the cases.

Hereafter, I further distinguish between *purely star-forming* (PSF) and *transition* galaxies, the former being within 1.5σ from the field fit, the latter lying below -1.5σ. With this cut, transition galaxies represent $\sim 24\%$ (7%) of the SF cluster (field) population and 9% (4%) of the full cluster (field) sample.

To have a closer view of the stellar mass dependence of the SFR, Figure 5.2 shows the $SSFR - M_*$ relation for star forming galaxies in clusters. Field galaxies are shown as reference. Indeed, the SSFR is a measure of how the ongoing star formation contributes to the mass growth for galaxies of different masses. Clusters and field galaxies follow a similar trend, with decreasing median SSFR at increasing mass, indicating that the mass growth rate at given stellar mass is lower for higher mass. The transition population is still well visible. These galaxies are building-up their mass at a lower rate than main sequence galaxies, as expected given the results discussed above for the SFR.

A further analysis of the SFR and SSFR distributions can be done looking at the SFR and SSFR normalized histograms for cluster and field star-forming galaxies in different stellar mass bins (Fig. 5.3). The population of cluster galaxies with reduced SFR/SSFR with respect to the field can be seen across the entire mass range, as confirmed also by a

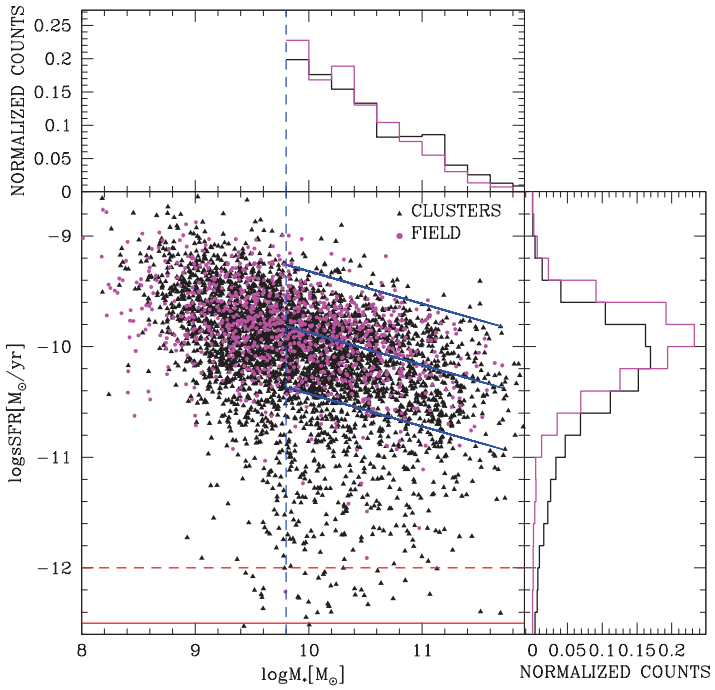

Figure 5.2: Main panel: SSFR-M_* relation for cluster (black triangles) and field (magenta circles) galaxies. The blue solid lines indicate the best fit of the field with 1.5σ error, the red solid (dashed) line the $\log sSFR = -12.5(-12)$ *limit. The blue vertical dashed line indicates the mass completeness limit. Upper panel: cluster (black) and field (magenta) mass distributions. Right panel: cluster and field SFR distributions above the mass completeness limit. Histograms are normalized to total and weighted for incompleteness.*

KS test, which firmly rejects the null hypothesis for all the stellar mass bins considered (P_{KS}=0.0,0.0 and 10^{-3} going from the least towards the most massive galaxies, for both SFR and SSFR).

5.3.2 Radial trends

It is now interesting to investigate the spatial distribution of transition galaxies within the clusters ($0< R/R_{200} <2$) and their impact on the SFR-M_* and SSFR-M_* relation. Figures 5.4 and 5.5 show star-forming galaxies in 6 different bins of projected cluster-centric distance; the field is reported for reference. The median SFRs and SSFRs of all SF galaxies, weighted for incompleteness, have been calculated in 4 mass bins. The quoted uncertainties on the medians are estimated as $1.253\sigma/\sqrt{N}$, where σ is the standard

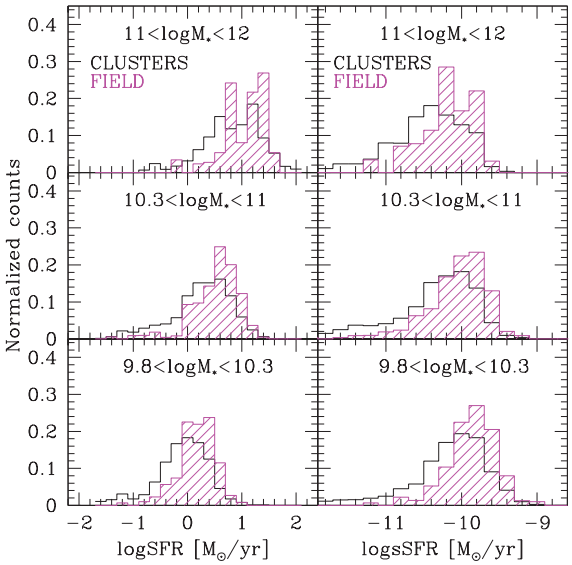

Figure 5.3: Histograms of the distributions for cluster (black) and field (magenta) star-forming galaxies above the mass completeness limit in stellar mass bins for logSFR *(left) and* log$SSFR$ *(right).*

deviation about the median and N is the number of galaxies (Rider, 1960).

Transition galaxies are mainly found within $0.6R_{200}$, where they represent more than 30% of all SF cluster galaxies and are able to significantly lower the median SFR-M_* relation. In these inner regions PSF galaxies are also lacking. The frequency of transition galaxies decreases with increasing distance until they almost disappear outside R_{200}.

I stress that for $R/R_{200} > 1.2$, that corresponds to the radius covered by most of the clusters, the small sample statistics prevents us from drawing solid conclusions, although results do not change if only the 11 clusters that reach $2R_{200}$ are considered.

Both mass and environment play an important role in driving galaxy evolution. The median mass is independent on distance, for PSF, transition and passive galaxies separately (plot not shown), indicating that there is no strong mass segregation. This result suggests that mass and position within the clusters are not strictly related and might play a different role in galaxy quenching.

I can therefore try to separate the two contributions and understand how the impact of the environment depends on the mass of the galaxy. The upper panel of Fig. 5.6 shows the incidence of each sub-population as a function of cluster-centric distance within two mass bins, while the lower panel shows the incidence of each sub-population as a function

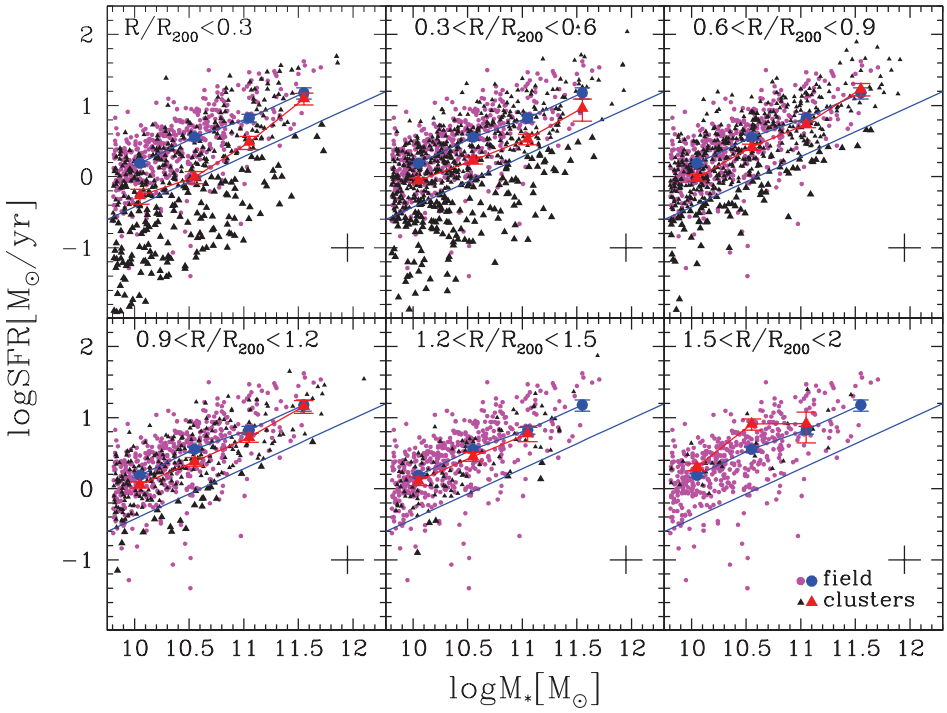

Figure 5.4: SFR-M_* relation above the mass completeness limit in 6 bins of cluster-centric distance, as indicated in the labels. Points and colors are as in Fig. 5.1; big triangles indicate transition galaxies. Blue (field) and red (clusters) big symbols are the medians of SF galaxies weighted for incompleteness in different mass bins; error-bars represent the uncertainty on the median. The blue slanting line shows the limit dividing PSF and transition galaxies. Typical error-bars on SFR and M_* are shown in the bottom-right of each panel.

of mass in two distance bins. Both the mass and radius separation values (respectively $M_* = 10^{10.5} M_\odot$ and $R/R_{200} = 0.6$) used to divide the sample are chosen to have similar numbers of galaxies in each bin. The transition to PSF galaxy ratio (top) strongly depends on distance, being ∼0.6 at $M_* > 10^{10.5} M_\odot$ and 0.8 at $10^{9.8} < M_* < 10^{10.5} M_\odot$ within $0.3 R_{200}$, and rapidly decreases going outward. The fraction of transition galaxies to the total (bottom) also decreases with distance, but is almost constant with mass, in agreement e.g. with Weinmann et al. (2011); Vulcani et al. (2015).

Passive and PSF galaxy fractions strongly depend on both distance and mass. Passive galaxies are the dominant population at all masses inside R_{200} and decrease going outwards, mirrored by PSF galaxies, in agreement with previous studies (e.g. Weinmann et al., 2006; Vulcani et al., 2011). Opposite trends are detected in the field, where PSF

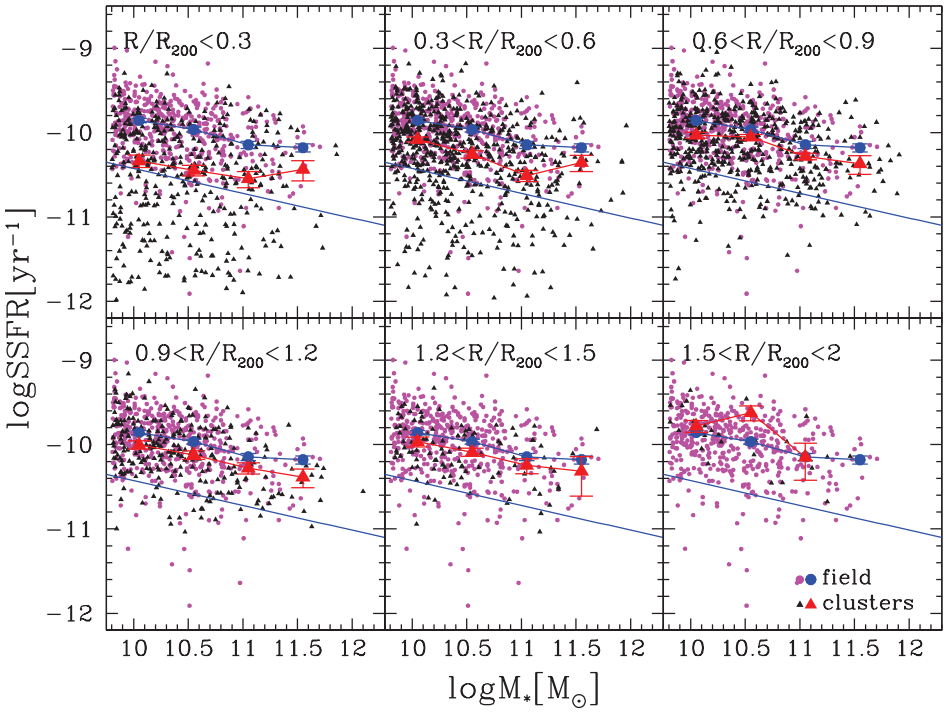

Figure 5.5: SSFR-M_* relation above the mass completeness limit in 6 bins of cluster-centric distance, as indicated in the labels. Points and colors as in Fig. 5.5

galaxies represent ∼70% of all galaxies at low masses and 50% at higher masses, while passive galaxies are ∼ 25% at low masses and are nearly as common as PSF galaxies at higher masses. In clusters, trends with mass are less pronounced within $0.6R/R_{200}$, where both PSF and passive fractions are almost constant, but well visible at larger distances, where they resemble what is observed in the field.

Overall, environmental effects seem to dominate within $0.6R_{200}$: the variation of the relative number of transition and PSF galaxies with distance is the main responsible of the decrease of the median SFR and of the change of the SFR-M_* relation seen in Fig. 5.1.

5.3.3 Galaxy properties and SFHs

It is interesting to analyze whether transition galaxies have different properties from the PSF galaxies.

Figure 5.7 shows how the LWA, MWA and (B-V) color change as a function of the

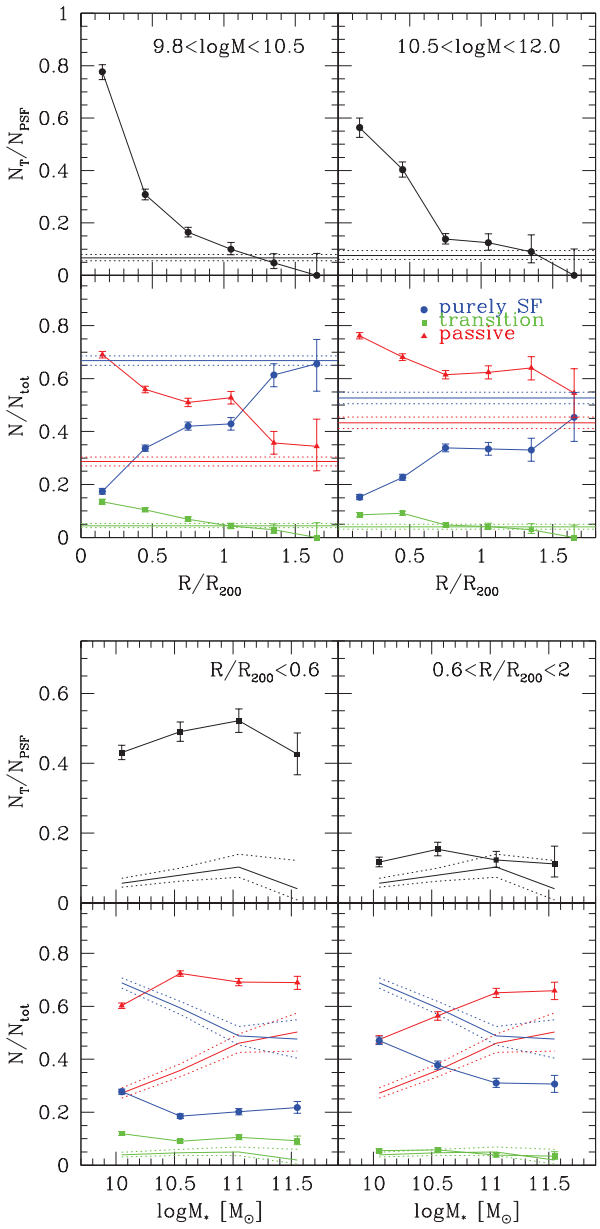

Figure 5.6: Galaxy fractions. Ratio of transition to PSF galaxies (top panels) and ratio of PSF, passive and transition galaxies to the total (bottom panels) as a function of R/R_{200} in 2 bins of mass (left) and as a function of M_* in 2 bins of cluster-centric distance (right). Points with error bars represent cluster fractions, solid and dotted lines represent field fractions and errors. Errors are binomial (Gehrels, 1986).

position on the SFR-M$_*$ plane for cluster member galaxies. Moving from left to right and top to bottom, galaxies show redder colors and are progressively older, with the transition population showing the largest values. The median LWA varies from ∼5 Gyr for transition galaxies to ∼2 Gyr for PSF galaxies, comparable with the field values for all SF galaxies. The same trend is found also for the MWA, but with a less marked gradient.

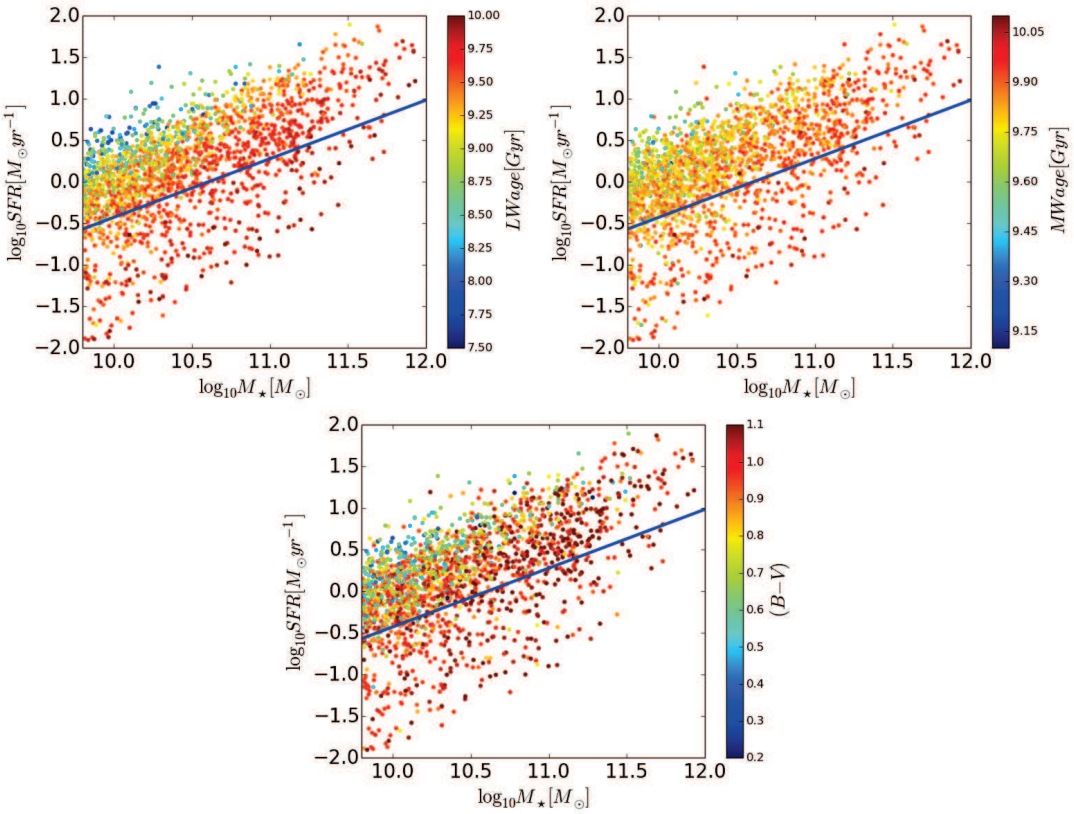

Figure 5.7: SFR-M$_*$ relation for cluster galaxies. The slanted solid blue line shows the limit dividing PSF and transition galaxies. Color-coded are the luminosity weighted age (upper left panel), the mass weighted age (upper right panel) and (B-V) color (lower panel).

I also inspected the SFHs of the different galaxy populations, to trace the evolutionary path of transition galaxies. The spectral analysis allowed us to derive an estimate of the SFRs at 12 different cosmic times (see section 4.1). However, there is an intrinsic degeneracy in the typical features of spectra of similar age, and this degeneracy increases for older stellar population spectra. There is, hence, an intrinsic limit to the precision of this method in determining the age of the stellar populations that compose a spectrum. The choice of the time interval in which SFRs estimates can be considered reliable accounts

for this aspect, and the initial 12 ages of the set of SSP spectra, i.e. the time intervals over which the SFR is assumed to be constant, were further binned into four intervals with $< t >= 3.9, 9.6, 12, 12.5$ Gyr and $\Delta t = 6.9, 4.6, 4.4, 0.6$ Gyr (see Guglielmo et al., 2015). Recall that the current SFR, used to separate galaxies, is taken to be the average during the last 20 Myr, thus is slightly different from the first bin of the SFHs.

To avoid the influence of the different mass distributions, I performed 100 Monte Carlo simulations. I randomly extracted a subsample of galaxies with the same mass distribution of PSF galaxies from the passive and transition samples and computed the mean SFR for each population, in the 4 age intervals. Errors on mean values have been computed as bootstrap standard deviations. Results are shown in Fig. 5.8.

Overall, the SFH decline gets steeper going from PSF to transition and passive galaxies. Consistently with the analysis of the LWAs, transition galaxies are clearly an evolved population with respect to PSF galaxies, having their SFR suppressed a long time ago (2-5 Gyr). A more accurate estimation of the quenching timescales is not possible due to the intrinsic capabilities of any spectrophotometric code to disentangle effects in such great detail.

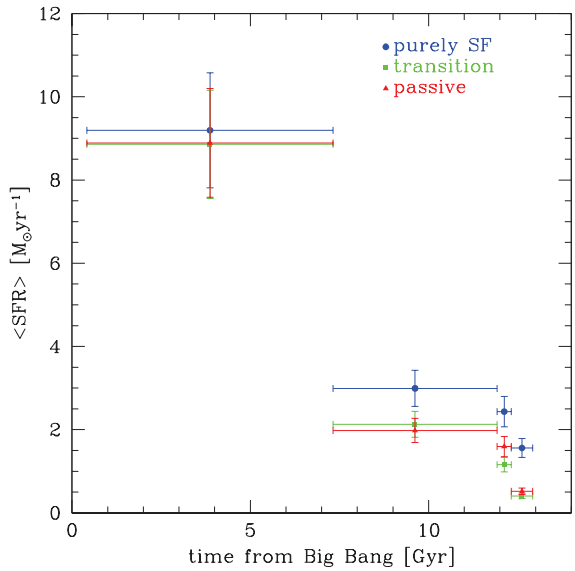

Figure 5.8: Mean SFR as a function of cosmic time for PSF galaxies (blue) and a sample of transition (green) and passive (red) galaxies mass-matched to the PSF population. Errors on the mean values are obtained using a bootstrap resampling.

5.4 Cluster properties

So far I have studied how the fraction and properties of the star forming population vary within clusters and I considered the clustercentric distance as a proxy for the local environment. A natural step forward is looking at the dependence on cluster properties exploiting the large range of σ_{cl} and L_X covered by the OmegaWINGS cluster sample.

Figure 5.9 shows the incidence of transition galaxies within the whole cluster population (bottom panels) and with respect to the PSF population (upper panels) as a function of cluster X-ray luminosity (left) and velocity dispersion (right). To mark the average trends group the cluster sample was grouped into five bins of σ and L_X with approximately the same number of objects; the results are shown as red points.
A mild increase of both fractions with σ_{cl} and L_X is visible. A Spearman correlation test, which assesses how well the relationship between two variables can be described using a monotonic function, gives coefficients of 0.18-0.31 and 0.26-0.28 for N_{TR}/N and N_{TR}/N_{PSF} respectively, with p-values greater than 0.10 thus no significant correlation is found.
To further check the significance of this correlation, I selected galaxies belonging to clusters in the higher and lower tails of the σ_{cl} and L_X distributions and compared the relative SFR-M_* relations (see figure 5.10).

No significant change is detectable in the median SFR-M_* relations, marked by blue and red big dots for the low L_X/σ_{cl} and high L_X/σ_{cl} samples respectively.

Moreover, the KS test on the weighted SFR distributions does not find any difference between these populations, supporting the null hypothesis that these samples are drawn from the same parent population (p-values of 0.46 and 0.06 for the L_X and σ SFR distributions). These results suggest that the star formation rate is insensitive to the mass of the structure in which the galaxy is embedded, in agreement with the findings of Lewis et al. (2002) who analyzed a sample of clusters in the 2dF survey with $0.05 < z < 0.1$. Vulcani et al. (2015), investigating the green valley population of galaxies in the PM2GC sample, also found no dependence on the host halo mass.

5.5 Discussion

If SF galaxies are affected by environmental mechanisms when they move from the field to groups or clusters, we should see a signature of this transformation that depends on the timescale over which it occurs.

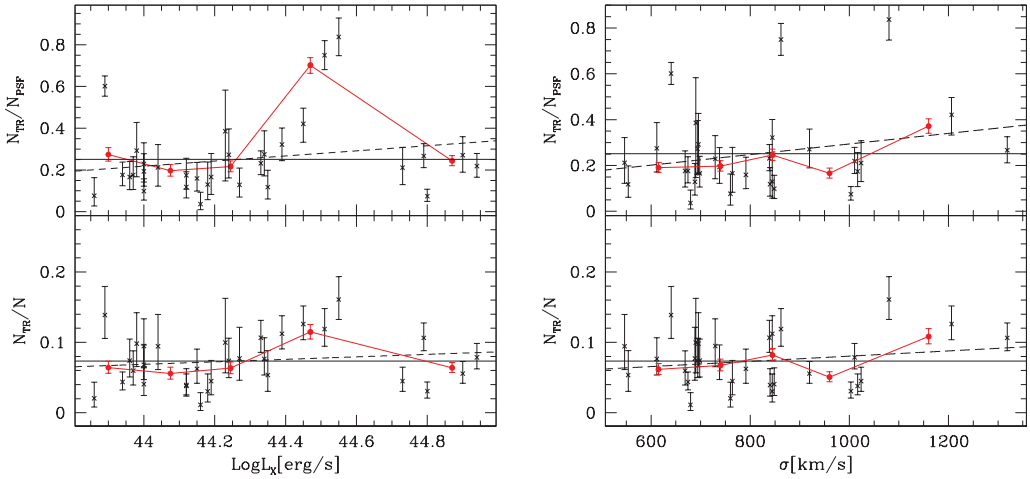

Figure 5.9: Fraction of transition galaxies as a function of the cluster X-ray luminosity (left) and velocity dispersion (right). Black points represent individual clusters, red points give the fractions in 5 equally populated bins. Lower panels: weighted fraction of transition galaxies among the whole population. Upper panels: weighted fraction of transition galaxies among the PSF population. Errors are binomial. Solid line: mean; dashed line: least square fit.

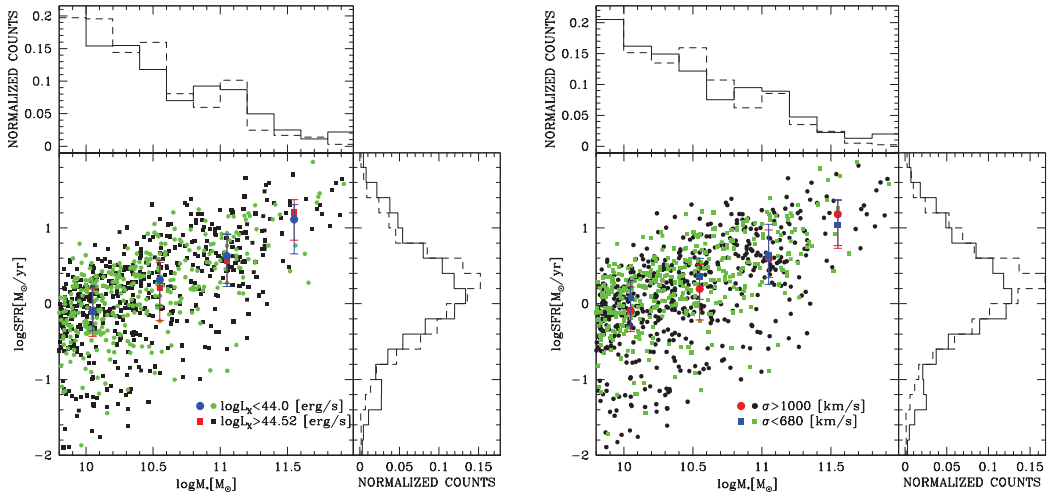

Figure 5.10: Main panel: SFR-M_* relation above the mass completeness limit for cluster galaxies within the highest/lowest bin of X-ray luminosity (left) and σ (right). Galaxies with $logL_X < 44.0$ [erg/s] or $\sigma < 680$ [km/s] are plotted as green squares while galaxies with $logL_X > 44.52$ [erg/s] or $\sigma > 1000$ [km/s] are plotted as black circles. Blue (lowest bin) and red (highest bin) big symbols are the medians of SF galaxies weighted for incompleteness in different mass bins. Upper panel: mass distributions. Right panel: SFR distributions. Histograms are normalized to total and weighted for incompleteness.

Comparing the SFR-M_* relation of SF galaxies in clusters and in the field and looking at variations as a function of the cluster-centric distance allow us to put constraints on both the range of environments where star formation is quenched and the average timescale over which it happens.

Rapid quenching processes would leave the SFR-M$_*$ relation unperturbed with respect to the field, moving SF galaxies directly to the red sequence. On the contrary, slow quenching would increase the number of galaxies with reduced SFRs resulting in a different SFR-M$_*$ relation. I found a population of low SF galaxies, which is rare in the field, suggesting that for these galaxies the transition from SF to passive occurs on a sufficiently long timescale to let us see them in the process of being quenched. We stress that our analysis cannot identify galaxies quenching on short timescales, that would move quickly from the SF MS to being passive. I showed that this slow process is confined to galaxies within R_{200} and that only within $0.6R_{200}$ this causes the median SFR-M$_*$ relation to detach from the observed field MS. Moreover, galaxy fractions in the inner regions ($R < 0.6R_{200}$), are found to be nearly constant with stellar mass.

The analysis of the SFHs, together with the variation of the properties of galaxies in the SFR-M$_*$ plane, support this scenario: transition galaxies have older LWAs and redder colors than MS galaxies and show reduced mean SFRs at least in the last $2-5$Gyr. Stellar mass seems to play a minor role, with the observed trends displaying a much weaker dependence on M$_*$ than on distance.

I cannot exclude that some transition galaxies are passive galaxies returning to the SF population due to accretion of gas-rich satellites or exchange of material during merging, but this channel seems improbable because of the many processes acting to remove gas or suppress the gas reservoir in clusters (see e.g. Bahé and McCarthy, 2015).

The results presented here agree with the conclusions of Vulcani et al. (2010) and Haines et al. (2013) at $z = 0.1 - 0.3$, who found that the SFRs of SF galaxies decline towards the cluster core from the values observed in the field. Also numerical simulations (e.g. Haines et al., 2015; Taranu et al., 2014; Oman et al., 2013) support the slow quenching scenario, finding kinematic segregation between normally star forming galaxies and those with reduced SFRs.

This analysis, together with the work of Patel et al. (2009) and Vulcani et al. (2010), who depicted a population of galaxies with reduced SFRs, at $0.4 < z \leq 0.8$, suggest that this transition population exists both at low and intermediate redshift clusters.

I conclude that, even if cluster galaxies can be as star-forming as field galaxies, there are significant differences in their SFR distributions. Clusters not only have a pre-existing

larger population of passive galaxies, but also show a tail of low star-forming galaxies that is rare in the field. This evidence is predicted for strangulation models, in which the diffuse gas halo is rapidly stripped at the passage through the intracluster medium leaving available to the galaxy only its reservoir of molecular gas to form stars (e.g., Bekki et al., 2002), but other physical processes such as ram pressure stripping cannot be excluded. Indeed, Boselli et al. (2016) recently showed that these results could also be explained in a scenario in which most of the gas is stripped on a short timescale (< 0.2 Gyr) at the first passage of the galaxy at the pericenter but the remaining reservoir could sustain a moderate star formation activity for longer times (1-3 Gyr) until full quenching is reached. Moreover, the long time scales associated with strangulation are also comparable to $\sim$ two crossing of a cluster (3-4 Gyr), a time sufficiently long to allow ram pressure stripping to reach its maximum for three times (see Boselli et al., 2014).

An other crucial effect that needs to be accounted is pre-processing (Dressler, 2004). Since a large fraction of cluster galaxies is accreted via small groups (McGee et al., 2009; De Lucia, 2011), the perturbing mechanisms can start to shape galaxy evolution well before the galaxy is within the massive cluster.

5.6 Summary

The star formation quenching depends on environment, but a full understanding of what mechanisms drive it is still missing. Exploiting a sample of galaxies with masses $M_* > 10^{9.8} M_\odot$, drawn from the WIde-field Nearby Galaxy-cluster Survey (WINGS) and its recent extension OmegaWINGS, I investigated the star formation rate as a function of stellar mass in galaxy clusters at $0.04 < z < 0.07$. I used non-member galaxies at $0.02<z<0.09$ as field control sample. The main results can be summarized as follows:

- There is a general agreement between the SFR-M_* relation of field and cluster galaxies, but a population of cluster galaxies with reduced SFRs, which is rare in the field, has been detected.

- These *transition* galaxies are mainly found within the cluster virial radius (R_{200}) but they impact on the SFR-M_* relation only within $0.6R_{200}$. The ratio of transition to PSF galaxies strongly depends on environment, being larger than 0.6 within $0.3R_{200}$ and rapidly decreasing with distance, while it is almost flat with M_*. No trend with the cluster velocity dispersion and X-ray luminosity have been detected.

- As galaxies move downward from the SFR-M_* main sequence, they become redder and present older luminosity and mass weighted ages.

These trends, together with the analysis of the star formation histories, suggest that transition galaxies have had a reduced SFR for the past 2-5 Gyr. These results are consistent with the hypothesis that the interaction of galaxies with the intracluster medium via strangulation causes a gradual shut down of star formation, giving birth to an evolved population of galaxies in transition from being star forming to becoming passive. However, other physical processes might also be responsible, such as for example ram pressure stripping that could be less efficient on certain orbits and remove only part of the gas in the disk.

6

Post starburst galaxies in different environments

In this Chapter, I exploit the combination of the WINGS and OmegaWINGS projects to study the properties of ~ 10000 *cluster member galaxies in an homogeneous sample at* $0.04 < z < 0.07$*. I investigate the occurrence and properties of post starburst galaxies in 32 clusters and compare them to those of passive and star forming galaxies. Trends are investigated as a function of both clustercentric distance and global cluster properties, i.e. cluster velocity dispersion and X-ray luminosity. Aim of this analysis is to shed light on the processes acting on these galaxies and the time scale needed to transform from one type to the other. Including also the PM2GC data sample, divided into groups, binaries and single galaxies, I study the dependence of the PSB fraction on the halo mass of the system.*

The following study is presented in Paccagnella et al. 2016 (submitted) and Paccagnella et al. in prep.

6.1 Introduction

Valuable insights to understand how the star forming population turns passive can be obtained by studying galaxies that appear to have intermediate properties and may be in the act of transitioning between the two main galaxy populations. This transition can occur on different time scales depending on the main process inducing the transformations

(Wetzel et al., 2013; Mok et al., 2013; Schawinski et al., 2014; Wheeler et al., 2014; Vulcani et al., 2015; Paccagnella et al., 2016). However, a clear picture describing the reasons why galaxies turn into passive following different paths and the properties of these galaxies is still missing.

Dressler and Gunn (1982), investigating cluster galaxies at intermediate redshifts, found a large number of spectra showing strong Balmer absorption lines and no emission and called them post-starburst galaxies. These features are typical of galaxies in which star formation had ended abruptly within the last 1-1.5 Gyr and therefore should have been affected by some of the aforementioned processes.

Since then, extensive spectrophotometric modeling (Couch and Sharples, 1987; Newberry et al., 1990; Poggianti and Barbaro, 1996; Abraham et al., 1996; Poggianti and Barbaro, 1997; Bekki et al., 2001; Poggianti, 2004) has found that the presence of strong hydrogen lines in absorption and the concomitant absence of emission lines, indicating no ongoing star formation, can be explained roughly decomposing the spectra into a combination of K giant star (or early type galaxy) spectrum and an A star spectrum. In general, A type stars - i.e. new born stars formed within the last 1 Gyr whose spectra are characterized by strong Balmer absorption lines - dominate the light of a galaxy about 0.5 Gyr after star formation stopped and leave their signature on the spectra visible for 1-1.5 Gyr. In contrast, O and B stars - more massive stars that die very quickly and emit the energetic photons able to ionize the gas that produce the emission lines - have no or very little contribution. This spectral combination, which explains the origin of the name "k+a" often used to describe post-starburst galaxies, can appear as a result of a star-bursting episode observed shortly after the star formation has rapidly stopped (for those galaxies with the strongest Balmer lines), or as a consequence of normal star formation that has been abruptly ended. Moreover, since A type stars have precisely known lifetimes, the evolution of this population can be used as a quenching clock.

The reason why post-starburst galaxies underwent an episode of star formation that was abruptly stopped is still matter of debate; any of the mentioned quenching mechanisms acting on a short time scale could make star formation cease, without or without a previous burst, producing a k+a spectrum. Important hints for solving this matter come from the study of the galaxy environments as different quenching mechanisms play different roles in different environments.

Galaxy mergers could be the dominant mechanism in the low-z field, where recent studies found a small but non negligible fraction of post starburst galaxies (Bekki et al., 2001; Quintero et al., 2004; Blake et al., 2004; Goto, 2005; Hogg et al., 2006; Mahajan,

2013), but they are less effective in clusters, due to the high velocity dispersions.

The origin of k+a galaxies in clusters is more probably related to the interaction of the infalling population with the hot and dense intra cluster medium (ICM). Indeed, as suggested by Dressler and Gunn (1982); Couch and Sharples (1987); Dressler and Gunn (1992); Poggianti et al. (1999); Poggianti (2004); Tran et al. (2003, 2004, 2007); Poggianti et al. (2009), the interaction of a gas rich galaxy with the hot high-pressure ICM via ram-pressure stripping might trigger a starburst and then clear the disk of neutral gas stopping star formation. The most striking evidence for this is perhaps in the Coma cluster, where the position of young post-starburst galaxies is strongly correlated with strong X-ray temperature gradients (Poggianti, 2004). While this picture is corroborated by observations of high and intermediate redshift clusters (Poggianti et al., 1999; Muzzin et al., 2014), in the local Universe several works (e.g. Blake et al., 2004; Goto, 2005) found that the majority (in number) of post starburst galaxies are outside of clusters and therefore argued that cluster specific processes are not likely to be the dominant source of fast quenching. Nonetheless, the few studies that investigated the fraction and properties of the local post-starburst cluster population (e.g. Caldwell and Rose, 1997; Poggianti, 2004; Fritz et al., 2014) found evidence of truncated star formation in a significant fraction of cluster members. A complete census of post-starburst galaxies in clusters and a homogeneous comparison with the field population is however still lacking, because of the paucity of the cluster samples studied and the different selection criteria adopted in these studies that do not allow fair intra-sample comparisons. In addition, local post starburst galaxies are often selected without constraints on the Hα line. This could be due to the choice of a selection criterium comparable to the one used at high redshift, where generally the spectral coverage does not allow to reach the Hα emission. As shown by Goto et al. (2003) and Blake et al. (2004), such selections suffer from high contamination from star forming galaxies.

6.2 The spectral classification

Focus of this chapter is to characterize the properties of galaxies showing different features on their spectra, therefore I relied on the measure of the EWs provided by SINOPSIS. I converted the observed EWs in rest frame values, simply dividing the measurements by $(1+z)$. As tested by Fritz et al. (2007) and section 4.1.1, based on the analysis of low S/N spectra, a 2Å limit was chosen for the oxygen forbidden lines: values above this threshold were considered unreliable for the EW of both [OII] and [OIII].

Based on the spectral classification originally proposed by Dressler et al. (1999) and Poggianti et al. (1999) and more recently described by Fritz et al. (2014), I subdivided the sample into three classes, according to the rest frame EWs of [OII] and Hδ, which are good indicators of current and recent star formation, respectively. When the [OII] is not detected, the equivalent width of [OIII] and Hβ are used instead. Differently from Fritz et al. (2014), this spectral classification exploits also the information on the Hα line: all spectra showing Hα in emission are directly classified as emission line galaxies, regardless of the other lines. According to Goto et al. (2003) a post-starburst sample selected ignoring this line could suffer from $\approx 50\%$ of contamination from Hα emitting galaxies. In this way we obtain a more robust classification, ensuring that there is no current star formation, in both the passive and post-starburst samples. The detailed description and the physical interpretation of this classification is discussed by Poggianti et al. (1999, 2009) and Fritz et al. (2014).

Briefly, spectra with any of the aforementioned emission lines belong to galaxies in which the star formation is currently contributing to the formation of the galaxy, and will thereafter be called emission line galaxies (EML).

Spectra with no emission lines, including Hα, are divided on the basis of on the strength of Hδ: k spectra, normally found in passively evolving elliptical galaxies, resembling those of K-type stars, with weak Hδ in absorption (Hδ <3 Å), and $k+a$ and $a+k$ spectra, displaying a combination of signatures typical of both K and A-type stars with strong Hδ in absorption (respectively $3 <$ H$\delta < 8\mathring{A}$ and H$\delta > 8\mathring{A}$). The former (k-type) will be thereafter called passive galaxies (PAS), the latter (both $k+a$ and $a+k$) post starburst galaxies (PSB).

Among the PSBs, the strength of Hδ is indicative of the initial condition associated with the main quenching event. Indeed an H$\delta > 6$ Å can be explained only if a burst of star formation involving high mass fractions (10-20%) happened prior to the sudden quenching and galaxies showing this feature are caught in an early phase of transition (Goto, 2004). In contrast, spectra with a moderate Hδ line could be both the result of the truncation of star formation in a normal star forming galaxy (thus no burst is required) or a late stage of evolution of the proper post-starburst galaxies. Broadly speaking, while all PSB galaxies with strong Hδ will later turn into PSBs with moderate Hδ, the opposite is not true. Therefore, I will sometimes discuss also the strong PSB (H$\delta > 6$ Å, hereafter sPSB) separately.

The automatic classification has been visually confirmed. Upon inspection, I noticed that in a number of cases the code had mis-identified emission lines (oxygen forbidden

Table 6.1: Weighted spectral numbers and fractions

Galaxy type	PAS		PSB		sPSB		EML	
	N	%	N	%	N	%	N	%
Clusters	8162 (4235)	55.7±0.4	1057 (560)	7.2±0.2	154 (80)	1.1±0.3	5441 (3029)	37.0±0.4
Field	415 (225)	19.7±0.8	28 (15)	1.3±0.2	7 (3)	0.3±0.1	1667 (923)	79.0±0.9

Table 6.2: Weighted Number (raw numbers in brackets) and percentage of the different spectral types for the magnitude-limited sample weighted for spectroscopic incompleteness and considering only galaxies inside 1.2R_{200}. The field sample, extracted from non-member galaxies in the WINGS+OmegaWINGS sample, has no radial limits. The proportion of PAS (k), PSB (k+a/a+k), strong PSB (PSB with EW(Hδ >=6) and EML galaxies are listed along with binomial errors.

lines and Hβ), measuring noise rather than real emission. The [OII] emission line, by coincidence, is located in a critical region of our spectra, being in the shortest wavelength regime covered by the spectrograph that often result quite noisy (see Smith et al., 2004). Moreover, I found that, in most cases, the Hβ and [OIII] emissions were mis-identified in spectra showing only one emission line. I visually inspected all the spectra where only one emission line was detected and, if necessary, changed the galaxy spectral type. Furthermore, I checked all the $k + a$ and $a + k$ candidates and excluded those with undetected emission line spectra, and I remeasured the Hδ EW for those galaxies with an automatic measure higher than 5 Å or with a comparable uncertainty.

6.3 Data Sample

One of the main goals of this chapter is to investigate the occurrence of PSB galaxies as a function of clustercentric distance; in particular I want to investigate the role of the cluster environment also beyond the virial radius. I therefore restrict this analysis to the clusters covered also by the OmegaWINGS observations. Among these, only the 32 clusters with a global spectroscopic completeness higher than $\approx 50\%$ are used.

Galaxies belonging to the final sample have a V magnitude brighter than 20 and a reliable measurement of EWs.

The AGN contribution was neglected. As pointed out by Alatalo et al. (2016), this could bias the results in the sense that if all emission-line spectra are excluded from the PSB sample, those galaxies in which emission lines are not linked to the star formation process, rather being excited by the AGN mechanism, are automatically excluded. Nonetheless, Guglielmo et al. (2015), analyzing a mass limited sample extracted from the original WINGS survey, estimated that the AGN contribution in the star forming galaxy

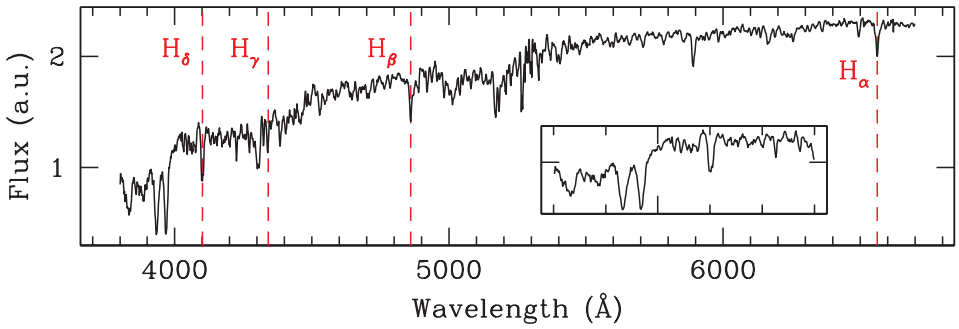

Figure 6.1: Rest frame composite spectrum of the post-starburst cluster sample. The inset shows a zoom in of the spectral region around Hδ.

population is approximately 1.6% and I estimated that this fraction will not remarkably change in the adopted sample. Thus, including these objects in the emission line galaxy population should not considerably affect the results. A more detailed analysis of emission line galaxies and their classification as star forming galaxies, transition objects and active galactic nuclei is presented, only for the WINGS sample, in Marziani et al. (2016).

The main sample consists of cluster members within $1.2R_{200}$ from the BCG, a distance that is reached by almost all the selected clusters (90%). I excluded galaxies at larger distances (the maximum radial coverage is approximately 2 R_{200} for member galaxies) because all these belong to clusters with very low velocity dispersion, so they might be a biased population non representative of the general trends. I also excluded BCGs, which have been shown not to be representative of the general cluster population (e.g. von der Linden et al., 2007; Fasano et al., 2010, and references therein).

Non-cluster-member galaxies with $0.035 < z < 0.08$ constitute our field control sample, used for reference. To avoid the introduction of possible systematics due to different criteria used to select galaxies, this field sample has been preferred to the PM2GC general field sample (see Chapter 3).

The final sample consists of 7824 cluster galaxies and 1163 field galaxies (respectively 14660 and 2110 galaxies, once weighted for incompleteness, see Cava et al., 2009, for a detailed explanation). The number of EML, PAS and PSB galaxies in the different environments is given in Table 6.2 and discussed below.

The cluster sample will be compared to the PM2GC data set presented in Chapter 3, restricting the analysis to galaxies brighter than the absolute magnitude limit of $M_B = -18.7$.

6.4 Results

In this section I present the results of the analysis on the cluster sample. I will first investigate the occurrence and the galaxy properties of the different spectral types (e.g. stellar masses, magnitudes, colors and morphologies), then I will investigate trends as a function of both clustercentric distance and the level of substructures in clusters. I will also focus on the position of the galaxies in a phase-space diagram and characterize the role of global cluster properties, i.e. cluster velocity dispersion and X-ray luminosity, in driving trends. Aim of our analysis is to shed light on the processes that induce a truncation of the star formation on short time scales and give rise to the existence of the PSB galaxies. Given our interest in this population, in Fig. 6.1 I show the composite spectrum of our PSBs, to visualize the main features of this population. The composite spectrum is obtained by summing the spectra of all the PSB galaxies in the cluster sample, after normalizing each spectrum by its mean value. The measured rest frame EW(Hδ) is greater than 4 Å, the other Balmer lines are well visible and no emission is detected.

6.4.1 Properties of the different galaxy populations

Table 6.2 presents the incidence of the different spectral types in clusters and in the field. The galaxy population in clusters is dominated by PAS galaxies, which represent 55.7±0.4% of all galaxies, while EML galaxies are 37.0±0.4% of all members. In the field, the contribution of the PAS and EML populations is reversed: nearly 80% of field galaxies show sign of ongoing star formation, while less than 20% are PAS. The fraction of PSB galaxies is significantly higher in clusters than in the field: 7.2±0.2% vs 1.3±0.2%. Note that our field sample might actually be biased towards galaxies belonging to filaments or structures falling into the main cluster that are difficult to separate. Furthermore, there are only 15 PSBs in the field, therefore the statistics in this environment is too poor to draw definitive conclusions. A more complete analysis of PSB galaxies as a function of the global environment, including galaxies in groups, binary systems and also single galaxies, will be presented in Section 6.6.

The relevance of the PSB cluster population is even more striking considering the fraction relative to the active population, which contains galaxies that are (EML) or have been (PSB) star-forming within the last 2 Gyr. The PSB to active fraction gives the "quenching efficiency" (see Poggianti et al., 2009) that is the efficiency in truncating the star formation in star-forming galaxies. PSB galaxies represent 16.3±0.5% of the cluster active population, in agreement also with the high redshift fractions derived by Poggianti

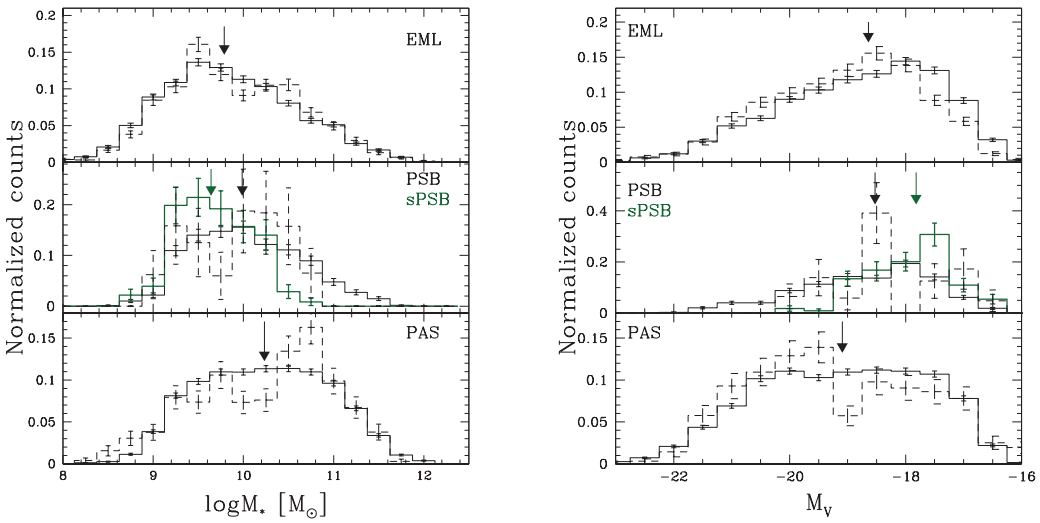

Figure 6.2: Number of cluster (solid) and field (dashed) galaxies in the three main spectral types as a function of stellar mass (left panel) and absolute V magnitude (right panel). Dark green histograms in the middle panels show the sPSB subsample. Arrows indicate the median value for each type. Errors are poissonian (Gehrels, 1986).

et al. (2009), while they make up for less than 2% in the field. Hence, clusters are far more efficient than the field in shutting off star formation in galaxies on a very short time scale.

Stellar mass and absolute V magnitude weighted distributions of galaxies of the different spectral types are presented in Fig. 6.2. The spectral classification, going from PAS to PSB, to EML galaxies, turns out to be, in both environments, a sequence of decreasing mean galaxy mass and increasing mean V magnitude. EML galaxies dominate the low mass/low luminosity tails of the distributions, while the contribution of the PAS population becomes more important going toward higher masses and luminosities. In order to test if the mass and magnitude distributions of the three populations are significantly different, I performed a Kolmogorov-Smirnov test. The results, comparing the distributions of PSBs to PASs and EMLs galaxies and PASs to EMLs, allow us to reject the null hypothesis that these populations are drawn from the same sample (P-values of the order of 0.0).

This picture fits the downsizing scenario (Cowie et al., 1996), in which star formation at higher redshifts was more active in more massive/luminous galaxies that are the first to turn into passive. The distribution of the properties of PSB galaxies are intermediate

between those of the PAS and EML populations. This is even clearer looking at the median values of the distributions for cluster galaxies indicated by the black arrows in Fig. 6.2 (the median masses are 9.78±0.01, 9.98±0.02 and 10.23±0.1, the median magnitudes are −18.64±0.02, −18.52±0.04, and −19.09±0.02 for EMLs, PSBs and PASs, respectively)

Field median values agree, within the standard errors, with the cluster ones indicating no strong environmental dependencies.

The absolute magnitude distribution of PSBs has its maximum around $M_V = -18.5$, with a deficit among the brightest galaxies ($M_V < -20.5$) with respect to both the EML and PAS populations. These characteristics were already visible in the sample described in Fritz et al. (2014) and are similar to those of the post-starburst population in the Coma cluster (Poggianti, 2004). In the cluster sample, 14±1% of the PSB galaxies are classified as sPSB; in the field, only 3/15 PSB galaxies are sPSB, making any conclusion statistically meaningless.

sPSB galaxies (dark green histograms in Fig. 6.2) span a narrower range of both absolute magnitude ($M_V > -19$) and stellar mass ($\log M_* < 10.5$) missing the high mass tail and luminosity. Other studies of PSB galaxies in the local universe (Mahajan, 2013; Wong et al., 2012) even found that the whole PSB population is restricted to the low-mass end of the stellar mass distribution. At these epochs most of the star formation is happening in low mass galaxies which are quenched during accretion into clusters (see also the phase space analysis in sect.6.4.5). Moreover, this suggests that only the least massive/luminous PSB galaxies undergo a phase of sPSB, and confirms the hypothesis that while all the sPSB galaxies will age and evolve into moderate PSB galaxies, not all PSBs have experienced the sPSB phase.

Figure 6.3 shows the absolute rest-frame color-magnitude diagram ($(B-V)$ vs V) for cluster galaxies of the different spectral classes. I recall that absolute magnitudes and rest-frame colors are given by the spectrophotometric model convolving the filters response curves with the spectrum . To subdivide galaxies into red and blue, I considered the color-magnitude red sequence of each WINGS cluster given in Valentinuzzi et al. (2011). I used the average value of the slope across all clusters and fix the quote 1σ below the average red sequence. Galaxies whose color lie above

$$(B-V)_{rf} = -0.045 \times V - 0.035$$

(black heavy line in Fig. 6.3) were assigned to the red sequence, the rest to the blue cloud.

As expected, most PAS galaxies present red colors (73.3±0.5%), while EML galaxies

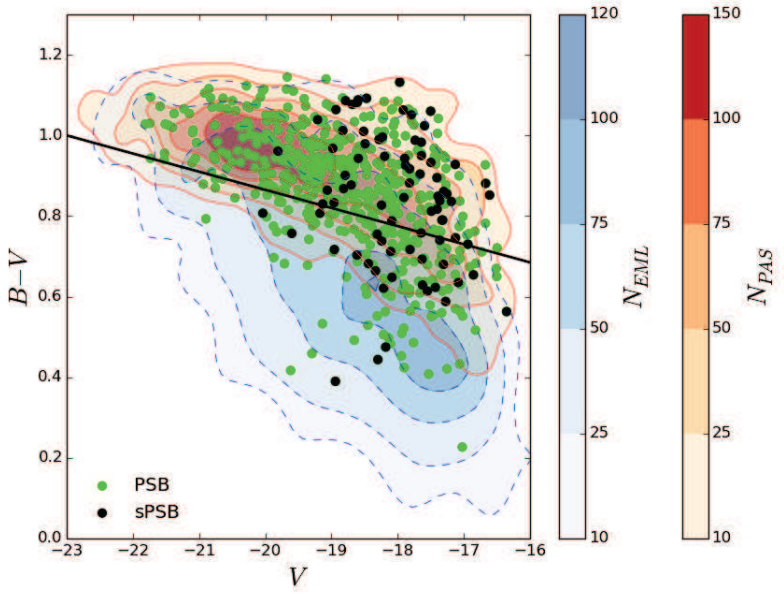

Figure 6.3: Rest-frame $(B-V)$-V relation for cluster galaxies of the different spectral types. Red-solid and blue-dashed contours: number densities of PAS and EML galaxies, respectively. Green dots: PSB; black dots: sPSB. The black line represents the selection limit we adopt to select red and blue galaxies.

are preferably bluer (75.2±0.6%). Also the majority of PSB and sPSB galaxies have red colors (73±1% and 59±4%, respectively), but span almost the entire color range, with a non negligible fraction of blue galaxies. This finding supports the idea that fast quenching of star formation immediately brings the galaxies to the red sequence, but also that a pure color-based selection is unable to uniquely distinguish between passive, star forming and galaxies that recently interrupted their star formation. Therefore a detailed spectral analysis is necessary to recognize the different galaxy sub-populations.

According to the picture described before, one would expect that sPSB galaxies have colors bluer than the rest of the PSB population (see, e.g., Poggianti, 2004). Figure 6.3 shows that this seems not to be the case in our sample. Even if blue galaxies are slightly more abundant within the sPSB population than within the whole PSB sample, still the majority of sPSB galaxies have red colors. One way to explain these results is to consider that, at low redshift, most of the stars in galaxies are old, and, as soon as the star formation is switched off, the galaxy becomes quickly red as the old stars dominated the integrated light. An alternative explanation could be the presence of dust. As already discussed in

Table 6.3: Weighted morphological percentages of PSB galaxies

	E	S0	LT
	%	%	%
PSB	28±1	45±2	27±1
sPSB	17±3	41±4	42±4

Table 6.4: Morphological percentages for the PSB and sPSB samples weighted for spectroscopic incompleteness. Errors are binomial.

Poggianti et al. (1999), the assumption that the progenitors of PSB galaxies are dusty starburst objects entails that dust reddening might affect also the post-starburst class. I tested this hypothesis by exploiting the average extinction values given by SINOPSIS and no trend with the EW of Hδ was found. This result might suggests that either sPSB galaxies are not more obscured than PSBs, or that the real EW values in absence of dust obscuration should be higher and that our EW estimates have to be considered as lower limits.

6.4.2 Morphologies

As mentioned in sec.4.2.1, a morphological classification is available for all PSB galaxies in our sample. The analysis of the morphological types can help to improve our understanding of the typical properties of this population.

Table 6.4 presents the percentage of galaxies of different morphological types for the whole PSB sample. 45±2% of the galaxies are classified as S0s, while the remaining sample is evenly divided between ellipticals (28±1%) and late-types (27±1%). Figure 6.4 illustrates the stellar mass distribution of the different morphological types.

Focusing on sPSB galaxies I found that while the fraction of S0s does not change within the errors (41±4%), that of late types and elliptical does: the former represent 42±4% of the total population, the latter 17±3%.

Several reasons might be at the origin of such different morphological distribution between the two samples.

The larger fraction of late-types among sPSB galaxies than among PSBs agrees with the hypothesis that these are younger objects in which the original disk structure has not yet been changed. Together with mass and luminosity distribution of sPSB galaxies (Fig. 6.2), this morphological mix could also indicate that the process responsible for the strong burst needed to create the observed spectral features is more effective on less

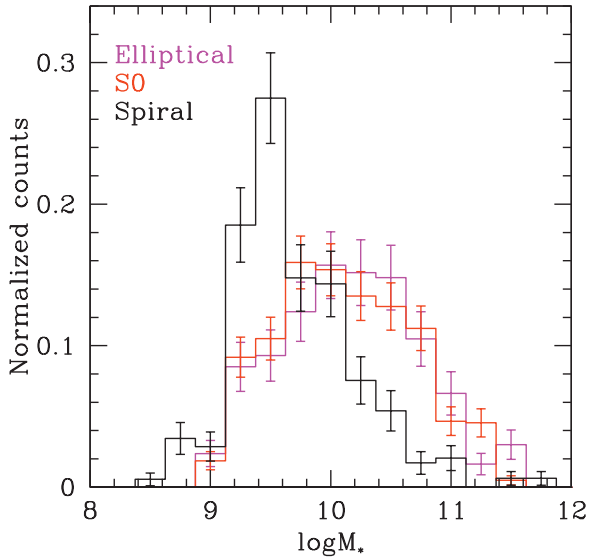

Figure 6.4: Mass distribution of PSB galaxies with different morphological type. Magenta, red and black histograms shows respectively the elliptical, S0 and spiral subsamples. Errors are poissonian.

massive galaxies with an high fraction of gas at the moment of infalling. As an alternative, invoking only ram pressure stripping as the main process responsible for the production of both PSB and sPSB galaxies, the observed morphologies could simply reflect the properties of the infalling population. At low redshifts, the amount of gas necessary to produce a burst of star formation as a consequence of the interaction of the galaxy, via ram pressure stripping, with the ICM, is mostly located in low-mass late-type systems while more massive galaxies are mostly early-types and gas deficient.

Similarly to the analysis of galaxy colors, the analysis of the morphologies shows that the majority of PSB galaxies cannot be recognized when using just a morphological classification, but a detailed spectral analysis is necessary.

6.4.3 Spatial distribution of the different spectral types

In the previous sections, I have shown that low-z clusters host a much larger fraction of post-starburst galaxies than the field, pointing towards a cluster-specific origin of the majority of this class of objects. To differentiate among possible quenching processes that can suddenly truncate the star formation in clusters I further investigated the radial

distribution of the different spectral classes, given that the clustercentric distance is a good tracer of the cluster density profile and is related with the time since infall into the cluster (Goto, 2004). Moreover, since the cluster crossing time is of the order of R_{200}/σ_{cl} (i.e. 2.5 Gyr), the clustercentric distance is also an approximate timescale sensitive to processes occurring on times $\leq$ Gyr. Processes that quench star formation gradually, such as strangulation, would induce radial gradients while processes acting on short time scales, e.g. ram pressure stripping, are more likely to cause distinctive signatures at the radii where they are most effective.

The bottom panel of Fig. 6.5 shows the incidence of each galaxy population (PAS, EML, PSB) as a function of clustercentric projected distance, in units of R/R_{200}.

As already mentioned, this analysis is limited to $1.2R_{200}$ not to bias our results towards clusters with low values of velocity dispersion. In agreement with previous results, (Weinmann et al., 2006; von der Linden et al., 2010; Vulcani et al., 2015) I found a pronounced relation between distance from the cluster center and the composition of the

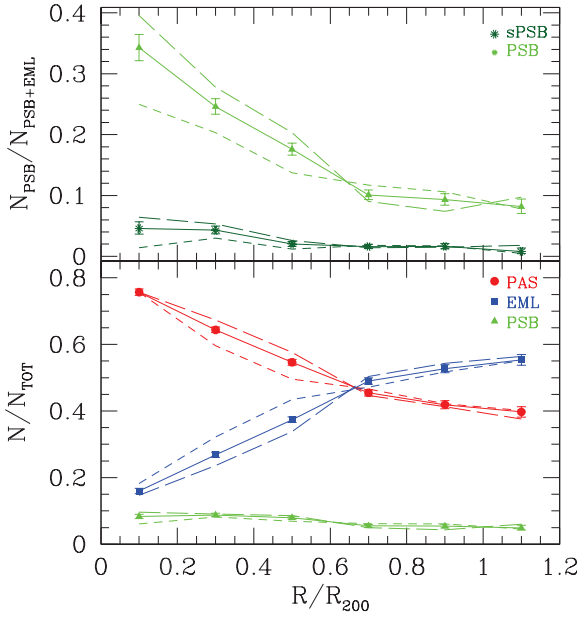

Figure 6.5: Ratio of post-starburst to active galaxies (top panels) and ratio of post-starburst, passive and emission line galaxies to the total (bottom panels) as a function of R/R_{200}. Points with error bars represent cluster fractions, dashed lines give the trends of the respective fractions in two bins of velocity dispersion σ ($\sigma < 840km/s$ -short dashed lines- and $\sigma > 840km/s$ -long dashed lines). Errors are binomial (Gehrels, 1986).

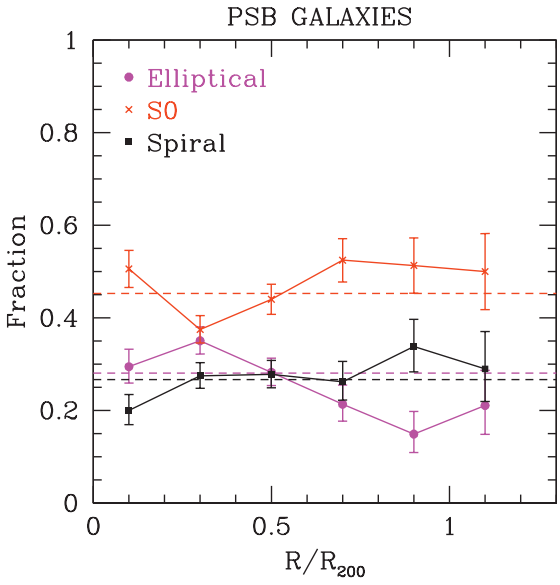

Figure 6.6: Morphological fractions for the whole PSB sample as a function of the clustercentric distance. Black squares refer to spiral galaxies, red crosses to S0s, magenta circles to ellipticals. The dashed lines mark the total fractions listed in table 6.4. Errors are defined as binomial errors.

galaxy population. PAS galaxies dominate the inner regions (∼70% at $R < 0.4R_{200}$), and their fraction decreases going outward of a factor of ∼2.5. In contrast, the fraction of EML galaxies is ∼ 60% at large clustercentric distances and rapidly declines towards the cluster center of a factor of 4. Despite their relatively small incidence, also the fraction of PSB galaxies depends on clustercentric distance, and their trend follows that of PAS: in the cluster cores PSBs are ∼2.5 as numerous as PSBs in the outskirts.

The upper panel of Fig. 6.5 shows the quenching efficiency ($PSB/(PSB+EML)$) as a function of the clustercentric distance. In the cluster cores, the ratio is ∼ 35%, indicating that even in these regions EMLs dominate the active population. The fraction strongly decreases from the cluster center to $0.6R_{200}$, of a factor of 3, while it is almost constant in the outer regions ($R/R_{200} > 0.7$). Also the incidence of sPSBs (black dots in the upper panel of Fig.6.5) among the active population increases toward the center, even if with a less steep trend.

These results might arise due to the different proportions in the population mix as a function of the global environment, i.e. different cluster halo mass. I therefore considered (see Fig. 6.5) two different cluster velocity dispersion bins, respectively with

$\sigma < 840\,km\,s^{-1}$ (short dashed line) and $\sigma > 840\,km\,s^{-1}$ (long dashed line) and found that the trends persist, being more pronounced in the high cluster mass bin.[1] A more detailed analysis of the dependence of the post-starburst fraction on the cluster global properties will be discussed in sect.6.4.6.

Considering the PSBs of different morphological types, I found that, overall, the incidence of ellipitcals, S0s and late-types does not change with clustercentric distance (Fig. 6.6), suggesting that there is no morphological segregation for PSBs.

6.4.4 Substructures

Clusters are generally characterized by the presence of substructures (Ramella et al., 2007; Biviano et al., 2002), which implies that merging between clusters and groups is a rather common physical process of cluster formation. This merging process has been found to affect greatly star formation histories of member galaxies and to eventually induce secondary starbursts (see Cohen et al., 2014; Bekki, 1999; Bekki et al., 2010). The coincidence of the position of the strongest k+a galaxies and the X-ray substructures in Coma found by Poggianti (2004) strengthens this scenario.

To check whether the presence of substructures alters the star formation in cluster galaxies, I computed the fractions of the PSB galaxies belonging to these systems. I used the catalogs of the OmegaWINGS substructures presented by Biviano et al. (in prep.), who define substructures and assign member galaxies to potential substructures exploiting the velocity distributions of galaxies in the cluster local density peaks.

30.4±0.4% of the member galaxies belong to substructures and, among these, 6.1±0.4% are PSB galaxies and 0.9±0.2% are sPSBs. The percentage of the PSBs is slightly lower than the value found for the same population when considering the entire galaxy sample (7.2±0.2%).

The same conclusion holds for the fraction of PSB and sPSB galaxies with respect to the active population. Thus, this type of analysis does not reveal a strong PSB enhancement in substructures.

I also investigated the fraction of PSB, PAS and EML galaxies in clusters characterized by different levels of relaxation. I used the parameter SUB defined in Biviano et al. (in prep.) that depends, among other things, on the fraction of member galaxies belonging to substructures, and consider three types of clusters: relaxed ($SUB = 0$), partly relaxed

[1] The value 840 km/s was chosen to approximately divide the galaxy sample in 2 equally populated bins.

($SUB = 1$) and unrelaxed ($SUB > 1$). In agreement with e.g. Cohen et al. (2015) and Biviano et al. (1997), I found a higher/lower fraction of EML/PAS galaxies in less relaxed clusters than in more-relaxed ones (0.34±0.01/0.58±0.01; 0.41±0.01/0.522±0.01 and 0.44±0.01/0.50±0.01 for SUB=0, SUB=1 and SUB> 1, respectively). Even more interestingly, the fraction of PSB galaxies also depends on the dynamical state of the cluster, following the trend of the PAS population: the PSB/PSB+EML fractions are 0.18±0.01, 0.14±0.01 and 0.12±0.01 for SUB=0, 1 and > 1, respectively. This is the opposite of what might be expected, if merging clusters were the most favorable environment for PSB production. Part of this trend might be due to the existence of the correlation between PSB fraction and L_X (Fig.6.9), as the average X-ray luminosity decreases going from more relaxed to less relaxed clusters (2.8, 2.7 and 1.3 $\times 10^{44}$ ergs^{-1} for SUB=0, 1, > 1). Moreover, the most unrelaxed clusters are in a sense clusters still in the formation process, in which the galaxy populations are still very similar to the unprocessed population of galaxies in the merging groups/clusters, therefore are still very rich of star-forming galaxies that have not experienced a massive cluster environment yet.

6.4.5 Phase space analysis

Many recent papers (Biviano et al., 2002; Haines et al., 2013; Oman et al., 2013; Muzzin et al., 2014; Jaffé et al., 2016) have shown that galaxy populations with different dynamical

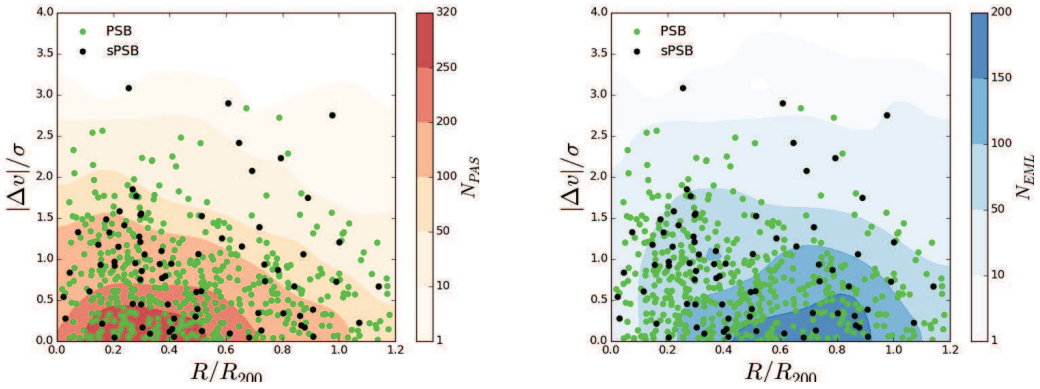

Figure 6.7: Observed stacked phase space diagram for cluster members. Clustercentric distances are in units of R_{200} and the absolute value of the line-of-sight velocities with respect to the cluster recessional velocities are normalized by the velocity dispersion of the cluster. PSB galaxies are represented by green points, sPSB galaxies by black points. They are over-plotted to PAS galaxies (left panel, red contours) and to EML galaxies (right panel, blue contours).

histories are well separated in the so-called phase space, which constrains the spatial position of a galaxy in the clusters, in units of R_{200}, and its peculiar velocity, Δv, normalized by the velocity dispersion of the cluster σ. Moreover, the theoretical phase space diagram derived from cosmological simulations retains information of the epoch of accretion of a galaxy, that can therefore be estimated based on the location of the galaxy in the diagram (Haines et al., 2015). The same is unfortunately not possible with observations, given the large uncertainties that induce the different populations to overlap on the plane. However, it is still possible to retrieve important clues about the dynamical histories of the different galaxy populations in clusters (see Mahajan et al., 2011; Oman et al., 2013; Muzzin et al., 2014; Hernández-Fernández et al., 2014; Haines et al., 2015; Jaffé et al., 2015, 2016). Indeed, the overall distribution of galaxies in the phase space strongly depends on the infall times: galaxies that where accreted earlier (i.e. virialized galaxies) typically occupy a triangular-shaped region while the recently accreted or infalling population permeates all projected velocities and radii. Combining this evidence with the well-established correlation between galaxy quiescence and environment, PAS galaxies are expected to form the majority of the virialized population while EML and PSB galaxies should belong to the infall or recently accreted sample.

Figure 6.7 shows the projected phase space obtained combining all clusters together for the different subpopulations separately. As expected, PAS galaxies are typically found in a triangular-shaped virialized region, which corresponds to the low velocity-low distance area, while EML galaxies are more spread in both radius and velocity. The PSB population, as already discussed, preferentially lies at small clustercentric distances ($R< 0.6R_{200}$), exhibiting anyway a non negligible spread in velocity. Their distribution is quite similar to the distribution of k+a's in high-z clusters found by Muzzin et al. (2014) who, comparing the observed phase-space diagram with simulations, concluded that the location of k+a galaxies can be interpreted with a rapid quenching timescale (0.1-0.5Gyr) happening at preferentially 0.5 R_{200}.

A 2D K-S test on Fig. 6.7 rejects the hypothesis that both PSB and EML and, with a slightly less significance, PSB and PAS galaxies are drawn from the same distribution (p-values respectively of 0.0 and 0.07), suggesting indeed that these populations are in different stages of their virialization process. The sPSB population can be better distinguished in terms of velocity rather than clustercentric distance: following the general radial trend of PSB galaxies, these galaxies have slightly higher velocities (median velocities of 0.67 ± 0.02 km/s and 0.87 ± 0.07 km/s for the PSB and sPSB population, respectively).

To better quantify the differences between the populations, following the procedure

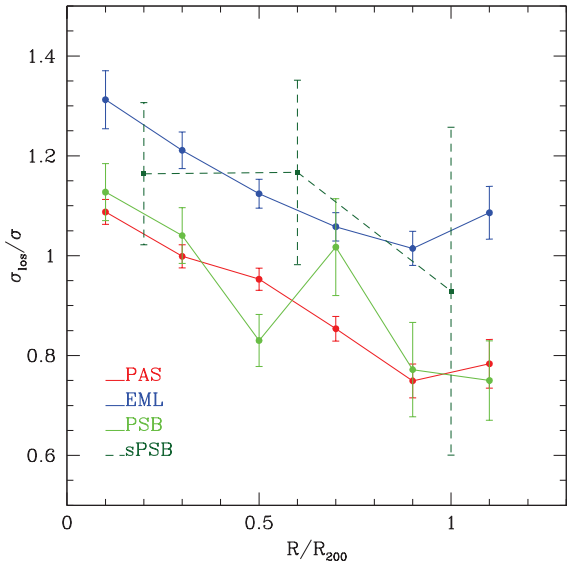

Figure 6.8: Velocity dispersion profiles ($\sigma_{LOS}(r)/\sigma$) of each galaxy population; colors refer to the different populations as described in the labels and as in Fig. 6.5. Errors are jackknife standard deviations (Efron, 1982).

adopted by Haines et al. (2015) for 75 simulated clusters at z= 0.0, Fig. 6.8 shows the mean normalized line of sight (LOS) velocity dispersion of each sub-population (σ_{LOS}/σ) in six bins of projected radial distance. The errors are obtained using the classical jackknife technique (Efron, 1982). Due to the low number statistics, the sPSB sample is divided only in three bins spanning the same radial range.

The different velocity dispersion profiles can be explained according to the dynamical evolution and accretion history of the galaxy populations.

PAS and EML galaxies are well separated, the former having low LOS-velocity dispersion at all radii with respect to the latter that displays, especially in the cluster core, higher values of σ. These trends are best reproduced by the virialized population, which was accreted at early epochs ($z > 0.4$), and by the most recently accreted and backsplash populations, respectively.

The profile of the PSB population follows the one traced by the PAS/virialized population, while sPSBs have remarkably larger velocity dispersions thus belonging to the more recently accreted population.

These findings fit well the scenario in which the strength of the EW(Hδ) sets a time line with higher values indicating a more recent quenching event. If the sPSBs are the

consequence of a starburst prior to a sudden quenching, the violent/sudden event that triggers the burst seems to happen on first infall; moderate PSBs could originate in the same way but are observed longer time after quenching (Poggianti et al., 2009).

6.4.6 Dependence of the spectral type fractions on cluster properties

So far I have shown how the fractions of the different subpopulations change as a function of the spatial location, both physical and dynamical, within the clusters.

I now examine if and how the fraction of PSB galaxies depends on the global properties of the clusters, such as velocity dispersion and X-ray luminosity, both proxy for the system total mass. It is still unclear whether cluster mass affects the amount of observed star formation. For example, several studies at high and intermediate redshifts (e.g. Finn et al., 2005; Poggianti et al., 2006) find an inverse correlation between star formation and cluster mass, while no such correlation is found in the nearby cluster population (e.g. Poggianti et al., 2006; Popesso et al., 2007).

All our clusters contain galaxies belonging to all the three main spectral classes, but the population mix in each cluster is quite different. To assess if these differences arise from a dependence on the cluster halo mass, for each cluster I computed the PSB fraction, weighted for completeness, among all galaxies and among the active population. For this analysis, I restricted the data to an absolute magnitude limited sample. This should prevent the introduction of possible systematics related to the selection criteria of the cluster sample. Member galaxies brighter than $M_V = -17.4$ were selected. This is the absolute magnitude corresponding to the $V = 20$ apparent magnitude limit of the most distant cluster.

The results are shown in Fig. 6.9 where the individual systems, indicated as black points, are shown as a function of velocity dispersion (left) and X-ray luminosity (right).

To mark the average trend I grouped the cluster sample into five bins of σ and L_X with approximately the same number of objects and show the results as red points. Both fractions (PSB/all and PSB/active galaxies) increase with the mass of the system, more significantly when we consider the X-ray luminosity rather than the velocity dispersion. A Spearman correlation test confirms all the trends at 99% level. This result is in line with the finding of Poggianti et al. (2009) for clusters in the EDisCS sample at $z \sim 0.5$, even if the strength of the correlations for our sample is lower (the Spearman test yields a 99.1% and 99.7% probability of a correlation with the velocity dispersion of their PSB/all and PSB/active fractions, respectively). On the contrary, it is at odds with the analysis

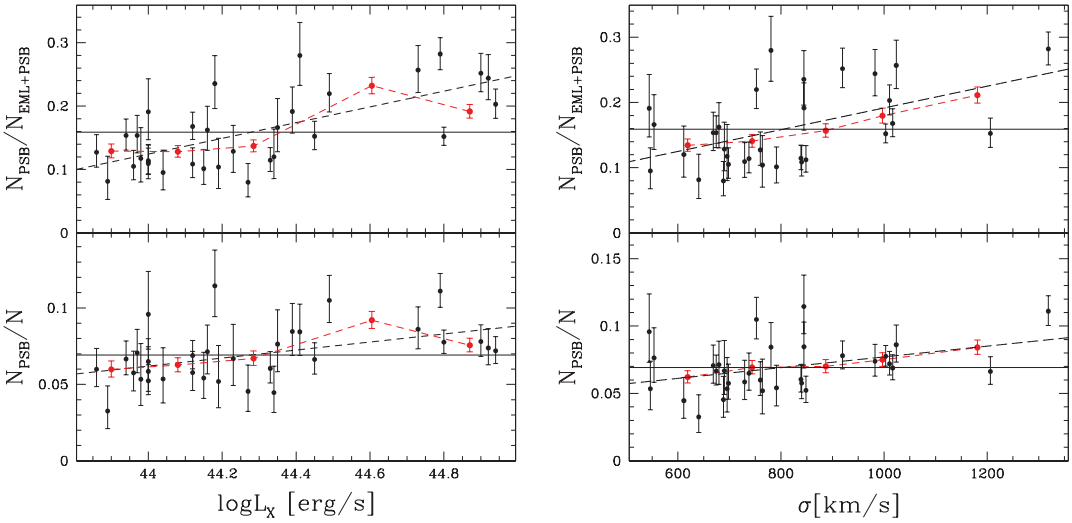

Figure 6.9: Fraction of post-starburst galaxies as a function of the cluster X-ray luminosity (left) and velocity dispersion (right). Black points represent individual clusters, red points give the fractions in 5 equally populated bins. Lower panels: weighted fraction of post-starburst galaxies among the whole population. Upper panels:weighted fraction of post-starburst galaxies among the active population. Errors are binomial. Solid black line: mean; black dashed line: least square fit.

performed by Fritz et al. (2014) on the restricted WINGS sample that did not see any correlation with neither the velocity dispersion nor the X-ray luminosity. Discrepancies could be due to several reasons, such as the different selection criteria for post-starburst galaxies (they did not use the information on the H_α line), the different cut in magnitude, the higher completeness and the larger area covered by our sample.

6.5 A comparison between PSBs and galaxies in transition

Exploiting the capabilities of the combined WINGS and OmegaWINGS samples, in this chapter I have investigated the properties and the spatial distribution of galaxies that are currently star-forming, that have recently interrupted their star formation and that are already passive in clusters at $0.04 < z < 0.07$. The main focus has been on PSB galaxies, to shed light on the processes that induce galaxies to undergo this particular phase during their life.

PSB galaxies are characterized by intermediate physical properties with respect to the EML and PAS galaxies, and are thought to be in a transition phase between these two populations: both their median stellar mass and magnitudes are in between the values

found for the other two populations. As expected given the fact that they have no ongoing star formation, PSB galaxies present colors similar to the PAS galaxies, even though at faint magnitudes they can also be as blue as the EML galaxies.

Almost half of the PSBs galaxies have been classified as S0s, while the incidence of elliptical and late-type galaxies depends on the strength of the measured Hδ: considering all PSBs, the fraction of ellipticals and late-types is similar, considering only the sPSB, late-type galaxies dominate the population.

The fraction of PSB galaxies decreases with increasing distance, suggesting that in the core of the clusters some mechanisms are inducing galaxy transitions. The same fraction also depends on the cluster properties and it steadily increases with increasing L_x and σ.

Moreover, PSBs do not concentrate as much in the low clustercentric distance-low velocity locus of the phase-space as virialized galaxies do. This, together with the fact that their velocity dispersion is quite intermediate between that of PAS and EML galaxies, especially for the sPSB galaxies, could lead to the interpretation that PSBs are a combination of galaxies with a mix of times-since infall (backsplash + virialized). Ideally, one should define the virial, infall and backsplash classes following the orbits of the particles using cosmological simulation. This task is beyond the scope of this work but will be addressed in forthcoming papers.

6.5.1 Slow and fast quenching mechanisms in clusters

As found by a large number of works (Couch & Sharples 1987, Poggianti & Barbaro 1996, Poggianti et al. (1999), Tran et al. (2007), and Muzzin et al. (2014)), PSB galaxies have to be generated by a fast acting mechanism ($\leq 10^8$ yr), while the k+a signature is observable approximately for 1-1.5 Gyr. As already discussed in Sec.6.1, spectra showing strong Balmer absorption lines and no emission are the result of a combination of an old stellar population above which A-type stars signatures are well visible. These stars, formed within the last Gyr, dominate the light of a galaxy where a recent star formation activity has ended abruptly and are visible for 1-1.5 Gyr (e.g. Poggianti, 2004, and references therein). Even though this is a quite efficient channel to transform galaxies from star forming to passive, it is definitely not the only one. For example, Patel et al. (2009); Vulcani et al. (2010) have found a population of galaxies in transition on long time scales (few Gyr) both in the local universe and at higher redshift ($z < 1$). Adopting a different approach, following the infall and orbits of galaxies in the vicinity of the 75 most massive clusters in the Millennium cosmological simulation, also Haines et al. (2015) support a

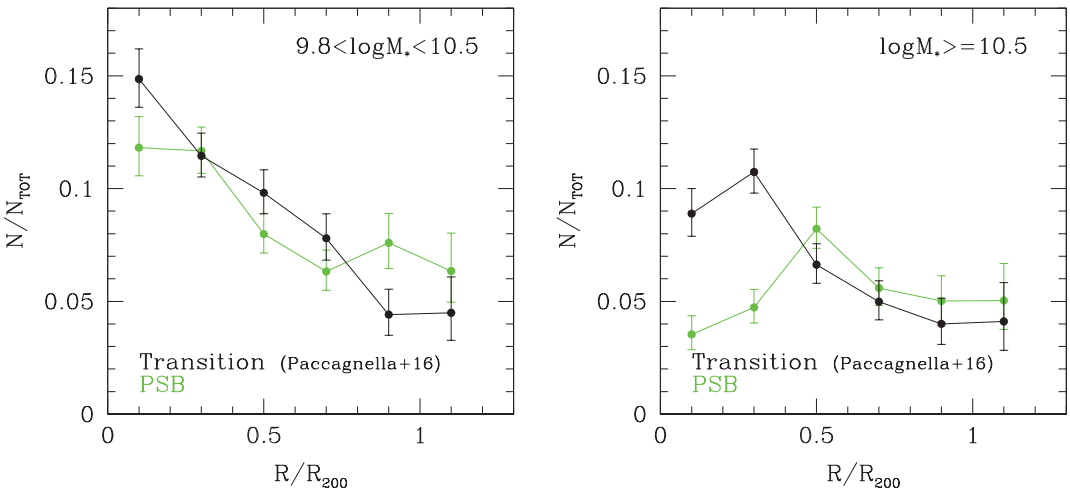

Figure 6.10: Radial distribution of transition galaxies (black) as defined by Paccagnella et al. (2016) and of PSB galaxies (green), in two bins of stellar mass. Errors are binomial.

slow quenching scenario, with a timescale of the order of 0.7-2 Gyr.

Seeking for objects in transition from being star forming to becoming passive, in the previous chapter, analyzing the SFR-M_* relation of local cluster galaxies in a mass-limited sample extracted from the WINGS+OmegaWINGS sample, I defined a sample of *transition galaxies*, whose star formation histories and properties suggest that they have had a reduced SFR for the past 2-5 Gyr. At least above the mass completeness limit, the fraction of transition galaxies strongly depends on environment, being almost negligible outside the virial radius and rising towards the center, making up for almost 30% of all star forming galaxies inside $0.6R_{200}$. These findings, together with the estimated quenching time scale, are consistent with the hypothesis that the interaction of galaxies with the intracluster medium via strangulation causes a gradual shut down of star formation, although also other mechanisms cannot be ruled out.

I am now in the position of directly comparing the slow quenching channel with the much faster one required to observe the typical post-starburst signatures. To do so, I consider only galaxies with stellar mass larger than the mass completeness limit of $10^{9.8} M_\odot$. 346 PSB galaxies (650 once weighted for completeness) enter the sample, of which only 32 (56) are sPSB. Above this limit, PSBs constitute 7.3±0.3% of the total population and all the environmental dependencies found for the whole sample persist. For comparison, I recall that above the same limit and the same clustercentric distance, 408 (780) galaxies

have been classified as in transition, and they constitute 9.0±0.3% of the entire population. By definition, being transition galaxies selected from the star forming population, there is no object entering both samples.

Therefore transition galaxies are only slightly more numerous than PSB galaxies. Starting from the logical assumption that both populations have their progenitors among star-forming galaxies, and assuming that the transition phase lasts for about twice the time (of the order of >2 Gyr) of the PSB visibility (∼1 Gyr), I conclude that the short timescale star-formation "quenching" channel contributes at least two times more than the long timescale one to the growth of the passive population.

Figure 6.10 investigates in detail where these two populations are found within the clusters. It shows the number of transition and PSB galaxies to the total number of galaxies, as a function of clustercentric distance. As done in sect. 5.3.2, two different mass bins are considered here, to also look for trends with stellar mass. For $\log M_* < 10.5$, PSB and transition galaxies present a similar anticorrelation between the fraction of PSB and transition objects and distance, even though PSB galaxies show a slightly flatter trend, being less numerous than transition galaxies in the core of the clusters and slightly more numerous outside the virial radius.

For $\log M_* > 10.5$, at large clustercentric distances, both populations present trends similar to those at lower masses, but in the cluster cores they present a drop in number. Such drop occurs only in the very cluster cores for transition galaxies, at $R < 0.5R_{200}$ for PSBs. Overall, it might be primarily due to the fact that in the cluster cores massive galaxies are already mostly passive, therefore the reservoir for transitioning galaxies is poorer than at lower masses. In addition, the different behavior seen for the two populations could be due to the visibility time-scales of the two populations, with PSBs disappearing faster than transition galaxies on the way to the cluster core.

As mentioned in sect.4.2.1, galaxies drawn from the WINGS sample (approximately all those located within 0.6 R_{200}), have been morphologically classified. I can therefore compare the morphologies of PSB and transition galaxies in the core of the clusters, to look for signs of a link between galaxy morphology and time scale of quenching. I considered the mass limited samples. Overall, among PSB galaxies, 40±2% are ellipticals, 44±2% are S0s and the remaining 16±2% are late-type galaxies. Transition galaxies have a much more numerous population of S0s, with a remarkable 56±2% at the expense of elliptical galaxies, accounting only for the 28±2%, while 16±2% are late-types.

No strong trends of the morphological mix with distance have been detected, as can be seen in figure 6.11. However, I stress that here only galaxies in the core of the clusters

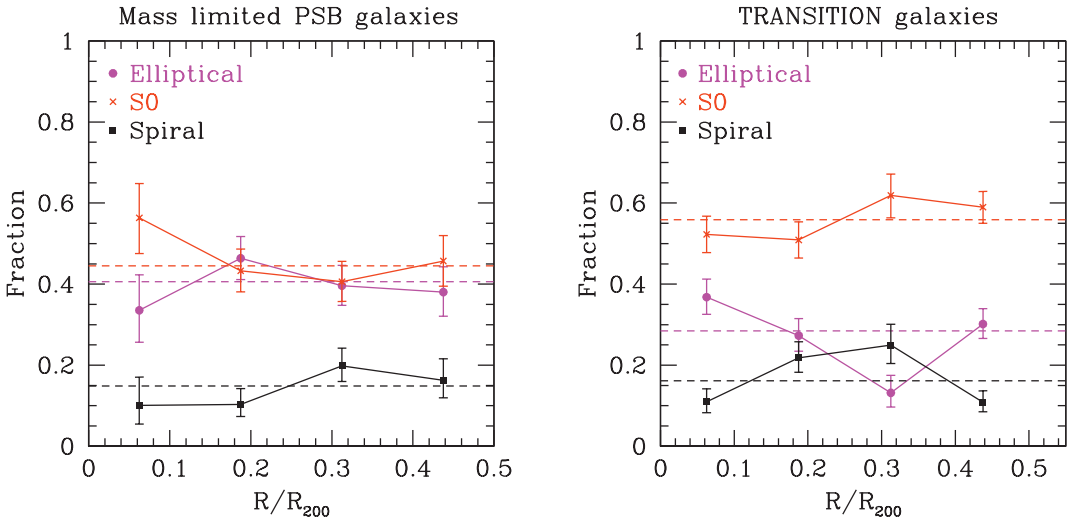

Figure 6.11: Morphological fractions for the mass limited sample of PSB (left) and transition galaxies (right) within 0.5 R/R_{200}. Black squares refer to spiral galaxies, red crosses to S0s, magenta circles to ellipticals. The dashed lines mark the total fractions. Errors are defined as binomial errors.

were considered, and no attempt to extrapolate trends at larger distances, where the morphological mix might be different, has been made. Moreover, this analysis is performed above the mass completeness limit of $10^{9.8} M_{\odot}$ and this cut excludes the vast majority of sPSB galaxies from our sample. This population has been found to have a distinct morphology from the whole population of PSB galaxies (see section 6.4.1).

Studies regarding slow and fast quenching should necessarily follow different approaches. As far as the post-starburst population is concerned, due to the high precision clocks imposed by lack of emission lines and by the A-type stars lifetime, there is a general agreement on the time-scales involved (see Quintero et al., 2004; Poggianti, 2004; Poggianti et al., 2009; Muzzin et al., 2014; Vulcani et al., 2015, etc.) and, based on these, ram pressure stripping has been proposed as main responsible mechanism. On the other hand, an hypothesis on the physical processes causing the slow quenching of a galaxy has to be made to estimate the time scales involved. Several authors have tried to estimate the quenching timescales of satellite galaxies through different approaches. Wetzel et al. (2013) proposed a mass dependent "delay-then-rapid" scenario in which star formation is quenched rapidly but only after a delay of 2-4 Gyr after infall. As an alternative Taranu et al. (2013) presented models where quenching occurs within a smaller radius, approximately $0.5 R_{200}$,

followed by an exponential decline of star formation over 3-3.5 Gyr.

6.5.2 Specific processes responsible for the objects in transitions in clusters

I found the majority of transition and PSB galaxies within the virial radius. From these results it seems clear that any of the proposed physical mechanisms (i.e. starvation or ram pressure stripping), which alter the star formation of infalling galaxies, is stronger in the central regions of the clusters, where the density and the temperature of the ICM (as well as the velocity of galaxies) reach their maxima. By comparing the cluster crossing times and the A-stars lifetime, we could also imagine an evolutionary sequence in which some of the PSBs (the low massive ones, as discussed in sect. 6.4.1) descend from sPSB galaxies, i.e. the ram pressure starts being effective at larger distances, generating the population of sPSB, while at smaller cluster-centric distances we only see the PSB galaxies. However, the comparison of the radial trends of the fractions of PSBs and transition galaxies does not allow to definitely ascertain whether the two populations have a different origin. Indeed, both could be due to ram pressure stripping, which efficiency and strength depend, among other things, on the orbit and on the orientation of the galaxy with respect to the ICM (Abadi et al., 1999).

If the ram pressure induces a sudden shut down of the star formation, the resulting quenched population is expected to have PSB features, maintaining the original structural properties, since nothing apart from gas loss would disturb its morphology. On the contrary, if the effect of the ram pressure is more gentle and the suppression of the star formation is slower, the resulting population is expected to have the features of the galaxies in transition presented in Chapter 5. However, the same population could originate also via strangulation, consistent with a gradual quenching corresponding to a time scale of 2 Gyr or more. Indeed, strangulation is expected to have the effect of removing the outer galaxy gas halo and prevent further infall of gas into the disk. On timescales of a few Gyr, the star formation would thus exhaust the available gas, quenching the star formation activity. Boselli et al. (2006) found that strangulation is unable to explain the structural properties of spiral galaxies in clusters, favoring the ram pressure stripping scenario.

In addition to ram pressure stripping and strangulation, other mechanisms might play a role, even though they most likely take place at larger distances form the cluster center.

As discussed for example by Treu et al. (2003) and reviewed by Boselli and Gavazzi (2006), quenching from gravitational interaction between galaxies (i.e. galaxy-galaxy in-

teractions, harassment) occurs preferentially outside the virial radius and at all radii, respectively, given the high velocity dispersions in the cluster cores that remarkably reduce the probability of pair interactions. Moreover, these kind of interactions act on the stellar component, producing selective morphological transformations that we do not observe in the transition or PSB populations.

I emphasize that this does not mean that galaxy-galaxy interactions have no effect at all on cluster galaxies. These processes might eventually become important, but generally after the gas has been removed by other processes.

6.6 PSB galaxies: from single galaxies to clusters

So far I focused on PSB galaxies in clusters, investigating their properties and spatial distribution. Moreover, I showed that the fraction of PSB galaxies slowly increases with the mass of the cluster and is significantly lower within the field environment, suggesting that any physical mechanism causing the PSB signature should correlate with the halo mass of the system in which the galaxy is embedded. Nevertheless, as already said, the field sample extracted from the OmegaWINGS survey (see sec. 6.3) is small (only 15 PSB galaxies) and could be contaminated by galaxies belonging to filaments or secondary structures falling into the main clusters. A detailed study of the PSB population considering the whole range of environments, going from single galaxies to groups and clusters can be done considering also the PM2GC galaxy sample (see chapter 3). This is an absolute magnitude limited sample, including only galaxies brighter than $M_B = -18.7$. To compare the different data sets, I applied the same magnitude cut of the PM2GC also to the OmegaWINGS sample. In OmegaWINGS this leaves 2805 member galaxies (5130 once weighted for spectroscopic incompleteness). The fractions of PSB, PAS and PSF galaxies in the different environments are listed in table 6.6.

The fraction of PAS/EML galaxies increases/decreases going from single galaxies to binaries, groups and clusters. The fraction of PSB galaxies grows from the poorest (only 1% in single galaxies) to the richest environments (4.5% in clusters).

In Section 3.3.3 I found that groups with a low fraction of interlopers can be distinguished based on their location onto the $logM_* - \sigma$ space. Distinguishing between high and low contaminated groups is important because interlopers, i.e. field galaxies selected as group members, could significantly alter the galaxy fractions. For this reason I selected only *real* groups and recalculated the percentages of the different spectral types. As expected, removing the contamination introduced by possible field galaxies lowers the

Table 6.5: Weighted spectral numbers and fractions in different environments

Environment	PAS		PSB		EML	
	N	%	N	%	N	%
Clusters	3125 (1660)	60.9±0.6	229 (119)	4.5±0.3	1776 (1026)	34.6±0.6
Groups (all)	373	36±1	31	3.0±0.6	629	61±1
Real groups	280	42±2	25	3.7±0.7	364	54±2
Binaries	111	23±2	10	2.0±0.6	365	75±1
Single galaxy	168	15±1	12	1.1±0.4	943	84±1
General field	652	25±1	53	2.0±0.3	1937	73±1

Table 6.6: Weighted Number (raw numbers in brackets for clusters) and percentage of the different spectral types for the absolute magnitude-limited samples ($M_B < -18.7$). The proportion of PAS (k), PSB (k+a/a+k) and EML galaxies are listed along with binomial errors. The fractions for the general field population that includes galaxies in the whole PM2GC sample are also listed.

fraction of EML galaxies (from 61±1% to 54±2%) and increases the fraction of PAS galaxies (from 36±1% to 42±2%). The percentage of PSB galaxies also increases, going from 3.0±0.6% to 3.7±0.7%. Anyway, considering only these groups, the halo mass range narrows, removing almost all groups with $M_{halo} < 10^{12.2}$ $M_\odot$.

It is now possible to study the PSB population as a function of the mass of the dark matter halo. Concerning the PM2GC sample, as extensively described in section 3.3.4, halo masses were computed thanks to the total stellar mass-to halo relation derived from the Millennium Simulation.

For the cluster sample, the halo mass has been estimated from the σ_{cl}, by means of the virial theorem, following Poggianti et al. (2006) (sec.2.2.2). For this analysis I adopted the cosmology of the Millennium Simulation ($H_0 = 73 kms^{-1}Mpc^{-1}$, $\Omega_m = 0.25$ and $\Omega_\Lambda = 0.75$). This means that the halo masses derived from eq.2.2 and listed in table 2.3 for the OmegaWINGS sample were recalculated accounting for the proper cosmology.

Considering the different environments together, namely single galaxies, binaries, groups and clusters, the halo mass range covered goes from 10^{11} $M_\odot$ to approximately 10^{15} $M_\odot$.

Figure 6.12 shows the PSB fraction with respect to the whole galaxy population (PAS+EML+PSB) as a function of the halo mass. A clear trend emerges: the fraction of PSB galaxies increases with the halo mass. If only real groups are considered, this trend is even more pronounced. Not only the incidence of PSB galaxies becomes more important going from single galaxies to clusters, but also the quenching efficiency ($N_{PSB}/N_{PSB+EML}$) significantly increases, as is shown in figure 6.13.

These results are in agreement with Poggianti et al. (2009) who performed a spectral analysis of galaxies in clusters, groups, poor groups and the field at $z = 0.4 - 0.8$ based on

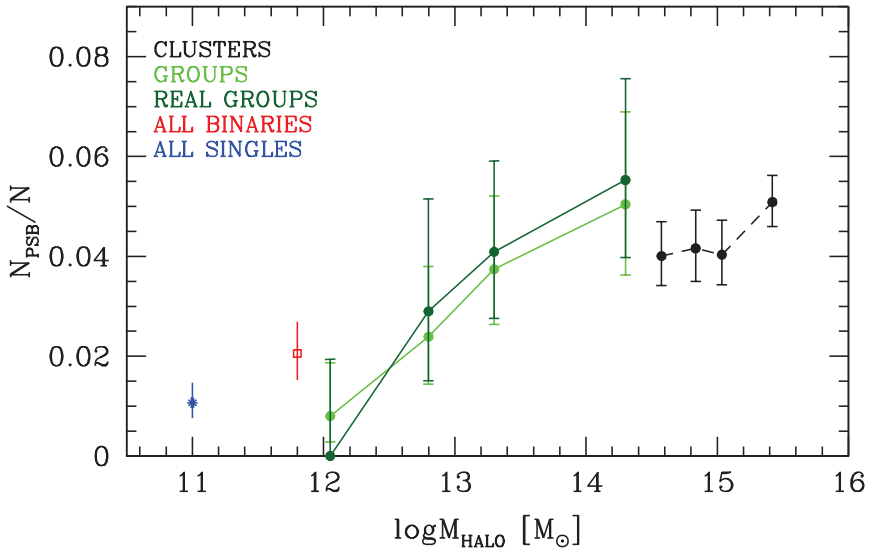

Figure 6.12: Fraction of PSB galaxies as a function of the halo mass for the absolute magnitude limited sample including OmegaWINGS cluster and the PM2GC sample. Black dots represent the cluster data; green(black) dots represent the PSB fractions in groups(real groups only). The red empty square and the blue cross at $LogM_{halo}$ =11.8 and 11 respectively show the value for binaries and single galaxies. Errors are binomial.

the ESO Distant Cluster Survey. They found that the incidence of $k+a$ galaxies at those redshifts depends strongly on environment: PSB's reside preferentially in clusters and, unexpectedly, in a subset of the groups that have a low fraction of [OII] emitters. In these environments, 20-30% of the recently star-forming galaxies have had their star formation activity recently truncated. In contrast, there are proportionally fewer $k+a$ galaxies in the field, the poor groups and groups with a high [OII] fraction. Also Dressler et al. (2013), examining the full range of environments sampled in the IMACS Cluster Building Survey at $0.31 < z < 0.54$, found that PSB galaxies strongly favor denser environments and their incidence increases going from the field to groups and clusters (see their figure 19(a)). At lower redshifts, Gavazzi et al. (2010), studying the PSB population within the Coma supercluster confirm this rising trend: the PSB fraction is found to significantly increase as a function of the local density, going from the cosmic web to groups and finally the cluster center.

The picture emerging from these works and from our analysis is that any physical mechanism responsible for the truncation of star formation on time-scales as short as or

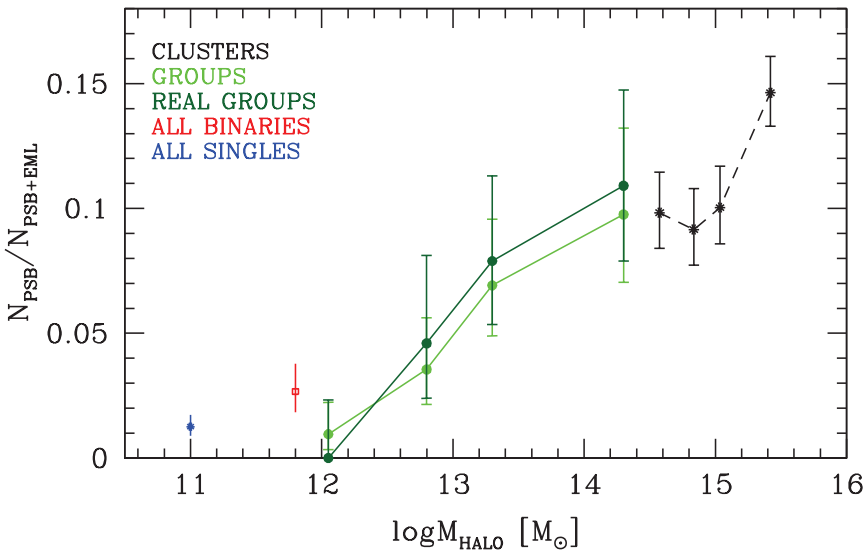

Figure 6.13: Fraction of PSB galaxies with respect to the active population (EML+PSB) as a function of the halo mass for the absolute magnitude limited sample including OmegaWINGS cluster and the PM2GC sample. Symbols and colors as in figure 6.12. Errors are binomial.

shorter than ∼100 Myr, that is the quenching timescale required to give origin to the PSB signature in a galaxy spectrum, must depend in some way on the global environment. The observed trend with halo mass for the cluster PSB population can be easily explained if the truncation is due to the interaction with the intracluster medium. As already discussed and extensively modeled (see for example Boselli et al. 2008) ram pressure stripping could be the driving mechanism. Concerning group PSBs, the strong observed correlations with halo mass could be explained as the natural sequence of intergalactic medium (IGM), with more massive systems having a denser IGM. When smaller systems as binaries or even single galaxies are included in the global picture, other processes might need to be considered. In these environments, the most obvious candidate mechanisms are close galaxy interactions or mergers. A merger could, at least temporarily, exhaust in a short time the available gas and thus give rise to a PSB spectrum. Several works support this scenario, from both the theoretical and observational point of view (Bekki et al., 2001; Goto, 2005; Blake et al., 2004, and references therein). Quite interestingly, theoretical simulations indicate that the PSB spectrum marks a late stage of the merging event, when the merging companion is no longer identifiable as the morphological signatures of

the merging.

Unfortunately, the PSB spectrum does not allow to distinguish between different mechanisms, establishing, as I said, only the time scale for the truncation of the star formation. Thus, any physical process that is able to abruptly shut down star formation needs to be considered.

6.7 Summary

In this chapter I have resorted to an observed magnitude limited sample of galaxies in clusters drawn from the WINGS and OmegaWINGS surveys to investigate the occurrence and the properties of galaxies of different types in 32 clusters at $0.04 < z < 0.07$. I classified the galaxies according to the different features detected in their spectra (presence/absence of [OII], Hδ and Hα) into passive (PAS), post starburst (PSB) and emission line (EML) galaxies. We have compared stellar population properties and location within the clusters of the different spectral types to obtain valuable insights on the physical processes responsible for the star formation quenching.

The main results can be summarized as follows.

- For $V < 20$, PAS represent $55.7 \pm 0.4\%$ of the cluster population within 1.2 virial radii, EML represent $37.0 \pm 0.4\%$ and PSBs $7.3 \pm 0.2\%$, 15% of which show strong Hδ in absorption (> 6Å, sPSB), indication of either a very recent quenching and/or a strong burst before quenching.

- PSBs have stellar masses, magnitudes, colors and morphologies intermediate between PAS and EML galaxies, typical of a population in transition from being star forming to passive. Interestingly, 45% of PSBs have S0 morphology, $28\pm1\%$ are ellipticals and $27\pm1\%$ are late types. Considering only sPSBs, the incidence of late-types increases to $42 \pm 4\%$ with a corresponding drops of ellipticals, which are only $17 \pm 3\%$.

- The incidence of PSBs increases from the cluster outskirts toward the cluster center and from the least toward the most luminous and massive clusters, defined in terms of L_X and velocity dispersion.

- The dynamical state of the clusters partially influences the incidence of PSBs. While the presence of substructures does not enhance the fraction of PSBs, the level of relaxation does: the fraction of PSBs is higher in relaxed clusters. At least part of this trend is due to the correlation between PSB fraction and L_X.

- The phase space analysis and the velocity dispersion profiles suggest that PSBs represent a combination of galaxies with different accretion histories. Moreover, the PSBs with the strongest Hδ are consistent with being recently accreted.

- Exploiting an absolute magnitude limited sample that includes also the PM2GC catalog ($M_B < -18.7$), I showed that the incidence of PSB galaxies increases as a function of halo mass, going from single galaxies, to binaries, groups and clusters.

PSBs are thought to be galaxies generated by fast acting mechanisms (quenching timescale $\leq 10^8$ yr) and this phase is expected to be observable approximately for 1-1.5 Gyr (e.g. Poggianti, 2004; Muzzin et al., 2014). This analysis suggests that as a galaxy is accreted onto a cluster, at first its properties are not strongly affected, but when it approaches the virialized region of the cluster, processes like ram pressure stripping or other interactions induce either a burst of the star formation with a subsequent fast quenching, or simply a fast quenching. As the shut off of the star formation occurs, the galaxy changes the features in its spectrum, but variations in color and morphology require longer time scales, therefore PSBs appear with a wide range of these properties. It is important to stress that the majority of those galaxies that are truncated on a short timescale cannot be recognized based on color or color+morphology, but only by performing a detailed spectral analysis.

The fraction of PSBs is similar to the fraction of galaxies in transition on longer timescales, as defined in the previous chapter, while the PSB visibility timescale is less than half that of the transitioning population. This suggests that the short timescale quenching channel contributes twice more than the long timescale process to the growth of the passive population. Hence, processes like ram pressure stripping appear to be more efficient than strangulation in affecting star formation in clusters.

In other environments, the fraction of PSB galaxies and the processes responsible for its existence might be considerably different. In agreement with Vulcani et al. (2015), I found an enhanced fraction of PSB galaxies in groups compared to isolated and binary systems. A complete characterization of the physical processes in these environments should include the interaction of galaxies with the intergalactic medium and the gravitational interactions between galaxies, that are expected to be more efficient in lower density regions.

7

Conclusions and Future work

The work presented in this thesis has been aimed at obtaining a better understanding of the processes that affect galaxies that reside in clusters. In particular I have investigated the effects of environment on the star formation activity within galaxies in the local Universe ($z < 0.1$). I have studied the suppression of star formation in cluster galaxies at two different stages of their evolution. On one hand, I have focused on cluster galaxies while they are still forming stars, but are already going through a process, or multiple processes, that affect the rate at which they form stars. On the other hand, I have analyzed galaxies just after their star formation has been strongly suppressed, and explored the different mechanisms that drove the transformation from actively star-forming to passive. In the following I summarize the main results.

Chapter 2 is dedicated to the presentation of the cluster sample, built matching the WINGS and OmegaWINGS galaxy catalogs. I summarized the main characteristic of WINGS and focused on the description of the new OmegaWINGS survey: I described the procedure used to measure redshifts, the computation of the velocity dispersions and membership assignments. The final catalog consists of 60 clusters in the redshift range $0.04 < z < 0.07$ and includes 11144 member galaxies with $V > 20$.

To complete the description of the data sample, in **Chapter 3** I presented the PM2GC catalog. Galaxies are selected according to their B rest frame magnitude ($M_B < -18.7$) and assigned to groups, binary or single systems thanks to a Friend of Friend algorithm. Exploiting a mock galaxy catalog built from semi analytic models run on the Millennium Simulation, I derived a simple method to distinguish high and low contaminated groups and obtained two functional formulations to compute halo masses from observable quantities: the stellar mass to halo relation, that links the halo mass to the stellar mass of the

most massive galaxy in the system, and the total stellar mass to halo relation.

In **Chapter 4** I discussed the methods adopted to compute the properties of the galaxy samples studied in the following analysis. The spectrophotometric code SINOPSIS has been used to derive properties as stellar masses, star formation rate, star formation histories, luminosity and mass weighted ages and to measure equivalent widths. I also presented the MORPHOT tool used to get the morphological classification from B and V images.

Exploiting the capabilities of the WINGS and OmegaWINGS samples, in **Chapter 5** I dealt with the relation between the star formation activity, galaxy stellar mass and environment exploiting a mass limited sample of galaxies extracted from the cluster samples with $0.04 < z < 0.07$ (see Chapter 2). I used non-member galaxies at $0.02<z<0.09$ as field control sample. Overall, I found agreement between the SFR-M_* relation in the two environments but I detected a population of cluster galaxies with reduced SFRs that is rare in the field. I thus divided star forming galaxies into *purely star forming* (PSF) and *transition* galaxies depending on the position on the SFR-M_* plane.

Investigating the spatial distribution of this transition population within the clusters ($0 < R/R_{200} < 2$), I found that they are mainly located within the cluster virial radius (R_{200}) while they are able to modify the median SFR-M_* relation only within $0.6R_{200}$. I also showed that the ratio of transition to PSF strongly depends on environment, being larger than 0.6 within $0.3R_{200}$ and rapidly decreasing with distance, while it is almost flat with M_*.

These trends, together with the analysis of the star formation histories and of the properties of galaxies, suggest that transition galaxies have had a reduced SFR for the past 2-5 Gyr. These results are consistent with the hypothesis that the interaction of galaxies with the ICM via strangulation causes a gradual shut down of star formation, giving birth to an evolved population of galaxies in transition from being star forming to becoming passive. However, other physical processes might also be responsible, such as for example ram pressure stripping that could be less efficient on certain orbits and remove only part of the gas in the disk.

In **Chapter 6** I investigated the occurrence and properties of galaxies of different types, classified according to the different features detected in their spectra (presence/absence of [OII], Hδ and Hα), resorting to an observed magnitude limited sample in clusters drawn from the WINGS and OmegaWINGS surveys. The main focus has been on post starburst (PSB) galaxies, to shed light on the processes that induce galaxies to undergo this particular phase during their life.

For $V < 20$, the PSB fraction is 7.3±0.2%, 15% of which show strong Hδ (EW($H\delta$) > 6 Å) in absorption (strong PSB, sPBS), indication of a burst before very recent quenching. PSBs have properties intermediate between passive (PAS) and emission line (EML) galaxies, typical of a population that have recently turned passive. The analysis of the morphological fractions also revealed some interesting features concerning sPSB galaxies, with an enhanced fraction of late types with respect to the whole PSB population. Their incidence decreases with clustercentric distance, suggesting that in the cluster cores some mechanisms are inducing galaxy transitions. Their frequency also depends on cluster properties, being slightly higher in more luminous/more massive clusters. Also the dynamical state of the clusters partially influences the incidence of PSBs, which is higher in relaxed clusters. The phase space analysis and the velocity dispersion profiles suggest that PSBs represent a combination of galaxies with different accretion histories and sPSB are consistent with being recently accreted.

The dependence on the cluster global properties suggest that any physical mechanism causing the PSB signature should correlate with the halo mass of the system in which the galaxy is embedded. To further inspect this, I studied the PSB population as a function of the mass of the dark matter halo including also the galaxy sample extracted from the PM2GC database and described in Chapter 3. In order to compare the different data sets, this magnitude limit was applied also to the WINGS+OmegaWINGS sample. I characterized the global environment by means of the halo mass: concerning the PM2GC, halo masses were computed thanks to the total stellar mass-to halo relation, while for the cluster sample it has been estimated from the cluster velocity dispersion.

The fraction of PSB galaxies and the quenching efficiency (the ratio of PSBs to the active population, defined to include PSB galaxies and galaxies of all emission-line types) increase with halo mass, that goes from 10^{12} to approximately $10^{15} M_{\odot}$.

The emerging picture is that, in the different environments, the PSB signatures in the galaxy spectra might be due to different physical mechanisms, which all produce a truncation of star formation on time-scales of the order of $\sim 10^8$ yr. In clusters, ram pressure stripping is most likely the dominant process, while in groups the observed strong correlations with halo mass could originate from other processes. The origin of PSB galaxies in smaller halos is probably related to the perturbation induced by close galaxy interactions or mergers.

The two galaxy populations analyzed in this work represent two possible pathways to transform a healthy star forming galaxy into one of the many passive galaxies populating clusters in the local Universe. The time scales involved anyway are quite different:

transition galaxies require a gradual quenching of star formation over a long time scale, t> 2Gyr, while the visibility timescale for PSBs is less than a half, t∼1Gyr, and the quenching timescale to produce such spectral signature is an order of magnitude shorter. Two main physical processes have been proposed to explain the origin of these galaxies: strangulation and ram pressure stripping. I concluded this analysis performing a comparison between PSB and transition galaxies. I found that the fraction of PSBs is similar to the fraction of transition galaxies, and that both these population preferentially lie within the virial radius, with quite similar radial trends. These results suggest that the short timescale quenching channel contributes twice more than the long timescale process to the growth of the passive population. Hence, processes like ram pressure stripping appear to be more efficient than strangulation in affecting star formation in clusters.

From this analysis two different scenarios can be depicted in which star formation can either be suddenly shut down and give origin to the PSB population, or more gently and progressively depressed (by strangulation, or by the same ram-pressure stripping), and produce the outliers in the SFR-mass relation.

In addition to ram pressure stripping and strangulation, other mechanisms might play a role, even though they should take place also at larger distances form the cluster center. Moreover, these kind of interactions act on the stellar component, producing selective morphological transformations that were not observed in the transition or PSB populations.

I emphasize that this does not mean that galaxy-galaxy interactions have no effect at all on cluster galaxies. These processes might eventually become important, but generally after the gas has been removed by other processes.

7.1 Future works

A lot of work has already been devoted to the study of star formation in cluster galaxies and the transformation of galaxies from star forming to passive, producing many significant results. However, several open questions emerged and in the future I plan to extend the work done in this Thesis to answer some of them.

So far I investigated the impact of environment measured as clustercentric distance and halo mass. In order to reach a better understanding of the environmental dependence of galaxy properties it is now necessary to combine these results with others where the environment is parametrized in terms of local density estimates, together with a theoretical understanding of what could influence the star formation activity and morphological transformations in galaxies. For these reasons I plan to exploit the local density catalogs of the OmegaWINGS targets that will be available in the next few months (Vulcani et al. in preparation).

In addition, I aim to characterize in detail the PSB galaxies in the PM2GC sample, identifying galaxies that show disturbed morphologies indicative of recent merging. This would allow to confirm the origin of this population in low-density environments. Concerning the cluster sample, a comparison with the X-ray residuals and temperature maps would also be useful to properly characterize the interaction of galaxies with the ICM.

All the environmental quenching mechanisms considered in this Thesis are sensitive to the path taken by the galaxies through the cluster. Strangulation is strongest near the cluster center. Ram pressure stripping varies with the local density of hot cluster gas and the relative velocity of the galaxy, both of which vary radially in the cluster. Mergers are more probable in the outskirts of clusters. Harassment is most effective during high speed encounters, which occur near the cluster core. Thus, another interesting step forward will be a detailed study of the orbital history of the different types of galaxies, comparing our results with simulations.

List of Figures

List of Tables

Bibliography

Abadi, M. G., Moore, B., and Bower, R. G. (1999). Ram pressure stripping of spiral galaxies in clusters. MNRAS, 308:947–954.

Abraham, R. G., Smecker-Hane, T. A., Hutchings, J. B., Carlberg, R. G., Yee, H. K. C., Ellingson, E., Morris, S., Oke, J. B., and Rigler, M. (1996). Galaxy Evolution in Abell 2390. ApJ, 471:694.

Alatalo, K., Cales, S. L., Rich, J. A., Appleton, P. N., Kewley, L. J., Lacy, M., Lanz, L., Medling, A. M., and Nyland, K. (2016). Shocked POststarbust Galaxy Survey. I. Candidate Post-starbust Galaxies with Emission Line Ratios Consistent with Shocks. ApJS, 224:38.

Bahé, Y. M. and McCarthy, I. G. (2015). Star formation quenching in simulated group and cluster galaxies: when, how, and why? MNRAS, 447:969–992.

Bai, L., Rieke, G. H., Rieke, M. J., Christlein, D., and Zabludoff, A. I. (2009). The Infrared Luminosity Functions of Rich Clusters. ApJ, 693:1840–1850.

Baldry, I. K., Balogh, M. L., Bower, R. G., Glazebrook, K., Nichol, R. C., Bamford, S. P., and Budavari, T. (2006). Galaxy bimodality versus stellar mass and environment. MNRAS, 373:469–483.

Balogh, M., Eke, V., Miller, C., Lewis, I., Bower, R., Couch, W., Nichol, R., Bland-Hawthorn, J., Baldry, I. K., Baugh, C., Bridges, T., Cannon, R., Cole, S., Colless, M., Collins, C., Cross, N., Dalton, G., de Propris, R., Driver, S. P., Efstathiou, G., Ellis, R. S., Frenk, C. S., Glazebrook, K., Gomez, P., Gray, A., Hawkins, E., Jackson, C., Lahav, O., Lumsden, S., Maddox, S., Madgwick, D., Norberg, P., Peacock, J. A., Percival, W., Peterson, B. A., Sutherland, W., and Taylor, K. (2004a). Galaxy ecology: groups and low-density environments in the SDSS and 2dFGRS. MNRAS, 348:1355–1372.

Balogh, M. L., Baldry, I. K., Nichol, R., Miller, C., Bower, R., and Glazebrook, K. (2004b). The Bimodal Galaxy Color Distribution: Dependence on Luminosity and Environment. ApJ, 615:L101–L104.

Balogh, M. L., Morris, S. L., Yee, H. K. C., Carlberg, R. G., and Ellingson, E. (1997). Star Formation in Cluster Galaxies at 0.2 ¡ Z ¡ 0.55. ApJ, 488:L75–L78.

Balogh, M. L., Navarro, J. F., and Morris, S. L. (2000). The Origin of Star Formation Gradients in Rich Galaxy Clusters. ApJ, 540:113–121.

Bamford, S. P., Nichol, R. C., Baldry, I. K., Land, K., Lintott, C. J., Schawinski, K., Slosar, A., Szalay, A. S., Thomas, D., Torki, M., Andreescu, D., Edmondson, E. M., Miller, C. J., Murray, P., Raddick, M. J., and Vandenberg, J. (2009). Galaxy Zoo: the dependence of morphology and colour on environment. MNRAS, 393:1324–1352.

Baugh, C. M., Benson, A. J., Cole, S., Frenk, C. S., and Lacey, C. G. (1999). Modelling the evolution of galaxy clustering. MNRAS, 305:L21–L25.

Baugh, C. M., Cole, S., Frenk, C. S., and Lacey, C. G. (1998). The Epoch of Galaxy Formation. ApJ, 498:504–521.

Baum, W. A. (1959). Population Inferences from Star Counts, Surface Brightness and Colors. PASP, 71:106–117.

Beers, T. C., Flynn, K., and Gebhardt, K. (1990). Measures of location and scale for velocities in clusters of galaxies - A robust approach. AJ, 100:32–46.

Beijersbergen, M., Hoekstra, H., van Dokkum, P. G., and van der Hulst, T. (2002). U-, B- and r-band luminosity functions of galaxies in the Coma cluster. MNRAS, 329:385–397.

Bekki, K. (1999). Group-Cluster Merging and the Formation of Starburst Galaxies. ApJ, 510:L15–L19.

Bekki, K. and Couch, W. J. (2003). Starbursts from the Strong Compression of Galactic Molecular Clouds due to the High Pressure of the Intracluster Medium. ApJ, 596:L13–L16.

Bekki, K., Couch, W. J., and Shioya, Y. (2002). Passive Spiral Formation from Halo Gas Starvation: Gradual Transformation into S0s. ApJ, 577:651–657.

Bekki, K., Owers, M. S., and Couch, W. J. (2010). Synchronized Formation of Starburst and Post-starburst Galaxies in Merging Clusters of Galaxies. ApJ, 718:L27–L31.

Bekki, K., Shioya, Y., and Couch, W. J. (2001). Formation and Evolution of E+A Galaxies in Dusty Starburst Galaxies. ApJ, 547:L17–L20.

Bell, E. F. and de Jong, R. S. (2001). Stellar Mass-to-Light Ratios and the Tully-Fisher Relation. ApJ, 550:212–229.

Bell, E. F., Papovich, C., Wolf, C., Le Floc'h, E., Caldwell, J. A. R., Barden, M., Egami, E., McIntosh, D. H., Meisenheimer, K., Pérez-González, P. G., Rieke, G. H., Rieke, M. J., Rigby, J. R., and Rix, H.-W. (2005). Toward an Understanding of the Rapid Decline of the Cosmic Star Formation Rate. ApJ, 625:23–36.

Bertelli, G., Bressan, A., Chiosi, C., Fagotto, F., and Nasi, E. (1994). Theoretical isochrones from models with new radiative opacities. A&AS, 106.

Bertin, E. and Arnouts, S. (1996). SExtractor: Software for source extraction. A&AS, 117:393–404.

Bhavsar, S. P. (1981). On galaxy morphology in small groups. ApJ, 246:L5–L9.

Biviano, A., Katgert, P., Mazure, A., Moles, M., den Hartog, R., Perea, J., and Focardi, P. (1997). The ESO Nearby Abell Cluster Survey. III. Distribution and kinematics of emission-line galaxies. A&A, 321:84–104.

Biviano, A., Katgert, P., Thomas, T., and Adami, C. (2002). The ESO Nearby Abell Cluster Survey. XI. Segregation of cluster galaxies and subclustering. A&A, 387:8–25.

Blake, C., Pracy, M. B., Couch, W. J., Bekki, K., Lewis, I., Glazebrook, K., Baldry, I. K., Baugh, C. M., Bland-Hawthorn, J., Bridges, T., Cannon, R., Cole, S., Colless, M., Collins, C., Dalton, G., De Propris, R., Driver, S. P., Efstathiou, G., Ellis, R. S., Frenk, C. S., Jackson, C., Lahav, O., Lumsden, S., Maddox, S., Madgwick, D., Norberg, P., Peacock, J. A., Peterson, B. A., Sutherland, W., and Taylor, K. (2004). The 2dF Galaxy Redshift Survey: the local E+A galaxy population. MNRAS, 355:713–727.

Blakeslee, J. P., Franx, M., Postman, M., Rosati, P., Holden, B. P., Illingworth, G. D., Ford, H. C., Cross, N. J. G., Gronwall, C., Benítez, N., Bouwens, R. J., Broadhurst, T. J., Clampin, M., Demarco, R., Golimowski, D. A., Hartig, G. F., Infante, L., Martel, A. R., Miley, G. K., Menanteau, F., Meurer, G. R., Sirianni, M., and White, R. L. (2003). Advanced Camera for Surveys Photometry of the Cluster RDCS 1252.9-2927: The Color-Magnitude Relation at z = 1.24. ApJ, 596:L143–L146.

Blanton, M. R., Lupton, R. H., Schlegel, D. J., Strauss, M. A., Brinkmann, J., Fukugita, M., and Loveday, J. (2005). The Properties and Luminosity Function of Extremely Low Luminosity Galaxies. ApJ, 631:208–230.

Bolzonella, M., Kovač, K., Pozzetti, L., Zucca, E., Cucciati, O., Lilly, S. J., Peng, Y., Iovino, A., Zamorani, G., Vergani, D., Tasca, L. A. M., Lamareille, F., Oesch, P., Caputi, K., Kampczyk, P., Bardelli, S., Maier, C., Abbas, U., Knobel, C., Scodeggio, M., Carollo, C. M., Contini, T.,

Kneib, J.-P., Le Fèvre, O., Mainieri, V., Renzini, A., Bongiorno, A., Coppa, G., de la Torre, S., de Ravel, L., Franzetti, P., Garilli, B., Le Borgne, J.-F., Le Brun, V., Mignoli, M., Pelló, R., Perez-Montero, E., Ricciardelli, E., Silverman, J. D., Tanaka, M., Tresse, L., Bottini, D., Cappi, A., Cassata, P., Cimatti, A., Guzzo, L., Koekemoer, A. M., Leauthaud, A., Maccagni, D., Marinoni, C., McCracken, H. J., Memeo, P., Meneux, B., Porciani, C., Scaramella, R., Aussel, H., Capak, P., Halliday, C., Ilbert, O., Kartaltepe, J., Salvato, M., Sanders, D., Scarlata, C., Scoville, N., Taniguchi, Y., and Thompson, D. (2010). Tracking the impact of environment on the galaxy stellar mass function up to z ˜ 1 in the 10 k zCOSMOS sample. A&A, 524:A76.

Boselli, A. (1994). Multifrequency windows on spiral galaxies. 4: Gas content and star formation on the Virgo cluster. A&A, 292:1–12.

Boselli, A., Boissier, S., Cortese, L., and Gavazzi, G. (2008). The Origin of Dwarf Ellipticals in the Virgo Cluster. ApJ, 674:742–767.

Boselli, A., Boissier, S., Cortese, L., Gil de Paz, A., Seibert, M., Madore, B. F., Buat, V., and Martin, D. C. (2006). The Fate of Spiral Galaxies in Clusters: The Star Formation History of the Anemic Virgo Cluster Galaxy NGC 4569. ApJ, 651:811–821.

Boselli, A., Cortese, L., Boquien, M., Boissier, S., Catinella, B., Gavazzi, G., Lagos, C., and Saintonge, A. (2014). Cold gas properties of the Herschel Reference Survey. III. Molecular gas stripping in cluster galaxies. A&A, 564:A67.

Boselli, A. and Gavazzi, G. (2006). Environmental Effects on Late-Type Galaxies in Nearby Clusters. PASP, 118:517–559.

Boselli, A., Roehlly, Y., Fossati, M., Buat, V., Boissier, S., Boquien, M., Burgarella, D., Ciesla, L., Gavazzi, G., and Serra, P. (2016). The quenching of the star formation activity in cluster galaxies. *ArXiv e-prints*.

Bouché, N., Dekel, A., Genzel, R., Genel, S., Cresci, G., Förster Schreiber, N. M., Shapiro, K. L., Davies, R. I., and Tacconi, L. (2010). The Impact of Cold Gas Accretion Above a Mass Floor on Galaxy Scaling Relations. ApJ, 718:1001–1018.

Bouy, H., Bertin, E., Barrado, D., Sarro, L. M., Olivares, J., Moraux, E., Bouvier, J., Cuillandre, J.-C., Ribas, Á., and Beletsky, Y. (2015). Messier 35 (NGC 2168) DANCe. I. Membership, proper motions, and multiwavelength photometry. A&A, 575:A120.

Bower, R. G., Benson, A. J., Malbon, R., Helly, J. C., Frenk, C. S., Baugh, C. M., Cole, S., and Lacey, C. G. (2006). Breaking the hierarchy of galaxy formation. MNRAS, 370:645–655.

Bower, R. G., Lucey, J. R., and Ellis, R. S. (1992). Precision Photometry of Early Type Galaxies in the Coma and Virgo Clusters - a Test of the Universality of the Colour / Magnitude Relation - Part Two - Analysis. MNRAS, 254:601.

Bressan, A., Granato, G. L., and Silva, L. (1998). Modelling intermediate age and old stellar populations in the Infrared. A&A, 332:135–148.

Brinchmann, J., Charlot, S., White, S. D. M., Tremonti, C., Kauffmann, G., Heckman, T., and Brinkmann, J. (2004). The physical properties of star-forming galaxies in the low-redshift Universe. MNRAS, 351:1151–1179.

Bruzual, G. and Charlot, S. (2003). Stellar population synthesis at the resolution of 2003. MNRAS, 344:1000–1028.

Buser, R. (1978). A systematic investigation of multicolor photometric systems. I - The UBV, RGU and UVBY systems. II - The transformations between the UBV and RGU systems. A&A, 62:411–430.

Butcher, H. and Oemler, Jr., A. (1978). The evolution of galaxies in clusters. I - ISIT photometry of C1 0024+1654 and 3C 295. ApJ, 219:18–30.

Butcher, H. R. and Oemler, Jr., A. (1984). Nature of blue galaxies in the cluster C11447 + 2619. Nature, 310:31–33.

Byrd, G. G., Keel, W. C., and Howard, S. (1990). A simulation survey of galaxy interactions. In Sulentic, J. W., Keel, W. C., and Telesco, C. M., editors, *NASA Conference Publication*, volume 3098 of *NASA Conference Publication*.

Caldwell, N. (1983). Structure and stellar content of dwarf elliptical galaxies. AJ, 88:804–812.

Caldwell, N. and Rose, J. A. (1997). The Butcher-Oemler Effect at Low Redshift: Spectroscopy of Five Nearby Clusters of Galaxies. AJ, 113:492.

Calvi, R., Poggianti, B. M., Fasano, G., and Vulcani, B. (2012). The distribution of galaxy morphological types and the morphology-mass relation in different environments at low redshift. MNRAS, 419:L14–L18.

Calvi, R., Poggianti, B. M., and Vulcani, B. (2011). The Padova-Millennium Galaxy and Group Catalogue (PM2GC): the group-finding method and the PM2GC catalogues of group, binary and single field galaxies. MNRAS, 416:727–738.

Calvi, R., Poggianti, B. M., Vulcani, B., and Fasano, G. (2013). The impact of global environment on galaxy mass functions at low redshift. MNRAS, 432:3141–3152.

Calzetti, D., Kinney, A. L., and Storchi-Bergmann, T. (1994). Dust extinction of the stellar continua in starburst galaxies: The ultraviolet and optical extinction law. ApJ, 429:582–601.

Cardelli, J. A., Clayton, G. C., and Mathis, J. S. (1989). The relationship between infrared, optical, and ultraviolet extinction. ApJ, 345:245–256.

Catinella, B., Schiminovich, D., Cortese, L., Fabello, S., Hummels, C. B., Moran, S. M., Lemonias, J. J., Cooper, A. P., Wu, R., Heckman, T. M., and Wang, J. (2013). The GALEX Arecibo SDSS Survey - VIII. Final data release. The effect of group environment on the gas content of massive galaxies. MNRAS, 436:34–70.

Cava, A., Bettoni, D., Poggianti, B. M., Couch, W. J., Moles, M., Varela, J., Biviano, A., D'Onofrio, M., Dressler, A., Fasano, G., Fritz, J., Kjærgaard, P., Ramella, M., and Valentinuzzi, T. (2009). WINGS-SPE Spectroscopy in the WIde-field Nearby Galaxy-cluster Survey. A&A, 495:707–719.

Chung, A., van Gorkom, J. H., Kenney, J. D. P., Crowl, H., and Vollmer, B. (2009). VLA Imaging of Virgo Spirals in Atomic Gas (VIVA). I. The Atlas and the H I Properties. AJ, 138:1741–1816.

Cohen, S. A., Hickox, R. C., and Wegner, G. A. (2015). Star Formation and Relaxation in 379 Nearby Galaxy Clusters. ApJ, 806:85.

Cohen, S. A., Hickox, R. C., Wegner, G. A., Einasto, M., and Vennik, J. (2014). Star Formation and Substructure in Galaxy Clusters. ApJ, 783:136.

Cole, S. (1991). Modeling galaxy formation in evolving dark matter halos. ApJ, 367:45–53.

Cole, S., Lacey, C. G., Baugh, C. M., and Frenk, C. S. (2000). Hierarchical galaxy formation. MNRAS, 319:168–204.

Colless, M. (1989). The dynamics of rich clusters. II - Luminosity functions. MNRAS, 237:799–826.

Colless, M., Dalton, G., Maddox, S., Sutherland, W., Norberg, P., Cole, S., Bland-Hawthorn, J., Bridges, T., Cannon, R., Collins, C., Couch, W., Cross, N., Deeley, K., De Propris, R., Driver, S. P., Efstathiou, G., Ellis, R. S., Frenk, C. S., Glazebrook, K., Jackson, C., Lahav, O., Lewis, I., Lumsden, S., Madgwick, D., Peacock, J. A., Peterson, B. A., Price, I., Seaborne, M., and Taylor, K. (2001). The 2dF Galaxy Redshift Survey: spectra and redshifts. MNRAS, 328:1039–1063.

Conselice, C. J. (2006). The fundamental properties of galaxies and a new galaxy classification system. MNRAS, 373:1389–1408.

Cooper, M. C., Coil, A. L., Gerke, B. F., Newman, J. A., Bundy, K., Conselice, C. J., Croton, D. J., Davis, M., Faber, S. M., Guhathakurta, P., Koo, D. C., Lin, L., Weiner, B. J., Willmer, C. N. A., and Yan, R. (2010). Absence of evidence is not evidence of absence: the colour-density relation at fixed stellar mass persists to z ˜ 1. MNRAS, 409:337–345.

Cooper, M. C., Griffith, R. L., Newman, J. A., Coil, A. L., Davis, M., Dutton, A. A., Faber, S. M., Guhathakurta, P., Koo, D. C., Lotz, J. M., Weiner, B. J., Willmer, C. N. A., and Yan, R. (2012). The DEEP3 Galaxy Redshift Survey: the impact of environment on the size evolution of massive early-type galaxies at intermediate redshift. MNRAS, 419:3018–3027.

Cortese, L., Catinella, B., Boissier, S., Boselli, A., and Heinis, S. (2011). The effect of the environment on the H I scaling relations. MNRAS, 415:1797–1806.

Cortese, L., Marcillac, D., Richard, J., Bravo-Alfaro, H., Kneib, J.-P., Rieke, G., Covone, G., Egami, E., Rigby, J., Czoske, O., and Davies, J. (2007). The strong transformation of spiral galaxies infalling into massive clusters at z ˜ 0.2. MNRAS, 376:157–172.

Couch, W. J., Barger, A. J., Smail, I., Ellis, R. S., and Sharples, R. M. (1998). Morphological Studies of the Galaxy Populations in Distant "Butcher-Oemler" Clusters with the Hubble Space Telescope. II. AC 103, AC 118, and AC 114 at Z = 0.31. ApJ, 497:188–211.

Couch, W. J., Ellis, R. S., Sharples, R. M., and Smail, I. (1994). Morphological studies of the galaxy populations in distant 'Butcher-Oemler' clusters with HST. 1: AC 114 AT Z = 0.31 and Abell 370 at Z = 0.37. ApJ, 430:121–138.

Couch, W. J. and Sharples, R. M. (1987). A spectroscopic study of three rich galaxy clusters at Z = 0.31. MNRAS, 229:423–456.

Cowie, L. L., Barger, A. J., Bautz, M. W., Brandt, W. N., and Garmire, G. P. (2003). The Redshift Evolution of the 2-8 keV X-Ray Luminosity Function. ApJ, 584:L57–L60.

Cowie, L. L., Songaila, A., Hu, E. M., and Cohen, J. G. (1996). New Insight on Galaxy Formation and Evolution From Keck Spectroscopy of the Hawaii Deep Fields. AJ, 112:839.

Cross, N. J. G., Driver, S. P., Liske, J., Lemon, D. J., Peacock, J. A., Cole, S., Norberg, P., and Sutherland, W. J. (2004). The Millennium Galaxy Catalogue: the photometric accuracy, completeness and contamination of the 2dFGRS and SDSS-EDR/DR1 data sets. MNRAS, 349:576–594.

Croton, D. J., Springel, V., White, S. D. M., De Lucia, G., Frenk, C. S., Gao, L., Jenkins, A., Kauffmann, G., Navarro, J. F., and Yoshida, N. (2006). The many lives of active galactic nuclei: cooling flows, black holes and the luminosities and colours of galaxies. MNRAS, 365:11–28.

Daddi, E., Dickinson, M., Morrison, G., Chary, R., Cimatti, A., Elbaz, D., Frayer, D., Renzini, A., Pope, A., Alexander, D. M., Bauer, F. E., Giavalisco, M., Huynh, M., Kurk, J., and Mignoli, M. (2007). Multiwavelength Study of Massive Galaxies at z˜2. I. Star Formation and Galaxy Growth. ApJ, 670:156–172.

De Lucia, G. (2010). Modelling the evolution of galaxies as a function of environment. In *JENAM 2010, Joint European and National Astronomy Meeting*, page 69.

De Lucia, G. (2011). Modelling the Evolution of Galaxies as a Function of Environment. *Astrophysics and Space Science Proceedings*, 27:203.

De Lucia, G. and Blaizot, J. (2007). The hierarchical formation of the brightest cluster galaxies. MNRAS, 375:2–14.

De Lucia, G., Kauffmann, G., and White, S. D. M. (2004). Chemical enrichment of the intracluster and intergalactic medium in a hierarchical galaxy formation model. MNRAS, 349:1101–1116.

De Lucia, G., Springel, V., White, S. D. M., Croton, D., and Kauffmann, G. (2006). The formation history of elliptical galaxies. MNRAS, 366:499–509.

De Propris, R., Colless, M., Driver, S. P., Couch, W., Peacock, J. A., Baldry, I. K., Baugh, C. M., Bland-Hawthorn, J., Bridges, T., Cannon, R., Cole, S., Collins, C., Cross, N., Dalton, G. B., Efstathiou, G., Ellis, R. S., Frenk, C. S., Glazebrook, K., Hawkins, E., Jackson, C., Lahav, O., Lewis, I., Lumsden, S., Maddox, S., Madgwick, D. S., Norberg, P., Percival, W., Peterson, B., Sutherland, W., and Taylor, K. (2003). The 2dF Galaxy Redshift Survey: the luminosity function of cluster galaxies. MNRAS, 342:725–737.

de Souza, R. E., Capelato, H. V., Arakaki, L., and Logullo, C. (1982). The galactic content of groups of galaxies. ApJ, 263:557–563.

Dekel, A. and Silk, J. (1986). The origin of dwarf galaxies, cold dark matter, and biased galaxy formation. ApJ, 303:39–55.

Delaye, L., Huertas-Company, M., and Mei, S. (2012). Mass-size relation at high redshift in different environments. In Boissier, S., de Laverny, P., Nardetto, N., Samadi, R., Valls-Gabaud, D., and Wozniak, H., editors, *SF2A-2012: Proceedings of the Annual meeting of the French Society of Astronomy and Astrophysics*, pages 455–459.

Desai, V., Dalcanton, J. J., Aragón-Salamanca, A., Jablonka, P., Poggianti, B., Gogarten, S. M., Simard, L., Milvang-Jensen, B., Rudnick, G., Zaritsky, D., Clowe, D., Halliday, C., Pelló, R., Saglia, R., and White, S. (2007). The Morphological Content of 10 EDisCS Clusters at 0.5 ¡ z ¡ 0.8. ApJ, 660:1151–1164.

Dressler, A. (1978a). A comprehensive study of 12 very rich clusters of galaxies. I - Photometric technique and analysis of the luminosity function. ApJ, 223:765–775.

Dressler, A. (1978b). A comprehensive study of 12 very rich clusters of galaxies. II - Dynamics. ApJ, 226:55–69.

Dressler, A. (1978c). Bautz-Morgan classes and the luminosity function for clusters of galaxies. ApJ, 222:23–28.

Dressler, A. (1980). Galaxy morphology in rich clusters - Implications for the formation and evolution of galaxies. ApJ, 236:351–365.

Dressler, A. (2004). Star-forming Galaxies in Clusters. *Clusters of Galaxies: Probes of Cosmological Structure and Galaxy Evolution*, page 206.

Dressler, A. and Gunn, J. E. (1982). Spectroscopy of galaxies in distant clusters. I - First results for 3C 295 and 0024 + 1654. ApJ, 263:533–545.

Dressler, A. and Gunn, J. E. (1992). Spectroscopy of galaxies in distant clusters. IV - A catalog of photometry and spectroscopy for galaxies in seven clusters with Z in the range of 0.35 to 0.55. ApJS, 78:1–60.

Dressler, A., Oemler, Jr., A., Butcher, H. R., and Gunn, J. E. (1994). The morphology of distant cluster galaxies. 1: HST observations of CL 0939+4713. ApJ, 430:107–120.

Dressler, A., Oemler, Jr., A., Couch, W. J., Smail, I., Ellis, R. S., Barger, A., Butcher, H., Poggianti, B. M., and Sharples, R. M. (1997). Evolution since z = 0.5 of the Morphology-Density Relation for Clusters of Galaxies. ApJ, 490:577–591.

Dressler, A., Oemler, Jr., A., Poggianti, B. M., Gladders, M. D., Abramson, L., and Vulcani, B. (2013). The IMACS Cluster Building Survey. II. Spectral Evolution of Galaxies in the Epoch of Cluster Assembly. ApJ, 770:62.

Dressler, A., Smail, I., Poggianti, B. M., Butcher, H., Couch, W. J., Ellis, R. S., and Oemler, Jr., A. (1999). A Spectroscopic Catalog of 10 Distant Rich Clusters of Galaxies. ApJS, 122:51–80.

Driver, S. P., Allen, P. D., Graham, A. W., Cameron, E., Liske, J., Ellis, S. C., Cross, N. J. G., De Propris, R., Phillipps, S., and Couch, W. J. (2006). The Millennium Galaxy Catalogue: morphological classification and bimodality in the colour-concentration plane. MNRAS, 368:414–434.

Driver, S. P., Liske, J., Cross, N. J. G., De Propris, R., and Allen, P. D. (2005). The Millennium Galaxy Catalogue: the space density and surface-brightness distribution(s) of galaxies. MNRAS, 360:81–103.

Drory, N. and Fisher, D. B. (2007). A Connection between Bulge Properties and the Bimodality of Galaxies. ApJ, 664:640–649.

Ebeling, H., Edge, A. C., Allen, S. W., Crawford, C. S., Fabian, A. C., and Huchra, J. P. (2000). The ROSAT Brightest Cluster Sample - IV. The extended sample. MNRAS, 318:333–340.

Ebeling, H., Edge, A. C., Bohringer, H., Allen, S. W., Crawford, C. S., Fabian, A. C., Voges, W., and Huchra, J. P. (1998). The ROSAT Brightest Cluster Sample - I. The compilation of the sample and the cluster log N-log S distribution. MNRAS, 301:881–914.

Ebeling, H., Stephenson, L. N., and Edge, A. C. (2014). Jellyfish: Evidence of Extreme Ram-pressure Stripping in Massive Galaxy Clusters. ApJ, 781:L40.

Ebeling, H., Voges, W., Bohringer, H., Edge, A. C., Huchra, J. P., and Briel, U. G. (1996). Properties of the X-ray-brightest Abell-type clusters of galaxies (XBACs) from ROSAT All-Sky Survey data - I. The sample. MNRAS, 281:799–829.

Efron, B. (1982). *The Jackknife, the Bootstrap and other resampling plans.*

Eggen, O. J., Lynden-Bell, D., and Sandage, A. R. (1962). Evidence from the motions of old stars that the Galaxy collapsed. ApJ, 136:748.

Elbaz, D., Daddi, E., Le Borgne, D., Dickinson, M., Alexander, D. M., Chary, R.-R., Starck, J.-L., Brandt, W. N., Kitzbichler, M., MacDonald, E., Nonino, M., Popesso, P., Stern, D., and Vanzella, E. (2007). The reversal of the star formation-density relation in the distant universe. A&A, 468:33–48.

Ellis, R. S., Smail, I., Dressler, A., Couch, W. J., Oemler, Jr., A., Butcher, H., and Sharples, R. M. (1997). The Homogeneity of Spheroidal Populations in Distant Clusters. ApJ, 483:582–596.

Elmegreen, B. G. and Efremov, Y. N. (1997). A Universal Formation Mechanism for Open and Globular Clusters in Turbulent Gas. ApJ, 480:235–245.

Evrard, A. E. (1991). Clues to galaxy activity from rich cluster simulations. MNRAS, 248:8P–10P.

Fabello, S., Kauffmann, G., Catinella, B., Li, C., Giovanelli, R., and Haynes, M. P. (2012). ALFALFA H I data stacking - III. Comparison of environmental trends in H I gas mass fraction and specific star formation rate. MNRAS, 427:2841–2851.

Faber, S. M. (1973). Variations in Spectral-Energy Distributions and Absorption-Line Strengths among Elliptical Galaxies. ApJ, 179:731–754.

Fasano, G., Bettoni, D., Ascaso, B., Tormen, G., Poggianti, B. M., Valentinuzzi, T., D'Onofrio, M., Fritz, J., Moretti, A., Omizzolo, A., Cava, A., Moles, M., Dressler, A., Couch, W. J., Kjærgaard, P., and Varela, J. (2010). The shapes of BCGs and normal ellipticals in nearby clusters. MNRAS, 404:1490–1504.

Fasano, G., Marmo, C., Varela, J., D'Onofrio, M., Poggianti, B. M., Moles, M., Pignatelli, E., Bettoni, D., Kjærgaard, P., Rizzi, L., Couch, W. J., and Dressler, A. (2006). WINGS: a WIde-field Nearby Galaxy-cluster Survey. I. Optical imaging. A&A, 445:805–817.

Fasano, G., Poggianti, B. M., Bettoni, D., D'Onofrio, M., Dressler, A., Vulcani, B., Moretti, A., Gullieuszik, M., Fritz, J., Omizzolo, A., Cava, A., Couch, W. J., Ramella, M., and Biviano, A. (2015). Morphological fractions of galaxies in WINGS clusters: revisiting the morphology-density paradigm. MNRAS, 449:3927–3944.

Fasano, G., Poggianti, B. M., Couch, W. J., Bettoni, D., Kjærgaard, P., and Moles, M. (2000). The Evolution of the Galactic Morphological Types in Clusters. ApJ, 542:673–683.

Fasano, G., Vanzella, E., Dressler, A., Poggianti, B. M., Moles, M., Bettoni, D., Valentinuzzi, T., Moretti, A., D'Onofrio, M., Varela, J., Couch, W. J., Kjærgaard, P., Fritz, J., Omizzolo, A., and Cava, A. (2012). Morphology of galaxies in the WINGS clusters. MNRAS, 420:926–948.

Ferland, G. J. (1996). *Hazy, A Brief Introduction to Cloudy 90.*

Fernandes, R. C., Leão, J. R. S., and Lacerda, R. R. (2003). The evolution of stars and gas in starburst galaxies. MNRAS, 340:29–42.

Ferreras, I., Charlot, S., and Silk, J. (1999). The Age and Metallicity Range of Early-Type Galaxies in Clusters. ApJ, 521:81–89.

Finlator, K. and Davé, R. (2008). The origin of the galaxy mass-metallicity relation and implications for galactic outflows. MNRAS, 385:2181–2204.

Finn, R. A., Zaritsky, D., McCarthy, Jr., D. W., Poggianti, B., Rudnick, G., Halliday, C., Milvang-Jensen, B., Pelló, R., and Simard, L. (2005). Hα-derived Star Formation Rates for Three z˜=0.75 EDisCS Galaxy Clusters. ApJ, 630:206–227.

Font, A. S., Bower, R. G., McCarthy, I. G., Benson, A. J., Frenk, C. S., Helly, J. C., Lacey, C. G., Baugh, C. M., and Cole, S. (2008). The colours of satellite galaxies in groups and clusters. MNRAS, 389:1619–1629.

Fossati, M., Fumagalli, M., Boselli, A., Gavazzi, G., Sun, M., and Wilman, D. J. (2016). MUSE sneaks a peek at extreme ram-pressure stripping events - II. The physical properties of the gas tail of ESO137-001. MNRAS, 455:2028–2041.

Fritz, J., Poggianti, B. M., Bettoni, D., Cava, A., Couch, W. J., D'Onofrio, M., Dressler, A., Fasano, G., Kjærgaard, P., Moles, M., and Varela, J. (2007). A spectrophotometric model applied to cluster galaxies: the WINGS dataset. A&A, 470:137–152.

Fritz, J., Poggianti, B. M., Cava, A., Moretti, A., Varela, J., Bettoni, D., Couch, W. J., D'Onofrio D'Onofrio, M., Dressler, A., Fasano, G., Kjærgaard, P., Marziani, P., Moles, M., and Omizzolo, A. (2014). WINGS-SPE. III. Equivalent width measurements, spectral properties, and evolution of local cluster galaxies. A&A, 566:A32.

Fritz, J., Poggianti, B. M., Cava, A., Valentinuzzi, T., Moretti, A., Bettoni, D., Bressan, A., Couch, W. J., D'Onofrio, M., Dressler, A., Fasano, G., Kjærgaard, P., Moles, M., Omizzolo, A., and Varela, J. (2011). WINGS-SPE II: A catalog of stellar ages and star formation histories, stellar masses and dust extinction values for local clusters galaxies. A&A, 526:A45.

Fujita, A., Martin, C. L., Mac Low, M.-M., and Abel, T. (2003). The Influence of Supershells and Galactic Outflows on the Escape of Ionizing Radiation from Dwarf Starburst Galaxies. ApJ, 599:50–69.

Fujita, Y. (1998). Quantitative Estimates of Environmental Effects on the Star Formation Rate of Disk Galaxies in Clusters of Galaxies. ApJ, 509:587–594.

Fumagalli, M., Fossati, M., Hau, G. K. T., Gavazzi, G., Bower, R., Sun, M., and Boselli, A. (2014). MUSE sneaks a peek at extreme ram-pressure stripping events - I. A kinematic study of the archetypal galaxy ESO137-001. MNRAS, 445:4335–4344.

Gallazzi, A., Charlot, S., Brinchmann, J., and White, S. D. M. (2006). Ages and metallicities of early-type galaxies in the Sloan Digital Sky Survey: new insight into the physical origin of the colour-magnitude and the Mg_2-σ_V relations. MNRAS, 370:1106–1124.

Gao, L., De Lucia, G., White, S. D. M., and Jenkins, A. (2004). Galaxies and subhaloes in ΛCDM galaxy clusters. MNRAS, 352:L1–L5.

Garilli, B., Maccagni, D., and Andreon, S. (1999). Composite luminosity function of cluster galaxies. A&A, 342:408–416.

Gavazzi, G. (1989). 21 centimeter study of spiral galaxies in the Coma supercluster. II - Evidence for ongoing gas stripping in five cluster galaxies. ApJ, 346:59–67.

Gavazzi, G., Boselli, A., Cortese, L., Arosio, I., Gallazzi, A., Pedotti, P., and Carrasco, L. (2006). Hα surface photometry of galaxies in nearby clusters. A&A, 446:839–845.

Gavazzi, G., Boselli, A., van Driel, W., and O'Neil, K. (2005). Completing H I observations of galaxies in the Virgo cluster. A&A, 429:439–447.

Gavazzi, G., Fumagalli, M., Cucciati, O., and Boselli, A. (2010). A snapshot on galaxy evolution occurring in the Great Wall: the role of Nurture at z = 0. A&A, 517:A73.

Gavazzi, G., Fumagalli, M., Fossati, M., Galardo, V., Grossetti, F., Boselli, A., Giovanelli, R., and Haynes, M. P. (2013a). Hα3: an Hα imaging survey of HI selected galaxies from ALFALFA. II. Star formation properties of galaxies in the Virgo cluster and surroundings. A&A, 553:A89.

Gavazzi, G., Savorgnan, G., Fossati, M., Dotti, M., Fumagalli, M., Boselli, A., Gutiérrez, L., Hernández Toledo, H., Giovanelli, R., and Haynes, M. P. (2013b). Hα3: an Hα imaging survey of HI selected galaxies from ALFALFA. III. Nurture builds up the Hubble sequence in the Great Wall. A&A, 553:A90.

Gehrels, N. (1986). Confidence limits for small numbers of events in astrophysical data. ApJ, 303:336–346.

Giovanelli, R. and Haynes, M. P. (1985). Gas deficiency in cluster galaxies - A comparison of nine clusters. ApJ, 292:404–425.

Girardi, M., Biviano, A., Giuricin, G., Mardirossian, F., and Mezzetti, M. (1993). Velocity dispersions in galaxy clusters. ApJ, 404:38–50.

Goto, T. (2004). Are E+A galaxies dusty-starbursts?: VLA 20 cm radio continuum observation. A&A, 427:125–130.

Goto, T. (2005). 266 E+A galaxies selected from the Sloan Digital Sky Survey Data Release 2: the origin of E+A galaxies. MNRAS, 357:937–944.

Goto, T., Nichol, R. C., Okamura, S., Sekiguchi, M., Miller, C. J., Bernardi, M., Hopkins, A., Tremonti, C., Connolly, A., Castander, F. J., Brinkmann, J., Fukugita, M., Harvanek, M., Ivezic, Z., Kleinman, S. J., Krzesinski, J., Long, D., Loveday, J., Neilsen, E. H., Newman, P. R., Nitta, A., Snedden, S. A., and Subbarao, M. (2003). Hδ-Strong Galaxies in the Sloan Digital Sky Survey: I. The Catalog. PASJ, 55:771–787.

Goto, T., Okamura, S., McKay, T. A., Bahcall, N. A., Annis, J., Bernard, M., Brinkmann, J., Gómez, P. L., Hansen, S., Kim, R. S. J., Sekiguchi, M., and Sheth, R. K. (2002). Composite Luminosity Functions Based on the Sloan Digital Sky Survey "Cut and Enhance" Galaxy Cluster Catalog. PASJ, 54:515–525.

Guglielmo, V., Poggianti, B. M., Moretti, A., Fritz, J., Calvi, R., Vulcani, B., Fasano, G., and Paccagnella, A. (2015). The star formation history of galaxies: the role of galaxy mass, morphology and environment. MNRAS, 450:2749–2763.

Gullieuszik, M., Poggianti, B., Fasano, G., Zaggia, S., Paccagnella, A., Moretti, A., Bettoni, D., D'Onofrio, M., Couch, W. J., Vulcani, B., Fritz, J., Omizzolo, A., Baruffolo, A., Schipani, P., Capaccioli, M., and Varela, J. (2015a). OmegaWINGS: OmegaCAM-VST observations of WINGS galaxy clusters. A&A, 581:A41.

Gullieuszik, M., Poggianti, B., Fasano, G., Zaggia, S., Paccagnella, A., Moretti, A., Bettoni, D., D'Onofrio, M., Couch, W. J., Vulcani, B., Fritz, J., Omizzolo, A., Baruffolo, A., Schipani, P., Capaccioli, M., and Varela, J. (2015b). VizieR Online Data Catalog: OmegaWINGS BV photometry (Gullieuszik+, 2015). *VizieR Online Data Catalog*, 358.

Gunn, J. E. and Gott, III, J. R. (1972). On the Infall of Matter Into Clusters of Galaxies and Some Effects on Their Evolution. ApJ, 176:1.

Haines, C. P., Pereira, M. J., Smith, G. P., Egami, E., Babul, A., Finoguenov, A., Ziparo, F., McGee, S. L., Rawle, T. D., Okabe, N., and Moran, S. M. (2015). LoCuSS: The Slow Quenching of Star Formation in Cluster Galaxies and the Need for Pre-processing. ApJ, 806:101.

Haines, C. P., Pereira, M. J., Smith, G. P., Egami, E., Sanderson, A. J. R., Babul, A., Finoguenov, A., Merluzzi, P., Busarello, G., Rawle, T. D., and Okabe, N. (2013). LoCuSS: The Steady

Decline and Slow Quenching of Star Formation in Cluster Galaxies over the Last Four Billion Years. ApJ, 775:126.

Hansen, S. M., McKay, T. A., Wechsler, R. H., Annis, J., Sheldon, E. S., and Kimball, A. (2005). Measurement of Galaxy Cluster Sizes, Radial Profiles, and Luminosity Functions from SDSS Photometric Data. ApJ, 633:122–137.

Hatton, S., Devriendt, J. E. G., Ninin, S., Bouchet, F. R., Guiderdoni, B., and Vibert, D. (2003). GALICS- I. A hybrid N-body/semi-analytic model of hierarchical galaxy formation. MNRAS, 343:75–106.

Haynes, M. P. and Giovanelli, R. (1984). Neutral hydrogen in isolated galaxies. IV - Results for the Arecibo sample. AJ, 89:758–800.

Henriksen, M. and Byrd, G. (1996). Tidal Triggering of Star Formation by the Galaxy Cluster Potential. ApJ, 459:82.

Hernández-Fernández, J. D., Haines, C. P., Diaferio, A., Iglesias-Páramo, J., Mendes de Oliveira, C., and Vilchez, J. M. (2014). Star formation activity and gas stripping in the Cluster Projected Phase-Space (CPPS). MNRAS, 438:2186–2200.

Hess, K. M. and Wilcots, E. M. (2013). Evolution in the H I Gas Content of Galaxy Groups: Pre-processing and Mass Assembly in the Current Epoch. AJ, 146:124.

Hester, J. A., Seibert, M., Neill, J. D., Wyder, T. K., Gil de Paz, A., Madore, B. F., Martin, D. C., Schiminovich, D., and Rich, R. M. (2010). IC 3418: Star Formation in a Turbulent Wake. ApJ, 716:L14–L18.

Hogg, D. W., Blanton, M. R., Eisenstein, D. J., Gunn, J. E., Schlegel, D. J., Zehavi, I., Bahcall, N. A., Brinkmann, J., Csabai, I., Schneider, D. P., Weinberg, D. H., and York, D. G. (2003). The Overdensities of Galaxy Environments as a Function of Luminosity and Color. ApJ, 585:L5–L9.

Hogg, D. W., Masjedi, M., Berlind, A. A., Blanton, M. R., Quintero, A. D., and Brinkmann, J. (2006). What Triggers Galaxy Transformations? The Environments of Poststarburst Galaxies. ApJ, 650:763–769.

Hubble, E. P. (1926). Extragalactic nebulae. ApJ, 64.

Huertas-Company, M., Mei, S., Shankar, F., Delaye, L., Raichoor, A., Covone, G., Finoguenov, A., Kneib, J. P., Le, F. O., and Povic, M. (2013a). The evolution of the mass-size relation for early-type galaxies from z $\sim$ 1 to the present: dependence on environment, mass range and detailed morphology. MNRAS, 428:1715–1742.

Huertas-Company, M., Shankar, F., Mei, S., Bernardi, M., Aguerri, J. A. L., Meert, A., and Vikram, V. (2013b). No Evidence for a Dependence of the Mass-Size Relation of Early-type Galaxies on Environment in the Local Universe. ApJ, 779:29.

Irwin, M. and Lewis, J. (2001). INT WFS pipeline processing. New A Rev., 45:105–110.

Jacoby, G. H., Hunter, D. A., and Christian, C. A. (1984). A library of stellar spectra. ApJS, 56:257–281.

Jaffé, Y. L., Aragón-Salamanca, A., De Lucia, G., Jablonka, P., Rudnick, G., Saglia, R., and Zaritsky, D. (2011). The colour-magnitude relation of elliptical and lenticular galaxies in the ESO Distant Cluster Survey. MNRAS, 410:280–292.

Jaffé, Y. L., Smith, R., Candlish, G. N., Poggianti, B. M., Sheen, Y.-K., and Verheijen, M. A. W. (2015). BUDHIES II: a phase-space view of H I gas stripping and star formation quenching in cluster galaxies. MNRAS, 448:1715–1728.

Jaffé, Y. L., Verheijen, M. A. W., Haines, C. P., Yoon, H., Cybulski, R., Montero-Castaño, M., Smith, R., Chung, A., Deshev, B. Z., Fernández, X., van Gorkom, J., Poggianti, B. M., Yun, M. S., Finoguenov, A., Smith, G. P., and Okabe, N. (2016). BUDHIES - III: the fate of H I and the quenching of galaxies in evolving environments. MNRAS, 461:1202–1221.

Kenney, J. D. P., Geha, M., Jáchym, P., Crowl, H. H., Dague, W., Chung, A., van Gorkom, J., and Vollmer, B. (2014). Transformation of a Virgo Cluster Dwarf Irregular Galaxy by Ram Pressure Stripping: IC3418 and Its Fireballs. ApJ, 780:119.

Kenney, J. D. P. and Koopmann, R. A. (1999). Ongoing Gas Stripping in the Virgo Cluster Spiral Galaxy NGC 4522. AJ, 117:181–189.

Kennicutt, Jr., R. C. and Kent, S. M. (1983). A survey of H-alpha emission in normal galaxies. AJ, 88:1094–1107.

Kobayashi, C., Springel, V., and White, S. D. M. (2007). Simulations of Cosmic Chemical Enrichment. MNRAS, 376:1465–1479.

Kodama, T. and Arimoto, N. (1997). Origin of the colour-magnitude relation of elliptical galaxies. A&A, 320:41–53.

Kodama, T., Arimoto, N., Barger, A. J., and Arag'on-Salamanca, A. (1998). Evolution of the colour-magnitude relation of early-type galaxies in distant clusters. A&A, 334:99–109.

Kodama, T. and Smail, I. (2001). Testing the hypothesis of the morphological transformation from field spiral to cluster S0. MNRAS, 326:637–642.

Kovač, K., Lilly, S. J., Knobel, C., Bschorr, T. J., Peng, Y., Carollo, C. M., Contini, T., Kneib, J.-P., Le Févre, O., Mainieri, V., Renzini, A., Scodeggio, M., Zamorani, G., Bardelli, S., Bolzonella, M., Bongiorno, A., Caputi, K., Cucciati, O., de la Torre, S., de Ravel, L., Franzetti, P., Garilli, B., Iovino, A., Kampczyk, P., Lamareille, F., Le Borgne, J.-F., Le Brun, V., Maier, C., Mignoli, M., Oesch, P., Pello, R., Montero, E. P., Presotto, V., Silverman, J., Tanaka, M., Tasca, L., Tresse, L., Vergani, D., Zucca, E., Aussel, H., Koekemoer, A. M., Le Floc'h, E., Moresco, M., and Pozzetti, L. (2014). zCOSMOS 20k: satellite galaxies are the main drivers of environmental effects in the galaxy population at least to z $\sim$ 0.7. MNRAS, 438:717–738.

Kuijken, K. (2011). OmegaCAM: ESO's Newest Imager. *The Messenger*, 146:8–11.

Kurtz, M. J. and Mink, D. J. (1998). RVSAO 2.0: Digital Redshifts and Radial Velocities. PASP, 110:934–977.

Lacey, C. and Silk, J. (1991). Tidally triggered galaxy formation. I - Evolution of the galaxy luminosity function. ApJ, 381:14–32.

Larson, R. B. (1974). Dynamical models for the formation and evolution of spherical galaxies. MNRAS, 166:585–616.

Larson, R. B. (1975). Models for the formation of elliptical galaxies. MNRAS, 173:671–699.

Larson, R. B., Tinsley, B. M., and Caldwell, C. N. (1980). The evolution of disk galaxies and the origin of S0 galaxies. ApJ, 237:692–707.

Lewis, I., Balogh, M., De Propris, R., Couch, W., Bower, R., Offer, A., Bland-Hawthorn, J., Baldry, I. K., Baugh, C., Bridges, T., Cannon, R., Cole, S., Colless, M., Collins, C., Cross, N., Dalton, G., Driver, S. P., Efstathiou, G., Ellis, R. S., Frenk, C. S., Glazebrook, K., Hawkins, E., Jackson, C., Lahav, O., Lumsden, S., Maddox, S., Madgwick, D., Norberg, P., Peacock, J. A., Percival, W., Peterson, B. A., Sutherland, W., and Taylor, K. (2002). The 2dF Galaxy Redshift Survey: the environmental dependence of galaxy star formation rates near clusters. MNRAS, 334:673–683.

Lidman, C., Rosati, P., Tanaka, M., Strazzullo, V., Demarco, R., Mullis, C., Ageorges, N., Kissler-Patig, M., Petr-Gotzens, M. G., and Selman, F. (2008). HAWK-I imaging of the X-ray luminous galaxy cluster XMMU J2235.3-2557. The red sequence at z = 1.39. A&A, 489:981–988.

Lilly, S. J., Carollo, C. M., Pipino, A., Renzini, A., and Peng, Y. (2013). Gas Regulation of Galaxies: The Evolution of the Cosmic Specific Star Formation Rate, the Metallicity-Mass-Star-formation Rate Relation, and the Stellar Content of Halos. ApJ, 772:119.

Lilly, S. J., Tresse, L., Hammer, F., Crampton, D., and Le Fevre, O. (1995). The Canada-France Redshift Survey. VI. Evolution of the Galaxy Luminosity Function to Z approximately 1. ApJ, 455:108.

Liske, J., Lemon, D. J., Driver, S. P., Cross, N. J. G., and Couch, W. J. (2003). The Millennium Galaxy Catalogue: 16¡=B$_{MGC}$¡ 24 galaxy counts and the calibration of the local galaxy luminosity function. MNRAS, 344:307–324.

Longhetti, M. and Saracco, P. (2009). Stellar mass estimates in early-type galaxies: procedures, uncertainties and models dependence. MNRAS, 394:774–794.

López-Cruz, O., Yee, H. K. C., Brown, J. P., Jones, C., and Forman, W. (1997). Are Luminous cD Halos Formed by the Disruption of Dwarf Galaxies? ApJ, 475:L97–L101.

Lotz, J. M., Primack, J., and Madau, P. (2004). A New Nonparametric Approach to Galaxy Morphological Classification. AJ, 128:163–182.

Lugger, P. M. (1986). Luminosity functions for nine Abell clusters. ApJ, 303:535–555.

Madgwick, D. S., Lahav, O., Baldry, I. K., Baugh, C. M., Bland-Hawthorn, J., Bridges, T., Cannon, R., Cole, S., Colless, M., Collins, C., Couch, W., Dalton, G., De Propris, R., Driver, S. P., Efstathiou, G., Ellis, R. S., Frenk, C. S., Glazebrook, K., Jackson, C., Lewis, I., Lumsden, S., Maddox, S., Norberg, P., Peacock, J. A., Peterson, B. A., Sutherland, W., and Taylor, K. (2002). The 2dF Galaxy Redshift Survey: galaxy luminosity functions per spectral type. MNRAS, 333:133–144.

Mahajan, S. (2013). Evidence for galaxies being pre-processed before accreted into clusters. MNRAS, 431:L117–L121.

Mahajan, S., Mamon, G. A., and Raychaudhury, S. (2011). The velocity modulation of galaxy properties in and near clusters: quantifying the decrease in star formation in backsplash galaxies. MNRAS, 416:2882–2902.

Martínez, H. J., Zandivarez, A., Merchán, M. E., and Domínguez, M. J. L. (2002). Galaxy groups in the 2dF Galaxy Redshift Survey: luminosity and mass statistics. MNRAS, 337:1441–1449.

Marziani, P., D'Onofrio, M., Bettoni, D., Poggianti, B. M., Moretti, A., Fasano, G., Fritz, J., Cava, A., Varela, J., and Omizzolo, A. (2016). Emission Line Galaxies and Active Galactic Nuclei in WINGS clusters. *ArXiv e-prints*.

McCarthy, I. G., Frenk, C. S., Font, A. S., Lacey, C. G., Bower, R. G., Mitchell, N. L., Balogh, M. L., and Theuns, T. (2008). Ram pressure stripping the hot gaseous haloes of galaxies in groups and clusters. MNRAS, 383:593–605.

McGee, S. L., Balogh, M. L., Bower, R. G., Font, A. S., and McCarthy, I. G. (2009). The accretion of galaxies into groups and clusters. MNRAS, 400:937–950.

McGee, S. L., Bower, R. G., and Balogh, M. L. (2014). Overconsumption, outflows and the quenching of satellite galaxies. MNRAS, 442:L105–L109.

Mei, S., Holden, B. P., Blakeslee, J. P., Ford, H. C., Franx, M., Homeier, N. L., Illingworth, G. D., Jee, M. J., Overzier, R., Postman, M., Rosati, P., Van der Wel, A., and Bartlett, J. G. (2009). Evolution of the Color-Magnitude Relation in Galaxy Clusters at z ˜ 1 from the ACS Intermediate Redshift Cluster Survey. ApJ, 690:42–68.

Mei, S., Holden, B. P., Blakeslee, J. P., Rosati, P., Postman, M., Jee, M. J., Rettura, A., Sirianni, M., Demarco, R., Ford, H. C., Franx, M., Homeier, N., and Illingworth, G. D. (2006). Evolution of the Color-Magnitude Relation in High-Redshift Clusters: Early-Type Galaxies in the Lynx Supercluster at z ˜ 1.26. ApJ, 644:759–768.

Mei, S., Raichoor, A., Stanford, A. S., Holden, B. P., Nakata, F., Rosati, P., Shankar, F., Tanaka, M., Ford, H. C., Huertas-Company, M., Illingworth, G. D., Kodama, T., Postman, M., Rettura, A., Blakeslee, J. P., Demarco, R., Jee, M. J., and Rick, W. (2012). The Evolution Of The Galaxy Mass-size Relation In Different Environments. In *American Astronomical Society Meeting Abstracts #219*, volume 219 of *American Astronomical Society Meeting Abstracts*, page 411.06.

Merluzzi, P., Busarello, G., Dopita, M. A., Haines, C. P., Steinhauser, D., Mercurio, A., Rifatto, A., Smith, R. J., and Schindler, S. (2013). ACCESS - V. Dissecting ram-pressure stripping through integral-field spectroscopy and multiband imaging. MNRAS, 429:1747–1773.

Mihos, J. C. (2004). The Evolution of Tidal Debris. In Duc, P.-A., Braine, J., and Brinks, E., editors, *Recycling Intergalactic and Interstellar Matter*, volume 217 of *IAU Symposium*, page 390.

Mihos, J. C. and Hernquist, L. (1994). Triggering of starbursts in galaxies by minor mergers. ApJ, 425:L13–L16.

Mo, H. J. and Fukugita, M. (1996). Constraints on the Cosmic Structure Formation Models from Early Formation of Giant Galaxies. ApJ, 467:L9.

Mok, A., Balogh, M. L., McGee, S. L., Wilman, D. J., Finoguenov, A., Tanaka, M., Giodini, S., Bower, R. G., Connelly, J. L., Hou, A., Mulchaey, J. S., and Parker, L. C. (2013). Efficient satellite quenching at $z\sim1$ from the GEEC2 spectroscopic survey of galaxy groups. MNRAS, 431:1090–1106.

Monaco, P., Fontanot, F., and Taffoni, G. (2007). The MORGANA model for the rise of galaxies and active nuclei. MNRAS, 375:1189–1219.

Moore, B., Katz, N., Lake, G., Dressler, A., and Oemler, A. (1996). Galaxy harassment and the evolution of clusters of galaxies. Nature, 379:613–616.

Moore, B., Lake, G., Quinn, T., and Stadel, J. (1999). On the survival and destruction of spiral galaxies in clusters. MNRAS, 304:465–474.

Moran, S. M., Ellis, R. S., Treu, T., Smith, G. P., Rich, R. M., and Smail, I. (2007). A Wide-Field Survey of Two z ˜ 0.5 Galaxy Clusters: Identifying the Physical Processes Responsible for the Observed Transformation of Spirals into S0s. ApJ, 671:1503–1522.

Moretti, A., Bettoni, D., Poggianti, B. M., Fasano, G., Varela, J., D'Onofrio, M., Vulcani, B., Cava, A., Fritz, J., Couch, W. J., Moles, M., and Kjærgaard, P. (2015). Galaxy luminosity functions in WINGS clusters. A&A, 581:A11.

Moretti, A., Gullieuszik, M., Poggianti, B., Paccagnella, A., Couch, W. J., Vulcani, B., Bettoni, D., Fritz, J., Cava, A., Fasano, G., D'Onofrio, M., and Omizzolo, A. (2017). OmegaWINGS: spectroscopy in the outskirts of local clusters of galaxies. *ArXiv e-prints*.

Moretti, A., Poggianti, B. M., Fasano, G., Bettoni, D., D'Onofrio, M., Fritz, J., Cava, A., Varela, J., Vulcani, B., Gullieuszik, M., Couch, W. J., Omizzolo, A., Valentinuzzi, T., Dressler, A., Moles, M., Kjærgaard, P., Smareglia, R., and Molinaro, M. (2014). WINGS Data Release: a database of galaxies in nearby clusters. A&A, 564:A138.

Moster, B. P., Somerville, R. S., Maulbetsch, C., van den Bosch, F. C., Macciò, A. V., Naab, T., and Oser, L. (2010). Constraints on the Relationship between Stellar Mass and Halo Mass at Low and High Redshift. ApJ, 710:903–923.

Muzzin, A., van der Burg, R. F. J., McGee, S. L., Balogh, M., Franx, M., Hoekstra, H., Hudson, M. J., Noble, A., Taranu, D. S., Webb, T., Wilson, G., and Yee, H. K. C. (2014). The Phase Space and Stellar Populations of Cluster Galaxies at z ˜ 1: Simultaneous Constraints on the Location and Timescale of Satellite Quenching. ApJ, 796:65.

Muzzin, A., Wilson, G., Yee, H. K. C., Gilbank, D., Hoekstra, H., Demarco, R., Balogh, M., van Dokkum, P., Franx, M., Ellingson, E., Hicks, A., Nantais, J., Noble, A., Lacy, M., Lidman, C., Rettura, A., Surace, J., and Webb, T. (2012). The Gemini Cluster Astrophysics Spectroscopic Survey (GCLASS): The Role of Environment and Self-regulation in Galaxy Evolution at z ˜ 1. ApJ, 746:188.

Nantais, J. B., Rettura, A., Lidman, C., Demarco, R., Gobat, R., Rosati, P., and Jee, M. J. (2013). Star-forming fractions and galaxy evolution with redshift in rich X-ray-selected galaxy clusters. A&A, 556:A112.

Nelan, J. E., Smith, R. J., Hudson, M. J., Wegner, G. A., Lucey, J. R., Moore, S. A. W., Quinney, S. J., and Suntzeff, N. B. (2005). NOAO Fundamental Plane Survey. II. Age and Metallicity along the Red Sequence from Line-Strength Data. ApJ, 632:137–156.

Newberry, M. V., Boroson, T. A., and Kirshner, R. P. (1990). Spectra of galaxies in clusters. II - Models for the spectra of postburst and stripped galaxies. ApJ, 350:585–596.

Noeske, K. G., Weiner, B. J., Faber, S. M., Papovich, C., Koo, D. C., Somerville, R. S., Bundy, K., Conselice, C. J., Newman, J. A., Schiminovich, D., Le Floc'h, E., Coil, A. L., Rieke, G. H., Lotz, J. M., Primack, J. R., Barmby, P., Cooper, M. C., Davis, M., Ellis, R. S., Fazio, G. G., Guhathakurta, P., Huang, J., Kassin, S. A., Martin, D. C., Phillips, A. C., Rich, R. M., Small, T. A., Willmer, C. N. A., and Wilson, G. (2007). Star Formation in AEGIS Field Galaxies since z=1.1: The Dominance of Gradually Declining Star Formation, and the Main Sequence of Star-forming Galaxies. ApJ, 660:L43–L46.

Nuijten, M. J. H. M., Simard, L., Gwyn, S., and Röttgering, H. J. A. (2005). The Canada-France-Hawaii Telescope Legacy Survey: The Morphology-Density Relation of Galaxies out to z ˜ 1. ApJ, 626:L77–L80.

Oesch, P. A., Carollo, C. M., Feldmann, R., Hahn, O., Lilly, S. J., Sargent, M. T., Scarlata, C., Aller, M. C., Aussel, H., Bolzonella, M., Bschorr, T., Bundy, K., Capak, P., Ilbert, O., Kneib, J.-P., Koekemoer, A. M., Kovač, K., Leauthaud, A., Le Floc'h, E., Massey, R., McCracken, H. J., Pozzetti, L., Renzini, A., Rhodes, J., Salvato, M., Sanders, D. B., Scoville, N., Sheth, K., Taniguchi, Y., and Thompson, D. (2010). The Buildup of the Hubble Sequence in the Cosmos Field. ApJ, 714:L47–L51.

Oman, K. A., Hudson, M. J., and Behroozi, P. S. (2013). Disentangling satellite galaxy populations using orbit tracking in simulations. MNRAS, 431:2307–2316.

Omizzolo, A., Fasano, G., Reverte Paya, D., De Santis, C., Grado, A., Bettoni, D., Poggianti, B., D'Onofrio, M., Moretti, A., Varela, J., Fritz, J., Gullieuszik, M., Cava, A., Grazian, A., and Moles, M. (2014). U-band photometry of 17 WINGS clusters. A&A, 561:A111.

Owers, M. S., Couch, W. J., Nulsen, P. E. J., and Randall, S. W. (2012). Shocking Tails in the Major Merger Abell 2744. ApJ, 750:L23.

Paccagnella, A., Vulcani, B., Poggianti, B. M., Moretti, A., Fritz, J., Gullieuszik, M., Couch, W., Bettoni, D., Cava, A., D'Onofrio, M., and Fasano, G. (2016). Slow Quenching of Star Formation in OMEGAWINGS Clusters: Galaxies in Transition in the Local Universe. ApJ, 816:L25.

Paolillo, M., Andreon, S., Longo, G., Puddu, E., Gal, R. R., Scaramella, R., Djorgovski, S. G., and de Carvalho, R. (2001). Luminosity function of clusters of galaxies. A&A, 367:59–71.

Patel, S. G., Holden, B. P., Kelson, D. D., Illingworth, G. D., and Franx, M. (2009). The Dependence of Star Formation Rates on Stellar Mass and Environment at z ˜ 0.8. ApJ, 705:L67–L70.

Peng, Y.-j., Lilly, S. J., Kovač, K., Bolzonella, M., Pozzetti, L., Renzini, A., Zamorani, G., Ilbert, O., Knobel, C., Iovino, A., Maier, C., Cucciati, O., Tasca, L., Carollo, C. M., Silverman, J., Kampczyk, P., de Ravel, L., Sanders, D., Scoville, N., Contini, T., Mainieri, V., Scodeggio, M., Kneib, J.-P., Le Fèvre, O., Bardelli, S., Bongiorno, A., Caputi, K., Coppa, G., de la Torre,

S., Franzetti, P., Garilli, B., Lamareille, F., Le Borgne, J.-F., Le Brun, V., Mignoli, M., Perez Montero, E., Pello, R., Ricciardelli, E., Tanaka, M., Tresse, L., Vergani, D., Welikala, N., Zucca, E., Oesch, P., Abbas, U., Barnes, L., Bordoloi, R., Bottini, D., Cappi, A., Cassata, P., Cimatti, A., Fumana, M., Hasinger, G., Koekemoer, A., Leauthaud, A., Maccagni, D., Marinoni, C., McCracken, H., Memeo, P., Meneux, B., Nair, P., Porciani, C., Presotto, V., and Scaramella, R. (2010). Mass and Environment as Drivers of Galaxy Evolution in SDSS and zCOSMOS and the Origin of the Schechter Function. ApJ, 721:193–221.

Poggianti, B. M. (2004). Modeling Stellar Populations in Cluster Galaxies. *Clusters of Galaxies: Probes of Cosmological Structure and Galaxy Evolution*, page 245.

Poggianti, B. M., Aragón-Salamanca, A., Zaritsky, D., De Lucia, G., Milvang-Jensen, B., Desai, V., Jablonka, P., Halliday, C., Rudnick, G., Varela, J., Bamford, S., Best, P., Clowe, D., Noll, S., Saglia, R., Pelló, R., Simard, L., von der Linden, A., and White, S. (2009). The Environments of Starburst and Post-Starburst Galaxies at z = 0.4-0.8. ApJ, 693:112–131.

Poggianti, B. M. and Barbaro, G. (1996). Starbursts and the Butcher-Oemler effect in galaxy clusters. A&A, 314:379–392.

Poggianti, B. M. and Barbaro, G. (1997). Indicators of star formation: 4000 Å break and Balmer lines. A&A, 325:1025–1030.

Poggianti, B. M., Bridges, T. J., Mobasher, B., Carter, D., Doi, M., Iye, M., Kashikawa, N., Komiyama, Y., Okamura, S., Sekiguchi, M., Shimasaku, K., Yagi, M., and Yasuda, N. (2001). A Photometric and Spectroscopic Study of Dwarf and Giant Galaxies in the Coma Cluster. III. Spectral Ages and Metallicities. ApJ, 562:689–712.

Poggianti, B. M., Calvi, R., Bindoni, D., D'Onofrio, M., Moretti, A., Valentinuzzi, T., Fasano, G., Fritz, J., De Lucia, G., Vulcani, B., Bettoni, D., Gullieuszik, M., and Omizzolo, A. (2013). Superdense Galaxies and the Mass-Size Relation at Low Redshift. ApJ, 762:77.

Poggianti, B. M., Fasano, G., Omizzolo, A., Gullieuszik, M., Bettoni, D., Moretti, A., Paccagnella, A., Jaffé, Y. L., Vulcani, B., Fritz, J., Couch, W., and D'Onofrio, M. (2016). Jellyfish Galaxy Candidates at Low Redshift. AJ, 151:78.

Poggianti, B. M., Smail, I., Dressler, A., Couch, W. J., Barger, A. J., Butcher, H., Ellis, R. S., and Oemler, Jr., A. (1999). The Star Formation Histories of Galaxies in Distant Clusters. ApJ, 518:576–593.

Poggianti, B. M., von der Linden, A., De Lucia, G., Desai, V., Simard, L., Halliday, C., Aragón-Salamanca, A., Bower, R., Varela, J., Best, P., Clowe, D. I., Dalcanton, J., Jablonka, P., Milvang-Jensen, B., Pello, R., Rudnick, G., Saglia, R., White, S. D. M., and Zaritsky, D. (2006). The Evolution of the Star Formation Activity in Galaxies and Its Dependence on Environment. ApJ, 642:188–215.

Poggianti, B. M. and Wu, H. (2000). Optical Spectral Signatures of Dusty Starburst Galaxies. ApJ, 529:157–169.

Popesso, P., Biviano, A., Böhringer, H., and Romaniello, M. (2006). RASS-SDSS Galaxy cluster survey. IV. A ubiquitous dwarf galaxy population in clusters. A&A, 445:29–42.

Popesso, P., Biviano, A., Romaniello, M., and Böhringer, H. (2007). RASS-SDSS galaxy cluster survey. VI. The dependence of the cluster SFR on the cluster global properties. A&A, 461:411–421.

Popesso, P., Böhringer, H., Romaniello, M., and Voges, W. (2005). RASS-SDSS galaxy cluster survey. II. A unified picture of the cluster luminosity function. A&A, 433:415–429.

Postman, M., Franx, M., Cross, N. J. G., Holden, B., Ford, H. C., Illingworth, G. D., Goto, T., Demarco, R., Rosati, P., Blakeslee, J. P., Tran, K.-V., Benítez, N., Clampin, M., Hartig, G. F., Homeier, N., Ardila, D. R., Bartko, F., Bouwens, R. J., Bradley, L. D., Broadhurst, T. J., Brown, R. A., Burrows, C. J., Cheng, E. S., Feldman, P. D., Golimowski, D. A., Gronwall, C., Infante, L., Kimble, R. A., Krist, J. E., Lesser, M. P., Martel, A. R., Mei, S., Menanteau, F., Meurer, G. R., Miley, G. K., Motta, V., Sirianni, M., Sparks, W. B., Tran, H. D., Tsvetanov, Z. I., White, R. L., and Zheng, W. (2005). The Morphology-Density Relation in z ˜ 1 Clusters. ApJ, 623:721–741.

Postman, M. and Geller, M. J. (1984). The morphology-density relation - The group connection. ApJ, 281:95–99.

Quilis, V., Moore, B., and Bower, R. (2000). Gone with the Wind: The Origin of S0 Galaxies in Clusters. *Science*, 288:1617–1620.

Quintero, A. D., Hogg, D. W., Blanton, M. R., Schlegel, D. J., Eisenstein, D. J., Gunn, J. E., Brinkmann, J., Fukugita, M., Glazebrook, K., and Goto, T. (2004). Selection and Photometric Properties of K+A Galaxies. ApJ, 602:190–199.

Raichoor, A. and Andreon, S. (2012). Galaxy mass, cluster-centric distance and secular evolution: their role in the evolution of galaxies in clusters in the last 10 Gyr. A&A, 543:A19.

Ramella, M., Biviano, A., Pisani, A., Varela, J., Bettoni, D., Couch, W. J., D'Onofrio, M., Dressler, A., Fasano, G., Kjørgaard, P., Moles, M., Pignatelli, E., and Poggianti, B. M. (2007). Substructures in WINGS clusters. A&A, 470:39–51.

Rasmussen, J., Mulchaey, J. S., Bai, L., Ponman, T. J., Raychaudhury, S., and Dariush, A. (2012). The Suppression of Star Formation and the Effect of the Galaxy Environment in Low-redshift Galaxy Groups. ApJ, 757:122.

Rawle, T. D., Altieri, B., Egami, E., Pérez-González, P. G., Richard, J., Santos, J. S., Valtchanov, I., Walth, G., Bouy, H., Haines, C. P., and Okabe, N. (2014). Star formation in the massive cluster merger Abell 2744. MNRAS, 442:196–206.

Renzini, A. (2006). Stellar Population Diagnostics of Elliptical Galaxy Formation. ARA&A, 44:141–192.

Rider, P. (1960). Variance of the Median of Small Samples from Several Special Populations. *Journal of the American Statistical Association*, 55:148–150.

Rowan-Robinson, M., Mann, R. G., Oliver, S. J., Efstathiou, A., Eaton, N., Goldschmidt, P., Mobasher, B., Serjeant, S. B. G., Sumner, T. J., Danese, L., Elbaz, D., Franceschini, A., Egami, E., Kontizas, M., Lawrence, A., McMahon, R., Norgaard-Nielsen, H. U., Perez-Fournon, I., and Gonzalez-Serrano, J. I. (1997). Observations of the Hubble Deep Field with the Infrared Space Observatory - V. Spectral energy distributions, starburst models and star formation history. MNRAS, 289:490–496.

Salim, S., Rich, R. M., Charlot, S., Brinchmann, J., Johnson, B. D., Schiminovich, D., Seibert, M., Mallery, R., Heckman, T. M., Forster, K., Friedman, P. G., Martin, D. C., Morrissey, P., Neff, S. G., Small, T., Wyder, T. K., Bianchi, L., Donas, J., Lee, Y.-W., Madore, B. F., Milliard, B., Szalay, A. S., Welsh, B. Y., and Yi, S. K. (2007). UV Star Formation Rates in the Local Universe. ApJS, 173:267–292.

Salpeter, E. E. (1955). The Luminosity Function and Stellar Evolution. ApJ, 121:161.

Sánchez, A. G., Baugh, C. M., Percival, W. J., Peacock, J. A., Padilla, N. D., Cole, S., Frenk, C. S., and Norberg, P. (2006). Cosmological parameters from cosmic microwave background measurements and the final 2dF Galaxy Redshift Survey power spectrum. MNRAS, 366:189–207.

Sandage, A. (2005). The Classification of Galaxies: Early History and Ongoing Developments. ARA&A, 43:581–624.

Sandage, A. and Visvanathan, N. (1978a). Color-absolute magnitude relation for E and S0 galaxies. III - Fully corrected photometry for 405 galaxies: Comparison of color distributions for E and S0 field and cluster galaxies. ApJ, 225:742–750.

Sandage, A. and Visvanathan, N. (1978b). The color-absolute magnitude relation for E and S0 galaxies. II - New colors, magnitudes, and types for 405 galaxies. ApJ, 223:707–729.

Schawinski, K., Urry, C. M., Simmons, B. D., Fortson, L., Kaviraj, S., Keel, W. C., Lintott, C. J., Masters, K. L., Nichol, R. C., Sarzi, M., Skibba, R., Treister, E., Willett, K. W., Wong, O. I., and Yi, S. K. (2014). The green valley is a red herring: Galaxy Zoo reveals two evolutionary pathways towards quenching of star formation in early- and late-type galaxies. MNRAS, 440:889–907.

Schechter, P. L. and Peebles, P. J. E. (1976). On the Significance of the Luminosities of First-Ranked Members of Sparse Groups of Galaxies. ApJ, 209:670–677.

Serra, P., Oosterloo, T., Morganti, R., Alatalo, K., Blitz, L., Bois, M., Bournaud, F., Bureau, M., Cappellari, M., Crocker, A. F., Davies, R. L., Davis, T. A., de Zeeuw, P. T., Duc, P.-A., Emsellem, E., Khochfar, S., Krajnović, D., Kuntschner, H., Lablanche, P.-Y., McDermid, R. M., Naab, T., Sarzi, M., Scott, N., Trager, S. C., Weijmans, A.-M., and Young, L. M. (2012). The ATLAS^{3D} project - XIII. Mass and morphology of H I in early-type galaxies as a function of environment. MNRAS, 422:1835–1862.

Sharp, R. and Parkinson, H. (2010). Sky subtraction at the Poisson limit with fibre-optic multi-object spectroscopy. MNRAS, 408:2495–2510.

Sheth, R. K. and Tormen, G. (2002). An excursion set model of hierarchical clustering: ellipsoidal collapse and the moving barrier. MNRAS, 329:61–75.

Smith, G. A., Saunders, W., Bridges, T., Churilov, V., Lankshear, A., Dawson, J., Correll, D., Waller, L., Haynes, R., and Frost, G. (2004). AAOmega: a multipurpose fiber-fed spectrograph for the AAT. In Moorwood, A. F. M. and Iye, M., editors, *Ground-based Instrumentation for Astronomy*, volume 5492 of Proc. SPIE, pages 410–420.

Smith, R. J., Lucey, J. R., Hammer, D., Hornschemeier, A. E., Carter, D., Hudson, M. J., Marzke, R. O., Mouhcine, M., Eftekharzadeh, S., James, P., Khosroshahi, H., Kourkchi, E., and Karick, A. (2010). Ultraviolet tails and trails in cluster galaxies: a sample of candidate gaseous stripping events in Coma. MNRAS, 408:1417–1432.

Solanes, J. M., Manrique, A., García-Gómez, C., González-Casado, G., Giovanelli, R., and Haynes, M. P. (2001). The H I Content of Spirals. II. Gas Deficiency in Cluster Galaxies. ApJ, 548:97–113.

Somerville, R. S. and Primack, J. R. (1999). Semi-analytic modelling of galaxy formation: the local Universe. MNRAS, 310:1087–1110.

Springel, V., White, S. D. M., Jenkins, A., Frenk, C. S., Yoshida, N., Gao, L., Navarro, J., Thacker, R., Croton, D., Helly, J., Peacock, J. A., Cole, S., Thomas, P., Couchman, H., Evrard, A., Colberg, J., and Pearce, F. (2005). Simulations of the formation, evolution and clustering of galaxies and quasars. Nature, 435:629–636.

Springel, V., White, S. D. M., Tormen, G., and Kauffmann, G. (2001). Populating a cluster of galaxies - I. Results at [formmu2]z=0. MNRAS, 328:726–750.

Stanford, S. A., Eisenhardt, P. R., and Dickinson, M. (1998). The Evolution of Early-Type Galaxies in Distant Clusters. ApJ, 492:461–479.

Sun, M., Jones, C., Forman, W., Nulsen, P. E. J., Donahue, M., and Voit, G. M. (2006). A 70 Kiloparsec X-Ray Tail in the Cluster A3627. ApJ, 637:L81–L84.

Tal, T., Dekel, A., Oesch, P., Muzzin, A., Brammer, G. B., van Dokkum, P. G., Franx, M., Illingworth, G. D., Leja, J., Magee, D., Marchesini, D., Momcheva, I., Nelson, E. J., Patel, S. G., Quadri, R. F., Rix, H.-W., Skelton, R. E., Wake, D. A., and Whitaker, K. E. (2014). Observations of Environmental Quenching in Groups in the 11 GYR since z = 2.5: Different Quenching for Central and Satellite Galaxies. ApJ, 789:164.

Taranu, D. S., Dubinski, J., and Yee, H. K. C. (2013). Mergers in Galaxy Groups. I. Structure and Properties of Elliptical Remnants. ApJ, 778:61.

Taranu, D. S., Hudson, M. J., Balogh, M. L., Smith, R. J., Power, C., Oman, K. A., and Krane, B. (2014). Quenching star formation in cluster galaxies. MNRAS, 440:1934–1949.

Tran, K.-V. H., Franx, M., Illingworth, G., Kelson, D. D., and van Dokkum, P. (2003). The Nature of E+A Galaxies in Intermediate-Redshift Clusters. ApJ, 599:865–885.

Tran, K.-V. H., Franx, M., Illingworth, G. D., Kelson, D. D., and van Dokkum, P. (2004). E+A galaxies in intermediate redshift clusters. In Diaferio, A., editor, *IAU Colloq. 195: Outskirts of Galaxy Clusters: Intense Life in the Suburbs*, pages 483–487.

Tran, K.-V. H., Franx, M., Illingworth, G. D., van Dokkum, P., Kelson, D. D., Blakeslee, J. P., and Postman, M. (2007). A Keck Spectroscopic Survey of MS 1054-03 (z = 0.83): Forming the Red Sequence. ApJ, 661:750–767.

Tremonti, C. A., Heckman, T. M., Kauffmann, G., Brinchmann, J., Charlot, S., White, S. D. M., Seibert, M., Peng, E. W., Schlegel, D. J., Uomoto, A., Fukugita, M., and Brinkmann, J. (2004). The Origin of the Mass-Metallicity Relation: Insights from 53,000 Star-forming Galaxies in the Sloan Digital Sky Survey. ApJ, 613:898–913.

Trentham, N., Sampson, L., and Banerji, M. (2005). The galaxy luminosity function from M_R=-25 to M_R=-9. MNRAS, 357:783–792.

Tresse, L. and Maddox, S. J. (1998). The H alpha Luminosity Function and Star Formation Rate at Z approximately 0.2. ApJ, 495:691–697.

Treu, T., Ellis, R. S., Kneib, J.-P., Dressler, A., Smail, I., Czoske, O., Oemler, A., and Natarajan, P. (2003). A Wide-Field Hubble Space Telescope Study of the Cluster Cl 0024+16 at z = 0.4. I. Morphological Distributions to 5 Mpc Radius. ApJ, 591:53–78.

Tyler, K. D., Bai, L., and Rieke, G. H. (2014). Star Formation Trends in the Unrelaxed, Post-merger Cluster A2255. ApJ, 794:31.

Tyler, K. D., Rieke, G. H., and Bai, L. (2013). Star-forming Galaxy Evolution in Nearby Rich Clusters. ApJ, 773:86.

Valentinuzzi, T., Poggianti, B. M., Fasano, G., D'Onofrio, M., Moretti, A., Ramella, M., Biviano, A., Fritz, J., Varela, J., Bettoni, D., Vulcani, B., Moles, M., Couch, W. J., Dressler, A., Kjærgaard, P., Omizzolo, A., and Cava, A. (2011). The red-sequence of 72 WINGS local galaxy clusters. A&A, 536:A34.

Valentinuzzi, T., Woods, D., Fasano, G., Riello, M., D'Onofrio, M., Varela, J., Bettoni, D., Cava, A., Couch, W. J., Dressler, A., Fritz, J., Moles, M., Omizzolo, A., Poggianti, B. M., and Kjærgaard, P. (2009). WINGS: a WIde-field nearby Galaxy-cluster survey. III. Deep near-infrared photometry of 28 nearby clusters. A&A, 501:851–864.

Valluri, M. (1993). Compressive tidal heating of a disk galaxy in a rich cluster. ApJ, 408:57–70.

van den Bergh, S. (1998). *Galaxy Morphology and Classification*.

van den Bosch, F. C., Aquino, D., Yang, X., Mo, H. J., Pasquali, A., McIntosh, D. H., Weinmann, S. M., and Kang, X. (2008). The importance of satellite quenching for the build-up of the red sequence of present-day galaxies. MNRAS, 387:79–91.

van Dokkum, P. G., Franx, M., Fabricant, D., Illingworth, G. D., and Kelson, D. D. (2000). Hubble Space Telescope Photometry and Keck Spectroscopy of the Rich Cluster MS 1054-03: Morphologies, Butcher-Oemler Effect, and the Color-Magnitude Relation at Z = 0.83. ApJ, 541:95–111.

van Dokkum, P. G. and Stanford, S. A. (2001). A Massive Disk Galaxy at z=1.34. ApJ, 562:L35–L38.

Varela, J., D'Onofrio, M., Marmo, C., Fasano, G., Bettoni, D., Cava, A., Couch, W. J., Dressler, A., Kjærgaard, P., Moles, M., Pignatelli, E., Poggianti, B. M., and Valentinuzzi, T. (2009). WINGS: A WIde-field Nearby Galaxy-cluster Survey. II. Deep optical photometry of 77 nearby clusters. A&A, 497:667–676.

Vijayaraghavan, R. and Ricker, P. M. (2013). Pre-processing and post-processing in group-cluster mergers. MNRAS, 435:2713–2735.

Visvanathan, N. and Sandage, A. (1977). The color-absolute magnitude relation for E and S0 galaxies. I - Calibration and tests for universality using Virgo and eight other nearby clusters. ApJ, 216:214–226.

Vollmer, B., Cayatte, V., Balkowski, C., and Duschl, W. J. (2001). Ram Pressure Stripping and Galaxy Orbits: The Case of the Virgo Cluster. ApJ, 561:708–726.

von der Linden, A., Best, P. N., Kauffmann, G., and White, S. D. M. (2007). How special are brightest group and cluster galaxies? MNRAS, 379:867–893.

von der Linden, A., Wild, V., Kauffmann, G., White, S. D. M., and Weinmann, S. (2010). Star formation and AGN activity in SDSS cluster galaxies. MNRAS, 404:1231–1246.

Vulcani, B., De Lucia, G., Poggianti, B. M., Bundy, K., More, S., and Calvi, R. (2014). What do Simulations Predict for the Galaxy Stellar Mass Function and its Evolution in Different Environments? ApJ, 788:57.

Vulcani, B., Poggianti, B. M., Aragón-Salamanca, A., Fasano, G., Rudnick, G., Valentinuzzi, T., Dressler, A., Bettoni, D., Cava, A., D'Onofrio, M., Fritz, J., Moretti, A., Omizzolo, A., and Varela, J. (2011). Galaxy stellar mass functions of different morphological types in clusters, and their evolution between z= 0.8 and 0. MNRAS, 412:246–268.

Vulcani, B., Poggianti, B. M., Fasano, G., Desai, V., Dressler, A., Oemler, A., Calvi, R., D'Onofrio, M., and Moretti, A. (2012). The importance of the local density in shaping the galaxy stellar mass functions. MNRAS, 420:1481–1494.

Vulcani, B., Poggianti, B. M., Finn, R. A., Rudnick, G., Desai, V., and Bamford, S. (2010). Comparing the Relation Between Star Formation and Galaxy Mass in Different Environments. ApJ, 710:L1–L6.

Vulcani, B., Poggianti, B. M., Fritz, J., Fasano, G., Moretti, A., Calvi, R., and Paccagnella, A. (2015). From Blue Star-forming to Red Passive: Galaxies in Transition in Different Environments. ApJ, 798:52.

Wang, Y., Yang, X., Mo, H. J., and van den Bosch, F. C. (2007). The Cross-Correlation between Galaxies of Different Luminosities and Colors. ApJ, 664:608–632.

Weinmann, S. M., Kauffmann, G., van den Bosch, F. C., Pasquali, A., McIntosh, D. H., Mo, H., Yang, X., and Guo, Y. (2009). Environmental effects on satellite galaxies: the link between concentration, size and colour profile. MNRAS, 394:1213–1228.

Weinmann, S. M., van den Bosch, F. C., and Pasquali, A. (2011). *The Dependence of Low Redshift Galaxy Properties on Environment*, page 29.

Weinmann, S. M., van den Bosch, F. C., Yang, X., and Mo, H. J. (2006). Properties of galaxy groups in the Sloan Digital Sky Survey - I. The dependence of colour, star formation and morphology on halo mass. MNRAS, 366:2–28.

Wetzel, A. R., Tinker, J. L., and Conroy, C. (2012). Galaxy evolution in groups and clusters: star formation rates, red sequence fractions and the persistent bimodality. MNRAS, 424:232–243.

Wetzel, A. R., Tinker, J. L., Conroy, C., and van den Bosch, F. C. (2013). Galaxy evolution in groups and clusters: satellite star formation histories and quenching time-scales in a hierarchical Universe. MNRAS, 432:336–358.

Wheeler, C., Phillips, J. I., Cooper, M. C., Boylan-Kolchin, M., and Bullock, J. S. (2014). The surprising inefficiency of dwarf satellite quenching. MNRAS, 442:1396–1404.

White, S. D. M. and Frenk, C. S. (1991). Galaxy formation through hierarchical clustering. ApJ, 379:52–79.

Whitmore, B. C. and Gilmore, D. M. (1991). On the interpretation of the morphology-density relation for galaxies in clusters. ApJ, 367:64–68.

Whitmore, B. C., Gilmore, D. M., and Jones, C. (1993). What determines the morphological fractions in clusters of galaxies? ApJ, 407:489–509.

Wijesinghe, D. B., Hopkins, A. M., Brough, S., Taylor, E. N., Norberg, P., Bauer, A., Brown, M. J. I., Cameron, E., Conselice, C. J., Croom, S., Driver, S., Grootes, M. W., Jones, D. H., Kelvin, L., Loveday, J., Pimbblet, K. A., Popescu, C. C., Prescott, M., Sharp, R., Baldry, I., Sadler, E. M., Liske, J., Robotham, A. S. G., Bamford, S., Bland-Hawthorn, J., Gunawardhana, M., Meyer, M., Parkinson, H., Drinkwater, M. J., Peacock, J., and Tuffs, R. (2012). Galaxy And Mass Assembly (GAMA): galaxy environments and star formation rate variations. MNRAS, 423:3679–3691.

Wilman, D. J., Oemler, Jr., A., Mulchaey, J. S., McGee, S. L., Balogh, M. L., and Bower, R. G. (2009). Morphological Composition of z ˜ 0.4 Groups: The Site of S0 Formation. ApJ, 692:298–308.

Wong, O. I., Schawinski, K., Kaviraj, S., Masters, K. L., Nichol, R. C., Lintott, C., Keel, W. C., Darg, D., Bamford, S. P., Andreescu, D., Murray, P., Raddick, M. J., Szalay, A., Thomas, D., and Vandenberg, J. (2012). Galaxy Zoo: building the low-mass end of the red sequence with local post-starburst galaxies. MNRAS, 420:1684–1692.

Woo, J., Dekel, A., Faber, S. M., Noeske, K., Koo, D. C., Gerke, B. F., Cooper, M. C., Salim, S., Dutton, A. A., Newman, J., Weiner, B. J., Bundy, K., Willmer, C. N. A., Davis, M., and Yan, R. (2013). Dependence of galaxy quenching on halo mass and distance from its centre. MNRAS, 428:3306–3326.

Yagi, M., Yoshida, M., Komiyama, Y., Kashikawa, N., Furusawa, H., Okamura, S., Graham, A. W., Miller, N. A., Carter, D., Mobasher, B., and Jogee, S. (2010). A Dozen New Galaxies Caught in the Act: Gas Stripping and Extended Emission Line Regions in the Coma Cluster. AJ, 140:1814–1829.

Yahil, A. and Vidal, N. V. (1977). The Velocity Distribution of Galaxies in Clusters. ApJ, 214:347–350.

Yang, X., Mo, H. J., and van den Bosch, F. C. (2003). Constraining galaxy formation and cosmology with the conditional luminosity function of galaxies. MNRAS, 339:1057–1080.

Yang, X., Mo, H. J., and van den Bosch, F. C. (2008). Galaxy Groups in the SDSS DR4. II. Halo Occupation Statistics. ApJ, 676:248–261.

Yang, X., Mo, H. J., van den Bosch, F. C., and Jing, Y. P. (2005). A halo-based galaxy group finder: calibration and application to the 2dFGRS. MNRAS, 356:1293–1307.

Yang, X., Mo, H. J., van den Bosch, F. C., Pasquali, A., Li, C., and Barden, M. (2007). Galaxy Groups in the SDSS DR4. I. The Catalog and Basic Properties. ApJ, 671:153–170.

York, D. G., Adelman, J., Anderson, Jr., J. E., Anderson, S. F., Annis, J., Bahcall, N. A., Bakken, J. A., Barkhouser, R., Bastian, S., Berman, E., Boroski, W. N., Bracker, S., Briegel, C., Briggs, J. W., Brinkmann, J., Brunner, R., Burles, S., Carey, L., Carr, M. A., Castander, F. J., Chen, B., Colestock, P. L., Connolly, A. J., Crocker, J. H., Csabai, I., Czarapata, P. C., Davis, J. E., Doi, M., Dombeck, T., Eisenstein, D., Ellman, N., Elms, B. R., Evans, M. L., Fan, X., Federwitz, G. R., Fiscelli, L., Friedman, S., Frieman, J. A., Fukugita, M., Gillespie, B., Gunn, J. E., Gurbani, V. K., de Haas, E., Haldeman, M., Harris, F. H., Hayes, J., Heckman, T. M., Hennessy, G. S., Hindsley, R. B., Holm, S., Holmgren, D. J., Huang, C.-h., Hull, C., Husby, D., Ichikawa, S.-I., Ichikawa, T., Ivezić, Ž., Kent, S., Kim, R. S. J., Kinney, E., Klaene, M., Kleinman, A. N., Kleinman, S., Knapp, G. R., Korienek, J., Kron, R. G., Kunszt, P. Z., Lamb, D. Q., Lee, B., Leger, R. F., Limmongkol, S., Lindenmeyer, C., Long, D. C., Loomis, C., Loveday, J., Lucinio, R., Lupton, R. H., MacKinnon, B., Mannery, E. J., Mantsch, P. M., Margon, B., McGehee, P., McKay, T. A., Meiksin, A., Merelli, A., Monet, D. G., Munn, J. A., Narayanan, V. K., Nash, T., Neilsen, E., Neswold, R., Newberg, H. J., Nichol, R. C., Nicinski, T., Nonino, M., Okada, N., Okamura, S., Ostriker, J. P., Owen, R., Pauls, A. G., Peoples, J., Peterson, R. L., Petravick, D., Pier, J. R., Pope, A., Pordes, R., Prosapio, A., Rechenmacher, R., Quinn, T. R., Richards, G. T., Richmond, M. W., Rivetta, C. H., Rockosi, C. M., Ruthmansdorfer, K., Sandford, D., Schlegel, D. J., Schneider, D. P., Sekiguchi, M., Sergey, G., Shimasaku, K., Siegmund, W. A., Smee, S., Smith, J. A., Snedden, S., Stone, R., Stoughton, C., Strauss, M. A., Stubbs, C., SubbaRao, M., Szalay, A. S., Szapudi, I., Szokoly, G. P., Thakar, A. R., Tremonti, C., Tucker, D. L., Uomoto, A., Vanden Berk, D., Vogeley, M. S., Waddell, P., Wang, S.-i., Watanabe, M., Weinberg, D. H., Yanny, B., Yasuda, N., and SDSS Collaboration (2000). The Sloan Digital Sky Survey: Technical Summary. AJ, 120:1579–1587.

Yoshida, M., Yagi, M., Komiyama, Y., Furusawa, H., Kashikawa, N., Koyama, Y., Yamanoi, H., Hattori, T., and Okamura, S. (2008). Strange Filamentary Structures ("Fireballs") around a Merger Galaxy in the Coma Cluster of Galaxies. ApJ, 688:918–930.